

**CHLORIDE TRANSPORT AND  
SALT TOLERANCE MECHANISMS  
IN PLANTS**

Dissertation  
zur Erlangung des Doktorgrades  
der Mathematisch-Naturwissenschaftlichen Fakultät  
der Christian-Albrechts-Universität zu Kiel

vorgelegt von  
Livia Saleh

Kiel; Dezember 2010



Referent/in: .....PD Dr. Christoph Plieth  
Korreferent/in: .....Prof. Dr. Wolfgang Bilger  
Tag der mündlichen .....10. Februar 2011  
Zum Druck genehmigt: Kiel, .....10. Februar 2011

# ABSTRACT

Sodium ( $\text{Na}^+$ ) and chloride ( $\text{Cl}^-$ ) are the most abundant ions found on arable land affected by salinity worldwide. Salinity interferes with plant growth and consequently limits crop production. While many studies focussed on the mechanisms of  $\text{Na}^+$  transport, accumulation and exclusion in plants under salt stress, the role of  $\text{Cl}^-$  is less investigated. Although, the interest on the mechanisms of  $\text{Cl}^-$  transport and its role in salt tolerance mechanisms is growing, there are still many unanswered questions.

The work presented here was intended to tackle some of these questions. Therefore, two closely related plant species considered extremes in salt tolerance were employed: the glycophyte *Arabidopsis thaliana* and the halophyte *Thellungiella salsuginea*. Screening germination and growth, and ionic and osmotic parameters of both plant species delivered surprising results. *Thellungiella* is in its early developmental stages not able to cope with high salinity, whereas *Arabidopsis* does germinate and grow even on 100 mM NaCl.

Both plant species, when exposed to high salinity, accumulate  $\text{Na}^+$  and  $\text{Cl}^-$  which seem to replace potassium and nitrate in the tissue, respectively. In addition, symptoms of iron deficiency were observed in both species. And indeed, iron deficiency could be confirmed by iron content measurements. The  $\text{Na}^+$  accumulation in *Thellungiella* is lower, revealing a possible trait of salt tolerance mechanism in this plant species.

In experiments run in parallel, calcium has been omitted in the growth medium leading to significant lower  $\text{Na}^+$  and  $\text{Cl}^-$  accumulations. This effect is in contrast to studies where the ameliorative role of calcium on salt stress symptoms was highlighted. In *Arabidopsis*, all screened parameters show a dependency on calcium, whereas in *Thellungiella* this is less obvious. Important in this context is the over-accumulation of iron in plants suffering from calcium deficiency. Both, free iron, and low-molecular-weight iron chelates in aerobic tissue cause the excess formation of reactive oxygen species (ROS) under abiotic stress.

Therefore, oxidative stress responses, such as changes in the total low molecular weight antioxidative capacity, superoxide scavenging activity, and the activity of peroxidases, catalases and glutathione reductases were examined. Particular assays were developed and optimised during this study. The results reveal different antioxidative responses to salinity in *Arabidopsis* and *Thellungiella*. Many of the antioxidative enzymes are heme-containing proteins. The measured iron deficiency in plants growing on 75 mM NaCl and above corresponds with the reduction in their activity. In contrast, calcium deficiency leads to a drastic increase in the abundance of peroxidases in *Arabidopsis* under salt stress. These peroxidases are possibly inactive in the plants, due the lack of calcium.

*In vivo* fluorescence ratiometric techniques were employed during this study to investigate anion transport and changes of cellular anion concentrations in living plant cells exposed to salt stress. In addition, cellular redox poise and pH were measured during salt treatment in *Arabidopsis* expressing appropriate fluorescent indicators. The effects of calcium, trivalent cations, polyamines, oxidative substances and inhibitors of anion transporters on the anion influx have been tested in course of this endeavour. The results show, that  $\text{Cl}^-$  influx is sensitive to extracellular pH, external Ca availability and the redox milieu. Due to contradictory results, a definite statement about the kind of transporters involved in NaCl-induced  $\text{Cl}^-$  influx could not be made.

By cloning and co-expressing members of the  $\text{Cl}^-$  channel family (ClCs) from *Arabidopsis thaliana* together with an anion-sensitive fluorescent indicator, the role of anion compartmentalisation under salt stress conditions was illuminated. A point mutation in the selectivity filter of a  $\text{NO}_3^-/\text{H}^+$  antiporter AtClC-A for example produces a change in the anion selectivity and thus a switch from  $\text{NO}_3^-$  to  $\text{Cl}^-$  transport into the vacuole. For further molecular and functional characterization, it has been attempted to purify the anion channel proteins.

# ZUSAMMENFASSUNG

Natrium ( $\text{Na}^+$ ) und Chlorid ( $\text{Cl}^-$ ) sind im Zusammenhang mit Versalzung landwirtschaftlich genutzter Flächen weltweit die häufigsten Ionen. Salz im Boden wirkt sich negativ auf das Pflanzenwachstum aus und führt so zu Ertragseinbußen. Bisher konzentrierte sich die Erforschung des Salzstresses in Pflanzen auf die Mechanismen von  $\text{Na}^+$ -Transport, -Akkumulation und -Ausschluss. Die Rolle von  $\text{Cl}^-$  ist hingegen weniger erforscht. Trotz zunehmenden Interesses an der Erforschung der  $\text{Cl}^-$ -Transportmechanismen, sind immer noch viele Fragen unbeantwortet.

Das Ziel der vorliegenden Arbeit war es einigen dieser Fragen nachzugehen. Dafür wurden zwei nahe verwandte Pflanzenarten ausgesucht, die sich in ihrer Salztoleranz stark unterscheiden: *Arabidopsis thaliana* gehört zu den Glykophyten und *Thellungiella salsuginea* wurde bisher als 'halophil' bezeichnet. Die Quantifizierung von Keimrate, Wachstum und Ionengehalt der auf verschiedenen Salzkonzentrationen gewachsenen Pflanzen, lieferten überraschende Ergebnisse. *Thellungiella* ist während früher Wachstumsstadien nicht in der Lage, mit hohen Salzkonzentrationen fertig zu werden. *Arabidopsis* hingegen keimt und wächst auf Konzentrationen bis zu 100 mM NaCl.

Beide Pflanzenarten akkumulieren auf hohen Salzkonzentrationen  $\text{Na}^+$  und  $\text{Cl}^-$ , welche dann Kalium und Nitrat im Gewebe verdrängen. Die Akkumulation von  $\text{Na}^+$  ist in *Thellungiella* niedriger. Dies könnte ein mögliches Salztoleranzmerkmal dieser Art sein. Zusätzlich wurden in beiden Spezies typische Eisenmangelsymptome beobachtet. Diese Beobachtungen konnten durch Messungen des Eisengehaltes bestätigt werden.

In parallelen Experimenten, wurde Kalzium im Wachstumsmedium weggelassen, was zu einer signifikant niedrigeren  $\text{Na}^+$ - und  $\text{Cl}^-$ -Akkumulation führte. Dieser Effekt steht im Widerspruch zu Studien, welche den positiven Einfluss von Kalzium auf die Salzstresssymptome hervorheben. *Arabidopsis* zeigt in allen gemessenen Parametern eine Kalziumabhängigkeit, die man bei *Thellungiella* nicht eindeutig beobachten kann. In diesem Zusammenhang wurde unter Kalziummangel eine übermäßige Akkumulation an Eisen beobachtet. Sowohl freies Eisen als auch Eisenchelate begünstigen in aeroben Geweben die Bildung reaktiver Sauerstoffspezies unter abiotischem Stress.

Aus diesem Grund wurden Änderungen in der gesamt-antioxidativen Kapazität, der Superoxid-scavenging Aktivität, der Peroxidase- und der Glutathion-Reduktase-Aktivitäten näher untersucht. Dazu wurden spezielle Verfahren entwickelt und optimiert. Die Ergebnisse zeigen, dass *Arabidopsis* und *Thellungiella* unterschiedlich auf Salzstress reagieren. Viele der antioxidativen Enzyme besitzen Eisen-Häm Komplexe. Der gemessene Eisenmangel in Pflanzen unter Salzstress (über 75 mM NaCl) korrespondiert mit der abgeschwächten Aktivität dieser Enzyme. Im Gegensatz dazu führt Kalziummangel zu einer übermäßigen Zunahme an Peroxidasen. Diese sind aber durch den Mangel an Kalzium in den Pflanzen vermutlich inaktiv.

Ratiometrische *in vivo*-Fluoreszenzmesstechniken wurden während dieser Studie genutzt, um Änderungen in der zellulären Anionenkonzentration und den damit verbundenen Anionentransport in Pflanzen unter Salzstress zu untersuchen. Mit Hilfe bestimmter Fluoreszenzindikatoren wurde zudem der Einfluß von Salz auf das zelluläre Redoxgleichgewicht und den  $\text{pH}_{\text{cyt}}$  untersucht. Getestet wurde insbesondere, wie Kalzium, trivalente Kationen, Polyamine, oxidative Substanzen und spezielle Inhibitoren auf den Anionentransport wirken. Die Ergebnisse zeigen eine Sensitivität des  $\text{Cl}^-$ -Einstroms gegenüber den Änderungen im externen pH, der Kalziumkonzentration und der Redoxumgebung. Eine eindeutige Aussage über die Identität der am NaCl-induzierten  $\text{Cl}^-$ -Einstrom beteiligten Transporter konnte nicht gewonnen werden.

Durch Klonierung und Ko-expression von Chloridkanälen (ClCs) zusammen mit einem Anionenindikator konnte aber die Anionenkompartimentalisierung beleuchtet werden. Eine Punktmutation im Selektivitätsfilter von AtClC-A führte zu einer Änderung in der Selektivität und dadurch zu einem Wechsel vom  $\text{NO}_3^-$ - zu  $\text{Cl}^-$ -Transport in die Vakuole. Für weitere strukturelle und funktionelle Charakterisierungen wurde die Aufreinigung der Anionenkanalproteine versucht.



# INDEX OF CONTENTS

<b>ABSTRACT .....</b>	<b>4</b>
<b>ZUSAMMENFASSUNG.....</b>	<b>5</b>
<b>INDEX OF CONTENTS.....</b>	<b>7</b>
<b>LIST OF PUBLICATIONS .....</b>	<b>10</b>
<b>LIST OF CONFERENCE CONTRIBUTIONS.....</b>	<b>10</b>
<b>LIST OF FIGURES.....</b>	<b>11</b>
<b>LIST OF TABLES.....</b>	<b>12</b>
<b>ABBREVIATIONS .....</b>	<b>13</b>
<b>1 INTRODUCTION .....</b>	<b>14</b>
<b>1.1 General aspects of salinity stress and tolerance mechanisms .....</b>	<b>14</b>
1.1.1 Ion fluctuations during salt stress.....	15
1.1.2 Oxidative stress and the antioxidative system.....	16
<b>1.2 Uptake and transport of chloride under salt stress in relation to salt tolerance .....</b>	<b>19</b>
1.2.1 Uptake of chloride by the plants .....	20
1.2.2 Uptake of chloride into the cell during salt stress .....	21
<b>1.3 Chloride channel (ClC) proteins.....</b>	<b>22</b>
1.3.1 Chloride channel proteins – the intracellular and tissue localisation .....	22
1.3.2 The structure dependent functionality of ClC proteins .....	27
<b>1.4 Electroneutral cation-chloride-cotransporters (CCCs).....</b>	<b>29</b>
<b>2 COMPARATIVE STUDY OF <i>ARABIDOPSIS THALIANA</i> AND <i>THELLUNGIELLA SALSUGINEA</i> DURING LONG-TERM SALT STRESS.....</b>	<b>30</b>
<b>2.1 MATERIALS AND METHODS .....</b>	<b>30</b>
2.1.1 Chemicals, consumables and equipment.....	30
2.1.2 Solutions and buffers .....	30
2.1.3 Plant treatment .....	30
2.1.4 Anion content measured by ion chromatography (IC).....	31
2.1.5 Cation content measured by atomic absorption spectroscopy (AAS) .....	31
2.1.6 Osmotic properties .....	32
<b>2.2 RESULTS .....</b>	<b>32</b>
2.2.1 Germination rate .....	32
2.2.2 Primary root length .....	33
2.2.3 The visible symptoms of salt stress and simultaneous calcium deficiency .....	34
2.2.4 Ionic component of salt stress .....	36
2.2.5 Osmotically active substances .....	40
<b>2.3 DISCUSSION .....</b>	<b>41</b>
2.3.1 <i>Thellungiella salsuginea</i> - the germination phenomenon .....	41
2.3.2 Organic osmolytes are not accumulated during salt stress in <i>A. thaliana</i> and <i>T. salsuginea</i> .....	42
2.3.3 Calcium alleviates symptoms of salt stress in plants .....	42
2.3.4 Iron availability .....	43
<b>3 RATIO-METRIC QUANTITATION OF GENERIC CELLULAR PARAMETERS <i>IN VIVO</i> DURING SHORT TERM SALT STRESS.....</b>	<b>45</b>
<b>3.1 MATERIAL AND METHODS .....</b>	<b>45</b>
3.1.1 Chemicals, consumables and equipment.....	45
3.1.2 Solutions and buffers .....	45

3.1.3 Bacterial strains .....	47
3.1.4 Characteristics of GFP-based indicators used in this study .....	47
3.1.4.1 pH-sensitive fluorescent indicators .....	48
3.1.4.2 Redox sensitive GFP-based indicator - S3roGFP .....	49
3.1.4.3 Genetically encoded chloride indicator - Clomeleon .....	51
3.1.4.4 Co-expression study with dsRED and PtGFP .....	53
3.1.5 Fluorescence imaging, calibration procedures and data processing .....	53
3.1.5.1 Ratio imaging workstation .....	53
3.1.5.2 Calibration of fluorescent indicators .....	55
3.1.5.3 Data analysis .....	55
3.1.5.4 In vivo experiments with transgenic plants .....	55
3.1.6 Cloning of chloride channels - RNA isolation and first-strand cDNA synthesis .....	56
3.1.7 Cloning of chloride channels - specific PCR .....	56
3.1.8 DNA isolation and ethanol precipitation .....	57
3.1.9 Restriction digest and ligation .....	57
3.1.10 Transformation of bacteria by electroporation .....	57
3.1.11 Isolation of DNA .....	58
3.1.12 Biolistic transformation of leek ( <i>Allium porrum</i> ) and onion ( <i>Allium cepa</i> ) epidermal cells .....	58
3.1.13 Purification of recombinant indicators and chloride channel proteins .....	60
3.1.13.1 Expression of proteins and cell lysis .....	60
3.1.13.2 Sodium Dodecyl Sulphate PolyAcrylamide Gel Electrophoresis (SDS PAGE) .....	61
3.1.13.3 Streptavidin affinity chromatography .....	61
3.1.13.4 Ni <sup>2+</sup> - NTA affinity chromatography .....	61
3.1.13.5 Gel filtration .....	62
3.1.13.6 Fast Protein Liquid Chromatography (FPLC) analysis .....	62
<b>3.2 RESULTS .....</b>	<b>63</b>
3.2.1 Ratiometric quantitation of salt stress-induced chloride influx .....	63
3.2.1.1 Chloride influx into Arabidopsis root cells exhibits two distinct phases- the fast “depolarisation phase” and the slow “saturation phase” .....	63
3.2.1.2 Chloride influx is dependent on calcium .....	64
3.2.1.3 Chloride flux is sensitive to diuretics and some anion channel inhibitors .....	66
3.2.1.4 Chloride influx is sensitive to trivalent cations .....	69
3.2.1.5 Chloride influx is inhibited by the polyamine spermine .....	69
3.2.1.6 Salt-stress induces changes in the cell redox environment .....	70
3.2.1.7 Influence of externally applied abscisic acid (ABA) on the chloride flux .....	72
3.2.2 Cloning of chloride channels .....	73
3.2.2.1 Cloning of AtClC-A .....	73
3.2.2.2 Mutation of the GPGIP motif in AtClC-A .....	74
3.2.2.3 Cloning of AtClC-B .....	74
3.2.2.5 Cloning of AtClC-C .....	75
3.2.2.6 Cloning of the other chloride channels .....	75
3.2.2.7 Cloning of AtCCC .....	76
3.2.3 Suitability of biolistic transformation for transient co-expression of a reporter and a target gene .....	77
3.2.4 The co-expression of Clomeleon and chloride channel constructs – effect on the chloride influx .....	78
3.2.4.1 Experiments with leek epidermal cells .....	78
3.2.4.2 Experiments with onion epidermal cells .....	78
3.2.4 Expression and purification of AtClC-A in bacterial system .....	80
<b>3.3 DISCUSSION .....</b>	<b>82</b>
3.3.1 NaCl-induced chloride influx into <i>Arabidopsis</i> root cells exhibits two distinct phases .....	82
3.3.2 Internal and external calcium availability differ in their effect on NaCl-induced chloride entry .....	83
3.3.3 Salinity induced chloride transport and the role of pH .....	84
3.3.4 Chloride flux is sensitive to diuretics and some anion channel inhibitors .....	84
3.3.5 Block of chloride flux by trivalent ions La <sup>3+</sup> , Gd <sup>3+</sup> , and Al <sup>3+</sup> .....	85
3.3.6 Inhibition of chloride influx by spermine .....	85
3.3.7 Chloride influx is redox-sensitive .....	85
3.3.8 AtClC-A mediates the nitrate influx into the vacuoles of onion epidermal cells .....	86



<b>4</b>	<b>FINGERPRINTING ANTIOXIDATIVE ACTIVITIES.....</b>	<b>88</b>
<b>4.1</b>	<b>MATERIAL AND METHODS .....</b>	<b>88</b>
4.1.1	Chemicals, consumables and equipment.....	88
4.1.2	Solutions and buffers .....	88
4.1.3	Processing of plant material.....	89
4.1.3.1	Growing and stress treatment of garden cress ( <i>Lepidium sativum</i> ).....	89
4.1.3.2	Growing and stress treatment of <i>Arabidopsis thaliana</i> and <i>Thellungiella salsuginea</i> .....	90
4.1.3.3	Processing of plant samples .....	90
4.1.4	Protein content measurements .....	91
4.1.5	Total antioxidative activity (TAC) assay .....	91
4.1.5.1	Principle of the TAC assay.....	91
4.1.5.2	Setting up the TAC assay .....	93
4.1.5.3	Assaying the plant samples .....	94
4.1.6	Luminol converting peroxidase assay .....	95
4.1.6.1	LUPO assay principle.....	95
4.1.6.2	Assaying the plant samples .....	95
4.1.7	Superoxide scavenging activity (SOSA) assay .....	96
4.1.7.1	XOD reaction mechanism .....	96
4.1.7.2	XOD assay .....	97
4.1.7.3	SOSA assay principle.....	98
4.1.7.4	Assaying plant samples .....	99
4.1.8	Catalase (CAT) assay.....	100
4.1.9	Glutathione reductase (GR) assay.....	100
<b>4.2</b>	<b>RESULTS .....</b>	<b>100</b>
4.2.1	Fingerprinting the antioxidative activities of <i>Lepidium sativum</i> during different abiotic stress situations .....	100
4.2.1.1	Salt stress.....	101
4.2.1.2	Drought stress.....	101
4.2.1.3	Heat stress .....	102
4.2.1.4	Cold stress .....	103
4.2.2	Fingerprinting the antioxidative activities of <i>Arabidopsis thaliana</i> and <i>Thellungiella salsuginea</i> during salt stress.....	104
<b>4.3</b>	<b>DISCUSSION .....</b>	<b>108</b>
4.3.1	Salt stress: a “two in one” challenge.....	108
4.3.2	Calcium controls the oxidative stress response in <i>Arabidopsis thaliana</i> .....	110
4.3.3	Drought stress .....	111
4.3.4	Heat stress .....	112
4.3.5	Cold stress.....	112
4.3.6	Tolerance and robustness .....	113
4.3.7	Redundancies in the ROS-scavenging system .....	114
<b>5</b>	<b>GENERAL DISCUSSION .....</b>	<b>116</b>
	<b>AKNOWLEDGMENTS.....</b>	<b>119</b>
	<b>EIDESSTATTLICHE ERKLÄRUNG .....</b>	<b>120</b>
	<b>REFERENCES .....</b>	<b>121</b>
	<b>SUPPLEMENTAL MATERIAL .....</b>	<b>139</b>

## LIST OF PUBLICATIONS

Saleh, L.; Plieth, C. 2010 "Total low molecular weight antioxidants as a summary parameter, quantified in biological samples by a chemiluminescent inhibition assay" *Nature Protocols* 5(10): 1627-1634

Saleh, L.; Plieth, C. 2010 "A coelenterazine-based luminescence assay to quantify high molecular weight superoxide anion scavenger activities" *Nature Protocols* 5(10): 1635-1641

Saleh, L.; Plieth, C. 2009 "Fingerprinting antioxidative activities in plants" *Plant Methods* 5:2  
doi:10.1186/1746-4811-5-2

## LIST OF CONFERENCE CONTRIBUTIONS

Saleh, L.; Plieth, C.; Mock, H.-P.; Mühling, K.-H.; Witzel, K "Antioxidative defence mechanisms in two contrasting barley genotypes under salt stress" Symposium Genetics of Plant Mineral Nutrition 2010 (30. September - 2. October 2010) Hannover, FRG - Abstract 121 p.161

Saleh, L., Plieth, C. "Low molecular weight antioxidants quantified by an integrated chemoluminescence assay." Botanikertagung 2009 (6.-10. September 2009) Leipzig, FRG - Abstract S16-26

Saleh, L., Plieth, C. "How do plants fight excessive superoxide formation under abiotic stress?" Botanikertagung 2009 (6.-10. September 2009) Leipzig, FRG - Abstract S16-23

Saleh, L., Plieth, C. "Changes in the antioxidative system in plants during abiotic stress" International Conference on 'Plant Abiotic Stress Tolerance' Vienna, Austria, (8.-11. February 2009) Abstract N44, p.63

Pohanke, J., Saleh, L., Plieth, C. "Ballistic bombardment allows transient co-expression to 100%" Botanikertagung 2007 (3.-7.9.2007) Hamburg, FRG - Conf.-Track 674 Abstract P08:3

Saleh, L., Plieth, C. "Internal and external Ca<sup>2+</sup> ion availabilities differ in controlling salt stress-induced chloride influx" Botanikertagung 2007 (3.-7.9.2007) Hamburg, FRG - Conf.-Track 662 Abstract P13:18

## LIST OF FIGURES

Figure 1: Interwoven character of salinity induced mechanisms.....	15
Figure 2: Ascorbate-glutathione cycle .....	19
Figure 3: Chloride channel proteins .....	24
Figure 4: Bacterial ClC structure .....	27
Figure 5: Comparison of germination rate of plants sown on full MS medium compared with plants sown on medium lacking calcium.....	32
Figure 6: Comparison of the primary root length of plants sown on full MS medium compared with plants sown on medium lacking calcium .....	33
Figure 7: Percentage difference between primary root lengths of <i>A.thaliana</i> and <i>T.salsuginea</i> grown at different salt concentrations .....	34
Figure 8: Two species contrasting in their salt tolerance grown at agar plates with different salt concentrations.....	35
Figure 9: Comparison of anion content in <i>Arabidopsis</i> and <i>Thellungiella</i> grown on substrates with different salt concentrations .....	37
Figure 10: The chloride to nitrate ratio.....	38
Figure 11: Cation content .....	39
Figure 12: Comparison of total osmolarity .....	40
Figure 13: Organic compatible solutes .....	41
Figure 14: Comparison of two recombinant pH-probes on a log-log scale .....	48
Figure 15: Fluorescence properties of genetically encoded pH-indicators.....	49
Figure 16: Fluorescence properties of genetically encoded redox indicator during oxidative and reducing treatment .....	50
Figure 17: pH sensitivity of the redox indicator .....	50
Figure 18: The emission spectra of Clomeleon .....	52
Figure 19: pH sensitivity of the genetically encoded Cl-indicator.....	53
Figure 20: Ratio imaging workstation .....	54
Figure 21: Scheme of the flow-through chamber assembly .....	55
Figure 22: Illustration of the gene gun with a vacuum chamber .....	59
Figure 23: Kinetics of chloride influx at different pH with two NaCl concentrations.....	63
Figure 24: Effect of internal calcium supply at the chloride influx during salt stress.....	64
Figure 25: Kinetics of chloride influx during salt stress at different CaCl <sub>2</sub> concentrations .....	65
Figure 26: Effect of different internal and external Ca availability on chloride influx.....	66
Figure 27: Block of calcium channels by nifedipine .....	66
Figure 28: Effect of the diuretic bumetanide on NaCl-induced chloride influx.....	67
Figure 29: Effect of the diuretic R-DIOA on NaCl-induced chloride influx .....	68
Figure 30: Effect of DMSO on the NaCl-induced chloride flux .....	68
Figure 31: Effect of the anion channel blocker DIDS on the cytoplasmic pH.....	69
Figure 32: Trivalent cation block of NaCl-induced chloride entry .....	69
Figure 33: Effect of polyamines on the NaCl-induced chloride flux .....	70
Figure 34: Influence of oxidizing substances on the Clomeleon emission ratio in <i>Arabidopsis</i> .....	70
Figure 35: Redox changes during salt and simultaneous oxidative treatment.....	71
Figure 36: pH changes during salt and simultaneous oxidative treatment .....	72
Figure 37: Direct effect of oxidative treatment on the anion indicator Clomeleon.....	72
Figure 38: Influence of ABA on the salt-induced chloride influx.....	73
Figure 39: PCR product (AtClC-A) visualised on a agarose gel .....	74
Figure 40: Temperature gradient PCR of AtClCA_mut .....	74
Figure 41: PCR products (AtClCB1 and B2) visualised on a agarose gel .....	75
Figure 42: PCR products (AtClC-C) visualised on a agarose gel.....	75
Figure 43: PCR products (AtClC-D, -E, -F and -G) visualised on a agarose gel .....	76
Figure 44: AtCCC visualised on a agarose gel .....	76
Figure 45: Biolistic bombardment allows transient co-expression to 100% .....	77
Figure 46: Chloride influx in onion epidermal cells expressing chloride channels during salinity treatment.....	79
Figure 47: Chloride/nitrate influx in onion epidermal cells expressing AtClC-A and mutated AtClC-A .....	80

Figure 48: 45 kDa endogenous bacterial protein is binding on the Ni <sup>2+</sup> -NTA column.....	80
Figure 49: Purification of AtClC-A on a gravity-flow Ni <sup>2+</sup> -NTA column .....	81
Figure 50: Purification of AtClC-A by the ÄKTA-purifier system .....	81
Figure 51: Purification of reduced AtClC-A on a gravity-flow Ni <sup>2+</sup> -NTA column.....	82
Figure 52: HRP-driven reaction cycle.....	92
Figure 53: The TAC assay procedure and data evaluation .....	93
Figure 54: The luminol converting peroxidase (LUPO) cycle.....	95
Figure 55: Proposed mechanism of oxidative (black cycle) and reductive (brown cycle) half-reactions of XOD and the interaction of superoxide with coelenterazine in the SOSA assay.....	97
Figure 56: The SOSA assay procedure and data evaluation .....	98
Figure 57: Stress-induced alterations in the antioxidative system of <i>Lepidium</i> .....	103
Figure 58: Comparison of constitutive antioxidative parameters in <i>Arabidopsis</i> and <i>Thellungiella</i> ....	104
Figure 59: Percentage change in TAC, LUPO, SOSA, CAT, and GR of plants exposed to salinity in comparison to untreated control plants .....	105
Figure 60: Fingerprints of antioxidant activities of salt-grown relatives differing in their salt tolerance .....	107
Figure 61: Influence of calcium deficiency on the antioxidative system of <i>Arabidopsis thaliana</i> and <i>Thellungiella salsuginea</i> plants.....	108

## LIST OF TABLES

Table 1: Characteristics of the <i>Arabidopsis thaliana</i> chloride channels. _____	26
Table 2: The parameters for measuring total Ca, K, Mg, Na and Fe contents via atomic absorption spectroscopy_____	31
Table 3: Bacterial strains used in this study _____	47
Table 4: Properties of fluorescent indicators used in this study _____	48
Table 5: Parameters of excitation beam path filters _____	54
for fluorescence imaging of different fluorescent indicators. _____	54
Table 6: Vectors used in this study _____	57
Table 7: Inhibitory effect on chloride influx_____	67

## ABBREVIATIONS

6xHis	6xHistidine	KCC	Potassium-Chloride-Cotransporter
A9C	Anthracene-9-Carboxylic acid	KPET	KPP+EDTA+Triton-X-100
AAS	Atomic Absorption Spectroscopy	LB	Luria Brothers
ABA	Abscisic Acid	LMW	Low Molecular Weight
ABRC	Arabidopsis Biological Resource Center	LUPO	Luminol converting Peroxidases
ABS	Absorption	MCS	Multiple Cloning Site
AO	Antioxidant	MDA	Monodehydroascorbate
AP	Aminophtalate	MDAR	Monodehydroascorbate Reductase
APX	Ascorbate Peroxidase	MES	2-(N-morpholino)ethanesulfonic Acid
ASC	Ascorbate	APS	Ammonium Persulfate
BSA	Bovine Serum Albumine	MS	Murashige & Skoog
BUME	Bumetanide	MWCO	Molecular Weight Cut-off
CaMV	Cauliflower Mosaic Virus	NADP	Nicotinamide adenine dinucleotide phosphate
CAT	Catalase	NADPH	Nicotinamide adenine dinucleotide phosphate (reduced form)
CBS	Cystathionine- $\beta$ -Synthetase	NCC	Sodium-Chloride -Cotransporter
CCC	Cation-Chloride-Cotransporter	Ni <sup>2+</sup> /NTA	Ni <sup>2+</sup> /Nitrilo Triacetic Acid
cDNA	copy Deoxyribonucleic Acid	NKCC	Sodium-Potassium-Chloride - Cotransporter
CFP	Cyan Fluorescent Protein	NPPB	Nitro-phenylpropylamino-benzoic Acid
CIC	Chloride Channel	OD	Optical Density
CTZ	Coelenterazine	ON	Over Night
CV	Column Volume	PAGE	Polyacrylamide Gel Electrophoresis
DHA	Dehydroascorbate	PBS	Phosphate Buffered Saline
DHAR	Dehydroascorbate Reductase	PCR	Polymerase Chain Reaction
DIDS	Diisothiocyanostilbene	POX	Peroxidase
DMSO	Dimethylsulphoxide	psmGFP	soluble modified GFP
DNA	Deoxyribonucleic Acid	ptGFP	<i>Ptilosarcus gurneyi</i> GFP
DNase	Deoxyribonuclease	PVDF	Polyvinylidene Fluoride
dNTP's	Deoxynucleotidetriphosphates	R-DIOA	R-(+)-Butylindazone, (Dihydroindenyl)Oxyalkanoic Acid
dsRED	<i>Discosoma</i> sp. Red Fluorescent Protein	RNA	Ribonucleic Acid
DTT	Dithiothreitol	RNase	Ribonuclease
DW	Dry Weight	roGFP	Redox-sensing GFP
EDTA	Ethylene Diamine Tetraacetic Acid	ROS	Reactive Oxygen Species
EGTA	Ethylene Glycol Tetraacetic Acid	RT	Room Temperature
KPP	Kaliumphosphat Puffer (potassium phosphate buffer)	SDS	Sodium Dodecyl Sulphate
FAD	Flavin Adenine Dinucleotide	SM	Standard Medium
FP	Fluorescent Protein	SOS	Salt Overly Sensitive
FPLC	Fast Protein Liquid Chromatography	SOSA	Superoxide Scavenging Activity
FRET	Förster Resonance Energy Transfer	StDv	Standard Deviation
FURO	Furosemide	Strep	Streptavidin
FW	Fresh Weight	TAC	Total Antioxidative Capacity
GFP	Green Fluorescent Protein	T-DNA	Transfer DNA
GPX	Glutathione Peroxidase	TGN	Trans Golgi Network
GR	Glutathione Reductase	TORA	Toramide
GSH	Glutathione (reduced state)	TRIS	Tris(hydroxymethyl)aminomethane
GSSG	Glutathione (oxidised state)	TriCa	TRIS+Calcium
HEPES	4-(2-hydroxyethyl)-1-piperazineethanesulfonic acid	TriCaT	TRIS+Calcium+Triton-X-100
HRP	Horseradish Peroxidase	UV	Ultraviolet
IAA-94	Indanyloxyacetic Acid 94	XOD	Xanthine Oxidase
IC	Ion-exchange Chromatography	YFP	Yellow Fluorescent Protein
IP3	Inositol Trisphosphate		
IPTG	Isopropyl $\beta$ -D-1-thiogalactopyranoside		

# 1 INTRODUCTION

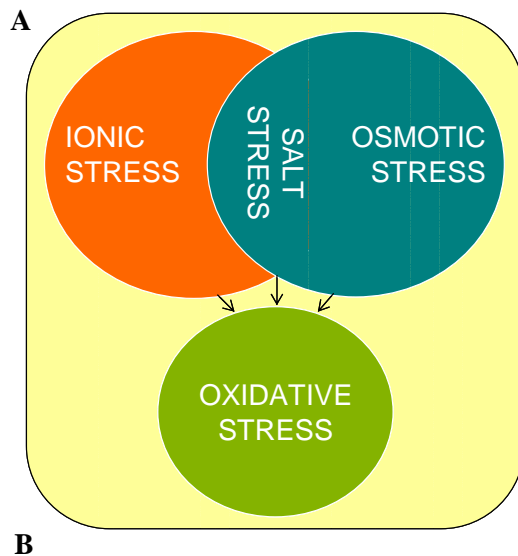
## 1.1 General aspects of salinity stress and tolerance mechanisms

Salinisation of arable land is a major limiting factor of crop production worldwide. Ill-conceived soil and water management practices lead to a worsening of the situation. In order to cope with this problem, the understanding of cellular processes in plants exposed to high salt concentrations is inevitable. Until now salt stress research has mainly focussed on Na<sup>+</sup>-transport and its cellular regulation. The genetic manipulation of the involved transport mechanisms led already to improvements of salt tolerance in model organisms and certain crop species. The transport of the concomitant anion - chloride - and the regulatory mechanisms did not receive appropriate attention. Characterisation of transporters involved in chloride uptake on molecular and cellular level would help to understand the role of chloride in salt stress tolerance mechanisms.

The factors determining salt tolerance in plants are very diverse. Excessive formation of reactive oxygen species (ROS) for example, is often considered the first process leading to cellular damage when stress situations arise. ROS are in plants balanced by a complex antioxidative system. The general assumption, as revealed by previous work, is that the capability to increase antioxidative activity during stress may represent a form of stress tolerance. Thus, plants having a higher capability to neutralize ROS also have a higher salt tolerance.

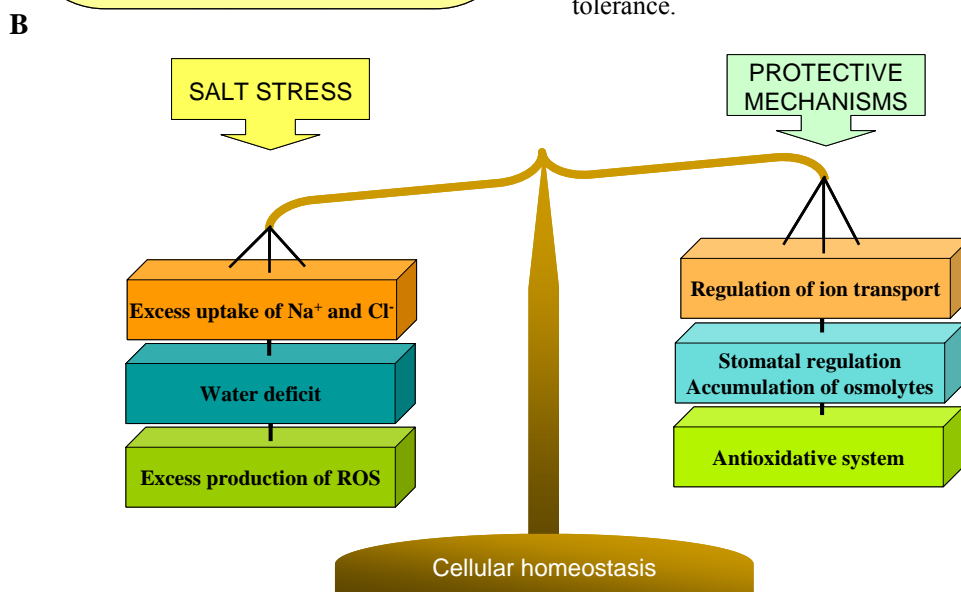
Salt stress mechanisms are complicated and comprise many different aspects of interwoven cellular activities (**Figure 1A**). For a good understanding of salt stress and tolerance, it is therefore necessary to keep many factors in mind (**Figure 1B**). Salinity causes:

- Osmotic stress and apparent drought symptoms (Chinnusamy *et al.*, 2006; Wang *et al.*, 2003; Zhu, 2001)
- Ion toxicity (Chinnusamy *et al.*, 2006; Serrano & Rodriguez-Navarro, 2001; Shabala, 2000; Zhu, 2001)
- Decreased uptake of nutritive cations, such as potassium and calcium (Asch *et al.*, 2000; Glenn *et al.*, 1999; Maathuis & Amtmann, 1999; Niu *et al.*, 1995; Shabala, 2000)
- Reduced uptake of anions such as nitrate and phosphate (Song *et al.*, 2009; Aslam *et al.*, 1984; Cerezo *et al.*, 1999; García-Sánchez *et al.*, 2003; Glass & Siddiqi, 1985; Kafkafi *et al.*, 1982)
- Excessive production of ROS (Hernández *et al.*, 1993; Rodríguez *et al.*, 2007)
- Adjustment of antioxidative system (Gossett *et al.*, 1994; Gomez *et al.*, 2004; Sreenivasulu *et al.*, 2000)



**Figure 1: Interwoven character of salinity induced mechanisms**

**A:** The plant is exposed to two aspects of high salinity: ionic and osmotic stress. Oxidative burst, characterised by excess production of reactive oxygen species (ROS), is known to be elicited by both stress kinds. **B:** This scheme depicts possible implications of high salinity on the plant cellular homeostasis. Due to uptake of toxic concentrations of  $\text{Na}^+$  and  $\text{Cl}^-$ , ionic imbalance is caused, leading to exclusion of other nutrients. The osmotic stress caused by over-accumulation of ions leads to water deficit and in its consequence to drought symptoms. Excessive ROS production leads to redox imbalance. Protective cellular mechanisms are counterbalancing these negative effects, thus contributing to salt tolerance.



### 1.1.1 Ion fluctuations during salt stress

Ion homeostasis of plants is dependent on transmembrane transport proteins that mediate ion fluxes, including  $\text{H}^+$  translocating ATPases and pyrophosphatases,  $\text{Ca}^{2+}$ -ATPases, secondary active transporters, antiporters and channels (Sze *et al.*, 1999).

For the membrane integrity and the maintenance of transport processes it is important, that the plasma membrane voltage remains negative in the cytoplasm with respect to outside (Teakle & Tyerman 2009). For maintaining the charge balance in the cell, it is crucial, that uptake of chloride is counterbalanced either by the uptake of a cation or by loss of another anion. It is well known that the presence of nitrate in soils can ameliorate the toxic effect of excess  $\text{Cl}^-$  (Bar *et al.*, 1997), seemingly due to the competitive effect of  $\text{NO}_3^-$  on  $\text{Cl}^-$  influx (Glass & Siddiqi, 1985; Kafkafi *et al.*, 1982; Song *et al.*, 2009; Abdolzadeh *et al.*, 2008; Adler & Wilcox, 1995). The opposite effect has also been described previously (Jabeen & Ahmad, 2009; Dias & Costa, 1983). In salt stress situations,  $\text{Na}^+$  is in the majority of cases in surplus. If  $\text{NO}_3^-$  is transported out and  $\text{Na}^+$

and  $\text{Cl}^-$  into the cell, then only from the charge balance view, it would become necessary to have a counter-cation to  $\text{Na}^+$ , moving out of the cell. This role is taken by  $\text{K}^+$ -leakage out of the cell possibly mediated through potassium outward rectifying channels (KORCs, Maathuis & Amtmann, 1999; Shabala, 2000; Tyerman & Skerrett, 1998; Chen *et al.*, 2007; Shabala *et al.*, 2006).

$\text{Na}^+$  is able to compete with  $\text{K}^+$  for binding sites of cytosolic enzymes. High  $\text{Na}^+$  concentrations in the cytosol consequently can disrupt certain enzymatic activities (Bhandal *et al.*, 1988; Tester & Davenport, 2003; Serrano & Kwang, 1996). Therefore it has been presumed, that maintaining a low cytosolic  $\text{Na}^+:\text{K}^+$  ratio is crucial for plants exposed to high salinity (Glenn *et al.*, 1999; Apse & Blumwald 2002). In *Arabidopsis thaliana*, the plasma membrane  $\text{Na}^+/\text{H}^+$  antiporter (SOS1 - Salt Overly Sensitive) is responsible for  $\text{Na}^+$  extrusion from cells (Shi *et al.*, 2000; Shi *et al.*, 2002). The activity of the antiporter was shown to be increased in salt stressed halophytes and glycophytes (Blumwald & Poole, 1987; Garbarino & DuPont, 1988; Staal *et al.*, 1991; Apse *et al.*, 1999). Another possibility to cope with high cytosolic  $[\text{Na}^+]$  is its compartmentation in the vacuole. ATPases (V-type) and pyrophosphatases are responsible for  $\text{H}^+$ -translocation into the vacuole and generation of  $\text{H}^+$  motive force across the tonoplast (Golldack & Dietz, 2001; Lüttge *et al.*, 1997; Zhen *et al.*, 1997). Salt treatment induces ATPase activity and  $\text{H}^+$  transport by V-type pumps (Dietz *et al.*, 2001; Ratajczak *et al.*, 1994; Binzel, 1995; Kabala & Klobus, 2008; Vera-Estrella *et al.*, 1999). In consequence of overexpression of transporters like the vacuolar  $\text{H}^+$ -PPase AVP1 (Gao *et al.*, 2006; Gaxiola *et al.*, 2001), the vacuolar  $\text{Na}^+/\text{H}^+$  antiporter *AtNHX1* (Apse *et al.*, 1999; Brini *et al.*, 2007; Zhang *et al.*, 2001) and other genes of the SOS pathway (Shi *et al.*, 2003; Yang *et al.*, 2009), salt tolerance was drastically increased.

A hypersaline environment results in a disruption of the ionic steady state not only for  $\text{Na}^+$  and  $\text{Cl}^-$  and  $\text{K}^+$ , but also for  $\text{Ca}^{2+}$  (Niu *et al.*, 1995; Shabala *et al.*, 2005).  $\text{NaCl}$  treatment causes cytosolic increase of  $\text{Ca}^{2+}$  (Gao *et al.*, 2004), which is hypothesized to work as a secondary messenger and to trigger stress responses (e.g. SOS1 transporter; Liu & Zhu, 1997; Pardo *et al.*, 1998). Calcium in addition is known to meliorate the growth of plants on saline soils (Shabala *et al.*, 2006; Hibbard, 1922; Marschner, 1995; Husain *et al.*, 2004).

### 1.1.2 Oxidative stress and the antioxidative system

Oxygen is used as the terminal electron acceptor in oxidative phosphorylation. However, when enzymatic redox chains become overreduced (transfer of unpaired single electrons), oxygen radicals are formed. Reactive oxygen species (ROS; hydrogen peroxide  $\text{H}_2\text{O}_2$ , singlet oxygen  $\text{O}^*$ , superoxide  $\text{O}_2^{\cdot-}$ , or hydroxyl radical  $\text{OH}^*$ ) play different roles *in vivo*. They are involved in energy production, regulation of cell growth and intracellular signalling specifically triggering antioxidative responses. Especially the latter feature gained more importance in the last years (Van Breusegem & Dat, 2006; Rhoads *et al.*, 2006; Gadjev *et al.*, 2006; Hancock *et al.*, 2006;

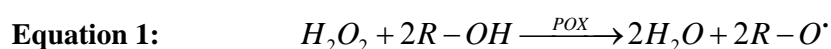


Desikan *et al.*, 2004; Mittler *et al.* 2004; Neill *et al.*, 2002a; Neill *et al.*, 2002b; Vranova *et al.*, 2002). The role of ROS as signals for gene expression and modulators of activities of key signalling molecules, such as MAP-kinases, Lsd1; WRKY75 and NIM/NPR1 has been elucidated (Gechev *et al.*, 2005; Rentel *et al.*, 2004; Desikan *et al.*, 2001; Vanderauwera *et al.*, 2005). However, all these examples are dealing with the regulatory mechanisms of programmed cell death due to environmental stress. Since ROS are unavoidable products of oxygen metabolism, enzymatic and non-enzymatic antioxidants are involved in order to balance the cellular redox homeostasis (Asada, 2006; Halliwell, 2006; Shigeoka *et al.*, 2002; Van Breusegem & Dat, 2006). The electron transport chains of chloroplasts and mitochondria produce significant amounts of superoxide radicals and, subsequently also H<sub>2</sub>O<sub>2</sub>. In peroxisomes, two sites have been identified for superoxide generation: xanthine oxidase and a membrane-bound oxidoreductase system (del Rio *et al.*, 1996; López-Huertas *et al.*, 1997; Bolwell & Wojtaszek, 1997). Moreover, peroxisomes contain H<sub>2</sub>O<sub>2</sub>-generating flavin oxidases, such as glycolate oxidase. Free iron and iron-chelates produce by interaction with H<sub>2</sub>O<sub>2</sub> and O<sub>2</sub><sup>•-</sup> (Fenton reaction and Haber-Weiß-reaction; Elstner, 1990) other reactive oxygen species - the hydroxyl radical.

During disadvantageous external conditions, especially in plants, ROS are produced in excess. Many studies show how and where their formation occurs (Hernández *et al.*, 1993; Rodríguez *et al.*, 2007; Van Breusegem *et al.*, 2008). Their excessive generation can be either due to malfunction of cellular metabolism or due to active generation of ROS by enzymes like NADPH-oxidases, amine oxidases or class III peroxidases (Almagro *et al.*, 2009; Sagi & Fluhr, 2006; Murphy *et al.*, 1998; Foreman *et al.*, 2003). ROS are damaging, since they attack lipids in cell membranes, proteins, carbohydrates, and DNA (Wiseman & Halliwell 1996). Oxidative stress is the term referred to, when an imbalance between production of ROS and the antioxidative system occurs in favour of the first (Wojtaszek, 1997; Sies, 1991). Consequently, this affects the redox environment on cellular level (Gutscher *et al.*, 2008; Meyer *et al.*, 2007; Rosenwasser *et al.*, 2010; Schwarzländer *et al.*, 2008).

Besides the main low-molecular-weight antioxidants (ascorbate, glutathione, tocopherol), and other metabolites, the antioxidative system of plants consists of specific ROS-scavenging enzymes.

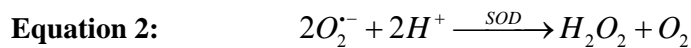
Different classes of heme and non-heme peroxidases (e.g. catalase, ascorbate peroxidase, glutathione peroxidase, peroxiredoxins) catalyse a transfer of two electrons to H<sub>2</sub>O<sub>2</sub>, many of them using redox-active molecules such as ascorbate and glutathione as electron and/or proton donors (**Equation 1**).



Their sub-cellular distribution varies greatly. In contrast to many other peroxidases, catalases are apparently absent in the chloroplast, whereas class III peroxidases reside only in the cell wall.

However, as already mentioned above, the latter are able to generate ROS such as superoxide and hydroxyl radical as a defence strategy against pathogen attack or wounding (Almagro *et al.*, 2009; Cosio & Dunand, 2009).

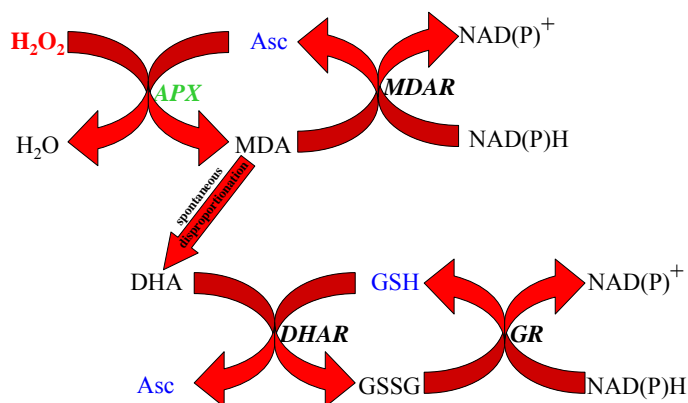
The superoxide anion ( $O_2^{\cdot-}$ ) is an oxygen species that is formed by single electron transfer from over-reduced redox enzymes to molecular oxygen.  $O_2^{\cdot-}$  has a short lifetime in living cells (Elstner, 1990) and is quickly disproportionated to  $H_2O_2$  and molecular oxygen.



Although a short living molecule, superoxide reacts very quickly with sensitive and critical cellular targets. Therefore, plants possess different defence mechanisms to keep  $O_2^{\cdot-}$  in check. On one hand, there are different superoxide dismutases (SODs) scavenging superoxide anions enzymatically (**Equation 2**; Abarca *et al.*, 2001; Alscher *et al.*, 2002; Morgan *et al.*, 2008; Bowler *et al.*, 1992; Scandalios, 1993). Three different families of SODs are known, depending on the metal cofactor at the active site of the enzyme – the Cu-ZnSODs, the FeSODs and the MnSODs. FeSOD isoenzymes can be found mostly in chloroplasts. Moran *et al.* (2003) have described a cytosolic FeSOD in cowpea root nodules. CuZnSODs are also located in the chloroplasts and cytosol, but can be found also in the apoplast. In contrast, the MnSOD isoenzymes reside in the mitochondria and peroxisomes (Bowler *et al.*, 1989; Alscher *et al.*, 2002). Many other non-enzymatic high-molecular-weight  $O_2^{\cdot-}$ -scavengers, on the other hand, are also found in plants (Kuda *et al.*, 2006) and may protect cellular components from radical attack.

The groups of antioxidative enzymes mentioned above are responsible for the direct scavenging of ROS. However, many enzymes are working indirectly by regenerating low-molecular-weight antioxidants. For example glutathione reductase, dehydroascorbate reductase and monodehydroascorbate reductase catalyse the reduction of glutathione and ascorbate pools through the ascorbate-glutathione cycle (**Figure 2**). Therefore, although having no direct scavenging function, they are a very important part of the antioxidative system in plants.

Ascorbate (ASC) alone or in cooperation with ascorbate peroxidase (APX) is known to be a potent ROS scavenger during stress exposure (Noctor & Foyer, 1998). It is oxidised to monodehydroascorbate (MDHA) and dehydroascorbate (DHA), which can be re-reduced to ASC by the ascorbate-glutathione pathway. The other most abundant low-molecular-weight antioxidant is glutathione. Under normal conditions the glutathione pool is nearly completely reduced (GSH), whereas due to excess production of ROS during stress, the glutathione is transiently oxidised (GSSG) in the ASC-GSH cycle (Foyer & Noctor, 2005).



**Figure 2: Ascorbate-glutathione cycle**

Hydrogen peroxide ( $\text{H}_2\text{O}_2$ ) is scavenged via the oxidation of ascorbate (Asc) by ascorbate peroxidase (APX) to monodehydroascorbate (MDHA), which can be converted back to Asc via monodehydroascorbate reductase (MDHAR) and dehydroascorbate reductase (DHAR). DHAR uses glutathione (GSH) as a reducing equivalent. The oxidised form of glutathione (GSSG) is then regenerated by glutathione reductase. Figure from Mittler (2002).

The pyridine nucleotide pair NADPH, NADH and their oxidized forms  $\text{NADP}^+$  and  $\text{NAD}^+$  are important redox-active components in the cell. NADH transfers electrons between the Krebs cycle and the mitochondrial electron transport chain and is used by the enzymes that catalyze substrate oxidation. NADPH plays a role in the chloroplast, being the last molecule produced from  $\text{NADH}^+$  by the light-driven electron chain and subsequently used in the Calvin cycle. Moreover,  $\text{NAD(P)H}$  is used by different enzymes to regenerate (reduce) other antioxidants within the ASC-GSH cycle (Berczi & Moller, 1998; Potters *et al.*, 2002; Hashida *et al.*, 2009). Their part in the antioxidative system of plants consequently lies in being a cofactor in antioxidant- regeneration mechanisms, rather than being redox buffers themselves (Noctor, 2006).

Although some effects of unfavourable environmental conditions on specific components of the antioxidative system are characterized, little is known about changes in the overall antioxidative capacity. This latter quantity is defined as the amount of ROS that can be scavenged by an antioxidative system. In contrast, antioxidative activity is the rate at which ROS are scavenged. It is expressed in terms of rate constants or as equivalent turnover rate of an antioxidative enzyme.

The capability to increase the total antioxidative capacity by de-novo synthesis of larger amounts of particular scavengers during stress may represent one form of stress tolerance. Another possibility may be an interactive cooperation between the different antioxidant species (Bartosz & Bartosz, 1999), producing a systemic antioxidative capacity greater than the sum of its components. A third hypothesis originating from results obtained during the study presented here is discussed in detail within the **Chapter 4**.

## 1.2 Uptake and transport of chloride under salt stress in relation to salt tolerance

The general difference between salt tolerant plant species (halophytes) and the salt sensitive ones (non-halophytes or glycophytes) can be defined by their success to germinate and propagate under saline conditions. Halophytes usually can withstand up to 3.5 M NaCl in the soil

(Flowers & Colmer, 2008; Flowers *et al.*, 1977), whereas glycophytes show impaired growth and stress-evoked damage in presence of much lower salt concentrations (>10 mM; Dajic, 2006; Greenway & Munns, 1980). Between plants of both groups variable levels in salt tolerance and/or sensitivity are found. Even the strategies to cope with salinity stress differ from genus to genus. They comprise mechanisms as different as phenological avoidance (plants, which complete their life cycle in the most favourable period of the year), salt secretion, salt exclusion, and salt accumulation and compartmentalisation (Dajic, 2006; Flowers *et al.*, 1977; Niu *et al.*, 1995).

The impact of chloride on salt stress symptoms and its contribution to the salt tolerance mechanisms in plants have been less investigated in the past. The majority of publications in this field focused mostly on the role of cations like  $\text{Na}^+$  and  $\text{K}^+$  (Flowers & Colmer, 2008; Shabala & Cuin, 2008; Shabala *et al.*, 2006). Since White & Broadley (2001) only recently the role of chloride under salt stress was reviewed by Teakle & Tyerman (2009). Chloride has long been considered as an inert anion being tolerated in a wide concentration range and as counter-ion to  $\text{K}^+$  responsible for cell turgor regulation and membrane depolarisation (Clarkson & Hanson, 1980; Barbier-Brygoo *et al.*, 2000). Nevertheless, many plant species (citrus trees, grapes, ...) are highly sensitive to high  $[\text{Cl}^-]$  (Shannon, 1997; Grattan & Grieve, 1998; Greenway & Munns, 1980), and even the term 'chloride toxicity' was established (White & Broadley, 2001), although the effects of chloride toxicity show a broad variability within species (Garthwaite *et al.*, 2005). Only in legumes and woody species like citrus and olive salt tolerance mechanisms were linked to chloride transport, compartmentalisation, and/or exclusion. Tissue concentrations of chloride in shoots and roots are negatively correlated to salt tolerance in some species, whereas in others the opposite is the case (more details in the review Teakle & Tyerman, 2009). Therefore, it is not necessarily true, that a reduced net  $\text{Cl}^-$  uptake, reduced xylem loading or efficient compartmentalisation of chloride characterize a salt tolerant plant. It can be characterized by its ability to keep the toxic effects of high chloride concentrations within such limits, that it is still able to complete its life cycle.

### 1.2 1 Uptake of chloride by the plants

Uptake of ions from the external environment through the cell walls of root cells is a passive process driven by diffusion or mass flow (Marschner, 1995). The primary cell wall consists of cross-linked cellulose, hemicellulose and glycoproteins which build pores with a maximum diameter of 5 nm (Carpita *et al.*, 1979). Since hydrated ions are only up to 20 % of the pore size, here no restriction for the movement of ions should occur.

In general, there are two pathways how the ions may be transported into the xylem: the symplastic and the apoplastic routes (Pitman, 1982; Clarkson, 1993). Since the Casparian strip in the walls of the endodermis blocks the apoplastic pathway for salts due to its hydrophobicity (Caspary, 1865/66; Marschner, 1995), ions can reach the transport system from the root to the shoot only by

passing plasma membranes (Köhler & Raschke, 2000). The symplastic pathway consequently involves at least two passages of ions through a membrane catalyzed by transport proteins (White & Broadley 2001). Plants exposed to sudden raised levels of  $[Cl^-]_{ext}$ , retain a large fraction of it in the root cells, mostly in the vacuole (Böszörményi & Cseh, 1961; Pitman, 1977; Storey & Walker, 1987), from where it is then translocated to the xylem. A constant level of chloride in the root is reached relatively fast; the translocation rate to xylem in contrast takes some hours to achieve a steady state (White & Broadley 2001). While the influx through plasma membrane continues with increasing  $[Cl^-]_{ext}$ , the flux of chloride from cytoplasm into the vacuole of root cells saturates at defined concentrations. Thus, it seems that the uptake of chloride into roots in general saturates too. The situation is different for the shoot.  $[Cl^-]_{shoot}$  increases proportionally with  $[Cl^-]_{ext}$  (Jeschke *et al.*, 1986; Jeschke & Wolf, 1988; Storey, 1995). Here, not only the uptake of chloride into the root plays a role. Other factors like the transpiration rate and the shoot growth rate impair the  $[Cl^-]_{shoot}$  (Greenway, 1965; Pitman, 1982; Storey, 1995; Moya *et al.*, 1999).

### 1.2.2 Uptake of chloride into the cell during salt stress

The principal driving forces for  $Cl^-$  movement at cellular level is the charge difference and the concentration gradient across the membrane, i.e. its electrochemical gradient. When the anion moves in the direction of its electrochemical gradient and through channels or carriers, then the transport is passive. A prerequisite for the passive influx of chloride is that the membrane potential is more positive than the equilibrium potential of chloride (**Equation 3**). This situation occurs, either when the external concentration of chloride is high compared to  $[Cl^-]_{cyt}$ , or when the plasma membrane is depolarised. The latter can be the result of high salinity due to excess  $Na^+$  crossing the cell membrane (Shabala *et al.*, 2003; Schachtman *et al.*, 1991; Blumwald *et al.*, 2000; Maathuis & Amtmann, 1999).

$$\text{Equation 3: } E_{eq,Cl^-} = \frac{RT}{zF} \ln \frac{[Cl^-]_o}{[Cl^-]_i}$$

$E_{eq,Cl^-}$  is the equilibrium potential for chloride, measured in volts

R is the universal gas constant, equal to  $8.314 \text{ joules} \cdot \text{K}^{-1} \cdot \text{mol}^{-1}$

T is the absolute temperature, measured in Kelvin

z is the number of elementary charges of the ion in question involved in the reaction

F is the Faraday constant, equal to  $96.485 \text{ J} \cdot \text{V}^{-1} \cdot \text{mol}^{-1}$

$[Cl^-]_o$  is the extracellular concentration of chloride

$[Cl^-]_i$  is the intracellular concentration of chloride

Electrophysiological studies of isolated wheat protoplasts at high salinity revealed an outward rectifying anion channel permeable to chloride (Skerrett & Tyerman, 1994). The apparent outward rectification of the channel was observed only when membrane was depolarised. By mediating anion influx, the membrane potential was restored. This passive entry of chloride at the onset of

salt stress would in consequence prevent further passive influx by holding the membrane potential at the equilibrium values for chloride.

Lorenzen *et al.* (2004) have shown a rapid increase in cytoplasmic chloride concentration using an anion sensitive fluorescent probe (Clomeleon) expressed in *Arabidopsis thaliana* root cells. Based on their findings the internal  $[Cl^-]_{\text{cyt}}$  saturates at about 75 mM after several hours when the outer  $[Cl^-]_{\text{out}}$  is adjusted to 100 mM. So, if there is a channel driven transport then this is the cellular concentration  $[Cl^-]_{\text{cyt}}$  at which the electro-motive force (emf, **Equation 4**) is zero:

$$\text{Equation 4: } emf = 0 = V_m + 59 \text{ mV} \cdot \log\left(\frac{100 \text{ mM}}{75 \text{ mM}}\right) = V_m + 7.4 \text{ mV}$$

In other words, a channel driven chloride entry into *Arabidopsis* root cells is possible only when the salt stress depolarisation is more positive than -7.4 mV.

Since there is evidence that depolarisation does not yield values more positive than -50 mV (Shabala *et al.*, 2003), a maximum of 14 mM chloride accumulation in the cell would be possible. Furthermore, Britto *et al.* (2004) have shown that the equilibrium potential for chloride in barley root cells exposed to 100 mM NaCl raises to nearly +40 mV. It is not conceivable, that in a living cell more positive membrane potential would occur in order to allow passive chloride influx. Therefore, active chloride transport is most likely to occur when the depolarisation phase is over and an equilibrium potential for chloride is established.

The active transport requires either chemical coupling to ATP hydrolysis or coupling of the transport to a second ion. Since calcium and at a lower extent also magnesium are able to inhibit the chloride influx, indications are given that the transport system for chloride is presumably coupled to a concomitant cation (Lorenzen *et al.*, 2004).

### 1.3 Chloride channel (ClC) proteins

#### 1.3.1 Chloride channel proteins – the intracellular and tissue localisation

It has been assumed, that in plants ClC proteins are involved in the transport of chloride (Hechenberger *et al.*, 1996, Lurin *et al.*, 1996). However, they are also able to mediate fluxes of other anions too ( $\text{NO}_3^-$ ,  $\text{I}^-$ ,  $\text{Br}^-$ ; De Angeli *et al.*, 2006; Geelen *et al.*, 2000). Since the discovery (Miller, 1982) and the cloning of the first member of this family from the torpedo ray electric organ (ClC-0, Jentsch *et al.*, 1990), many homologues have been identified in many organisms (**Figure 3**, Gurnett *et al.*, 1995; Klock *et al.*, 1994, Jentsch *et al.*, 1999, Maduke *et al.*, 2000, Fahlke *et al.*, 2001). In *Arabidopsis thaliana*, seven homologous genes were found (*AtClC-a* to *-g*; **Table 1**, **Figure 3**, Hechenberger *et al.*, 1996). The lack of an expression system suitable for electrophysiological studies of plant chloride channels still complicates a detailed understanding of

their transport characteristics. Until now, quantitative trait loci analyses (Harada *et al.*, 2004; Loudet *et al.*, 2003), mutational analyses (Harada *et al.*, 2004; Jossier *et al.*, 2010), and co-localisation studies (Marmagne *et al.*, 2007; Teardo *et al.*, 2005; Moradi, 2009) provided insight into their functions and their intracellular and tissue localisation. Despite the strongly conserved structural assembly of known animal ClCs, there are functional dissimilarities (Dutzler *et al.*, 2006; 2007). Some work as gated chloride channels, while others have antiporter properties. We can find the same situation also in *Arabidopsis*, where some members of this family are indeed functional chloride channels.

#### *AtClC-A*

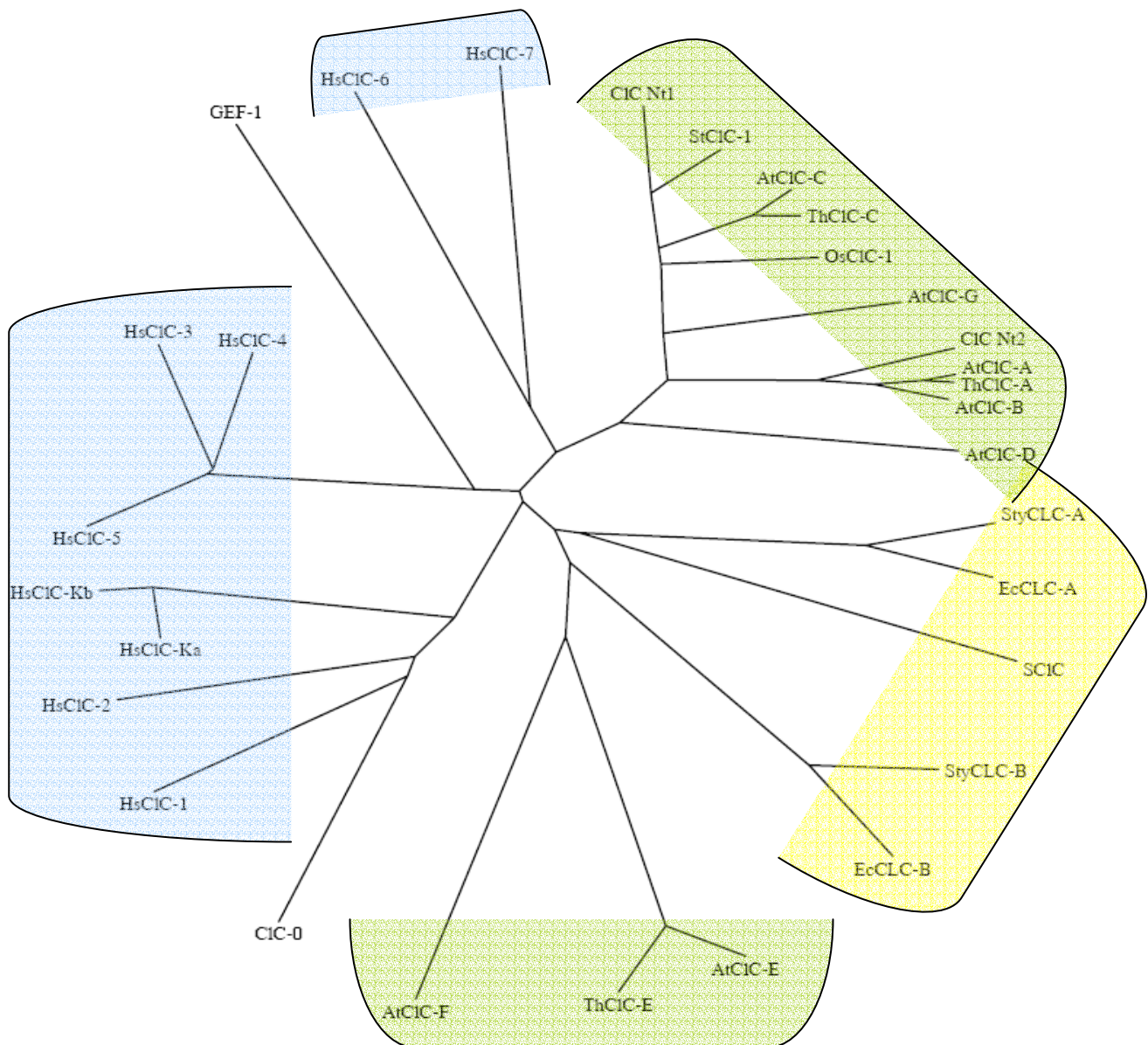
However, recent studies have shown that nitrate transport mediated by AtClC-A (DeAngeli *et al.*, 2006) and AtClC-B (Von der Fecht-Bartenbach *et al.*, 2010) across the tonoplast, is coupled to a proton counter flux. This does not correlate with the definition of a channel per se. Thus, AtClC-A was characterised as a  $1 \text{ H}^+ / 2 \text{ NO}_3^-$  antiporter (DeAngeli *et al.*, 2006), mediating slight outward rectifying currents, responsible for the nitrate influx into the vacuole. Microarray analyses of ClCs have shown the strongest day-time variation corresponding with the diurnal nitrate changes, with the transcript occurrence of AtClC-A and AtClC-B.

#### *AtClC-B*

The function of AtClC-B is not clear yet. One very recent electrophysiological study in *Xenopus laevis* oocytes suggests its possible role in the anion release out of the vacuole (Von der Fecht-Bartenbach *et al.*, 2010). Anyway, the missing inward currents could be simply explained by low cytoplasmic concentration of nitrate in oocytes. Therefore, it cannot be ruled out that AtClC-B is primarily responsible for the influx and accumulation of nitrate in the vacuoles of *Arabidopsis*.

#### *AtClC-C*

The next member of this family, AtClC-C, is localised in the tonoplast, too. Mutational analysis revealed its role in  $\text{NO}_3^-$  accumulation (Harada *et al.*, 2004). The homozygous *cclc-1* transposon insertion mutants grown on various external nitrate concentrations had significantly lower nitrate content. However, unlike the AtClC-A mutant, the *cclc-1* plants showed altered contents of chloride, malate, and citrate (Harada *et al.*, 2004), which may indicate a broader anion selectivity of AtClC-C. A very recent study (Jossier *et al.*, 2010) shows new physiological functions of this protein, which are directly connected with the transport of chloride through the tonoplast.



**Figure 3: Chloride channel proteins**

The dendrogram indicates the degree of similarity between CLC proteins from human (highlighted blue), animals (ClC-0), yeast (GEF-1), bacteria (highlighted yellow), and plants (highlighted green): CLC-0 (P35522) from *Torpedo marmorata*; HsCLC-1 (P35523), HsCLC-2 (P51788), HsCLC-3 (P51790), HsCLC-4 (P51793), HsCLC-5 (P51795), HsCLC-6 (P51797), HsCLC-7 (P51798), HsCLC-Ka (P51800), and HsCLC-Kb (P51801), all from *Homo sapiens*; StyCLC-A (Q8ZRP8) and StyCLC-B (Q8ZRP5) from *Salmonella typhimurium*; GEF1 (P37020) from the yeast *Saccharomyces cerevisiae*; EcCLC-A (P37019) and EcCLC-B (P76175) from *Escherichia coli*; SCLC (P74477) from *Synechocystis sp.*; CLC-Nt1 (Q40485) and CLC-Nt2 (Q9XF71) from *Nicotiana tabacum*; AtCLC-A (P92941), AtCLC-B (P92942), AtCLC-C (Q96282), AtCLC-D (P92943), AtCLC-E (Q8GX93), AtCLC-F(Q8RXR2), and AtCLC-G (P60300) all from *Arabidopsis thaliana*; ThClC-A (D3YP02), ThClC-C (D3YP03), ThClC-E (D3YP04) all from *Thellungiella salsuginea*; StCLC-1 (P93567) from *Solanum tuberosum*; and OsCLC-1 (Q8LPA2) from *Oryza sativa*. All CLC proteins are identified by Swiss-Prot/TrEMBL references (updated version from 2010)



ClCc T-DNA insertion mutant plants were shown to be hypersensitive to NaCl and KCl and to have altered stomatal movement in response to ABA treatment and light. The authors consider AtClC-C to play a very important role in regulation of chloride homeostasis, stomatal movement and consequentially in the salt tolerance mechanisms.

#### *AtClC-D*

AtClC-D is localized in the *trans*-Golgi network (TGN), where in cooperation with H<sup>+</sup>-V-ATPase it is probably responsible for optimal acidification of the compartment by transporting counter anions like chloride or nitrate. It possibly also works as a proton-coupled chloride transporter. The anion content of *clcd-1* plants was not affected by the loss of AtClC-D; only the root growth was impaired. A weak promoter activity was observed in most organs, but was most prominent in the roots of germinating seedlings and in cotyledons of 5-day-old seedlings. In contrast, 28-day-old plants have shown a higher activity in the hydathodes and in flowers (Von der Fecht Bartenbach, 2007).

#### *AtClC-E and -F*

AtClC-E and AtClC-F share more similarity with prokaryotic chloride channels than the other *Arabidopsis* ClCs (**Figure 3**). Fusion proteins with GFP/DsRed2 have shown their localisation in thylakoids and *cis*-Golgi vesicles and to some extent to *trans*-Golgi cisternae, respectively (Marmagne *et al.*, 2007). The latter finding is in contrast with a report from Teardo *et al.* (2005), where a chloroplast localization of a putative ClC channel in spinach sharing sequence similarity with AtClC-F was shown.

The presence of only one glutamate residue in the external binding site (see **Section 1.3.2**) indicates a Cl<sup>-</sup> channel character of both proteins. In agreement with the subcellular localization, AtClC-E expression is higher in green tissues compared with roots. Furthermore, the phenotype of *clce* mutants is closely related to photosynthetic activity.

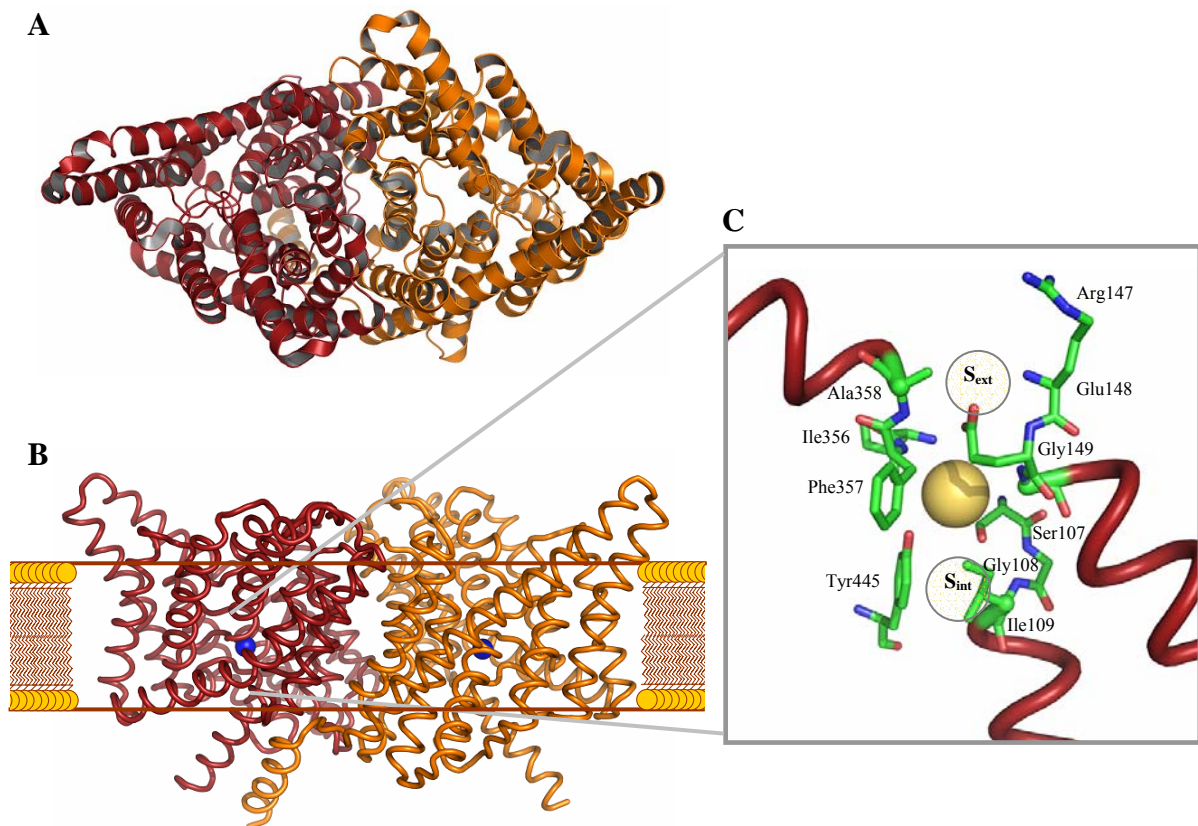
**Table 1: Characteristics of the *Arabidopsis thaliana* chloride channels.**

Summarized are the general properties of the proteins, their proposed intracellular localisation, the residues within their selectivity filters suggesting their substrate specificity.

Protein	TAIR annotation	Gene Bank accession	Gene Size (bp)	Protein size (AA)	Suggested selectivity	Intracellular localization	Amino acid residues constituting for:			Reference
							Selectivity filter	Ext.binding site for A <sup>-</sup>	Ext.binding site for H <sup>+</sup>	
<b>AtClC-A</b>	AT5G40890	NM_123454 gi:30693694	2328	775	H <sup>+</sup> /NO <sub>3</sub> <sup>-</sup>	Vacuole	GPGIP	E	E	De Angeli <i>et al.</i> , 2006
<b>AtClC-B</b>	AT3G27170	NM_113631 gi:30688669	2343	780	? H <sup>+</sup> /NO <sub>3</sub> <sup>-</sup>	Vacuole	GPGIP	E	E	Gaxiola <i>et al.</i> , 1998; Lv <i>et al.</i> , 2009
<b>AtClC-C</b>	AT5G49890	NM_124367 gi:30695773	2340	779	H <sup>+</sup> /Cl <sup>-</sup>	Vacuole	GSGIP	E	E	Lv <i>et al.</i> , 2009; Von der Fecht-Bartenbach <i>et al.</i> , 2010
<b>AtClC-D</b>	AT5G26240	NM_122525 gi:30690172	2379	792	? H <sup>+</sup> /Cl <sup>-</sup>	Trans- Golgi	GSGIP	E	E	von der Fecht-Bartenbach <i>et al.</i> , 2007
<b>AtClC-E</b>	AT4G35440	NM_119709 gi:18418748	2133	769	NO <sub>3</sub> <sup>-</sup>	Chloroplast	ESAGK	E	S	Marmagne <i>et al.</i> , 2007
<b>AtClC-F</b>	AT1G55620	NM_104438 gi:30695980	2346	781	Cl <sup>-</sup>	Cis-Golgi	EILDQ	E	T	Marmagne <i>et al.</i> , 2007
<b>AtClC-G</b>	AT5G33280	NM_122852 gi:30692599	2292	775	? Cl <sup>-</sup>	Vacuole	GSGIP	A	E	-

### 1.3.2 The structure dependent functionality of ClC proteins

The X-ray derived structure of two prokaryotic ClC Cl<sup>-</sup> channels from *Salmonella typhimurium* (StClC, **Figure 4**) and *Escherichia coli* (EcClC) and further mutational analyses provided an insight into the molecular basis of the anion selectivity of these channels (**Figure 4C**; Dutzler *et al.*, 2002; Dutzler *et al.*, 2003; Bergsdorf *et al.*, 2009; Dutzler, 2006; 2007). The proteins consist of a complex transmembrane transport domain and soluble regulatory domains, the cystathionine- $\beta$ -synthetase domains (CBS1 and CBS2). The crystal structure of the StClC reveals a homodimer, which is probably also the functional state of the protein (**Figure 4A, B**).



**Figure 4: Bacterial ClC structure**

**A:** Cartoon representation of the StClC dimer from the extracellular point of view. **B:** Positions of Cl<sup>-</sup> ions (blue spheres) within the ribbon representation of the StClC dimer from within the membrane. The brown lines show the approximate thickness of the lipid bilayer. **C:** The ClC pore, showing the position of the Cl<sup>-</sup> ion in the central binding site (yellow sphere), the other two manually added circles represent the proposed positions of the Cl<sup>-</sup> ion in the external and internal binding sites respectively. Figures reproduced from the PDB entry 1KPL (Dutzler *et al.*, 2002) by the PyMol Software.

Despite their similar characteristics as there were the basic structural architecture, selectivity for anions and a modulation of the gating by both chloride and protons (Dutzler, 2006; Jentsch, 2008; Miller, 2006; Zifarelli & Pusch, 2007; Pusch *et al.*, 2006; Chen, 2004), the distinct functionality of ClC channels and antiporters was hypothesised to be based in the energetics of their conformational changes (Lisal & Maduke, 2009).

Several amino acid residues recognized as essential for the coupling and gating mechanisms can be found in the crystal structure of EcClC (Dutzler *et al.*, 2002; Dutzler *et al.*, 2003) as well as in the amino acid sequences of several *Arabidopsis* ClC proteins. The central binding site (**Figure 4C**) is created by the <sup>564</sup>Tyr residue (numbering for AtClC-A) and the serine residue of the motif GSGIP/GPGIP. The internal and the external binding site (**Figure 4C**) are formed by main-chain amide nitrogen atoms of less conserved amino acid residues and by conserved motifs GK/REGP and GXFXP, respectively (Dutzler *et al.*, 2002; Dutzler *et al.*, 2003).

Together these three sites form the channel pore, which allows the passing of chloride along its electrochemical gradient. The permeability of the ClC proteins by the halogen ions Cl<sup>-</sup> and Br<sup>-</sup> was firstly demonstrated by Rychkov *et al.* (1998). This function can be impaired by bigger inorganic and organic anions (SCN<sup>-</sup> > ClO<sub>4</sub><sup>-</sup> > Cl<sup>-</sup> > Br<sup>-</sup> > NO<sub>3</sub><sup>-</sup> ~ ClO<sub>3</sub><sup>-</sup> > I<sup>-</sup> >> BrO<sub>3</sub><sup>-</sup> > HCO<sub>3</sub><sup>-</sup> >> methanesulfonate ~ cyclamate ~ glutamate).

There is a strong functional coupling between ion conduction and gating (Richard & Miller, 1990; Pusch *et al.*, 1995; Chen & Miller, 1996, Rychkov *et al.*, 1998). This means that Cl<sup>-</sup> is the current-carrying substrate passing through the pore, and it acts as an allosterical regulator of the channel's gates by binding in the pore. Once bound, the Cl<sup>-</sup> influences the open probability, giving rise to properties such as voltage-dependent gating in some ClC Cl<sup>-</sup> channels (Pusch *et al.*, 1995; Chen & Miller, 1996).

The substrate specificity of the ClC proteins depends on the conserved GSGIP residue. The AtClC-A protein contains a proline instead of the serine in the GSGIP motif. P to S mutation in ClC-A resulted in a Cl<sup>-</sup>/H<sup>+</sup> antiporting activity, while the wild type Cl<sup>-</sup>-coupling is insignificant (Bergsdorf *et al.*, 2009). The opposite was achieved by mutating S to P in the mammalian ClC-5 protein, resulting in a coupled NO<sub>3</sub><sup>-</sup> instead of Cl<sup>-</sup> transport (Zifarelli & Pusch, 2009). In the external binding site (**Figure 4C**) two glutamates at positions 203 and 270 (numbering in AtClC-A) are important for the functionality of the ClC proteins. Except AtClC-G (GK**A**PG) all other *Arabidopsis* ClCs carry glutamate (E) at this position (**Table 1**). The importance of this particular residue was recognized only by chance. Mutation of the glutamate to alanine in EcClC resulted in an additional halogen anion in the crystal structure (Dutzler *et al.*, 2003). The glutamate is proposed to mimic a chloride anion and by binding the external binding site (**Table 1**) leading to the closure of the channel. The mutation causes a blockade of the channel closure (Dutzler *et al.*, 2003; Dutzler, 2006; 2007; Jian *et al.*, 2004).

In transporters the mutation of the glutamate residue has a different effect. For example in AtClC-A it resulted in uncoupled anion conductances, indicating a role of <sup>203</sup>Glu in the coupling of the transport of protons to the anions (Bergsdorf *et al.*, 2009). This effect was observable in other ClC transporters, too (Accardi & Miller, 2004; Zdebik *et al.*, 2008). Complete disruption of the anion

currents was achieved by mutating the <sup>270</sup>Glu to an alanine in AtClC-A. However, the currents were restored by the uncoupling Glu<sup>203</sup>Ala mutation (Bergsdorf *et al.*, 2009). This indicates a hand-over mechanism in the coupling of the anion to the proton flux, in which the <sup>270</sup>Glu, located at the cytoplasmic site, binds protons and hands them over to the gating <sup>203</sup>Glu (Accardi *et al.*, 2005; Dutzler, 2007; Lim & Miller, 2009; Zdebik *et al.*, 2008).

### 1.4 Electroneutral cation-chloride-cotransporters (CCCs)

CCCs are secondary active transporters mediating the transport of Cl<sup>-</sup> coupled to K<sup>+</sup> and/or Na<sup>+</sup> across the plasma membrane (Haas, 1994). CCCs from animals are divided into four different groups, due to the symport mechanism and their sensitivity to various inhibitors (Colmenero-Flores *et al.*, 2007; Gamba, 2005). There are the benzothiadiazine (or thiazide)-sensitive Na<sup>+</sup>-Cl<sup>-</sup> cotransporters (NCCs); the sulfamoylbenzoic (or bumetanide)- sensitive Na<sup>+</sup>-K<sup>+</sup>-2Cl<sup>-</sup> (NKCCs) and Na<sup>+</sup>-Cl<sup>-</sup> cotransporters; and the dihydroindenylxy-alkanoic acid (DIOA)-sensitive K<sup>+</sup>-Cl<sup>-</sup> cotransporter (KCCs). However, NKCCs and KCCs can be inhibited by high concentrations of DIOA or loop diuretics, respectively (Gamba, 2005). The CCC family is in animals responsible for homeostasis of the most abundant electrolytes, K<sup>+</sup>, Na<sup>+</sup> and Cl<sup>-</sup>, and therefore important for cell ionic and osmotic regulation in secretory and absorptive epithelia (reviewed by Delpire & Mount, 2002; Gamba, 2005).

Harling *et al.* (1997) described the first putative CCC from tobacco (AXI4) with a high homology to the KCCs from animals. The intended role in the promotion of auxin-dependent cell division was disproved by Schell *et al.* (1999). However, the functional characterisation of CCCs in plants was at this time still pending.

Only few years ago, Colmenero-Flores *et al.* (2007) described a bumetanide-sensitive Na<sup>+</sup>-K<sup>+</sup>-2Cl<sup>-</sup>-cotransporter from *Arabidopsis* (AtCCC1) in *Xenopus* oocyte – system. It shares a 60% similarity (in terms of sequence homology) with KCCs and only a ~ 46 % similarity with sodium-dependent NCCs and NKCCs. However, Colmenero-Flores *et al.* (2007) showed that AtCCC1 is dependent on the coexistence of all three ions (Na<sup>+</sup>, K<sup>+</sup> and Cl<sup>-</sup>). Furthermore, due to its localised expression in the pericycle and other parenchyma cells bordering xylem vessels in cotyledon tips, plant vasculature, root tips and axillary buds, they hypothesised a role of AtCCC1 in long-distance Cl<sup>-</sup>-transport.

## CHAPTER 2

# COMPARATIVE STUDY OF *ARABIDOPSIS THALIANA* AND *THELLUNGIELLA SALSUGINEA* DURING LONG-TERM SALT STRESS

## 2.1 MATERIALS AND METHODS

### 2.1.1 Chemicals, consumables and equipment

All used chemicals, equipment and other consumables and their sources are listed in the **Suppl\_material 1-3**.

### 2.1.2 Solutions and buffers

#### 1xMS agar plates

4.4 g/l ready-to-use MS medium  
(containing macro and micro salts+vitamins)  
pH adjusted with KOH to 5.8  
1.2 % plant agar  
autoclaved

#### Calcium-free agar plates

macro salts were prepared individually according to the  
composition of ready-to-use MS medium without CaCl<sub>2</sub>  
1/1000 dilution of 1000 x MS vitamin stock  
1 g/l MS micro salts  
pH adjusted with KOH to 5.8  
1.2 % plant agar  
autoclaved

#### 1 x MS vitamin stock

10.31 g MS vitamins in 100 ml Milli-Q water

### 2.1.3 Plant treatment

Seeds of *Arabidopsis thaliana* Col-0 and its salt tolerant relative *Thellungiella salsuginea* known also as *Thellungiella halophila* ecotype Shandong were surface-sterilized by chlorine gas for 6 h (Bent, 2006), and sown on sterile vertical agar plates under laminar flow hood. The 1xMS agar plates were supplemented with different NaCl concentrations (0 mM, 50 mM, 75 mM, 100 mM, 125 mM, 150 mM, 175 mM, 200 mM NaCl). In parallel the seeds were sown on 1xMS plates lacking CaCl<sub>2</sub> prepared with the same quantities of sodium chloride as before. The plants were then grown in a climate chamber at 21°C with 16 h photoperiod (50 μE, white fluorescent lamps Osram L36 W/77). Germination rate and the primary root length were determined in adequate intervals as specified in the figure legends (**Figures 5, 6 and 7**). Four weeks after sowing, whole plants were harvested and washed thoroughly with distilled water to remove the remaining agar and contaminative salts. The excess water was removed with a paper towel and the material was shock frozen in liquid N<sub>2</sub>. The plant material was stored at -80°C, until needed for further experiments.

### 2.1.4 Anion content measured by ion chromatography (IC)

For determination of the total anion content (chloride, nitrate, sulphate, and phosphate) frozen plant material was ground in liquid nitrogen with mortar and pestle and mixed with 1 ml Milli-Q water (resistance  $18.2 \text{ M}\Omega \text{ cm}^{-1}$ ) per 250 mg fresh weight sample in 15 ml polypropylene tubes. The samples were vortexed thoroughly and placed in boiling water for 5 min. The tubes were vortexed every 60 sec in between. After 5 min the material was placed on ice for 30 min to cool down. A centrifugation step followed ( $4^\circ\text{C}$ , 3800 rpm/3000 g, 30 min) to separate the liquid from unwanted solid material. The prepared plant extracts can be stored at  $-80^\circ\text{C}$  until further processing.

For the separation of the aqueous phase 250  $\mu\text{l}$  chloroform were pipetted into a new 2 ml tube. The plant extract was diluted 1:10 with Milli-Q water, added to the chloroform to reach an end-volume of 1.5 ml and vortexed thoroughly. After centrifugation (11.000 rpm/9875 g, 10 min,  $4^\circ\text{C}$ ) the aqueous phase was recovered and the polar components were purified through a reversed-phase Strata C18-E column. The columns were equilibrated with methanol and used for purification accordingly to manufacturers' instructions. 200  $\mu\text{l}$  of the recovered sample were used for analysis by ion chromatography (ICS-2500; Dionex, Idstein, DE) using an IonPac AS11 Hydroxide-Selective Anion-Exchange Column (Dionex, Idstein, DE). The ions were eluted with 50 mM NaOH. Calculation and analysis of the chromatograms were done using the Chromeleon 6.6 software (Dionex, Idstein, DE).

### 2.1.5 Cation content measured by atomic absorption spectroscopy (AAS)

Total Ca, K, Mg, Na and Fe contents of the plant material used above were measured by means of AAS (AA S-series; Thermo Scientific Inc., Bonn, DE). Samples were prepared by dry ashing. First, the plant material was dried at  $65^\circ\text{C}$  for 48 h and powdered with a tissue homogenizer (Precellys, PeqLab, Erlangen, DE). 40 mg of dried, powdered samples were ashed in fireclay crucibles at  $550^\circ\text{C}$  in a muffle furnace for 5 hours. 2 ml 0.35 M  $\text{HNO}_3$  were added and incubated for 5 hours (mixing every  $\frac{1}{2}$  hour) before addition of 9 ml of Milli-Q water. The samples were then filtered through ashless filter paper (Whatman<sup>®</sup> #42). 5 ml sample dilutions were prepared as indicated in the **Table 2** by adding 250  $\mu\text{l}$  releasing agent (if any) and filled up to 5 ml with Milli-Q water.

**Table 2: The parameters for measuring total Ca, K, Mg, Na and Fe contents via atomic absorption spectroscopy**

Parameters	Elements				
	Na	K	Ca	Mg	Fe
Wavelength (nm)	598	589	422.8	285.2	248.5
Releasing agent	KCl	CsCl <sub>2</sub>	LaCl <sub>3</sub>	LaCl <sub>3</sub>	None
Dilution	1:50 (1:100)	1:50 (1:100)	1:20	1:20	No

### 2.1.6 Osmotic properties

The osmolarity was measured on a freezing point depression osmometer (O30; Gonotec, Berlin, DE). The osmolarity of water extracts obtained from the hot water extraction for IC and of water extracts made from dried (65°C for 48 h) and powdered plant material for AAS, was measured. The differences resulting from fresh:dry weight ratio were compared to get an internal control.

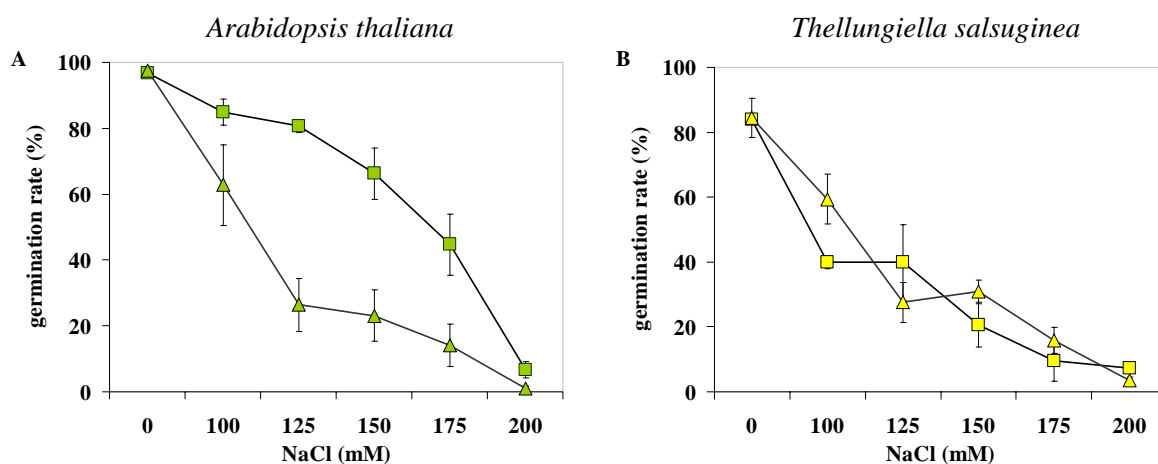
To obtain an approximate value of soluble organic osmotically active substances, the inorganic part comprising all major ions measured via IC and AAS was subtracted from the data obtained from osmometer measurements.

## 2.2 RESULTS

For salt stress treatments, *Arabidopsis thaliana* Col 0 and *Thellungiella salsuginea* seeds were sown on vertical agar plates containing 1xMS medium supplemented with different NaCl concentrations (as indicated in figure legends) and grown for 4 weeks. Since calcium is known to ameliorate the effects of salt stress in plants, it was omitted in parallel growth experiments.

### 2.2.1 Germination rate

In both plant species, the germination rate declines with increasing salt concentration. In *Arabidopsis thaliana* (Figure 5A) even 3 mM CaCl<sub>2</sub> have a positive effect on the germination under saline conditions.



**Figure 5: Comparison of germination rate of plants sown on full MS medium compared with plants sown on medium lacking calcium.**

The germination rate is plotted against NaCl concentration. **A:** *Arabidopsis thaliana* plants growing on full MS (green squares) and on full MS without CaCl<sub>2</sub> (green triangles) **B:** *Thellungiella salsuginea* plants growing on full MS agar plates (yellow squares) in comparison to plants growing on full MS without CaCl<sub>2</sub> (yellow triangles). The NaCl concentration is indicated in the figure legend. Each data point represents the average of five biological replicates corresponding to plants grown on 5 agar plates. Error bars represent StDv. If not seen, the StDv is equal to or below the symbol size.

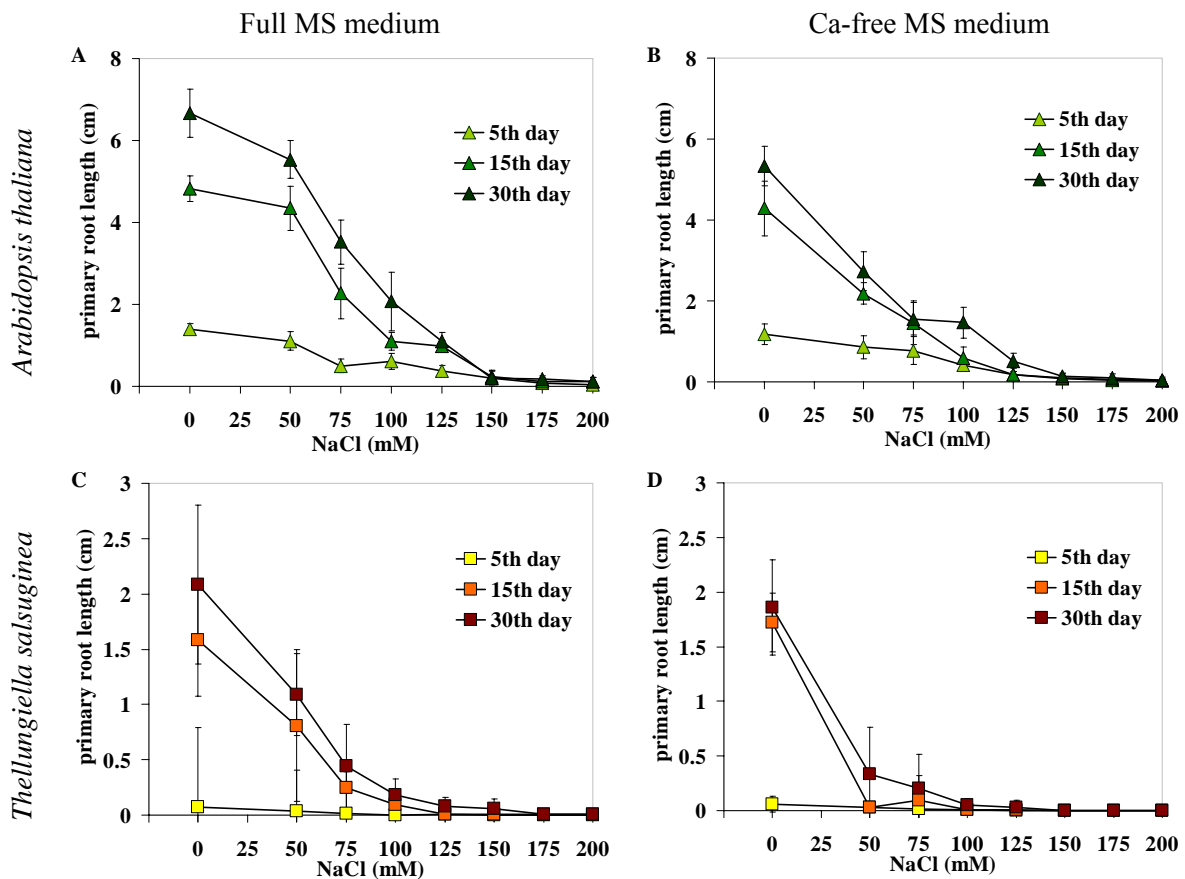
In some cases this improvement becomes obvious as a threefold higher germination rate compared to the calcium lacking plants. Omitting calcium leads to a significant reduction of the germination



rate. However, the screening of *Thellungiella salsauginea* shows different results (**Figure 5B**). Firstly, the germination rate of *Thellungiella* ( $83\pm 3\%$ ) under non-saline conditions is lower than that of *Arabidopsis* ( $99.4\pm 0.6\%$ ). Secondly, there are no significant changes in the number of seedlings, when omitting calcium in the growth medium. And the most interesting point is that the germination rate declines nearly to zero already at 200 mM NaCl. This is discussed later in more detail.

### 2.2.2 Primary root length

Primary root length was used here as a growth parameter for plants sown on media with different salt concentrations. As above also plants lacking calcium were screened for their root growth. As expected, root length decreases with increasing NaCl concentration in the medium with both plant species (**Figures 6 and 7**).

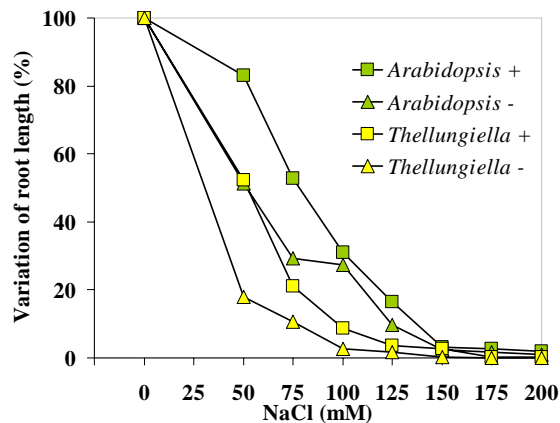


**Figure 6: Comparison of the primary root length of plants sown on full MS medium compared with plants sown on medium lacking calcium.**

The root length is plotted against NaCl concentration. **A:** *Arabidopsis thaliana* plants growing on full MS and **B:** on full MS without  $\text{CaCl}_2$  **C:** *Thellungiella salsauginea* plants growing on full MS agar plates in comparison to **D:** plants growing on full MS without  $\text{CaCl}_2$ . The day of evaluation is indicated in the figure legend. Each data point represents the average of 20 plants. Error bars represent StDv.

*Arabidopsis thaliana* has in general a higher root growth when compared to *Thellungiella salsauginea*. It also becomes obvious that the growth of *Thellungiella* varies from plant to plant (see

error bars in **Figure 6C, D**). Roots of plants exposed to salinity grown on Ca-free medium (**Figure 6B, D**) show reduced length when compared to plants grown on full MS medium. With *Arabidopsis* even at 50 mM NaCl their growth is suppressed significantly (**Figure 6B**). More prominent is this effect with *Thellungiella* (**Figure 6D**). Here, with the majority of germinated seedlings no particular root growth is observable.





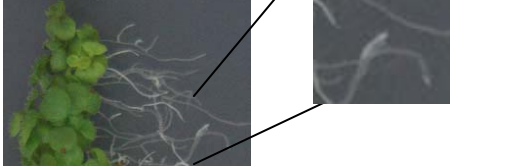









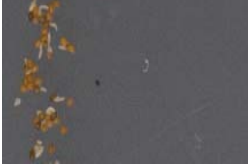


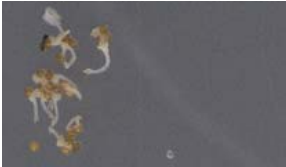

**Figure 7: Percentage difference between primary root lengths of *A.thaliana* and *T.salsuginea* grown on different salt concentrations**

The percentage variation of root lengths is plotted against NaCl concentration. 100 % corresponds to root length of plants grown at control conditions. *Arabidopsis thaliana* plants growing for 30 days on full MS (+, green squares) and on full MS without CaCl<sub>2</sub> (-, green triangles) are compared with *Thellungiella salsuginea* plants growing on full MS (+, yellow squares) and on full MS without CaCl<sub>2</sub> (-, yellow triangles). Curves are extrapolated from data shown in **Figure 6**. Error bars are given in the mentioned figure.

The percentage change in the root growth shown in **Figure 7** emphasizes once more the unexpected behaviour of the salt tolerant plant. While in *Arabidopsis* a 50 % reduction of root growth occurs at 75 mM NaCl (**Figure 7**, green squares), in *Thellungiella* it can be seen already at 50 mM NaCl (**Figure 7**, yellow squares). More pronounced is the difference when comparing plants grown on calcium free medium (**Figure 7**, green and yellow triangles). In *Thellungiella* the root growth declines by 80 % at 50 mM NaCl, whereas with *Arabidopsis* only a 50 % inhibition is visible.

### 2.2.3 The visible symptoms of salt stress and simultaneous calcium deficiency

**Figure 8** depicts the changes in the plant growth status due to exposure to salinity. With *Arabidopsis thaliana* 50 mM NaCl cause an increase in the number of lateral roots. Their number increases up to concentrations of 100 mM NaCl. The leaf area does not change due to 50 mM NaCl. From 75 mM NaCl up to 200 mM NaCl the leaf area continuously decreases. The overall phenotype at salt concentrations above 50 mM NaCl is stunted, and the thickness of leaves increases. The most interesting finding is that the tips of lateral roots of *Arabidopsis* plants grown on above 75 mM NaCl are swollen (**Figure 8**, inset). Although there are no other evidences, this symptom is tightly connected with iron deficiency (Römheld & Marschner, 1981; Landsberg, 1996; Moog *et al.*, 1995)) and is discussed in the **Section 2.3.4**.

	Full MS medium				Ca-free MS medium			
	0mM NaCl	50mM NaCl	100mM NaCl	200mM NaCl	0mM NaCl	50mM NaCl	100mM NaCl	200mM NaCl
<i>Arabidopsis thaliana</i>			 					
<i>Thellungiella salsuginea</i>								

**Figure 8: Two species contrasting in their salt tolerance grown on agar plates with different salt concentrations**

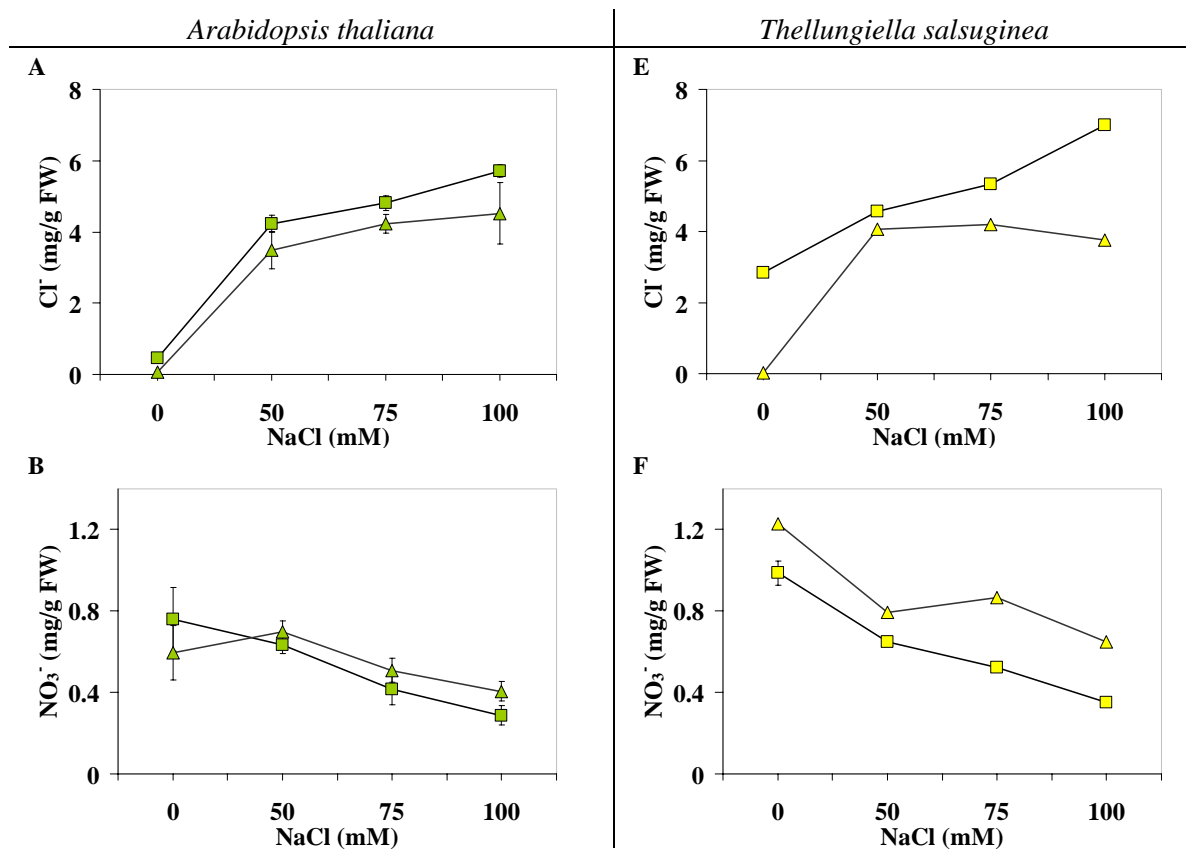
Seeds of salt sensitive *Arabidopsis thaliana* and salt-tolerant *Thellungiella salsuginea* were grown for 4 weeks on full MS medium and in parallel on Ca-free MS medium. The pictures shown here were taken on the 20th day after sowing.

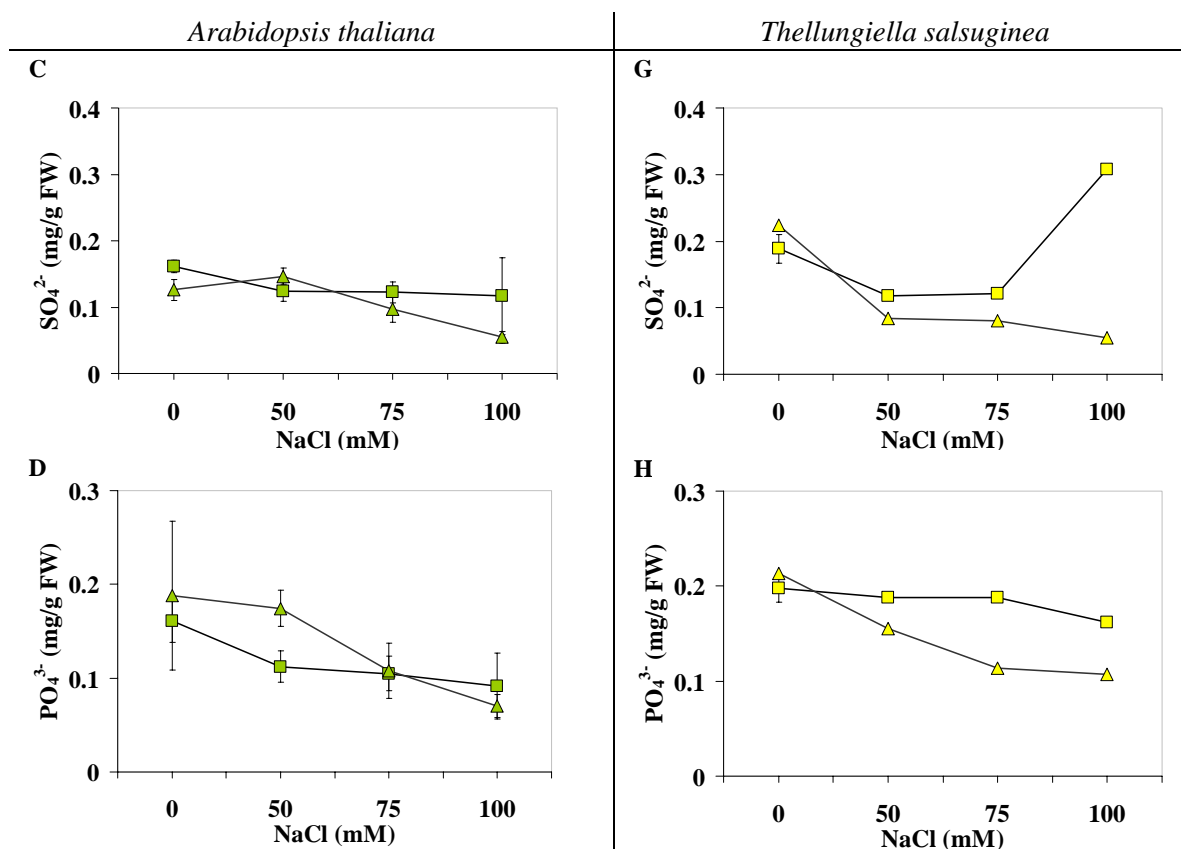
Even though *Arabidopsis* germinated at 200 mM NaCl, after 20 days and over this period, the plants did not grow further. *Arabidopsis* grown on Ca-free medium showed symptoms of Ca deficiency. Some of the plants were completely bleached and the overall fitness of the plants was reduced. Plants exposed to simultaneous salt treatment were stunted, the rosettes were significantly smaller and the leaf area partially reduced. Above 100 mM NaCl the germination and the growth rate were inhibited considerably.

With *Thellungiella* a different situation is given. The growth rate at control conditions differs greatly from plant to plant. However, mild salinity (50 mM NaCl) causes symptoms of iron deficiency (chlorotic leaves and swollen root tips). Although simultaneous calcium deficiency has in *Thellungiella* no particular effect on the germination (**Figure 5B**), the overall growth is massively inhibited already at 50 mM NaCl in the growth medium.

### 2.2.4 Ionic component of salt stress

In an attempt to understand mechanisms of salt tolerance, ion accumulation was compared in two related but in their salinity tolerance distinct plant species, one glycophytic (*Arabidopsis thaliana*) and the second halophytic (*Thellungiella salsuginea*).



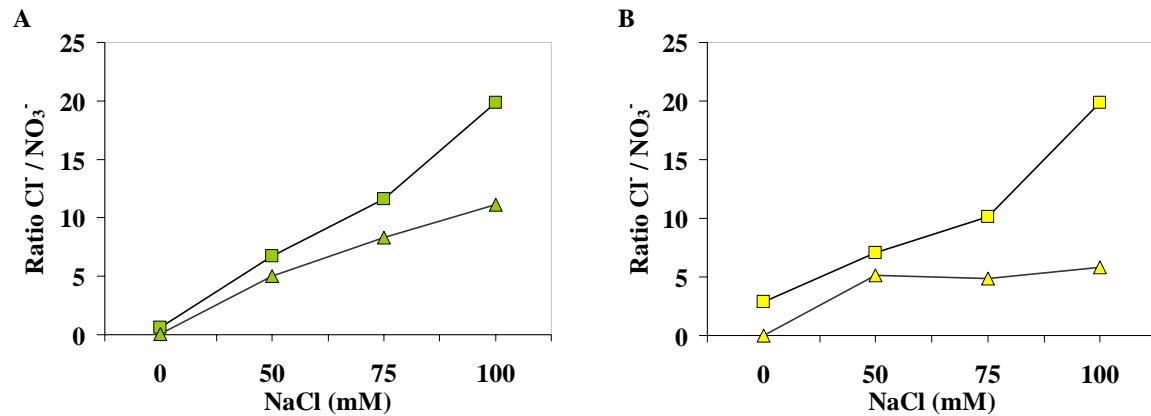


**Figure 9: Comparison of anion content in *Arabidopsis* and *Thellungiella* grown on substrates with different salt concentrations**

**A:** Chloride, **B:** nitrate, **C:** sulphate and, **D:** phosphate content of *Arabidopsis thaliana* plants grown on NaCl containing MS agar plates (green squares) compared to plants grown on medium lacking calcium (green triangles). **E:** Chloride, **F:** nitrate, **G:** sulphate and, **H:** phosphate content of *Thellungiella salsuginea* plants grown on NaCl containing MS agar plates (yellow squares) compared to plants grown on medium lacking calcium (yellow triangles). The anion content is related to the fresh weight (FW). Results are obtained from 3 biological replicates each with 3 technical replicates, i.e. the StDv shown as error bars refers to a mean of 9. If not seen, standard deviation is below the symbol size.

Both plant species showed very low growth rates on substrates with 100 mM NaCl and above (**Figures 7, 8**). Therefore, only plants grown on  $\leq 100$  mM were screened for their anion and cation content by IC and AAS, respectively. The results are displayed in **Figures 9, 10** and **11**.

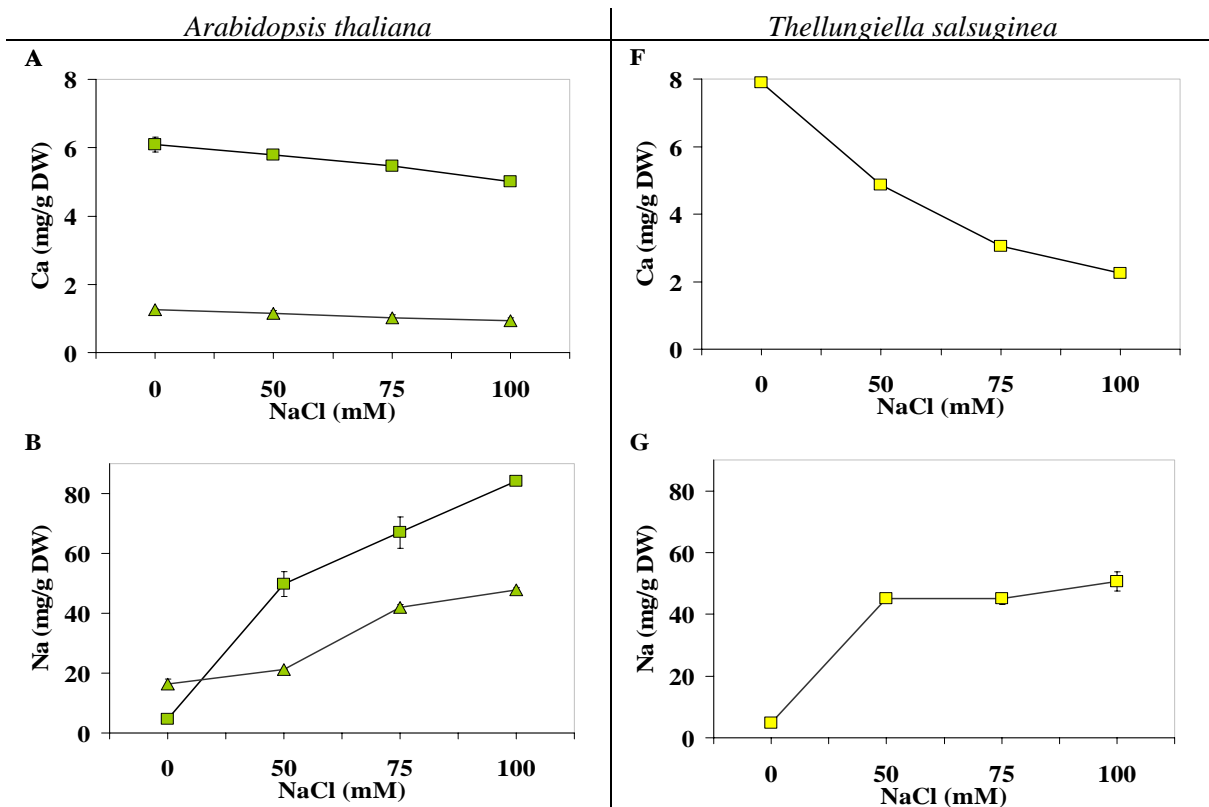
*Thellungiella salsuginea* plants grown on full MS have a higher [Cl<sup>-</sup>], when compared to plants grown on 1xMS (**Figure 9E**). The rate of chloride accumulation at increasing NaCl in the medium is nearly half that of *Arabidopsis thaliana* (**Figure 9A**). Anyway, chloride exclusion seems not to play a role in salt tolerance mechanisms neither in *Arabidopsis thaliana* nor in *Thellungiella salsuginea*; they both accumulate chloride up to 7 mg·g<sup>-1</sup> fresh weight (FW) at high salt concentrations (**Figure 9A, E**). Nitrate is probably secreted by the plants due to its replacement by chloride. Furthermore, the effect of calcium deficiency on the anion content of salt treated plants is more pronounced in *Thellungiella*. Significant differences can be seen with all four measured anions (**Figures 9**). This suggests a calcium mediated anion influx during salt stress in *Thellungiella salsuginea*.

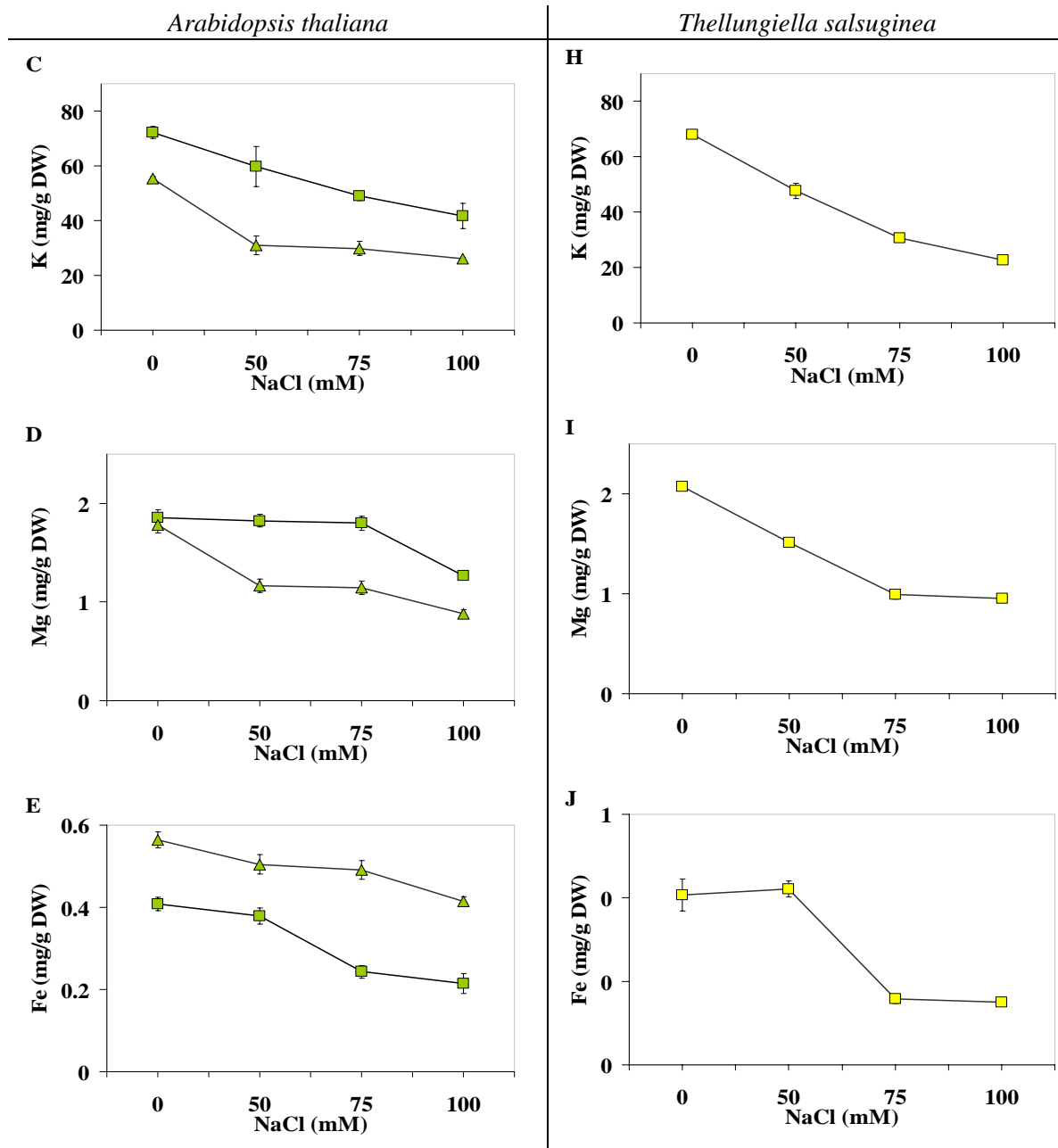


**Figure 10: The chloride to nitrate ratio**

The figure shows the dependency of nitrate exclusion on uptake of chloride during salt stress. **A:** *Arabidopsis thaliana* plants grown on different NaCl concentrations on full MS agar plates (green squares) are compared to plants grown on calcium lacking medium (green triangles). **B:** *Thellungiella salsuginea* plants grown on different NaCl concentrations on full MS agar plates (yellow squares) and on calcium lacking medium (yellow triangles).

The chloride to nitrate ratio rises in both plant species grown on full MS up to 20 at 100 mM NaCl (**Figure 10**), whereas the plants exposed to additional calcium deficiency show differences. The ratio of *Arabidopsis thaliana* plants steadily increases but at a lower rate when compared to the control plants. In contrast, the salt tolerant relative accumulates less chloride at higher salt concentrations, therefore the chloride to nitrate ratio remains at the same level for all three screened NaCl concentrations, when grown without calcium.





**Figure 11: Cation content**

**A-E** Comparison of cation content of *Arabidopsis thaliana* grown for 4 weeks on NaCl containing full MS agar plates (green squares) and plants grown on calcium free medium (green triangles); **F-J** *Thellungiella salsuginea* (yellow squares) plants grown for 4 weeks on NaCl containing full MS agar plates. The plants grown on calcium free medium did not deliver sufficient amount of material for AAS measurements. The NaCl concentration is indicated in the figure legend. The cation content is related to the dry weight (DW). Results include 3 biological replicates each measured 3 times, i.e. the StDv indicated by error bars refers to 9 data points. If not seen, standard deviation is equal to or below the symbol size.

**Figure 11** displays differences in cation content between both plant species. *Thellungiella salsuginea* shows more prominent calcium loss during salt stress treatment compared to *Arabidopsis thaliana* (**Figure 11A**). The progression of sodium accumulation (**Figure 11B**) in the salt tolerant relative is lower, revealing a possible trait of salt tolerance mechanism in this plant species. All three remaining cations (potassium, magnesium and iron) are lost from both species

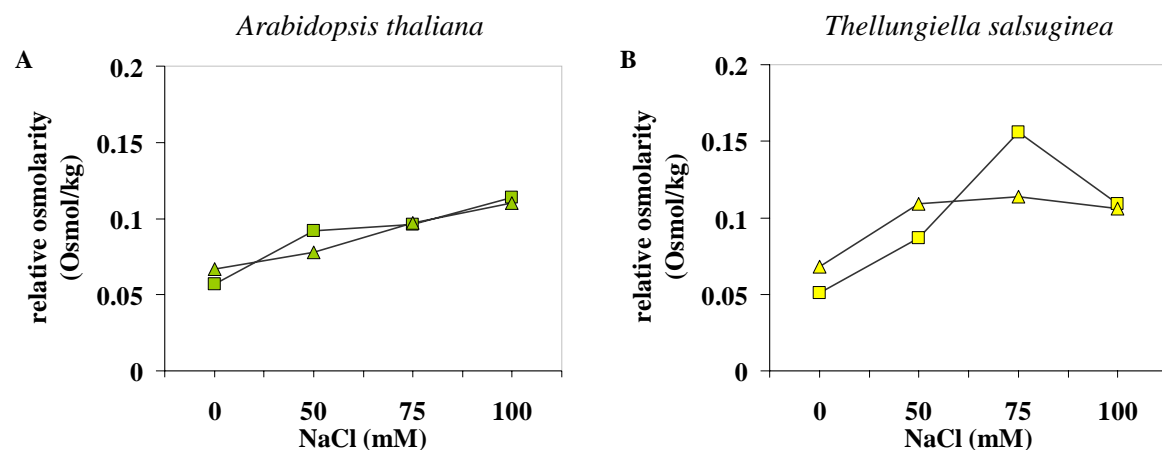
upon salt stress, with distinct patterns. As for potassium (**Figure 11C**), the loss is more prominent in *Thellungiella salsuginea*, but the general trend is the same for both. However, the magnesium graph (**Figure 11D**) shows a break point at 75 mM NaCl, where [Mg] of *Arabidopsis* starts to decline. *Thellungiella* in contrast reaches here its lowest [Mg].

During long term salt stress, *Thellungiella salsuginea* plants show apparent symptoms of iron deficiency (**Figure 8**). Therefore, iron content was also measured using AAS. 50 mM NaCl added to the full MS medium caused only a non significant lowering of the iron content. Addition of 75 mM NaCl however provokes a reduction of the  $[Fe^{2+}]$  below  $0.2 \text{ mg}\cdot\text{g}^{-1}$  DW in *Thellungiella salsuginea* and only marginally above this value in *Arabidopsis thaliana* (**Figure 11E**). Thus, a critical iron content in *Thellungiella salsuginea* is reached. This is in line with findings from Häussling *et al.*, 1985, who worked with grape-vine.

However, high salinity and simultaneous calcium deficiency did not cause iron deficiency. The iron content of plants grown on medium lacking calcium was nearly 1.5 times higher than in plants on full MS. The possible reasons are discussed in the **Section 2.3.4**.

### 2.2.5 Osmotically active substances

Beneficial effects against damage by drought and high salinity have been documented when transgenic plants contained or accumulated osmotically active metabolites, such as proline (Kishor *et al.*, 1995), glycine-betaine (Holmström *et al.*, 2000), and mannitol (Tarczynski *et al.*, 1993). The metabolites have been shown to accumulate in wild type plants during salt stress (Chen *et al.*, 2007; Szabados & Savouré, 2010).



**Figure 12: Comparison of total osmolarity**

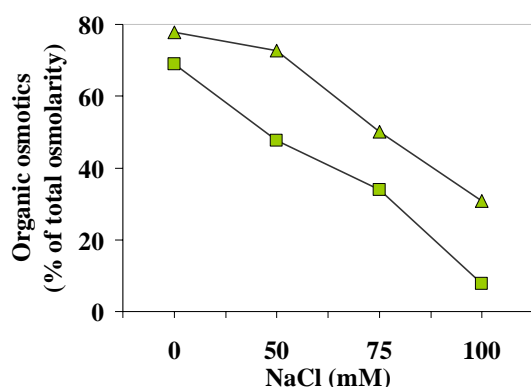
**A:** *Arabidopsis thaliana* (green squares) and **B:** *Thellungiella salsuginea* (yellow squares) plants grown for 4 weeks on NaCl containing full MS agar plates compared each to plants grown on medium without calcium (triangles). The NaCl concentration is indicated in the figure legend. Results are obtained from 3 technical replicates. Standard deviation is below the symbol size.

Here, in order to investigate their role in salt tolerance mechanisms osmolarity of plant extracts was measured. Total osmolarity of *Arabidopsis thaliana* plants exposed to salt stress (**Figure 12A**)



continuously rises about twofold with increasing NaCl concentration in the both growth media. The results are different, when assaying *Thellungiella salsuginea* (**Figure 12B**).

Total osmolarity of plant extracts (**Figure 12**) consists of two components: the ionic and the organic. The approximate osmolarity of the ionic component was calculated from the data obtained by AAS and IC. All measured anions and cations were included in the calculation, and the fresh/dry weight-ratio was taken into account. The organic component was then calculated as the difference of the ionic component and the total osmolarity of plant extracts (**Figure 13**).



**Figure 13: Organic compatible solutes**

Contribution of organic solutes to the total osmolarity of *Arabidopsis thaliana* sown on 1xMS medium (squares) and on 1xMS medium lacking calcium (triangles). The percentage contribution of organic solutes to the total osmolarity is plotted against NaCl concentration. Results are obtained from 3 technical replicates. Standard deviation is below the symbol size.

## 2.3 DISCUSSION

Two relatives differing in their salt tolerance, the glycophyte *Arabidopsis thaliana* and the halophyte *Thellungiella salsuginea*, were studied here by comparative analysis of their germination rate, growth parameters, ion accumulation and osmotic properties when germinating and grown on salt containing medium. Calcium is known to ameliorate the negative effects of salinity on plants (Shabala *et al.*, 2003; Hussain *et al.*, 2004; Shabala *et al.*, 2006). Therefore, the impact of calcium withdrawal on salt treated plants was studied in parallel experiments.

### 2.3.1 *Thellungiella salsuginea* - the germination phenomenon

*Thellungiella salsuginea* was shown to have a significantly higher tolerance to moderate salinity (100 mM NaCl) than *Arabidopsis thaliana* and is able to withstand concentrations even up to 500 mM NaCl (Orsini *et al.*, 2010; Volkov & Amtmann, 2003; Inan *et al.*, 2004). Nevertheless, it was also described, that the germination rate of *Thellungiella salsuginea* decreases markedly with increasing salt concentrations in the environment (Inan *et al.*, 2004; Orsini *et al.*, 2010). Partially the plants show a delay in germination of 3 to 4 months (Inan *et al.*, 2004). This phenomenon is not dependent on the salt concentration and is shared by several other halophytes too (Flowers *et al.*, 1977). It has been considered a protective strategy to ensure maximal survival (Inan *et al.*, 2004). The *Thellungiella salsuginea* ecotype Shandong, used for this study, grows in the coastal regions of northeast China. Seasonal changes in the salinity and nutrient content occur. In particular, during

summer due to rapid evaporation of water, surface of the soil has higher salinity and higher water potential (Khan & Gul, 2002). Seed germination in arid and semi-arid regions usually occurs after the winter, when heavy rains reduce soil surface salinity. This could be a possible explanation for the germination phenomenon in *Thellungiella salsuginea*, too.

### 2.3.2 Organic osmolytes are not accumulated during salt stress in *A. thaliana* and *T. salsuginea*

One protective mechanism to balance the changes in osmotic potential during salt stress is the accumulation of compatible solutes such as glycinebetaine, proline, polyols and sucrose within the cell (Tester & Davenport, 2003; Khedr *et al.*, 2003). Although the accumulation of the osmotic compounds mentioned above was not measured separately, the osmolarity measurements (**Figure 13**) suggest, that no additional organic osmolytes are synthesised during salt stress. In general, the use of ions for osmotic adjustment is energetically more favourable than de-novo synthesis of organic osmolytes especially under stress conditions (Raven, 1985). This seems to be also true for the presented experiments.

### 2.3.3 Calcium alleviates symptoms of salt stress in plants

Calcium functions as a structural component; it coordinates stable but reversible intermolecular linkages mostly in the cell wall and plasma membrane by bridging phosphate and carboxylate groups of phospholipids and proteins (Coldwell & Haug, 1981; Legge *et al.*, 1982; Marschner, 1995). It is therefore fundamental for membrane integrity and stability. Consequently, during calcium-deficiency low-molecular-weight solutes leak out of the cell (Van Goor, 1966) and severe deficiency leads to general disintegration of membrane structures and loss of cell compartmentation (Hecht-Buchholz, 1979, Marschner, 1995).

Thus, calcium is required in the external medium for the normal growth and in order to regulate the selectivity of ion uptake and to prevent solute leakage from the cytoplasm. At low calcium availability, an exchange of membrane bound calcium with other ions takes place (e.g.  $\text{Na}^+$ ,  $\text{K}^+$ , and  $\text{H}^+$ ). Consequently, a determining factor for this process is the concentration of other ions in the medium. Due to high external concentrations of heavy metals (Wallace *et al.*, 1966), or protons, which are able to replace the calcium at its external binding sites, its requirement is increased. High external concentrations of sodium as they occur during salt stress, lead to exchange of calcium at the binding sites with sodium (La Haye & Epstein, 1971; Lynch *et al.*, 1987; Rengel & Elliot, 1992; Marschner, 1995). The cation content measurements of *Arabidopsis thaliana* presented in **Figure 11A, B** confirm this statement. The calcium concentration decreases with increasing [Na] in the medium. Although both plant species lose calcium due to salinity, in *Thellungiella salsuginea* this loss is much more pronounced (**Figure 11F**). The data from germination screening (**Figure 5**)

deliver another hint. It becomes obvious, that in the salt sensitive plant the external calcium concentration of approx. 3 mM  $\text{CaCl}_2$  is sufficient to ameliorate the negative effects of salinity on germination (**Figure 5A**). In *Thellungiella salsuginea* the ameliorative effect of calcium cannot be seen, probably due to higher exchange of calcium with sodium at the external binding sites. The negative effect of NaCl on germination was previously shown in other halophytes grown in coastal regions (Gul & Khan, 2006). Furthermore, Gul & Khan (2006) have approved the ameliorative effect of 10 mM  $\text{Ca}^{2+}$  on germination of certain halophytic species. Thus, 3 mM  $\text{CaCl}_2$  in the 1xMS growth medium as used for the experiments presented here, are obviously not sufficient enough for *Thellungiella salsuginea*.

Although calcium stimulates the germination of *Arabidopsis* at moderate salinity, the plants grown at normal conditions have a higher chloride to nitrate ratio (**Figure 10A**), thus they obviously accumulate more chloride. Also sodium is accumulated at higher extent. This is in contrast with previous findings that calcium alleviates sodium uptake (Cramer, 2002; Henriksson & Henriksson, 2005).

Potassium is obviously leaking out from cells due to salinity (**Figure 11C, H**). Leakage of  $\text{K}^+$  is more prominent when there is lack of calcium. Since more Na is accumulated during calcium starvation, the Na:K ratio due to salinity remains the same in Ca-containing and Ca-deficient plants.

### 2.3.4 Iron availability

Plants grown on alkaline soils, suffer generally from low availability of nutrients (Lindsay, 1984). The same is true for salt affected soils (Cerdeira & Martinez, 1988; Keutgen & Pawelzik, 2009; Turan *et al.*, 2010). High sodium accumulation in the soil favours the formation of alkaline salts such as sodium bicarbonate, which increase the pH. Amongst others the uptake of iron is limited (Shrivastava *et al.*, 1993; Turan *et al.*, 2010). Consequently, plants grown on saline-sodic soils suffer from iron deficiency. Severe chlorosis, accompanied by a significant biomass reduction belongs to its symptoms.

There are two strategies, how plants fight low iron availability. The first one, found in dicots and non-graminaceous monocots, comprises the release of protons by plasma membrane  $\text{H}^+$ -ATPases, and thus the extracellular reduction of Fe (de Vos *et al.*, 1986; Bienfait, 1988). Therefore, proton secretion by plasma membrane  $\text{H}^+$ -ATPases and reduction capacity as well as Fe(II) transport are enhanced under Fe-deficient growth conditions (Schmidt, 2003).

The other strategy, found in graminaceous plants, is based on the release of iron hexadentate chelators, so called phytosiderophores (PS). The Fe(III)-PS complexes are then taken up by the plants. Salt treated barley plants for example develop more lateral roots than plants grown at normal conditions and show a highly stimulated phytosiderophore release (Yousfi *et al.*, 2007).

Here, *Thellungiella salsuginea* plants germinating on saline medium containing more than 75 mM NaCl showed symptoms of iron deficiency such as severe chlorosis. In *Arabidopsis* swollen tips of lateral roots could be observed (**Figure 8**). As described by Häussling *et al.* (1985) iron deficiency occurs at values  $\leq 0.2$  mg Fe·g<sup>-1</sup> DW. The iron content measured in *Thellungiella salsuginea* reaches this value and is only insignificantly higher in *Arabidopsis thaliana* (**Figure 11E**). Free iron and low-molecular-weight iron chelates can in aerobic systems cause the formation of reactive oxygen species, such as hydroxyl radical (OH<sup>•</sup>) (Halliwell & Gutteridge, 1986). Among others, this species is involved in lipid peroxidation (Elstner, 1991). In order to avoid further ROS production, the iron has to be tightly bound or incorporated into storage proteins (ferritins), which allow controlled reversible oxidation-reduction reactions (Briat *et al.*, 2010; Fobis-Loisy *et al.*, 1995; Briat *et al.*, 1995 Marschner, 1995).

The uptake of iron is obviously responsive to calcium. Calcium withdrawal causes in *A. thaliana* a prominent increase in the iron content (**Figure 11E**). In *Thellungiella salsuginea* this increase is much more pronounced than in *A. thaliana* (**Suppl\_Material 4**). A decreased ion selectivity of the transporting system due to low calcium could be one explanation (Marscher, 1995).

Another explanation can be either a direct or indirect effect of calcium on the reduction of extracellular iron. It has been shown, that calcium-dependent phosphorylation negatively regulates the function of the plasma membrane H<sup>+</sup>-ATPase (Lino *et al.*, 1998). Lack of calcium could impair this regulation; trigger the release of protons and thus a release of iron from the medium.

NADPH was suggested to be the electron donor for the Fe(III) reduction by the action of NADPH oxidase (Bienfait, 1988; Cakmak *et al.*, 1987). Its activity was found to be increased in iron-deficient roots. Interestingly, NADPH oxidase contains two EF-hand motifs, suggesting that calcium may play a role in the regulation of its activity (Keller *et al.*, 1998; Grant & Loake, 2000; Sagi & Fluhr, 2001, Sagi & Fluhr, 2006).

An iron responsible transporter (*IRT1*; At4g19690) was found in *Arabidopsis thaliana* to be highly up-regulated during iron deficiency and subsequently to account for the iron nutrition (Eide *et al.*, 1996; Vert *et al.*, 2002). Yet, no direct connection between calcium starvation and increased iron uptake seems to be described until now.

The influence of changes in cation content caused by the different treatments (salinity, calcium withdrawal) on the activity of certain antioxidative enzymes is shown in **Chapter 4** and discussed in more detail in **Chapter 5**.

## CHAPTER 3

# RATIOMETRIC QUANTITATION OF GENERIC CELLULAR PARAMETERS *IN VIVO* DURING SHORT TERM SALT STRESS

To investigate salt stress-induced chloride influx and its regulation, experiments using *in vivo* fluorescence ratiometry with *Arabidopsis* expressing GFP-based indicators like Clomeleon, pHluorins and roGFPs were performed. Another task was to clone and to express chloride channels from *Arabidopsis thaliana* in order to characterize their role in chloride transport under salt stress. On the one hand, selected channels were together with a fluorescent anion indicator Clomeleon expressed in a plant system (here *Allium porrum* and *Allium cepa* epidermal cells). On the other hand, expression of AtClC-A in a bacterial system and further purification were carried out, in order to obtain sufficient amounts of protein for reconstitution in liposomes and subsequent functional characterisation.

### 3.1 MATERIAL AND METHODS

#### 3.1.1 Chemicals, consumables and equipment

All used chemicals, equipment and other consumables and their sources are listed in the **Suppl\_materials 1-3**.

#### 3.1.2 Solutions and buffers

Media for growing plants:

<u>1xMS agar</u>	4.4 g/l Murashige & Skoog medium pH adjusted with KOH to 5.8 1.2 % plant agar autoclaved
------------------	---------------------------------------------------------------------------------------------------

Buffers for purification of GFP-based indicators:

<u>Wash buffer I (WB1)</u>	100 mM KPP pH 7.4
<u>Wash buffer I reduced</u>	100 mM Tris-HCl pH 7.5 5 mM DTT degassed
<u>Wash buffer II (WB2)</u>	5 mM imidazole in wash buffer I
<u>Wash buffer II reduced</u>	5 mM imidazole in reduced wash buffer I
<u>Elution buffer (EB)</u>	500 mM imidazole in wash buffer I
<u>Elution buffer (reduced)</u>	500 mM imidazole in reduced wash buffer I

## Buffers for purification of AtCIC-A:

<u>Solubilization buffer</u>	50 mM Tris-HCl pH 7.4 150 mM NaCl 200 mg/l lysozyme 20 mg/l DNaseI 1 Complete mini tablet per 20 ml buffer
<u>Wash buffer I (WB1)</u>	50 mM Tris-HCl pH 7.5 150 mM NaCl
<u>Wash buffer I reduced (WB1 reduced)</u>	50 mM Tris-HCl pH 7.5 150 mM NaCl 5 mM $\beta$ -mercaptoethanol degassed
<u>Wash buffer II (WB2)</u>	5 mM imidazole in wash buffer I
<u>Wash buffer II reduced (WB2 reduced)</u>	5 mM imidazole in reduced wash buffer I
<u>Elution buffer (EB)</u>	500 mM imidazole in wash buffer I
<u>Elution buffer (reduced)</u>	500 mM imidazole in reduced wash buffer I

## Buffers for FPLC analysis of AtCIC-A:

<u>Wash buffer I for FPLC</u>	50 mM Tris-HCl pH 7.5 150 mM NaCl filtered (0.22 $\mu$ m filter) and degassed
<u>Wash buffer II for FPLC</u>	10 mM imidazole in wash buffer I filtered (0.22 $\mu$ m filter) and degassed
<u>Elution buffer for FPLC</u>	50 mM Tris-HCl pH 7.5 150 mM NaCl 100 mM imidazole filtered (0.22 $\mu$ m filter) and degassed

## Buffers for SDS-PAGE:

<u>SDS-PAGE running buffer</u>	250 mM Tris-HCl 2 M glycine 1 % (w/v) SDS
<u>SDS-PAGE 7.5 % stacking gel</u>	1.2 ml deionized H <sub>2</sub> O 0.6 ml Tris/HCl pH 6.8 0.45 ml acrylamide/N,N'-methylenebisacrylamide 30 $\mu$ l 10 % SDS 3 $\mu$ l TEMED 30 $\mu$ l 10 %APS
<u>SDS-PAGE 15 % separative gel</u>	1.4 ml deionized H <sub>2</sub> O 1.6 ml Tris/HCl pH 8.8 3 ml acrylamide/N,N'-methylenebisacrylamide 60 $\mu$ l 10 % SDS 6 $\mu$ l TEMED 100 $\mu$ l 10 %APS
<u>Coomassie staining solution</u>	0.1 % (w/v) Coomassie brilliant blue R250 40 % (v/v) ethanol 10 % (v/v) acetic acid brought up to the end volume with deionized water
<u>Coomassie destaining solution</u>	30 % (v/v) ethanol 10 % (v/v) acetic acid brought up to the end volume with deionized water

Buffers and solutions for flow-trough experiments:

<u>Standard medium (SM) stock</u>	100 mM KCl 100 mM CaCl <sub>2</sub> 100 mM MgCl <sub>2</sub> diluted 1 :1000 in the flow-through medium
<u>NaCl (pH 6)</u>	5 mM MES (with or without SM, as described in the figure legends) 50 mM, 100 mM or 150 mM NaCl supplemented with different modulators as described in the figure legends adjusted to pH6 with KOH
<u>NaCl (pH8)</u>	5 mM HEPES 100 mM or 150 mM NaCl adjusted to pH8 with KOH
<u>KCl (pH6)</u>	5 mM MES + SM 50 mM, 100 mM and 150 mM KCl adjusted to pH 6 with KOH
<u>KNO<sub>3</sub> (pH6)</u>	5 mM MES + SM 50 mM, 100 mM and 150 mM KNO <sub>3</sub> adjusted to pH 6 with KOH

### 3.1.3 Bacterial strains

**Table 3: Bacterial strains used in this study**

<i>Escherichia coli</i>	Genotype background	Reference
<b>M15[pREP4]</b>	<i>Nal<sup>S</sup> Str<sup>S</sup> Rif<sup>S</sup> Thi<sup>-</sup> lac<sup>-</sup> ara<sup>+</sup> gal<sup>+</sup> mtl<sup>-</sup> F<sup>-</sup> recA<sup>+</sup> uvr<sup>+</sup> lon<sup>+</sup></i> [pREP4 Kan <sup>r</sup> ]	Qiagen (Hilden, DE)
<b>SG13009[pREP4]</b>	<i>Nal<sup>S</sup> Str<sup>S</sup> Rif<sup>S</sup> Thi<sup>-</sup> lac<sup>-</sup> ara<sup>+</sup> gal<sup>+</sup> mtl<sup>-</sup> F<sup>-</sup> recA<sup>+</sup> uvr<sup>+</sup> lon<sup>+</sup></i> [pREP4 Kan <sup>r</sup> ]	Qiagen (Hilden, DE)
<b>XL1-Blue</b>	<i>recA1 endA1 gyrA96 thi-1 hsdR17 supE44 relA1 lac</i> [F <sup>'</sup> <i>proAB lacIqZΔM15 Tn10</i> (Tetr)]	Stratagene (La Jolla, USA)

### 3.1.4 Characteristics of GFP-based indicators used in this study

Green fluorescent protein (GFP) isolated from the jellyfish *Aequorea victoria* (Shimomura *et al.*, 1962; Chalfie *et al.*, 1994) has become a common tool for cell and molecular biologists to visualize sub-cellular structures and localisation of specific proteins; analysis of protein-protein interactions and detecting changes in cellular and sub-cellular parameters, i.e. ion fluctuations, changes in pH or redox environment. They all require genetic manipulation of the original GFP in order to change its spectral properties. In addition, FPs from organisms other than *Aequorea victoria* have been found useful for specific investigations, e.g. PtGFP from the orange seapen (*Ptilosarcus gurneyi*) for detecting pH changes (Schulte *et al.*, 2006). In course of this endeavour countless FPs of different spectral characteristics and different applicability were produced by introducing specific mutations (Fricker *et al.*, 2006; Day & Davidson, 2009 and the references cited therein).

Cross-sensitivities are often major drawbacks when fluorescent proteins are engineered to indicators for studies of different cellular properties. During salt stress in plants other cellular

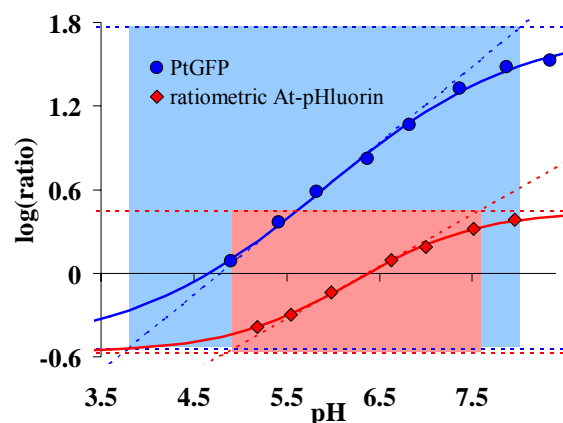
parameters, such as the pH or the redox milieu may change. Therefore, it was necessary to screen the different indicators for cross-sensitivities.

**Table 4: Properties of fluorescent indicators used in this study**

FP variant	Parameters to be quantified	Excitation maxima (nm)	Emission maxima (nm)	Isoexcitation point (nm)
ptGFP	pH	395 and 475	540	438
ratiometric pHluorin	pH	395 and 475	508	428
S3roGFP	Redox status	395(oxidized) 395 and 475(reduced)	508	424
Clomeleon	Anions	434	475 and 535	513
dsRED	Expression level	470	520	406

### 3.1.4.1 pH-sensitive fluorescent indicators

Two ratiometric pH-sensitive FPs were used in this study as cytoplasmic pH indicators. Ratiometric At-pHluorin (ratiometric GFP, Miesenböck *et al.*, 1998; Gao *et al.*, 2004; Schulte *et al.*, 2006) has pH-dependent spectra with an optimal dynamic response in the interval pH 5.6 – pH 7.8 (**Figures 14 and 15**), which makes it suitable for cytoplasmic pH measurements. The other pH-sensitive FP (PtGFP) was previously used in *Arabidopsis thaliana* to detect pH changes (Schulte *et al.*, 2006). PtGFP has a broader pH-responsiveness, an excellent dynamic ratio range (**Figures 14 and 15**) and a better acid stability (Schulte *et al.*, 2006).

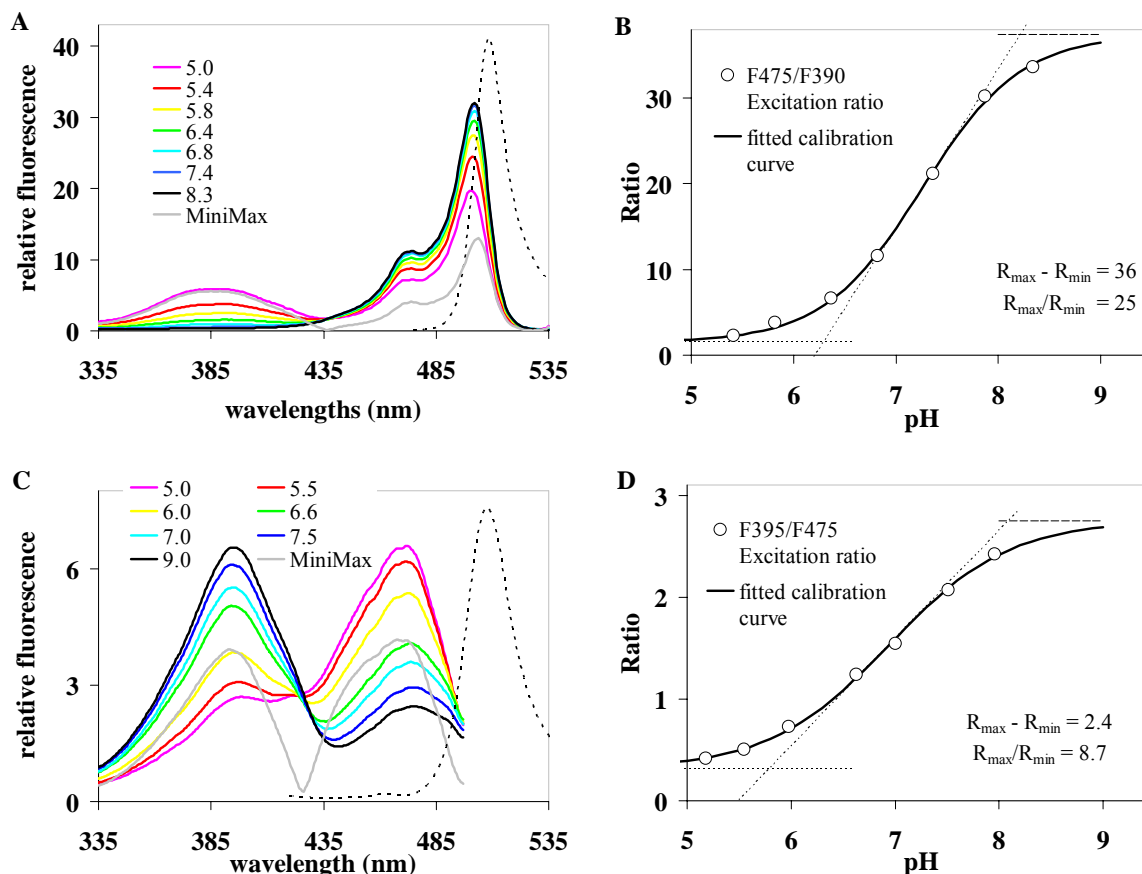


**Figure 14: Comparison of two recombinant pH-probes on a log-log scale**

The areas of best responsiveness are highlighted by coloured rectangles: ratiometric pHluorin in red (excitation ratio  $R_{ex} = F_{390}/F_{475}$  at  $\lambda_{em} = 508$  nm), and PtGFP in blue (excitation ratio  $R_{ex} = F_{475}/F_{390}$  at  $\lambda_{em} = 540$  nm). Data adapted from Schulte *et al.* (2006).

Both proteins, pHluorin and PtGFP, are double excitation indicators (**Table 4; Figure 15**). With PtGFP the fluorescence ratio  $F_{475}/F_{390}$  and with ratiometric pHluorin ratio  $F_{390}/F_{475}$  was taken as a measure for pH.





**Figure 15: Fluorescence properties of genetically encoded pH-indicators.**

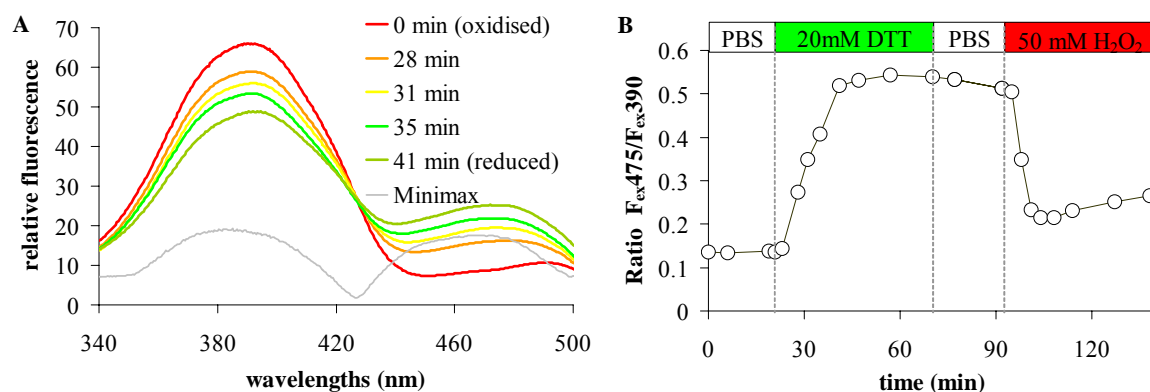
Spectra taken at different pHs are given for PtGFP (A), and ratiometric pHluorin (C). Corresponding ratio curves are on the right hand side (B, D). **A:** Excitation spectra of PtGFP at  $\lambda_{em} = 540$  nm. The dotted line represents the emission spectrum ( $\lambda_{ex} = 470$  nm) corresponding to pH = 7.4. **B:** Dependency of fluorescence excitation ratios  $R(475_{ex}/390_{ex}; 540_{em})$  of PtGFP on pH. **C:** Excitation spectra of ratiometric pHluorin at  $\lambda_{em} = 508$  nm. The dotted line represents the emission spectrum ( $\lambda_{ex} = 390$  nm) corresponding to pH 7.5. **D:** Dependency of fluorescence excitation ratios  $R(395_{ex}/475_{ex}; 508_{em})$  of ratiometric pHluorin on pH. All spectra are normalized by their area. The grey curve in each set of spectra (A, C) represents the corresponding minimax spectrum (maximum fluorescence difference for each wavelength). Its minimum designates the isosbestic point. Sigmoidal Boltzmann function was fitted to the ratio data (B, D). Figures adapted from Schulte *et al.* (2006)

Schulte *et al.* (2006) measured the fluorescence spectra of both pH-probes *in vitro* with purified protein to search for possible chloride and redox cross-sensitivities. They found, that the chloride sensitivities in the range of  $0 < [Cl^-] < 1$  M (at pH = 7.5 in 50 mM Hepes) are negligible and that there are also no noteworthy spectral differences between reduced (20 mM DTT in degassed PBS) and oxidized probes (50 mM  $H_2O_2$  in PBS).

#### 3.1.4.2 Redox sensitive GFP-based indicator - S3roGFP

To obtain a redox sensitive ratioable indicator with negligible pH sensitivity, in a previous work (Schmidt, 2005) mutations were introduced into the “soluble modified” psmGFP (Davis and Vierstra 1998; ABRC stock number: CD3-326). Accordingly to Dooley *et al.* (2004) and Hanson *et al.* (2004) certain amino acid residues were changed to cysteines ( $S_{147}C$ ,  $N_{149}C$ ,  $S_{202}C$ ,  $Q_{204}C$ ). The

residues are able to form disulphide bonds during oxidation, thereby changing the spectral properties of the protein (**Figure 16**, Schmidt *et al.*, 2007).

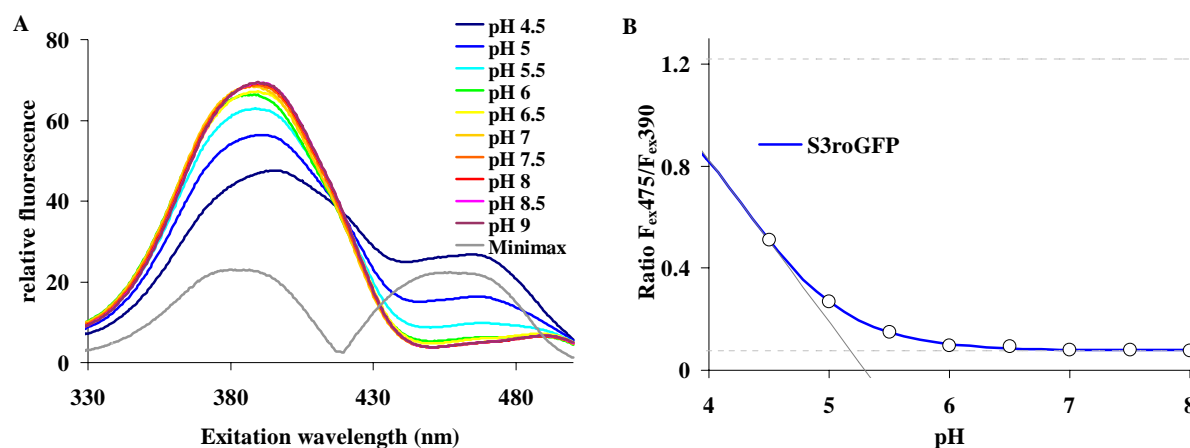


**Figure 16: Fluorescence properties of genetically encoded redox indicator during oxidative and reducing treatment**

**A:** Excitation spectra of purified S3roGFP taken during dialysis against a reducing DTT-buffer. All spectra are normalized by their area **B:** Time course of fluorescence ratios  $R(475_{ex}/390_{ex}; 560_{em})$  from S3roGFP during dialysis against reducing and oxidising buffers. Data from Schmidt (2005); Schmidt *et al.* (2007).

Plants stably expressing the S3roGFP in the cytoplasm were produced in previous work (Schmidt, 2005). Later on targeting sequences for peroxisomes and mitochondria were introduced (Thierbach, 2006). With this indicator it is now possible to quantify changes in the cytoplasmic, peroxisomal and mitochondrial redox environment using dual excitation fluorescence ratiometry.

S3roGFP shows in physiologically relevant pH range (pH 6.3 to 9.5) no changes in its spectral properties (**Figure 17**).

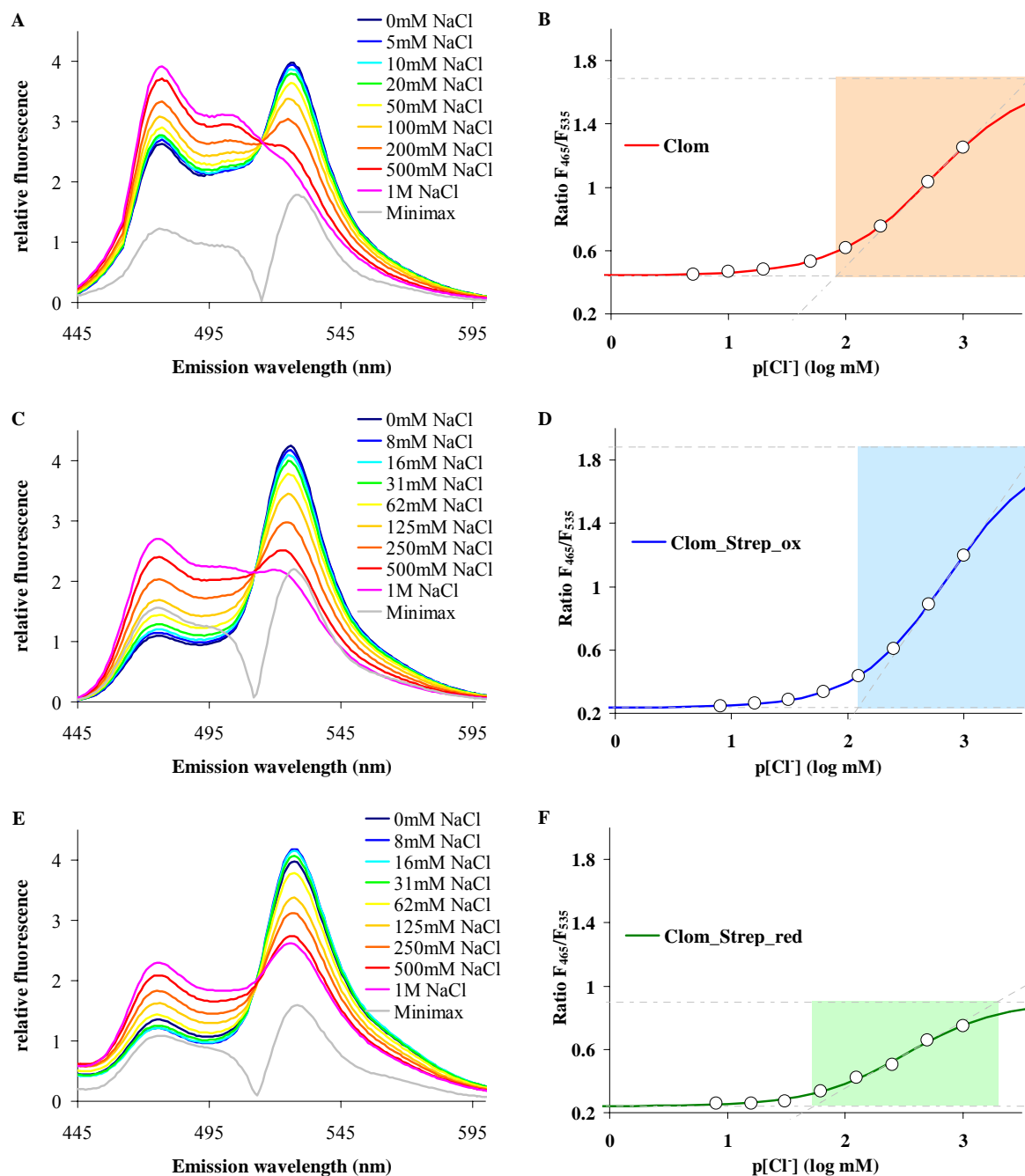


**Figure 17: pH sensitivity of the redox indicator**

**A:** Excitation spectra of S3roGFP at  $\lambda_{em} = 560$  nm at different pH. All spectra are normalized by their area. The grey curve represents the corresponding minimax spectrum. **B:** Dependency of fluorescence excitation ratios  $R(475_{ex}/390_{ex}; 560_{em})$  of S3roGFP on pH. Sigmoidal Boltzmann function was fitted to the ratio data. Data adapted from Schmidt, 2005.

### 3.1.4.3 Genetically encoded chloride indicator - Clomeleon

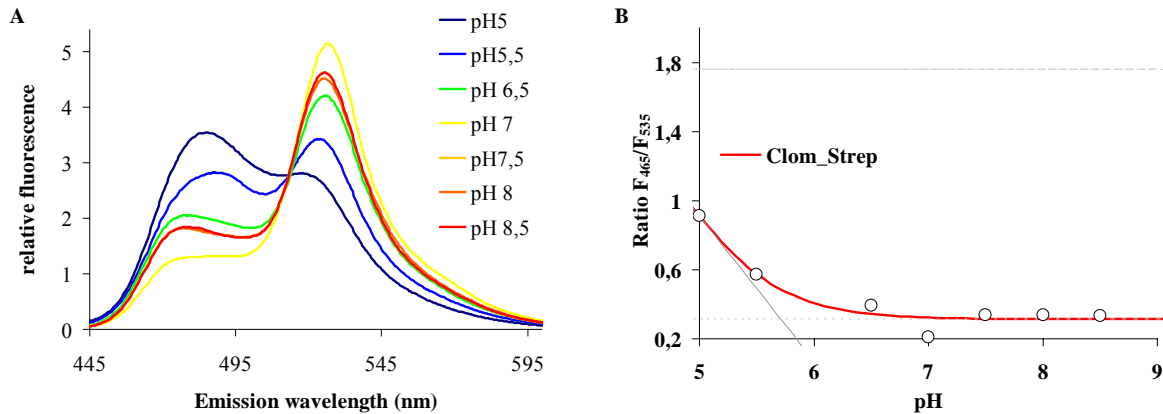
To monitor changes of  $[Cl^-]$  in the cytoplasm of plant cells an anion sensitive indicator named Clomeleon was used (Kuner, Augustine, 2000). The indicator consists of two fluorescent molecules – topaz YFP and the CFP, whose spatial arrangement allows Förster resonance energy transfer (FRET). FRET is a fast excited state reaction, where energy is transmitted radiationless from a fluorescent molecule (donator, here CFP) to a near receiver molecule (acceptor, here topaz YFP). FRET is a dipole-dipole interaction in the near field. Thus, an overlap of the dipole fields of both, the donator and the acceptor (2-10 nm), is necessary. If the acceptor is also a fluorescent molecule, energy is emitted as fluorescent light. Illumination of Clomeleon with blue light (434 nm) excites the CFP (480 nm), and triggers radiationless FRET to YFP (530 nm). The CFP itself fluoresces weakly. By increasing the chloride concentration, the YFP continuously loses its absorbance properties (**Figure 18**). The  $Cl^-$  binding at two sites of the YFP near the chromophore converts the protein into a non-absorbing state (Kuner & Augustine, 2000; Wachter *et al.*, 2000). Consequently, the ratio of CFP to YFP emission maxima can be calibrated in terms of  $[Cl^-]$  and thus Clomeleon can be used as a ratiometric indicator for  $[Cl^-]$  (**Figure 18B**). In order to quantify chloride concentrations in plants, *Arabidopsis thaliana* was stably transformed with Clomeleon and used for *in vivo* measurements previously (Lorenzen *et al.*, 2004). The spectral properties of Clomeleon expressed in plant cells were different from Clomeleon protein purified with N-terminal His-tag. This was possibly due to cleavage by proteases during purification. This gave shorter fragments of the indicator protein and consequently a spectral shift in favour of the CFP emission (**Figure 18A, B**). Therefore a Strep II tag was cloned at the C-terminus and the protein was purified with the help of both tags. The emission spectra under normal (oxidized) conditions were recorded (**Figure 18C, D**). Still, the comparison with emission ratios from plants was not satisfactory. The cytoplasm of plants has a reducing environment. Therefore, Clomeleon was again purified, however under reducing conditions (5 mM DTT) and the spectral properties were analyzed (**Figure 18E, F**). Reduced and oxidized Clomeleon produce different emission spectra. The YFP-derived peak at 535 nm is higher with all screened NaCl concentrations when Clomeleon is reduced. Hence, only the reduced spectra can be used for calibration and for reliably converting the results obtained from *in planta* studies into chloride concentrations. Since Clomeleon is also  $NO_3^-$  sensitive (Lorenzen *et al.*, 2004), the conversion to absolute  $[Cl^-]$ , especially in plants grown on nitrate containing media, would not deliver precise values. Therefore, all results from superfusion experiments (**Figures 23 - 47**) display only the relative changes in the emission ratio  $F_{465}/F_{535}$ , when dealing with Clomeleon, during different treatments.



**Figure 18: The emission spectra of Clomeleon**

The proteins were purified by **A**: His-tag only with oxidized buffers **C**: His-tag and Strep tag with oxidized buffers **E**: His-tag and Strep tag with reduced buffers. The schemes in A, C and E show the normalized spectra in presence of different chloride concentrations. All spectra are normalized by their area. The gray curves represent the corresponding minimax spectra (maximum fluorescence difference for each wavelength). Each minimum designates the isosbestic point. **B**, **D** and **F**: Dependency of the respective fluorescence emission ratios  $R(434_{ex}; 465_{em} \text{ and } 535_{em})$  of Clomeleon on chloride. A sigmoidal Boltzmann function was fitted to the ratio data.

Also pH cross-sensitivities of Clomeleon were screened in course of this study (**Figure 19**). In the cytoplasm of plant cells a pH around 7.6 is present. Thus, even an extreme change in the pH by 1 unit would affect Clomeleon only insignificantly.



**Figure 19: pH sensitivity of the genetically encoded Cl<sup>-</sup>indicator**

**A:** Emission spectra of Clomeleon (Clom-Strep) at  $\lambda_{\text{ex}} = 434$  nm under reduced conditions and different pH. **B:** Dependency of fluorescence emission ratios  $R(434_{\text{ex}}/465_{\text{em}}; 535_{\text{em}})$  of reduced Clomeleon on pH. All spectra are normalized by their area. Sigmoidal Boltzmann function was fitted to the ratio data.

#### 3.1.4.4 Co-expression study with dsRED and PtGFP

Biolistic micro-projectile bombardment (**Section 3.1.12**) is widely used for transient protein expression in plant cells. However, the efficiency of this procedure often varies and protein expression is mostly invisible. Therefore, it is useful to co-express a fluorescent reporter protein in order to easily distinguish transfected cells from unaffected ones within the bombarded specimen. However, the expression of the reporter does not necessarily report the expression of the target gene and vice versa, the absence of fluorescence in a cell is not necessarily equivalent to the absence of the co-bombarded target gene. The percentage of co-expression within the bulk of cells was assumed to be dependent on the molar ratio of both constructs used for coating the microparticles. In order to verify this hypothesis two constructs were used for co-transfection of leek epidermal cells: a peroxisomal PtGFP and a cytosolic red fluorescent protein (DsRed), both in a pART7 vector under the control of a single CaMV 35S-promoter. Gold particles were coated with different molar ratios of the reporter constructs. The biolistic bombardment procedure was performed as described in **Section 3.1.12**. A fluorescence ratio imaging workstation (**Section 3.1.5.1**) was used to quantify red ( $F_{\text{ex}470}; F_{\text{em}620}$ ) and green ( $F_{\text{ex}470}; F_{\text{em}530}$ ) fluorescence from whole cells. The  $F_{\text{em}530}/F_{\text{em}620}$ -ratio was correlated over a wide range with the molar ratio of the DNA constructs used for co-bombardment (**Figure 45**).

### 3.1.5 Fluorescence imaging, calibration procedures and data processing

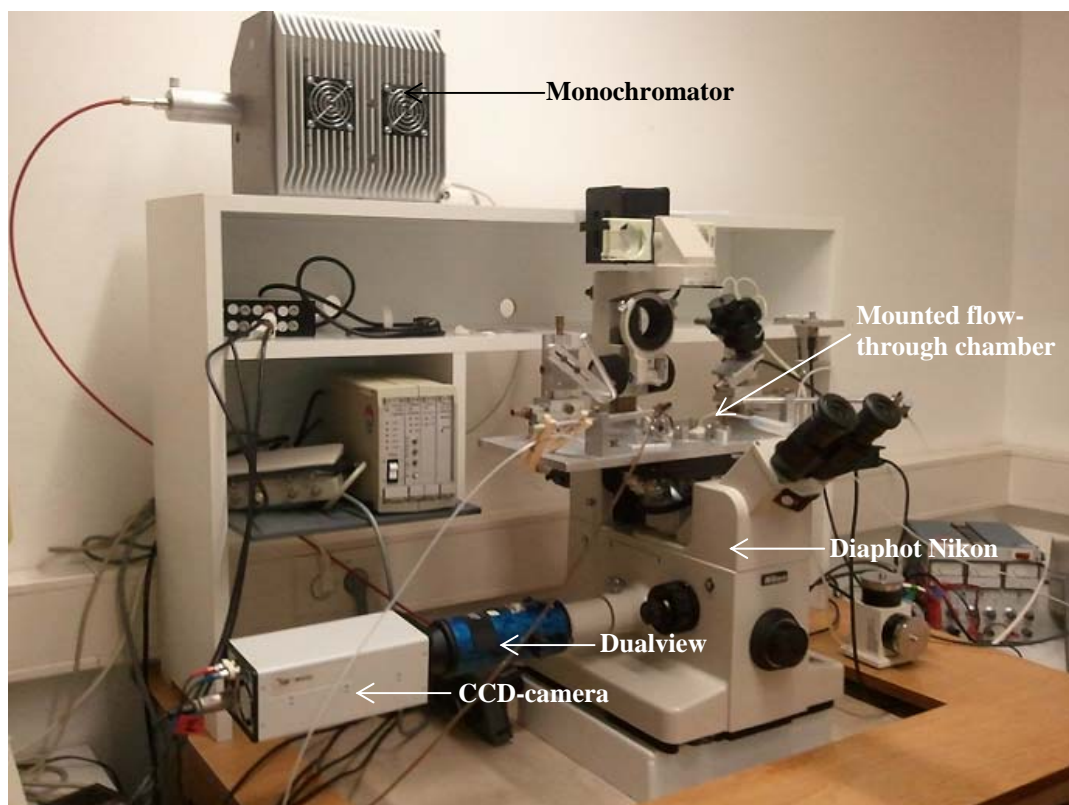
#### 3.1.5.1 Ratio imaging workstation

Fluorescence imaging was performed essentially as described (Gao *et al.*, 2004; Lorenzen *et al.*, 2004). Briefly, fluorescence images were taken with a ratio imaging system from TILL-Photonics fitted to an inverted microscope (**Figure 20**, Diaphot, Nikon, Düren DE) using light from a monochromator (Polychrome IV, TILL Photonics, DE). In the excitation beam path a filter cube

supplemented with filters and mirrors for each protein as indicated in the **Table 5**. For dual emission image recording a MultiSpec Micro-Imager DUAL VIEW (manufactured by Optical Insights, LLC) was mounted onto the microscope. An image splitting filter holder allowed using this assembly for all other measurements too, simply by switching between multi-spectral (split-field) and full-spectrum (full-field) imaging. A CCD-camera (Imago QE, TILL Photonics, DE) was connected to the DUAL VIEW and the TILLVision 4.0 software (TILL Photonics, DE) was used to collect images.

**Table 5: Parameters of excitation beam path filters for fluorescence imaging of different fluorescent indicators.**

FP variant	Excitation beam path	
	Filter	Dichroic mirror
ptGFP	HQ 535/50	500 dextr
Ratiometric GFP	HQ 535/50	500 dextr
S3roGFP	HQ 535/50	500 dextr
Clomeleon	Additional filter 435.8 nm	455 delp
dsRED/GFP	HC-BS 493/574	



**Figure 20: Ratio imaging workstation**

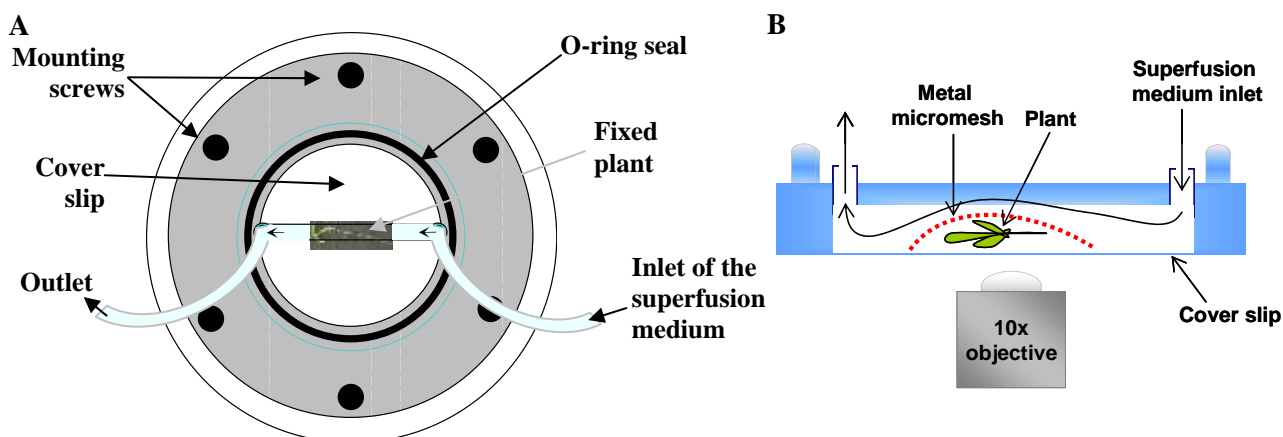
### 3.1.5.2 Calibration of fluorescent indicators

To calibrate recombinant fluorescent proteins *in vitro*, they need to be purified first (Section 3.1.13). The purified indicator proteins were assessed spectroscopically. Fluorescence spectra (Figures 15-19) of the proteins were taken with a fluorescence spectrometer (F-2500, Hitachi, Tokyo, JP or Cary Eclipse, Varian, US). The proteins were diluted 1:1000 (PtGFP, ratiometric pHluorin) and 1:500 (S3roGFP and Clomeleon) in 3 ml of the corresponding buffer placed in an acrylic cuvette. The buffers used are indicated in the respective figure legends (Figures 15-19) and their composition is listed in the **Suppl\_material 5**.

### 3.1.5.3 Data analysis

Spectra were normalized by their integral (i.e. the mean of fluorescence values over all scanned wavelengths  $\lambda$ ). The minimax spectrum  $F_{\text{minimax}}(\lambda)$  of a set of spectra is determined by subtracting the minimal fluorescence from the maximal fluorescence at each wavelength within the obtained set of spectra (i.e. within the scanned analyte concentration range). The isosbestic point ( $\lambda_{\text{iso}}$ ) is determined by looking for the global minimum in the minimax spectrum. Ideally, the minimax spectrum is zero at the isosbestic point (i.e.  $F_{\text{minimax}}(\lambda_{\text{iso}}) = 0$ ). The ratiometric sensitivity  $S$  is defined here by the integral of the minimax spectrum. Depending on the reporter protein analyzed, the sensitivity  $S$  is calculated either from the set of its excitation spectra ( $S_x$ ) or from its set of emission spectra ( $S_m$ ). The Boltzmann fit has been applied for fitting sigmoidal curves to calibration data. The fit parameter of the Boltzmann includes  $R_{\text{min}}$ ,  $R_{\text{max}}$ , and the apparent pK of the calibrated indicator. Fitting has been performed using Origin 7.0 (OriginLab Corp., Northampton, MA, USA).

### 3.1.5.4 *In vivo* experiments with transgenic plants



**Figure 21: Scheme of the flow-through chamber assembly**

**A:** Scheme of the flow-through chamber with fixed plant material **B:** Cross-section of the flow-through chamber.

For *in vivo* recording of fluorescence ratios transgenic *Arabidopsis* plants stably expressing the FPs, were grown on vertical agar plates for 6 – 14 days. Whole plants were placed in a perfusion chamber (**Figure 21**), fixed with metal micromesh, mounted in the ratio imaging workstation, and perfused with different solutions as indicated in the figure legends of the Result section. Fluorescence images were taken every 12 s. The hairy root segments of the maturation zone of the root were chosen as the region of interest for all experiments with *Arabidopsis* plants.

### 3.1.6 Cloning of chloride channels - RNA isolation and first-strand cDNA synthesis

*Arabidopsis thaliana* plants were grown for RNA isolation on sterile vertical agar plates containing 1.2 % plant agar and 1xMS medium for 3 weeks. Whole plants were harvested, except for the cloning of the cation-chloride-cotransporter (CCC). Here, the plants were grown sterile vertical agar plates containing 1.2 % plant agar and 1xMS medium supplemented with 50 mM NaCl in order to induce the expression of the transporter. Since the CCC is predominantly found at the xylem border, only the roots of plants were harvested. The material was shock frozen in liquid nitrogen and ground with mortar and pestle. The thawing of the ground plant material was avoided, in order to keep the RNAses inactivated. The RNA was isolated with a RNA plant isolation kit (Peqlab, Erlangen, DE) according to manufacturer's instructions. The concentration was then measured by NanoDrop ND-1000 (Peqlab, Erlangen, DE) and the quality of RNA tested on a 0.8 % agarose gel, stained with ethidium bromide, visualised by the GelDoc 2000 using the Quantity One 4.2.1. software (Bio-Rad, München, DE). Possible contaminations by genomic DNA were dealt with by DNase digestion in a first approach. Since problems occurred with complete inactivation of the DNase before starting the cDNA synthesis, this step was omitted for all following reactions and the size of the fragments after the PCR reaction was taken as a determining factor.

For first-strand cDNA synthesis 1 µg of RNA was mixed with 1 µl Oligo(dT)<sub>15</sub> primer (Promega, Mannheim, DE), brought to an end volume of 15 µl with nuclease-free water, and incubated for 10 min at 65°C. The mix was immediately placed on ice. 1 µl 40 mM dNTP's, 4 µl ImProm-II™ 5x reaction buffer and 1 µl ImProm-II™ reverse transcriptase (Promega, Mannheim, DE) were added and incubated for 60 min at 42°C. Reverse transcriptase was heat-inactivated at 75°C for 15 min.

### 3.1.7 Cloning of chloride channels - specific PCR

For the PCR reactions with specific primers 5 µl of the cDNA synthesis product were used. 5 µl 4x GoTaq® green buffer (Promega, Mannheim, DE), 1.5 µl 25 mM MgCl<sub>2</sub>, 1 µl 40 mM dNTP's, 1 µl forward primer (10 pMol), 1 µl reverse primer (10 pMol), 0.3 µl/1.5 Units GoTaq® Polymerase (Promega, Mannheim, DE) were added to the synthesis product and adjusted to an end volume of 20 µl with nuclease-free water. A gradient PCR was carried out for all primer pairs as a first step to identify the optimal conditions. Subsequent reactions were carried out with primer specific



annealing temperatures (**Suppl\_material 6**) and elongation times corresponding to the length of the given construct (see **Introduction**; **Table 1**). The PCR reaction mix was applied on a 0.8 % agarose gel, stained with ethidium bromide and visualised on a GelDoc 2000 using the Quantity One 4.2.1. software (Bio-Rad, München, DE).

### 3.1.8 DNA isolation and ethanol precipitation

The fragments with the appropriate size were cut out of the gel and purified through a self-made filter. The gel slice was put in a 0.5 ml tube filled with filter material (JBL Symec) with a small hole in the bottom. This tube was capped, placed in a 1.5 ml tube and centrifuged for 5 min at 3.200 rpm/2800 g at RT. The flow-trough was collected in the lower tube and the volume was determined for ethanol precipitation.

1/10 Vol 1 M NaAc pH 5.5 and 2.5 Vol 100 % ethanol were added and mixed together thoroughly. The tube was for 2 min placed in liquid N<sub>2</sub> (or 30 min at -80°C alternatively) and spun down for 5 min at full speed and 4°C. The supernatant was removed completely and the pellet was mixed with 500 µl of 70 % ethanol. Another centrifugation step followed (as above) and the pellet was dried completely. The pellet was then taken up in nuclease-free water and used for restriction digests according to the cloning strategies for each chloride channel (**Suppl\_materials 7-15**).

### 3.1.9 Restriction digest and ligation

Restriction digests were performed according to the cloning strategies individually designed for each channel (**Suppl\_materials 7-15**) with enzymes and buffers obtained from Promega and NEB (**Suppl\_material 3**). The purified chloride channel DNA obtained from specific PCR was digested with two enzymes either in parallel or in two subsequent steps. The destination vectors (**Table 6**, **Suppl\_material 16**) were digested in the same way and dephosphorylated with SAP thereafter in order to minimize the re-ligation possibility.

**Table 6: Vectors used in this study**

Vector	Characteristics	Reference
pBluescript®II SK(+/-) pBluescript®II KS(+/-)	PT3, PT7, fl origin, Amp <sup>R</sup> , <i>lac</i> -operon, MCS	Stratagene (La Jolla, USA)
pQE30	PT5, <i>lac</i> -operon, RBS, ATG, His-Tag, MCS, ori Col E1, Amp <sup>R</sup>	Qiagen (Hilden, DE)
pART7	fl origin, 35S CaMV-promotor, MCS, Amp <sup>f</sup> , ocs-terminator	Gleave (1992)

The ligation reaction was assembled in a vector:insert molar ratio of 1:1 or 1:3, depending on the size of the insert, using the T4-DNA ligase (Promega, DE).

### 3.1.10 Transformation of bacteria by electroporation

Before electroporation, the DNA from the ligation was ethanol-precipitated (**Section 3.1.8**) to remove excess salts and taken up in 10 µl Milli-Q H<sub>2</sub>O. If the DNA was obtained from a plasmid purification procedure (**Section 3.1.11**), additional ethanol precipitation was omitted. The DNA

concentration never exceeded 150 µg/µl. Aliquots of frozen electro-competent cells were thawed on ice. 45 µl of cells were mixed with 5 µl of the ligation mix and transferred into a pre-cooled electroporation cuvette (gap width = 1 mm). Gene Pulser<sup>®</sup>II (Bio-Rad, DE) was adjusted to a voltage of 1.8 kV for transformation of *E.coli* and 1.2 kV for transformation of *A. tumefaciens*; the resistor to 200 Ω in the low range and 500 Ω in the high range; and the capacitor to 25 µF. The cuvette was placed into the electroporation device. The electroporation itself was performed by a single short electrical pulse (time constant  $RC = \tau = 5$  ms). Immediately after transformation 300 µl of LB medium without antibiotics were added into the cuvette, mixed with the bacteria-DNA suspension and transferred into a fresh 1.5 ml tube. The bacterial cells were allowed to grow for 45 min or even longer (depending on the size of the plasmid) at 37°C to replicate a sufficient copy number of the inserted plasmid. Afterwards, the cells were spread onto an LB-agar plate with the respective antibiotics in order to select the transformed from untransformed cells. The plates were kept at 37°C over night. The success of ligation was verified by an adjacent colony PCR reaction with respective primer pairs.

### 3.1.11 Isolation of DNA

Small amounts of DNA for control restriction digest and subsequent sequencing were isolated from 5 ml ON cultures using the QIAprep Spin miniprep kit (Qiagen, Hilden, DE) and/or the Plasmid Quick pure kit (Macherey-Nagel, Düren, DE) according to manufacturer's instructions. The only difference to the given protocols included the usage of pre-warmed Milli-Q water instead of the elution buffer to elute the DNA from the spin columns. The concentration of DNA, measured by NanoDrop ND-1000 (Peqlab, Erlangen, DE), averages between 80 and 200 ng/µl.

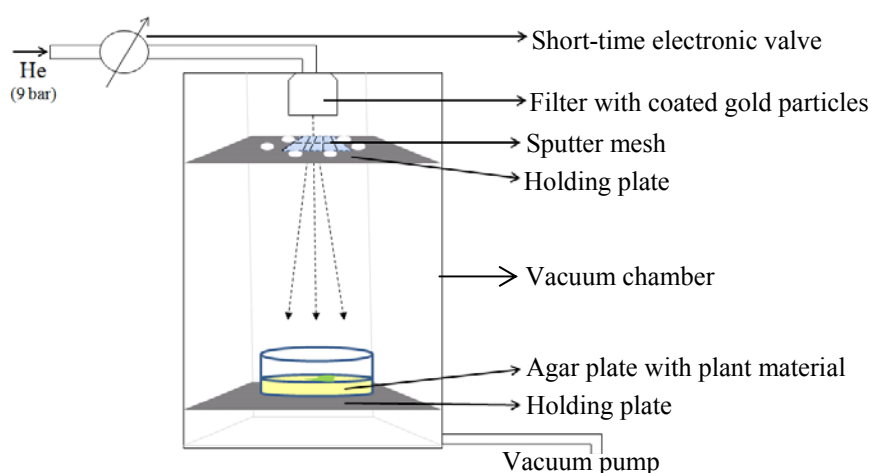
Isolation of larger amounts of DNA was performed by the CompactPrep Plasmid Midi Kit (Qiagen, Hilden, DE) from 50-100 ml ON cultures. These amounts (600-1200 ng/µl) were needed for the cloning procedures and for the biolistic transformation of leek and onion epidermal cells.

### 3.1.12 Biolistic transformation of leek (*Allium porrum*) and onion (*Allium cepa*) epidermal cells

At least 8 months are necessary to obtain sufficient number of stably transformed *Arabidopsis thaliana* plants with the floral dip method (Clough & Bent, 1998). To achieve results faster and more effectively, transient transformation procedure is of advantage. Therefore, biolistic transformation (Klein *et al.*, 1987; Sanford *et al.*, 1987) was applied in order to get transformed plants in much shorter time. Since in *Arabidopsis thaliana* all chloride channels are expressed constitutively, it is also possible, that some of them have redundant functions (Moradi, 2009). All co-expression studies of individual channel constructs with chloride indicators were therefore carried out in leek and onion epidermal cells.

Gold particles (Chempur, Karlsruhe, DE, diameter 1.5 - 4  $\mu\text{m}$ ) were prepared by washing a small portion (50-100 mg) twice with 500  $\mu\text{l}$  of 100 % ethanol and three times with sterile Milli-Q water. The excess water was removed completely and the pellet was dried for 30 min at RT. The gold particles were dissolved in water (0.25 mg/ $\mu\text{l}$  w/v) and 20  $\mu\text{l}$  aliquots (approx. 5 mg particles) were prepared and stored at  $-20^{\circ}\text{C}$  until further procedures. One aliquot of gold particles coated with 8-10  $\mu\text{g}$  DNA is sufficient for 5 transformations (biolistic shots). Leek and onions were obtained in a local supermarket. The epidermis was peeled carefully and pieces as large as possible were placed on 1.2 % agar plates containing 1 x MS medium.

One aliquot of gold particles was spun down and the water removed. The respective vector DNA (plant expression vector pART 7 carrying the gene of interest) was diluted or concentrated to obtain a final amount of 8-10  $\mu\text{g}$  in a volume up to 50  $\mu\text{l}$  and added to the gold pellet. For the co-expression of two constructs, 8-10  $\mu\text{g}$  of each construct were adjusted to give an equimolar ratio. The remaining volume (to 50  $\mu\text{l}$ ) was filled up with nuclease-free water. Then 50  $\mu\text{l}$  of 2.5 M  $\text{CaCl}_2$  (sterile-filtered) were added and mixed thoroughly on a vortex. Keeping the sample vortexing, 20  $\mu\text{l}$  of 0.1 M spermidine (sterile-filtered) were added. The tube was then vortexed for further 2.5 min. 3x100  $\mu\text{l}$  of 100 % ethanol ( $-20^{\circ}\text{C}$ ) were subsequently added to the vortexing sample. The tube was closed and immediately transferred to liquid  $\text{N}_2$  for 2 min for complete precipitation of the DNA. The DNA attached to the particles was spun down at full speed for 4 min. The supernatant was removed completely, in order to avoid clumping of gold particles. The pellet was resuspended in 50  $\mu\text{l}$  of nuclease-free water and evenly distributed on 5 Swinnex filters (Millipore, Medford, USA). The prepared plates and the filters were placed in a custom-made gene gun with vacuum chamber (**Figure 22**; reproduced from original deposited at the University of Freiburg).



**Figure 22: Illustration of the gene gun with a vacuum chamber**

Vacuum was applied ( $<100$  mBar) and a volume of ca. 3 ml of helium gas at 9 bar was released to shoot the particles onto the sample. All steps after dissolving the particles in water were carried out as quickly as possible, to minimize the release of DNA from the particles. The transformed

epidermis pieces were incubated in tightly closed Petri dishes over night in the dark at room temperature. The next days the results of the transient transformation were examined by fluorescence microscopy.

### 3.1.13 Purification of recombinant indicators and chloride channel proteins

In order to purify recombinant fluorescent indicators for *in vitro* calibration (Section 3.1.5.2), the column affinity chromatography was applied. The tagged proteins were purified and concentrated through a *Strep*-Tactin sepharose column and/or Ni<sup>2+</sup>/NTA-agarose column.

Purifying soluble membrane proteins requires a sophisticated protocol, which depends on the protein to be purified. For *Arabidopsis thaliana* chloride channels the protocol from Dutzler *et al.* (2002), which was originally used for purification of chloride channels from *Escherichia coli* and *Salmonella typhimurium* was adapted.

#### 3.1.13.1 Expression of proteins and cell lysis

*Escherichia coli* SG13009 competent cells (Qiagen, Hilden, DE) were transformed with the respective pQE30 vector carrying the gene of interest. 250 ml bacterial cultures in LB-medium were grown (rotary shaker, 37°C, 200 rpm). To prevent foaming 40 mg/l of Simethicon® (Ratiopharm, DE) were admixed to the LB-medium. The production of protein was induced by adding 1 mM IPTG at an OD<sub>600</sub> = 0.8-1. The cells were kept shaking at 37° for 1 hour after addition of IPTG, before the temperature was decreased to 20°C for 5°hours. The bacterial cultures were centrifuged with 4.700 g at 4°C for 1 hour (Multifuge Heraeus 3 S-R, VWR, DE) and the cell pellet from 250 ml bacterial culture was resuspended in 10 ml ice-cold KPP buffer. The suspension was then placed on ice and sonicated on level 5 (Sonoplus 2200 equipped with the sonotrode MS 73, Bandelin, DE) 3 x 1 min at 30 % power. The sonicated cells were kept at -20 C for 30 min and centrifuged subsequently with 4700 g for 1 hour at 10 C to remove the bacterial debris. When the suspension was clear, a subsequent filtration through a 0.45 µm membrane filter was omitted.

For test expression of AtClC-A only 50 ml bacterial cultures in LB-medium were grown (rotary shaker, 37°C, 200 rpm), whereas for purification of larger amounts of protein, 4-6 l cultures were needed. To prevent foaming Simethicon® (Ratiopharm, DE) was added as described above. The IPTG induction and further incubation were performed as described above. The bacterial cultures were centrifuged with 4.700 g at 4°C for 1 hour (Multifuge Heraeus 3 S-R, VWR, DE) and the cell pellet from 1 l bacterial culture was resuspended in 10 ml solubilization buffer. The subsequent sonification was applied as above. Afterwards, n-dodecyl-β-D-maltoside or other non-ionic detergents were added to reach 50 mM and the suspension was kept at room temperature for 2 hours. After the incubation the cell debris was separated from the dissolved protein by centrifuging it twice at 75.600 g (Avanti J-25 equipped with JA-10 rotor, Beckmann Coulter, DE).

For FPLC analysis the suspension was diluted to reach a volume of 50 ml with the solubilization buffer containing n-dodecyl- $\beta$ -D-maltoside and filtered through a 0.2  $\mu$ m PVDF membrane filter, in order to avoid plugging of the capillaries and valves of the ÄKTA Purifier system by cell debris.

#### 3.1.13.2 *Sodium Dodecyl Sulphate PolyAcrylamide Gel Electrophoresis (SDS PAGE)*

SDS-PAGE was performed according to a modified protocol from Shapiro *et al.* (1967). To detect the chloride channel proteins a 15 % separation gel with 7.5 % stacking gel was used. The purified protein mixtures were boiled in reducing Laemmli buffer (Laemmli, 1970). The gel was run at a constant current of 40 mA in a vertical electrophoresis system (Bio-Rad, DE). As a reference, LMW marker was used, containing 6 protein calibration standards as described in the manufacturer's manual. Coomassie staining (over night on a horizontal shaker) and destaining (until the non-specific staining disappeared) were carried out.

#### 3.1.13.3 *Streptavidin affinity chromatography*

Purification with two subsequent affinity chromatography steps was established for Clomeleon. In addition to the N-terminal His-tag, on the C-terminus of the proteins a *Strep*-tag II was cloned (**Suppl. material 17**). Using two affinity chromatography steps (N-terminal His-tag and C-terminal Strep II-tag) sequentially, it is possible to obtain highly purified protein without protease-cleaved fragments. The protein purification using the Strep-tactin sepharose columns (IBA, Göttingen, DE) was performed according to the manufacturer's instructions. Subsequently, a Ni<sup>2+</sup>-NTA affinity chromatography was carried out and the protein purified by gel filtration.

#### 3.1.13.4 *Ni<sup>2+</sup>-NTA affinity chromatography*

Ni<sup>2+</sup>-NTA (nitrilotriacetic acid, Qiagen, Hilden, DE) resin was used for purifying recombinant FPs carrying an affinity tag of six consecutive histidine residues - the 6xHis tag. By cloning of the fluorescent protein-DNA in frame into the MCS of the pQE30 vector, the tag is attached to the N-terminus of the protein automatically during translation. This allows the purification of the protein by Ni<sup>2+</sup>-NTA affinity chromatography.

2 ml of the Ni<sup>2+</sup>-NTA resin were pipetted into a 10 ml polypropylene column. The beads were equilibrated with 10 CV WB1 and the protein suspension was loaded on the column. The beads were mixed with protein suspension thoroughly. The bound protein was washed with 10 CV WB2. To elute the protein from the beads 3 ml of EB were applied. Only the fluorescent fractions were collected and directly applied on the gel filtration column (NAP 25). The same procedure was utilized for reduced proteins. Reducing buffers were used instead the standard buffers. The column was washed with 10 CV of WB1 and stored in 20 % ethanol. The same procedure was utilized for reduced proteins. Reducing buffers (up to 5 mM DTT) were used instead the standard buffers.

In order to test the protein expression and solubilization conditions for AtClC-A, affinity chromatography was applied. For purification of chloride channel protein the same procedure as above was used with buffers as described in the **Section 3.1.2**. To elute the protein from the beads 3 ml of EB were applied and 6x0.5 ml fractions were collected.

#### *3.1.13.5 Gel filtration*

NAP-25 gel filtration columns were used for purification of the FP suspension from imidazole. The equilibration, loading and washing of the column were carried out according the manufacturers instructions by using wash buffer 1 (WB1). The elution was carried out with 3 ml WB1 and the fluorescent fraction was collected. The resin was washed with 10 CV of WB1 and stored in 20 % ethanol.

The 6 fractions of the chloride channel protein eluted from the Ni<sup>2+</sup>-NTA column were first analyzed by SDS-PAGE. Subsequently, the fractions containing the desired protein were pooled and applied on the equilibrated NAP-25 column (not more than 2 ml). The equilibration was carried out by washing it six times with WB1. If the volume of the pooled fractions was lower than 2 ml, the remaining volume was filled up with WB1. The proteins were eluted with 3 ml WB1, 6 fractions were collected and analyzed on the SDS-PAGE.

#### *3.1.13.6 Fast Protein Liquid Chromatography (FPLC) analysis*

With the FPLC it is possible to elute the protein bound onto an affinity column with a continuous concentration gradient of the competitive substance. Therefore, firstly FPLC was applied with a protein in order to determine the best purification conditions. The second step was performed with well-defined conditions for obtaining a reasonable amount of pure protein. The FPLC analysis was carried out on the ÄKTA Purifier (GE Healthcare, DE) with a 1 ml HisTrap<sup>TM</sup> HP column (GE Healthcare, DE) at 4°C. The system was operated via external computer by the UNICORN®-Software (GE Healthcare, DE). The conductivity and the absorption at 280 nm and 254 nm were measured during entire purification procedure by a conductivity detector (Cond-900) and a UV-detector (UV-900), respectively.

According to the manufacturer's instructions the column was equilibrated and washed with 10 column volumes (CV) of filtered 20 % ethanol and subsequently with the same volume of Milli-Q water and wash buffer I, all at a flow rate of 0.5 ml/min. A super-loop capillary was attached to the injection valve, washed with the wash buffer I and into it the protein suspension (50 ml, **Section 3.1.13.1**) was loaded. A maximum pressure of 0.45 mPa was set up with a flow rate depending on the purity of the injected sample (up to 0.8 ml/min, but mostly much lower). After the sample was loaded on the column, the column was washed with the wash buffer II until a stable conductivity was achieved and a continuous concentration gradient between 10 (wash buffer II)

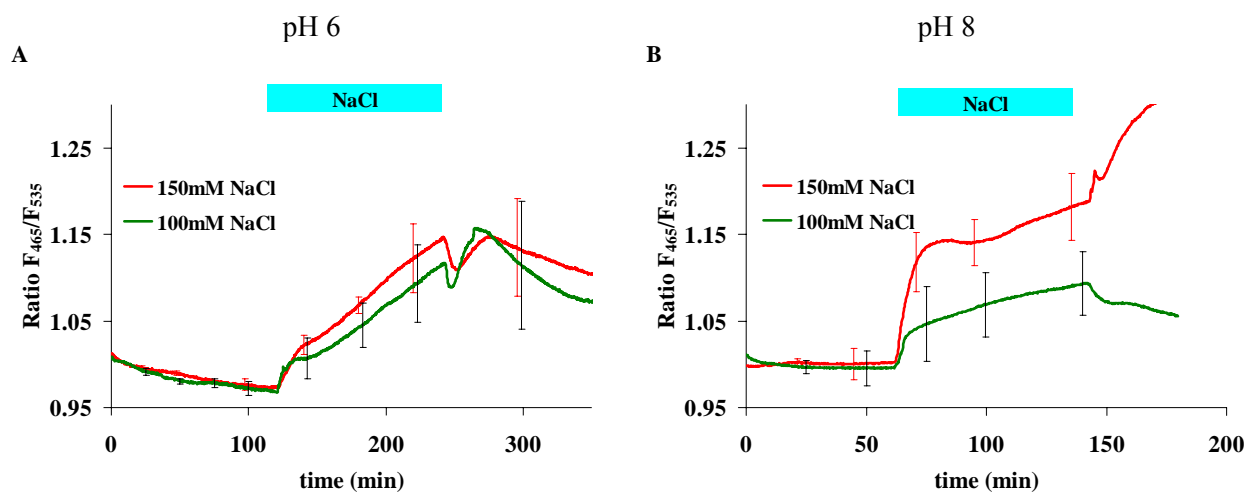
and 100 mM imidazole (elution buffer) was run. 1 ml fractions were collected in glass-tubes (placed in a fraction-collector) until the entire gradient has passed and subsequently analyzed by SDS-PAGE.

## 3.2 RESULTS

### 3.2.1 Ratiometric quantitation of salt stress-induced chloride influx

#### 3.2.1.1 Chloride influx into *Arabidopsis* root cells exhibits two distinct phases- the fast “depolarisation phase” and the slow “saturation phase”

High external concentrations of NaCl (150 mM) were applied to *Arabidopsis* root cells expressing Clomeleon. The results show, that the chloride influx exhibits two distinct phases during exposure to salt stress (**Figure 23A**). The faster part of the kinetic lasts for few minutes and is named here the “depolarisation phase”, describing the assumed passive chloride influx due to sodium triggered membrane depolarisation (more details in the **Section 1.2.2**). After a while (approximately 8 min) the chloride influx declines and a second phase begins – the slow “saturation phase”. Both phases are dependent on the extracellular pH. When changing the pH of the flow-through medium from pH 6 (**Figure 23A**) to pH 8 (**Figure 23B**), the application of 150 mM NaCl (**Figure 23B**, red curve) leads to exaggerated chloride influx during the depolarisation phase. This suggests that protons may play a role. An effect of higher pH is also visible in the saturation phase. High pH obviously inhibits the chloride influx with both screened NaCl concentrations. These results are discussed later in the **Section 3.3.3**.

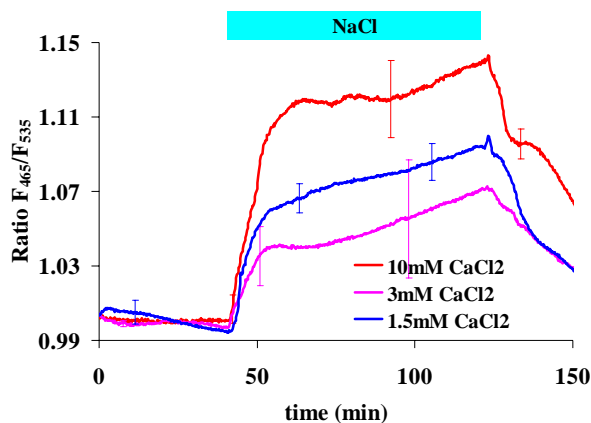


**Figure 23: Kinetics of chloride influx at different pH with two NaCl concentrations**

Flow-through *in vivo* experiments with *Arabidopsis thaliana* plants grown on full MS. Experiments were carried out in a buffer system containing **A**: 5 mM MES/KOH (pH = 6.0) with no SM (no additional salts); and **B**: 5 mM HEPES/KOH (pH = 8.0) with no SM. 100 mM and 150 mM NaCl were applied after 120 min (A) and 60 min (B). All curves are averages from 5 independent experiments. The data were normalized by the mean of the time interval  $5 \text{ min} \leq t \leq 15 \text{ min}$ . Error bars represent StDv.

### 3.2.1.2 Chloride influx is dependent on calcium

The differences in chloride influx due to changing  $[Ca^{2+}]$  in the external flow-through medium and varying internally available  $[Ca^{2+}]$  were elaborated (**Figure 24**). The latter was achieved by growing *A. thaliana* plants expressing Clomeleon on 0.5 x MS agar plates without  $CaCl_2$ , with 1.5 mM  $CaCl_2$  (standard  $[Ca^{2+}]$ ) and 10 mM  $CaCl_2$ , respectively. In order to remove calcium completely, EGTA was added to the growth medium. However, EGTA completely inhibited the germination (data not shown). The results of flow-through salt stress experiments with different internal  $[Ca^{2+}]$  availability (**Figure 24**) deliver at first glance inconsistent results. Plants grown on 0.5 x MS (1.5 mM  $CaCl_2$ ) show an enhanced chloride influx in comparison to plants grown on full MS (3 mM  $CaCl_2$ ); whereas 10 mM  $CaCl_2$  in the growth medium has an accelerating effect. This effect can only be seen in the first phase, the saturation phase is largely unaffected. Possible reasons for these findings are considered in the **Section 3.3.2**. To eliminate the possibility that added chloride (20 mM) caused the contradictory results, the same superfusion experiments were carried out with plants grown on 50 mM NaCl. No differences in chloride influx compared to control experiments could be found (data not shown).

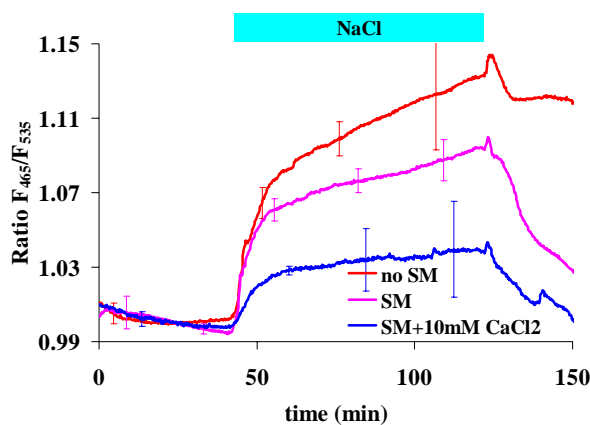


**Figure 24: Effect of internal calcium supply at the chloride influx during salt stress**

Superfusion experiments with *Arabidopsis thaliana* plants grown on half strength MS (blue curve), full MS (pink curve) and full MS containing altogether 10 mM  $CaCl_2$ . Experiments were carried out in a buffer system containing 5 mM MES/KOH (pH = 6.0) supplemented with SM (0.1 mM  $CaCl_2$ , 0.1 mM  $MgCl_2$ , 0.1 mM KCl). 150 mM NaCl were applied after 40 min. All curves are averages from 4 independent experiments. The data were normalized by the mean of the time interval  $5 \text{ min} \leq t \leq 15 \text{ min}$ . Error bars represent StDv.

The results of flow-through experiments with *Arabidopsis thaliana* plants expressing Clomeleon grown on half strength MS show that the extent and the rate of the chloride import are also regulated by external  $[Ca^{2+}]$  (**Figure 25**). Omitting  $Ca^{2+}$  during the entire experiment, leads to acceleration of chloride influx during the fast phase (**Figure 25**, red curve). Addition of 10 mM  $CaCl_2$  inhibits the “depolarisation phase”. Generally, the higher the externally applied  $[Ca^{2+}]$ , the less pronounced is the first phase. During the “saturation phase” a dependency on external  $[Ca^{2+}]$  becomes obvious too. **Figure 25** (blue curve) shows for example, that 10 mM  $CaCl_2$  are able to inhibit the chloride influx considerably during in this phase.



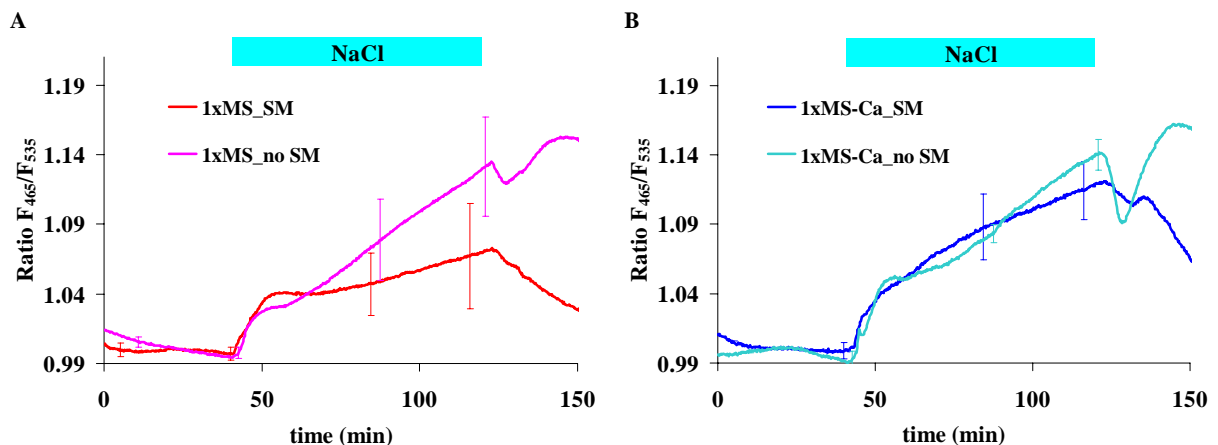


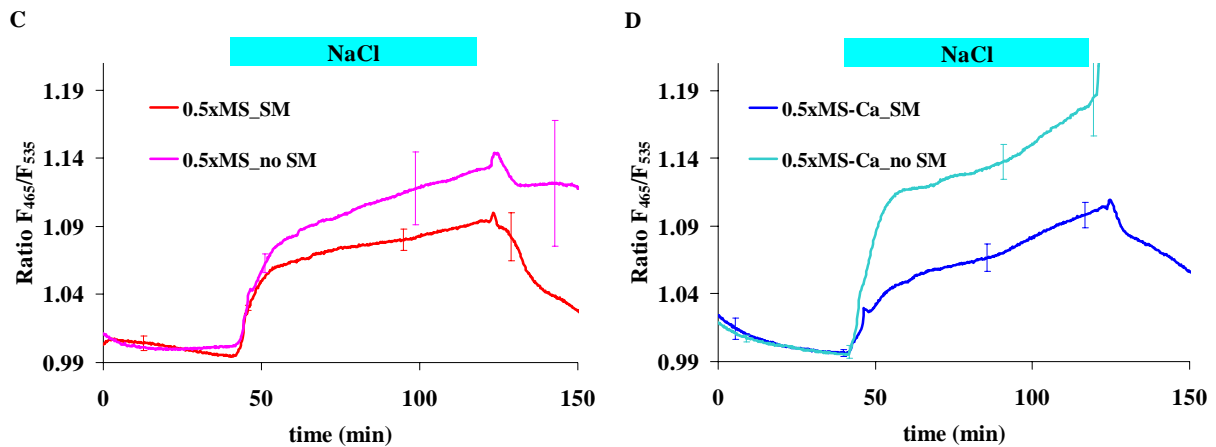
**Figure 25: Kinetics of chloride influx during salt stress at different  $\text{CaCl}_2$  concentrations**

*Arabidopsis thaliana* plants grown on half strength MS were treated with a buffer system containing 5 mM MES/KOH (pH = 6.0) with no additional salts (no SM); or supplemented with 0.1 mM  $\text{CaCl}_2$ , 0.1 mM  $\text{MgCl}_2$ , 0.1 mM KCl (SM); or 10 mM  $\text{CaCl}_2$ , 0.1 mM  $\text{MgCl}_2$ , 0.1 mM KCl (SM+10 mM  $\text{CaCl}_2$ ). 150 mM NaCl were applied after 40 min. All curves are averages from 5 independent experiments. The data were normalized by the mean of the time interval  $5 \text{ min} \leq t \leq 15 \text{ min}$ . Error bars represent StDv.

Different kinetics were obtained with plants grown on 1 x MS agar plates by superfusing them with buffers with or without SM during the entire experiment (**Figure 26A**). When compared to plants grown on 0.5 x MS (**Figure 26B**) the effect of the internally available calcium is visible. In plants having higher internal  $[\text{Ca}^{2+}]$  the additional  $\text{CaCl}_2$  in the flow-through medium does not alter the “depolarisation phase” (**Figure 26A**). However, the chloride concentration in the cytoplasm increases during the “saturation phase” much faster and after 80 minutes salt treatment the emission ratio reaches the same level as with plants grown on 0.5 x MS (**Figure 26B**, pink curve).

When comparing the  $\text{Cl}^-$  kinetics in plants grown on Ca-free 0.5xMS (**Figure 26D**, dark blue) and Ca-free 1xMS (**Figure 26B**, dark blue) it becomes obvious, that all other ingredients of the MS medium have no significant impact on the  $\text{Cl}^-$  transport, when Ca is present in the flow-through medium. However, omitting external calcium causes in plants grown on half strength MS (**Figure 26D**, light blue curve) increased chloride influx, probably due to instabilities of the plasma membrane. This is most prominent during washing-out the salt. Here, the hypo-osmotic shock obviously causes a rupture of the membrane. The effect of external and internal calcium availability is discussed in detail in the **Section 3.3.2**.

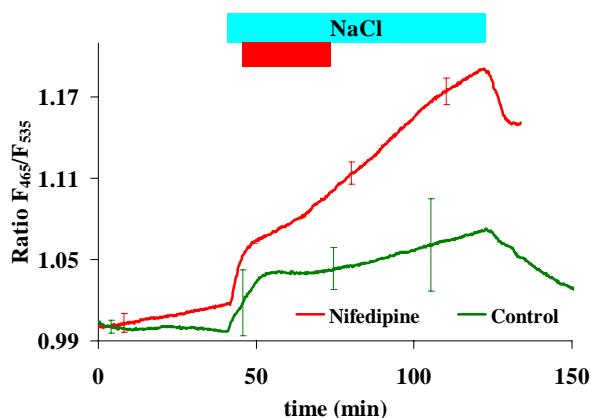




**Figure 26: Effect of different internal and external Ca availability on chloride influx**

Flow-through *in vivo* experiments with 6-14 days-old *Arabidopsis thaliana* plants expressing Clomeleon grown (A, B) on full MS either containing (1xMS) or lacking  $\text{CaCl}_2$  (1xMS-Ca). (C, D) represent plants grown on half strength MS either containing (0.5xMS) or lacking  $\text{CaCl}_2$  (0.5xMS-Ca). Each pair of experiments was carried out in a buffer system containing 5 mM MES/KOH (pH = 6.0) with no additional salts (no SM); or supplemented with 0.1 mM  $\text{CaCl}_2$ , 0.1 mM  $\text{MgCl}_2$ , 0.1 mM KCl (SM). 150 mM NaCl were applied after 40 min. All curves are averages from 5 independent experiments. The data were normalized by the mean of the time interval  $5 \text{ min} \leq t \leq 15 \text{ min}$ . Error bars represent StDv ( $n = 5$ ).

In order to determine how the externally applied calcium can influence the chloride transport, a calcium channel blocker - nifedipine - was used (Figure 27). Nifedipine, a dihydropyridine, blocks  $\text{Ca}^{2+}$  entry by binding to the  $\alpha_1$  subunit of voltage-gated channels (Tsien & Tsien, 1990). In the perfusion sequence, it was applied approximately 5 min after onset of salt stress, i.e. still in the “depolarisation phase”. Not surprising was, that no significant change in the depolarisation phase occurred. The effect of the calcium channel blocker on the “saturation phase” is comparable to the perfusion experiments without SM (Figure 26A, pink curve).



**Figure 27: Block of calcium channels by nifedipine**

Flow-through experiment with *Arabidopsis* root cells expressing Clomeleon, perfused with 5 mM MES/KOH, pH6 with SM; treated with 150 mM NaCl ( $t = 40 \text{ min}$ ) and 100  $\mu\text{M}$  nifedipine ( $t = 45 \text{ min}$ ). In the respective control experiment, plants were only treated with salt. Plants were grown on 1xMS for 6-12 days. The graph represents an average of at least 4 experiments. The data were normalized by the mean of the time interval  $5 \text{ min} \leq t \leq 15 \text{ min}$ . Error bars represent StDv.

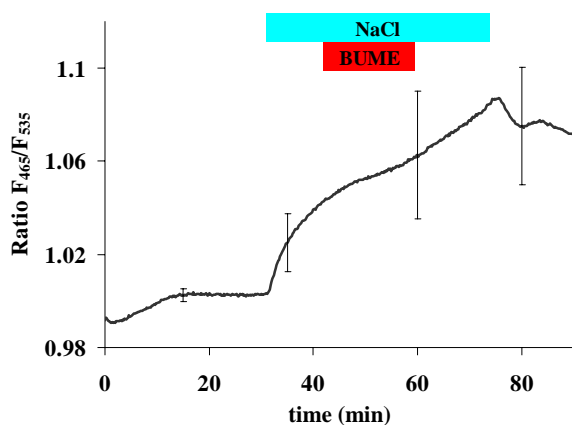
### 3.2.1.3 Chloride flux is sensitive to diuretics and some anion channel inhibitors

There are certain indications, that chloride under salt stress does not only enter the cell via anion channels, but probably is also transported via cation-chloride-cotransporters. At the plasma membrane of plant cells different chloride channels can be found. Only one putative cation-

chloride-cotransporter (AtCCC) localised probably at the plasma membrane was reported. In *Xenopus* oocytes, it was characterised as a bumetanide-sensitive  $\text{Na}^+\text{-K}^+\text{-2Cl}^-$ -cotransporter (NKCC, Colmenero-Flores *et al.*, 2007). Bumetanide belongs to the group of loop diuretics inhibiting the NKCCs specifically. In order to test what kind of channels and/or transporters play a role in the NaCl-induced chloride entry, the effect of different groups of diuretics and some typical channel blocker and inhibitors was characterised in more detail. Since the side effects of diuretics on plants are not adequately investigated, the results should be interpreted with caution (Section 3.3.4). The experiments with *A. thaliana* plants expressing Clomeleon were aimed on the “saturation phase” only, as here active chloride influx is proposed (Lorenzen *et al.*; 2004; Teakle & Tyerman, 2009).

The results of the experiments show that the diuretics (Figure 28, Table 7, highlighted gray) inhibiting the NKCCs in mammalian cells such as bumetanide (BUME, 100  $\mu\text{M}$ ), furosemide (FURO, 100  $\mu\text{M}$ ) and torasemide (TORA, 100  $\mu\text{M}$ ) have a capability to inhibit also chloride entry into plant cells partially (Colmenero-Flores *et al.*, 2007).

The inhibition rate is comparable to that of a known anion channel blocker indanyloxyacetic acid 94 (IAA-94, 100  $\mu\text{M}$ ); and twice as low as the inhibiting power of anthracene-9-carboxylic acid (A9C, 100  $\mu\text{M}$ ), also a potent anion channel inhibitor. 4, 4'-diisothiocyanatostilbene-2, 2'-disulfonic acid (DIDS, 5  $\mu\text{M}$ ) shows 60 % of the inhibiting capacity of A9C, whereas another anion channel blocker 5-nitro 9-(3-phenylpropylamino)benzoic acid (NPPB) appears to be ineffective (Table 7).



**Figure 28: Effect of the diuretic bumetanide on NaCl-induced chloride influx**

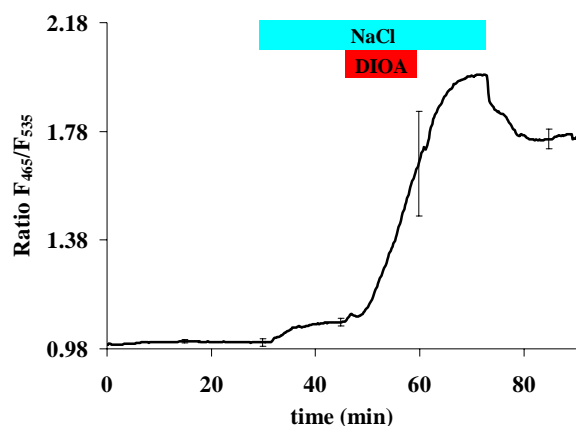
Flow-through experiments with *Arabidopsis* root cells expressing Clomeleon, perfused with 5 mM MES/KOH (pH6) without SM; treated with 150 mM NaCl ( $t = 30$  min) and 100  $\mu\text{M}$  bumetanide ( $t = 45$  min). Plants had been grown on 1xMS for 6-12 days. The graph represents an average of 5 experiments. The data were normalized by the mean of the time interval  $5 \text{ min} \leq t \leq 15 \text{ min}$ . Error bars represent StDv

**Table 7: Inhibitory effect on chloride influx**

Inhibitor	Inhibition rate (%)
A9C	$98 \pm 4.6$
DIDS	$60 \pm 10.8$
IAA 94	$46 \pm 30.1$
<b>TORA</b>	<b><math>52 \pm 5.7</math></b>
<b>BUME</b>	<b><math>48 \pm 18.1</math></b>
<b>FURO</b>	<b><math>41 \pm 30.8</math></b>

The inhibition rate was calculated as a percentage decrease in the slope of the emission ratio of control experiments (without inhibitor) for the time interval  $45 \text{ min} \geq t \leq 60 \text{ min}$ . Data obtained from 5 experiments each, as shown in Figure 28. The CCC inhibitors are highlighted gray.

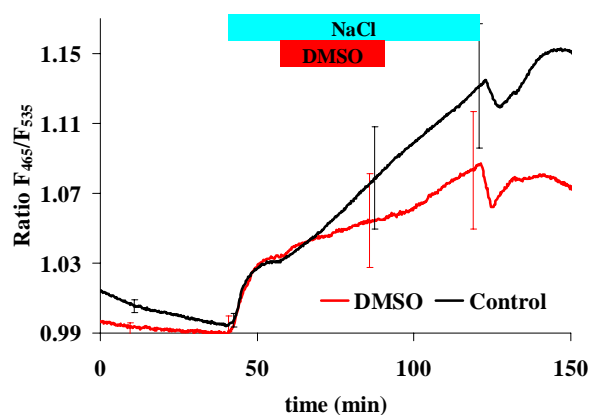
Further, hydrochlorothiazide; the thiazide-analogue xipamide (inhibitors of NCCs), dihydroindenylloxy-alkanoic acid (DIOA, inhibitor of KCCs), niflumic acid and flufenamic acid (chloride channel blocker) were tested in 100  $\mu$ M concentration. All of them show similar patterns in the dynamics of chloride influx. Even at micromolar concentrations they appear able to strongly accelerate the chloride influx (**Figure 29**).



**Figure 29: Effect of the diuretic R-DIOA on NaCl-induced chloride influx**

Flow-through experiment with *Arabidopsis* root cells expressing Clomeleon, perfused with 5 mM MES/KOH, pH6 without SM; treated with 150 mM NaCl ( $t = 30$  min) and 100  $\mu$ M DIOA ( $t = 45$  min). Plants had been grown on 1xMS for 6-12 days. The graph represents an average of 5 experiments. The data were normalized by the mean of the time interval  $5 \text{ min} \leq t \leq 15 \text{ min}$ . Error bars represent StDv

For control, the effect of dimethyl sulfoxide DMSO (**Figure 30**), in which some of the substances were solubilized (**Suppl\_material 18**), had to be tested. The results show, that DMSO is able to inhibit the NaCl-induced chloride influx slightly. This would not explain the prominent increase in the ratio during application of these inhibitors.

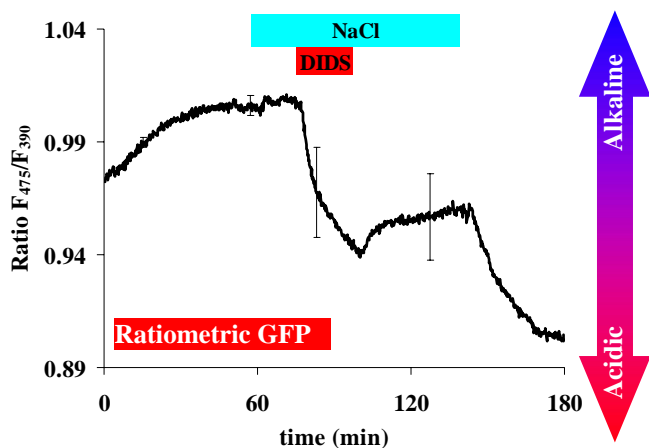


**Figure 30: Effect of DMSO on the NaCl-induced chloride flux**

Changes in chloride flux during salt (150 mM NaCl,  $t = 40$  min) and DMSO (360  $\mu$ l/l;  $t = 55$  min) treatment in root cells of *Arabidopsis* plants expressing Clomeleon. The perfusion buffer consisted of 5 mM MES/KOH, pH 6 without SM. Plants had been grown on 1xMS for 6-12 days. The data are averages of at least 3 independent experiments. The data were normalized by the mean of the time interval  $5 \text{ min} \leq t \leq 15 \text{ min}$ . Error bars represent StDv.

Since all of the substances are weak acids, and may acidify the cytoplasm (Plieth *et al.*, 1997) the next step was to test their effect on the cytoplasmic pH. Therefore, the pH indicators ptGFP or ratiometric GFP were utilized and indeed all of the substances mentioned above (DIOA, niflumic acid, flufenamic acid, xipamide) caused a prominent decrease in the cytoplasmic pH, which would affect Clomeleon. Due to the pH effect on Clomeleon the data are not implemented here. Also DIDS, which was shown before (**Table 7**) to inhibit the chloride influx, caused a change in the cytoplasmic pH (**Figure 31**). The **Figure 31** shows that the pH change caused by application of DIDS would not have a significant effect on Clomeleon, which is only slightly pH sensitive in the

range from pH6 to pH8 (**Figure 19**). So the results obtained with Clomeleon can be in this case regarded as reliable. The most interesting finding is that after washing out the salt, the pH continuously decreases. However, except DIDS, the other substances with an inhibiting effect listed in the **Table 7** had no significant influence on the pH (data not shown).

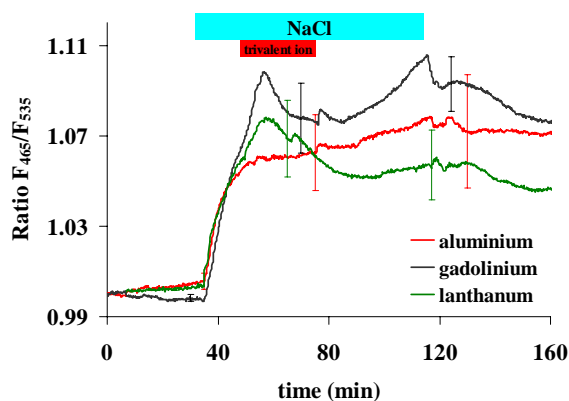


**Figure 31: Effect of the anion channel blocker DIDS on the cytoplasmic pH**

Flow-through experiment with *Arabidopsis* root cells expressing the pH indicator ratiometric GFP, perfused with 5 mM MES/KOH, pH6 without SM; treated with 150 mM NaCl ( $t = 30$  min) and 5  $\mu$ M DIDS. Plants had been grown on 1xMS for 6-12 days. The graph represents an average of 5 independent experiments. The data were normalized by the mean of the time interval  $5 \text{ min} \leq t \leq 15 \text{ min}$ . Error bars represent StDv. A shift in the ratio of 0.05 corresponds to a pH shift of approximately 0.08 units.

#### 3.2.1.4 Chloride influx is sensitive to trivalent cations

It was previously shown (Lorenzen *et al.* 2004) that the trivalent cation  $\text{La}^{3+}$ , a non-selective anion channel blocker (Lewis & Spalding, 1998), is able to block salt stress-induced chloride flux into *Arabidopsis* root cells. The measurements performed here with  $\text{Gd}^{3+}$  and  $\text{Al}^{3+}$  show (**Figure 32**) that both are also potent inhibitors of chloride transport. The washing out of the trivalent cations shows that in the case of  $\text{Al}^{3+}$  and  $\text{La}^{3+}$  the block is irreversible, whereas  $\text{Gd}^{3+}$  mediates a block in chloride flux comparable to  $\text{Ca}^{2+}$ , which can be partially reversed by washing it out.



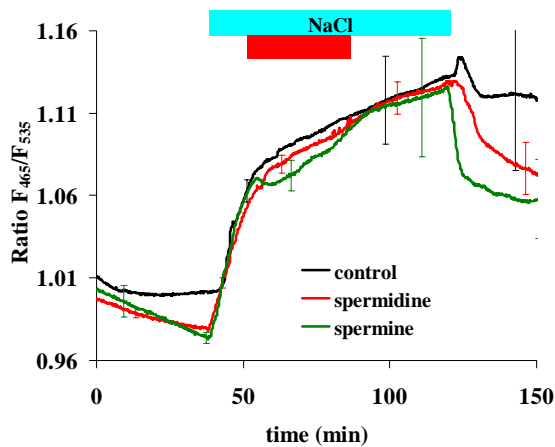
**Figure 32: Trivalent cation block of NaCl-induced chloride entry**

*Arabidopsis thaliana* root cells expressing Clomeleon were perfused with 5 mM MES/KOH, pH6 without SM; treated with 150 mM NaCl ( $t = 30$  min) and 2 mM  $\text{AlCl}_3$ ,  $\text{GdCl}_3$  and  $\text{LaCl}_3$  ( $45 \text{ min} \leq t \leq 80 \text{ min}$ ), respectively. The plants had been grown for 6-14 days on 0.5xMS. Each curve is an average of 4 independent experiments. The data were normalized by the mean of the time interval  $5 \text{ min} \leq t \leq 15 \text{ min}$ . Error bars represent StDv.

#### 3.2.1.5 Chloride influx is inhibited by the polyamine spermine

Several studies (Yamaguchi *et al.*, 2006; Erdei *et al.*, 1996) point out the important role of polyamines (spermidine, spermine and putrescine) in plant stress responses. Supplementing the plants with exogenous polyamines can improve their stress adaptation process (Lakra *et al.*, 2006;

Ndayiragije & Lutz, 2006). The mechanisms are still unclear, but one possible hypothesis can be the direct effect on the plasma membrane ion channels (Williams, 1997; Shabala *et al.*, 2007).



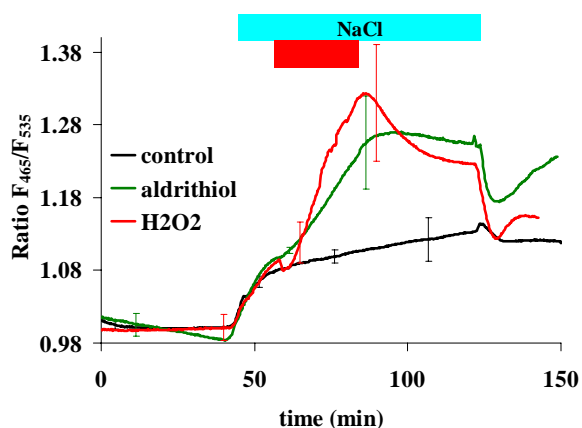
**Figure 33: Effect of polyamines on the NaCl-induced chloride flux**

Changes in chloride flux during salt and PA treatment in root cells of *Arabidopsis* plants expressing Clomeleon. Plants had been grown on 0.5xMS and perfused with buffers without SM. The data are averages of at least 4 independent experiments and were normalized by the mean of the time interval  $5 \text{ min} \leq t \leq 15 \text{ min}$ . Error bars represent StDv.

Measurements show (**Figure 33**), that only spermine (1 mM) transiently and slightly inhibits NaCl-induced chloride flux, whereas spermidine (0.5 mM) seems to be ineffective. However, more prominent is the effect, that the chloride is washed out of the root cells ( $t > 120 \text{ min}$ ) more easily when polyamines in millimolar concentrations were applied before. This indeed suggests a possible function of spermine and spermidine in stress adaptation processes.

### 3.2.1.6 Salt-stress induces changes in the cell redox environment

Oxidative agents such as  $\text{H}_2\text{O}_2$  and aldrithiol do - in contrast to di- and trivalent cations - accelerate any NaCl-induced chloride uptake (**Figure 34**). The acceleration is 8-fold for 10 mM  $\text{H}_2\text{O}_2$ , and 7-fold for 0.1 mM aldrithiol, calculated as a percentage change of the slope of the emission ratio for the time interval  $60 \text{ min} \geq t \leq 80 \text{ min}$  compared to control experiments (without oxidising substances).

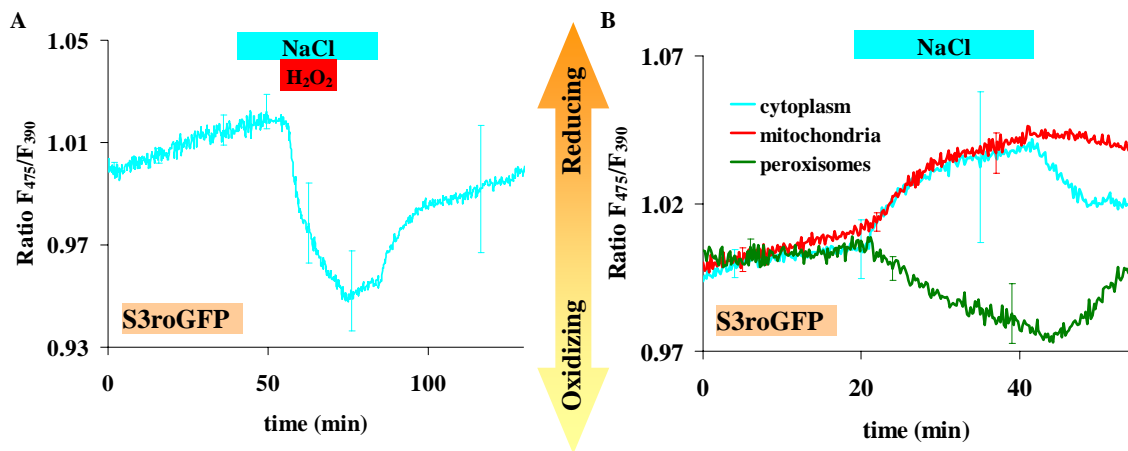


**Figure 34: Influence of oxidizing substances on the Clomeleon emission ratio in *Arabidopsis***

*A. thaliana* plants expressing Clomeleon grown on 0.5 x MS for 6-14 days were treated 150 mM NaCl and with 0.1 mM aldrithiol and 10 mM  $\text{H}_2\text{O}_2$ . Control represents only salt treated plants without additives. All data are averages of 5 independent experiments and were normalized by the mean of the time interval  $5 \text{ min} \leq t \leq 15 \text{ min}$ . Error bars represent StDv.

In order to see, what effect the oxidative treatment combined with salt stress has on the redox environment, S3roGFP expressing *Arabidopsis* plants were also treated with 150 mM NaCl and

10 mM  $H_2O_2$ . When applying the same perfusion sequence as in **Figure 34**, at first sight no notable redox changes during salt treatment could be detected (**Figure 35A**;  $t = 40\text{min}$  to  $54\text{ min}$ ).

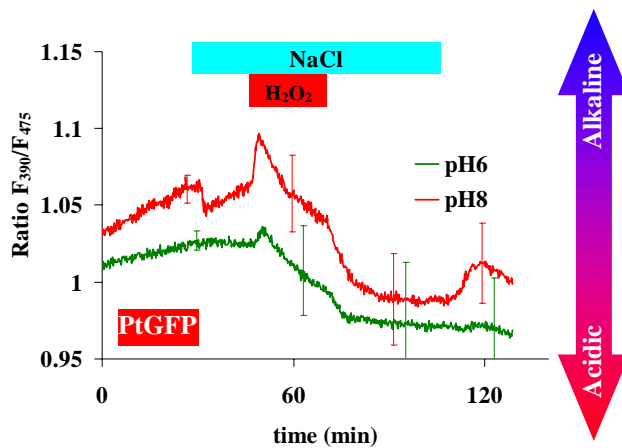


**Figure 35: Redox changes during salt and simultaneous oxidative treatment**

**A:** Redox changes during salt treatment (150 mM NaCl, 5 mM MES, SM; pH6) and addition of 10 mM  $H_2O_2$  in root epidermal cells of *Arabidopsis* expressing *S3roGFP* in cytoplasm and **B:** Redox changes in cytoplasm, mitochondria and peroxisomes during salt treatment only. All data are means of at least four independent experiments and were normalized by the mean of the time interval  $5\text{ min} \leq t \leq 15\text{ min}$ . The error bars represent StDv. Plants had been grown for 6-14 days.

A closer look at the redox milieu in cytoplasm, mitochondria and peroxisomes, revealed minor changes in all three compartments (**Figure 35B**). Interesting here is that after washing out the salt both, the cytoplasmic and the peroxisomal indicators approach their previous redox state, whereas the mitochondrial remains reduced.

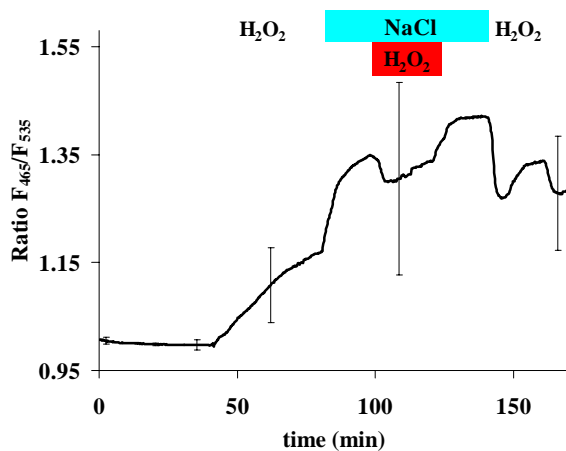
However, under the influence of additional 10 mM  $H_2O_2$  (**Figure 35A**;  $t = 54\text{ min}$  to  $70\text{ min}$ ) the cytoplasmic indicator was oxidised as can be seen by a decrease of the  $F_{475}/F_{390}$ -ratio. During washout of the oxidant (**Figure 35A**;  $t = 70\text{ min}$  to  $82\text{ min}$ ) there was no regeneration of the cytoplasmic milieu, leading to the finding, that salt stress inhibits the reducing power or antioxidant capacity. The indicator was reduced back only when the salt stress treatment was released (i.e. when salt was washed out; **Figure 35A**;  $t > 85\text{ min}$ ). Due to salt treatment (pH6) no significant changes with the cytoplasmic pH indicator are seen (**Figure 36**). The application of 10 mM  $H_2O_2$ , however, causes an acidification. At a higher pH of the flow-trough media,  $H_2O_2$  had a more prominent acidifying effect on the pH indicator.



**Figure 36: pH changes during salt and simultaneous oxidative treatment**

pH changes during salt treatment (150 mM NaCl, 5 mM MES, SM; pH6) and addition of 10 mM H<sub>2</sub>O<sub>2</sub> in root epidermal cells of *Arabidopsis* expressing the pH indicator PtGFP are shown. All data are means of at least four independent experiments and were normalized by the mean of the time interval 5 min ≤ t ≤ 15 min. The error bars represent StDv. Plants had been grown for 6-14 days.

Since Clomeleon is redox sensitive (**Figure 18**), it became necessary to test the influence of oxidative treatment on Clomeleon, before interpreting the obtained results. Therefore, *A. thaliana* plants expressing Clomeleon were exposed to 10 mM H<sub>2</sub>O<sub>2</sub> prior to salt treatment. The results show (**Figure 37**), that the indicator is indeed oxidised by H<sub>2</sub>O<sub>2</sub>, manifested as an increase in the ratio (t = 40 min to 80 min). Furthermore, when salt stress is applied an accelerated chloride influx is observable (t = 80 min). Reapplication of H<sub>2</sub>O<sub>2</sub> during salt treatment causes a transient inhibition of the chloride flux.



**Figure 37: Direct effect of oxidative treatment on the anion indicator Clomeleon**

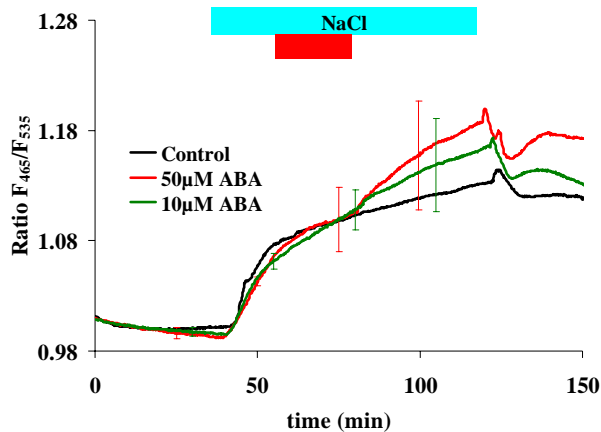
*Arabidopsis thaliana* root cells expressing Clomeleon were perfused with 5 mM MES/KOH, pH6 without SM; treated with 10 mM H<sub>2</sub>O<sub>2</sub> (t = 40 min), and 150 mM NaCl (t = 80 min). During the salt treatment 10 mM H<sub>2</sub>O<sub>2</sub> were applied once more (90 min ≤ t ≤ 110 min). The plants had been grown for 6-14 days on 0.5xMS. Data represent the average of 4 independent experiments and were normalized by the mean of the time interval 5 min ≤ t ≤ 15 min. Error bars represent StDv.

### 3.2.1.7 Influence of externally applied abscisic acid (ABA) on the chloride flux

The phytohormone ABA plays a regulatory role in many physiological processes in plants. Different adverse environmental conditions such as salt, water, drought, and temperature stress result in increased amounts of ABA. Recent studies have demonstrated the importance of ABA in modulation of adaptive responses at gene-level in plants exposed to stress (Zhu *et al.*, 2005; Sridha & Wu, 2006). Also the modulation of anion and cation channels by ABA was described in stomatal guard cells (Pei *et al.*, 2000). To examine the role of ABA on the NaCl-induced chloride influx, *A.thaliana* plants expressing Clomeleon were treated with 150 mM NaCl and 10 μM and



50  $\mu\text{M}$  ABA, respectively. The results show (**Figure 38**) no particular influence of ABA on the chloride influx during its application. Only after releasing the treatment, chloride influx is accelerated. This effect is more pronounced when higher ABA concentrations are used.



**Figure 38: Influence of ABA on the salt-induced chloride influx**

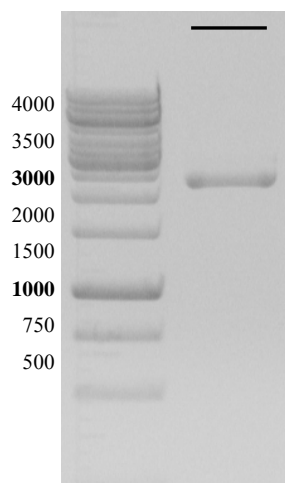
*Arabidopsis thaliana* plants expressing Clomeleon grown on 0.5 MS for 6-14 days were treated with 150 mM NaCl only (control). 10  $\mu\text{M}$  and 50  $\mu\text{M}$  ABA were added during the salt treatment at  $t = 55$  min and washed out at  $t = 75$  min. All data are means of 5 independent experiments and were normalized by the mean of the time interval  $5 \text{ min} \leq t \leq 15 \text{ min}$ . Error bars represent StDv.

### 3.2.2 Cloning of chloride channels

The cloning of *Arabidopsis thaliana* chloride channels was carried out in order to express the channels in suitable plant and bacterial systems for functional studies. After isolation of mRNA from *Arabidopsis thaliana*, cDNA was produced by reverse transcription. Since problems occurred during inactivation of DNase, the digestion step was omitted and the possibility of contamination with genomic DNA remained. Therefore PCR with chloride channel specific primers run on the cDNA delivered to some extent two kinds of fragments. The genomic DNA- and the cDNA-delivered fragments could be distinguished by their size on agarose gel. Since very different sizes were expected, reasonable lowering of the elongation time in the PCR led to amplification of the shorter fragment only, due to the discontinued extension by the used DNA-polymerase. The fragments were cloned into pBluescript or directly into pQE30 or pART7 (**Suppl\_materials 7-15**). The pBluescript vector was used only for sub-cloning because of its blue-white screening capability. The aim was to clone chloride channel DNA into plant (pART7) and bacterial (pQE30) expression vectors for further investigations.

#### 3.2.2.1 Cloning of AtClC-A

AtClC-A from *Arabidopsis thaliana* was purchased from ABRC as a cDNA clone in the cloning vector pUNI 51 (Stock #C104829). After sequencing (**Suppl\_material 7**), suitable primers with two additional restriction sites each (**Suppl\_material 6**) were used to amplify a 2370 bp long fragment (**Figure 39**), which was cloned directly to the pART7 vector. From here, the AtClC-A was cloned into a bacterial expression vector pQE30.

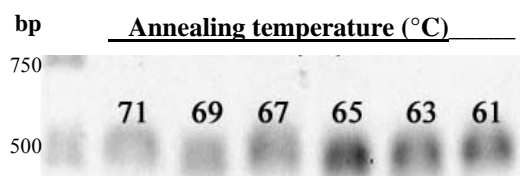


**Figure 39: PCR product (AtCIC-A) visualised on a agarose gel**

Products of a PCR reaction performed with the commercially available pUNI51\_AtCICA vector with CICAfor1 and CICArev1 primer pair. The desired product has a size of 2370 bp. A 1 kb DNA-ladder (Promega) was used as a size standard.

### 3.2.2.2 Mutation of the GPGIP motif in AtCIC-A

The GS/PGIP motif determines the anion selectivity. Bergsdorf *et al.* (2009) have previously shown in *Xenopus* oocytes that an exchange of proline to serine within this motif in AtCIC-A leads to higher selectivity for chloride than for nitrate. A point mutation (C479T) was introduced with help of modified primers into the GPGIP motif leading to P160S exchange (**Suppl\_material 7**). A PCR with the respective primers delivered an approximately 500 bp long fragment (**Figure 40**). The nucleotide exchange was proved by sequencing (**Suppl\_material 7**).

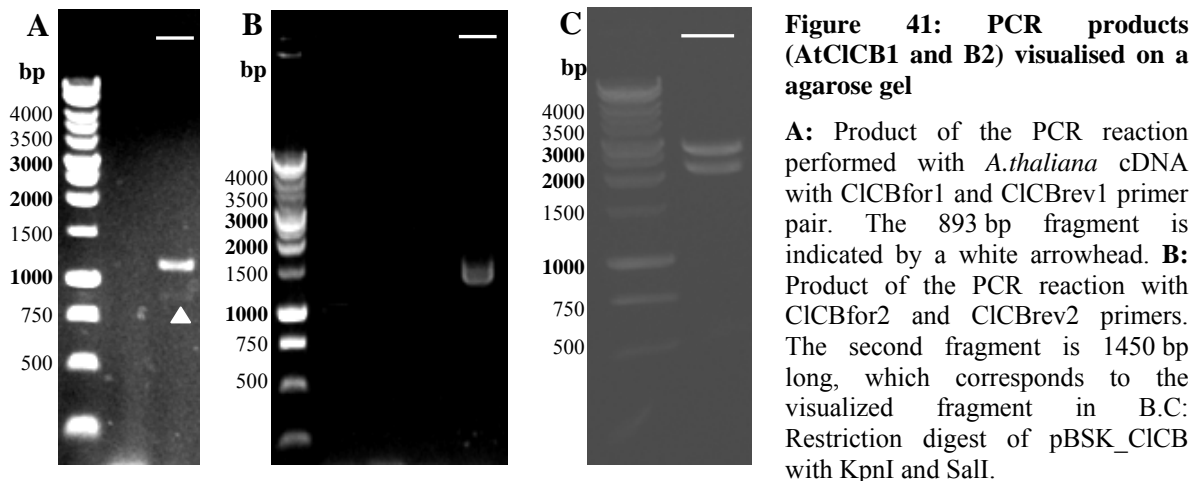


**Figure 40: Temperature gradient PCR of AtCICA\_mut**

PCR reaction was performed with the pUNI51\_AtCICA vector as template using the CICAfor1 and CICAmut\_rev primer pair. Temperature gradient was run with annealing temperatures as indicated by the numbers. The 65°C annealing temperature was chosen as the most suitable.

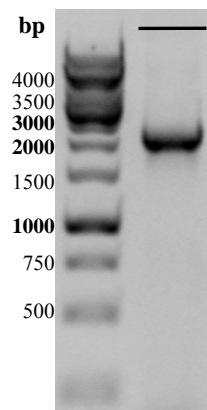
### 3.2.2.3 Cloning of AtCIC-B

AtCIC-B was divided in two fragments (**Suppl\_material 8**). Both fragments were amplified by PCR from *Arabidopsis thaliana*-cDNA. The first fragment (CICB1) was approximately 900 bp long (**Figure 41A**) and the second (CICB2) about 1450 bp long (**Figure 41B**). Both fragments were cloned separately into pBluescript vector and verified by sequencing (**Suppl\_material 8**). Then both fragments were combined together in pBluescript (**Figure 41C**). A subsequent cloning into a pART7 vector was carried out (data not shown).



### 3.2.2.5 Cloning of AtCIC-C

AtCIC-C lacks an appropriate restriction enzyme recognition site in the middle of its DNA. Therefore, it was cloned in one fragment from *Arabidopsis thaliana*-cDNA (**Suppl\_material 9**) into a pART7 vector. The respective primers were used for the amplification of a 2340 bp long fragment (**Figure 42**). The additional restriction sites were used for cloning into the pART7 vector. The obtained clones were verified by sequencing (**Suppl\_material 9**).

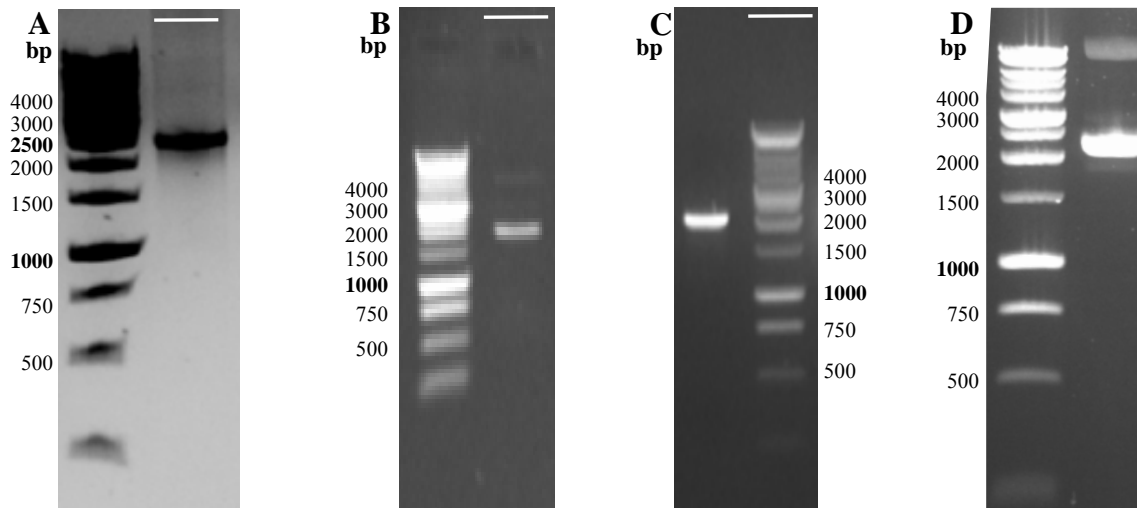


**Figure 42: PCR products (AtCIC-C) visualised on an agarose gel**

Product of the PCR reaction performed with *A.thaliana* cDNA with CICCfor and CICCrev primer pair. The band corresponds to the site of AtCIC-C (above 2000 bp).

### 3.2.2.6 Cloning of the other chloride channels

Similarly to AtCIC-C, the other chloride channels (AtCIC-D, E, F, and G) were cloned into the pART7 vector in only one fragment (**Suppl\_materials 10-14**). The PCR reactions with *A.thaliana* cDNA using the appropriate forward and reverse primers (**Suppl\_material 6**) delivered different fragments. For AtCIC-D, -F and -G approximately 2400 bp long fragments could be visualized; for AtCIC-E a fragment of approximate size about 2100 bp were obtained (**Figure 43**). These were then cloned into a pART7 vector and verified by sequencing (**Suppl\_materials 10-14**)

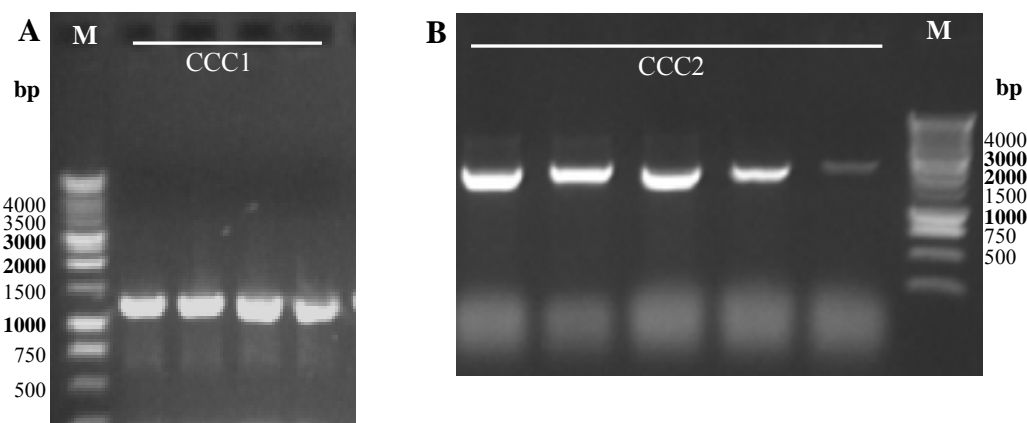


**Figure 43: PCR products (AtCIC-D, -E, -F and -G) visualised on a agarose gel**

**A:** PCR performed with *A.thaliana* cDNA with CICDfor and CICDrev primer pair. **B:** PCR performed with *A.thaliana* cDNA with CICEfor and CICErev primer pair. **C:** PCR performed with *A.thaliana* cDNA with CICFfor and CICFrev primer pair. **D:** PCR performed with *A.thaliana* cDNA with CICGfor and CICGrev primer pair.

### 3.2.2.7 Cloning of AtCCC

AtCCC was amplified by PCR in two fragments with a length of approximately 1300 bp (**Figure 44A**) and 2000 bp (**Figure 44B**) using the respective primers. Both, CCC1 and CCC2 were cut out of the gel and cloned (**Suppl\_material 15**) into a pBluescript vector. The subsequent sequencing showed the correctness of CCC1, whereas CCC2 was found to be a genomic DNA amplificate, containing intron sequences (highlighted gray in the **Suppl\_material 15**). Therefore further subcloning was discontinued.

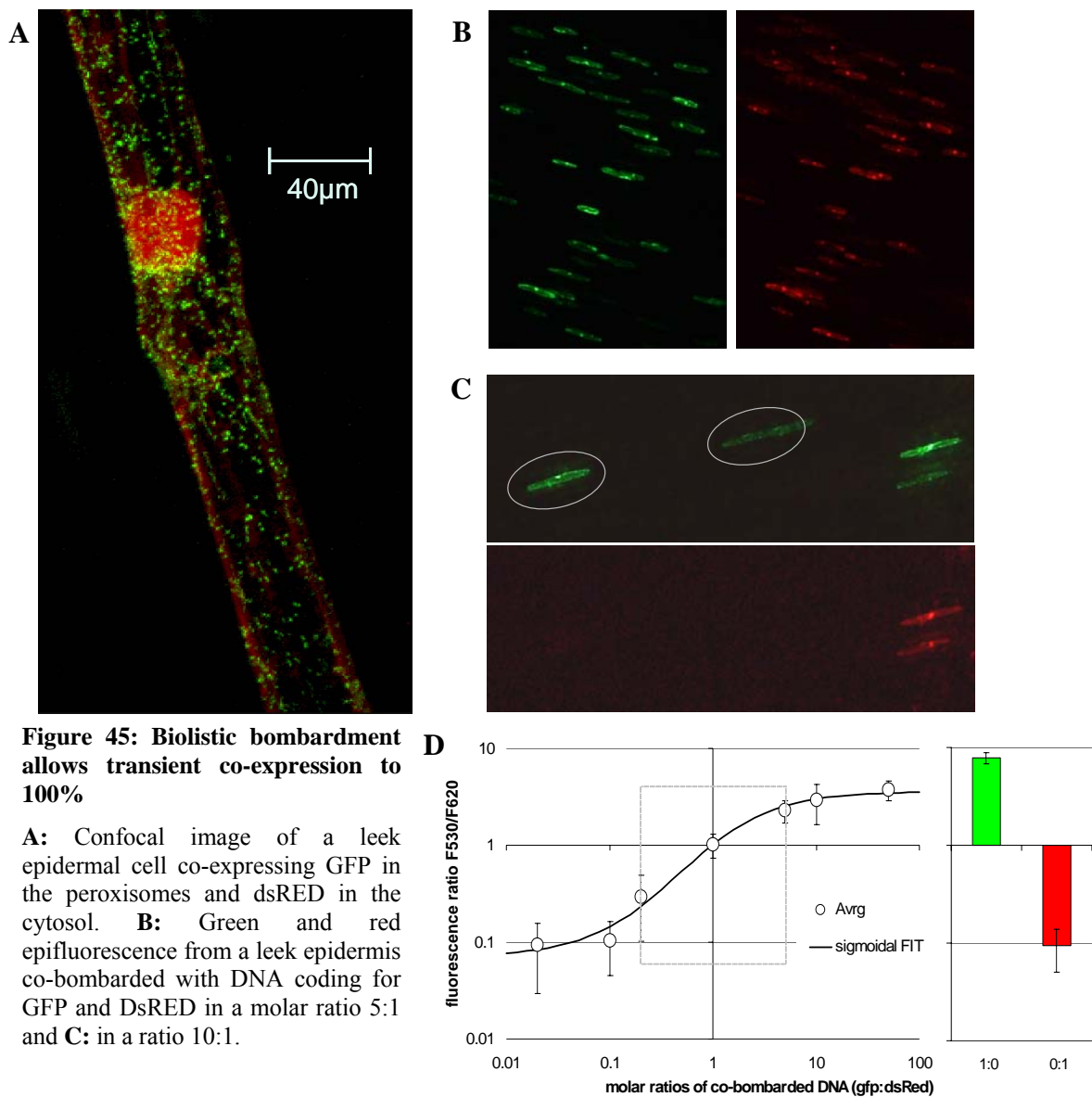


**Figure 44: AtCCC visualised on a agarose gel**

**A:** Product of the PCR reaction performed with *A.thaliana* cDNA with CCCfor1 and CCCrev1 primer pair. The 1301 bp fragment can be seen. **B:** Product of the PCR reaction with CCC2 and CCCrev2 primers. The second fragment should be 1626 bp long, which is not the size of the obtained fragment (around 2000 bp).

### 3.2.3 Suitability of biolistic transformation for transient co-expression of a reporter and a target gene

For functional studies of chloride channels a transient transformation procedure - biolistic bombardment - was used in order to obtain results in a reasonable time period. At first it was necessary to test, whether it is possible to use this method for a simultaneous expression of Clomeleon measuring the chloride flux and the selected chloride channel. The co-expression efficiency of the biolistic transformation method was tested with different molar ratios of two DNAs coding for different FP's (DsRED and PtGFP) expressed in the cytoplasm and peroxisomes, respectively (**Figure 45A**).



**Figure 45: Biolistic bombardment allows transient co-expression to 100%**

**A:** Confocal image of a leek epidermal cell co-expressing GFP in the peroxisomes and dsRED in the cytosol. **B:** Green and red epifluorescence from a leek epidermis co-bombarded with DNA coding for GFP and DsRED in a molar ratio 5:1 and **C:** in a ratio 10:1.

**D:** Ratios of integrated green and red fluorescence from cells co-bombarded with different molar ratios of the corresponding DNA-constructs. The boxed area gives the range of 100% co-expression. The green column represents fluorescence of cells transfected only with DNA coding for PtGFP and the red column represents the fluorescence of cells transfected with DsRED. Average data are of >7 cells. Error bars represent StDv

The expression level as monitored by fluorescence intensity integrated over the whole cell also depends on the total amount of DNA shot in. Therefore, ratio imaging has been employed to quantify this effect. The  $F_{em530}/F_{em620}$  ratio is correlated over a wide range with the molar ratio of the DNA constructs used for co-bombardment. Co-expression was 100% within the molar range of  $1:5 < \text{GFP/DsRed ratio} < 5:1$  (**Figure 45B, D**). Outside this interval, cells expressing only one of the two co-bombarded constructs could be observed (**Figure 45C**). Hence, simply a 1:1 mixture of reporter and of target gene DNA can be used to coat particles for co-transfection. Thereby, it is not necessary to precisely adjust the molar ratio. The reporter reliably displays the expression of the co-transfected target gene within the range of molar ratios given in **Figure 45D**.

### 3.2.4 The co-expression of Clomeleon and chloride channel constructs – effect on the chloride influx

For *in vivo* measurements of chloride influx, Clomeleon was used as a ratiometric indicator. From the chloride channel constructs in plant expression vector pART7 only four were chosen for co-transformation of leek and onion cells: AtCIC-A, AtCICAmut, AtCIC-C and AtCIC-F. All three wild type channels exhibit different transport properties and intracellular localisation. AtCIC-A and AtCIC-C are localised at the tonoplast of vacuoles (Lv *et al.*, 2009; DeAngeli *et al.*, 2006, Gaxiola *et al.*, 2002), AtCIC-F at the trans-Golgi membrane (Marmagne *et al.*, 2007). Furthermore, AtCIC-A and AtCIC-C possess different residues in their anion selectivity filter, constituting for nitrate and chloride selectivity respectively. The molar ratio for co-transformation of the target gene and Clomeleon was defined at 1:1, being in the range for effective co-expression shown in **Figure 45D**. However, the presence of the chloride channel protein was not confirmed.

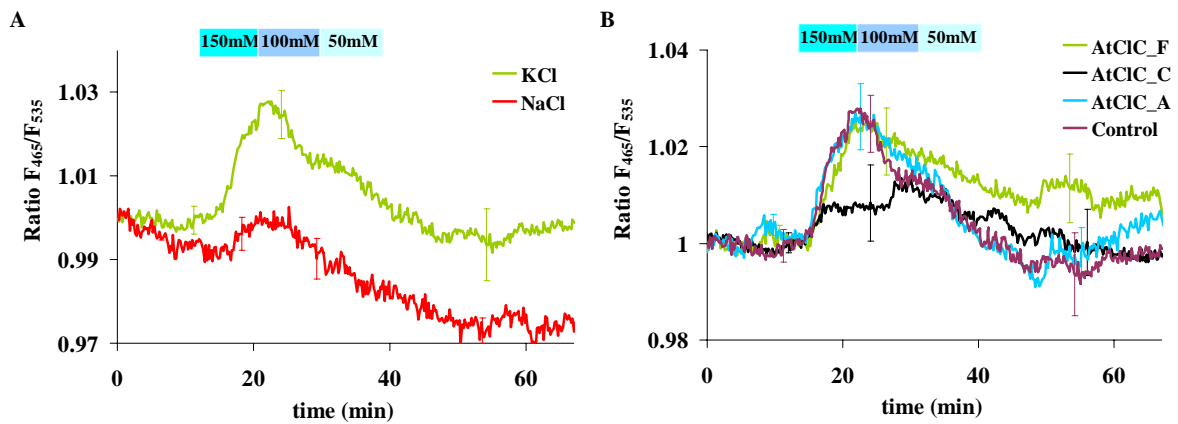
#### 3.2.4.1 Experiments with leek epidermal cells

Leek epidermal cells expressing Clomeleon produced inconsistent data. One reason may be that the flow-through medium reaches only the upper and the lower side of the multilayered epidermis, whereas the buried cells are not directly exposed to salt. To overcome this problem, the object of study was changed and onion epidermal cells were chosen for further experiments. The epidermis of onion is unilayered, allowing the direct contact of all transformed cells with the flow-through medium.

#### 3.2.4.2 Experiments with onion epidermal cells

The flow-through experiments with onion epidermis cells expressing Clomeleon have shown an almost insignificant NaCl - induced chloride influx into the cytoplasm during salt treatment (**Figure 46A**). However, washing out the salt at once caused irreversible cell damage due to hypoosmotic shock (data not shown). This fact underlines the hypothesis, that hypoosmotic shock

is more incisive for the plant cells than hyperosmolarity caused at the onset of salt treatment (Chapter 4, Section 4.3.1). Therefore, in all experiments the salt was washed out stepwise.

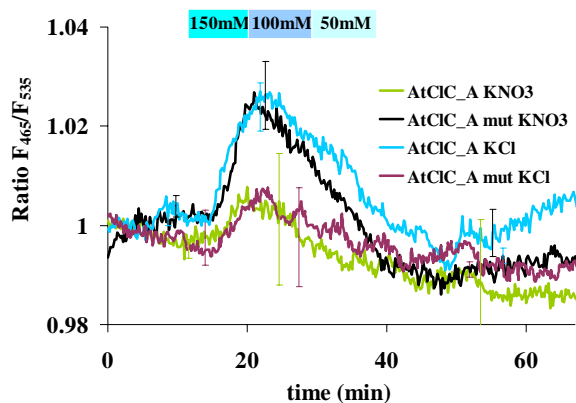


**Figure 46: Chloride influx in onion epidermal cells expressing chloride channels during salinity treatment**

**A:** The onion epidermis expressing Clomeleon was perfused with 5 mM MES/KOH, pH6 supplemented with SM; treated with 150 mM NaCl/KCl ( $t = 10$  min) and the salt treatment was released by lowering the NaCl/KCl concentration every 10 min. **B:** The epidermis cells were co-bombarded with Clomeleon and the respective *A.thaliana* chloride channel as depicted in the figure legend. The same perfusion sequence was applied using only KCl. Each curve shows the average of at least 4 independent experiments. The data were normalized by the mean of the time interval  $2 \text{ min} \leq t \leq 10 \text{ min}$ . Error bars represent StDv.

When applying NaCl on the cells, only a slight influx of chloride could be observed (Figure 46A, red curve). The situation changed when KCl was used instead (green curve). The chloride influx here is much more pronounced (Figures 46A; green curve). Co-expression of Clomeleon with three different *Arabidopsis thaliana* chloride channels (AtCIC-A,-C,-F) treated with KCl is shown in Figure 46B. Co-expression of Clomeleon and the chloride channels AtCIC-A and -F caused no particular change in the chloride influx when compared to cells expressing Clomeleon only (Figure 46B) In contrast the AtCIC-C transfected cells show a different chloride influx kinetics, suggesting a pronounced translocation of chloride into the vacuole. The anion selectivity of chloride channels lies in the GS/PGIP residues (Dutzler *et al.*, 2000, 2002, Bergsdorf *et al.*, 2009). AtCIC-A carries a proline instead of a serine in this particular motif, and this constitutes for nitrate selectivity. In order to test the nitrate influx into the cytoplasm, the flow-through experiments were carried out with  $\text{KNO}_3$  instead of KCl (Figure 47). The nitrate influx into the cytoplasm was lower, since the AtCIC-A compartmentalises nitrate in the vacuole more effectively than chloride. Consequently, the concentration in the cytoplasm is lowered. P to S mutation in the GPGIP motif of AtCIC-A selectivity filter causes higher affinity to chloride, which is observable in the flux studies with KCl and  $\text{KNO}_3$ . Here, the influx of chloride compared to wild type AtCIC-A measurements is less pronounced (Figure 47).

Onion epidermal cells over-expressing wild type AtCIC-C, carrying the GSGIP selectivity motif, show similar kinetics of chloride influx during salt treatment as with mutated AtCIC-A (Figure 47B, black curve).



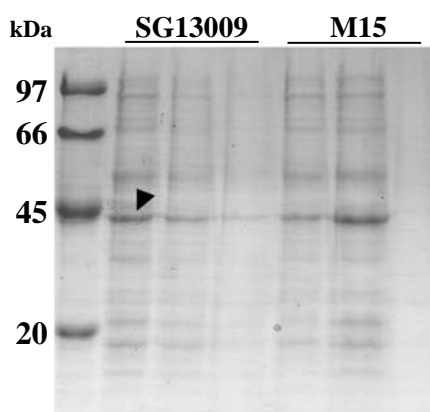
**Figure 47: Chloride/nitrate influx in onion epidermal cells expressing AtCIC-A and mutated AtCIC-A**

The onion bulb epidermis co-expressing Clomeleon and the channel proteins as depicted in the legend was perfused with 5 mM MES/KOH, pH6 supplemented with SM; and treated with 150 mM KCl or KNO<sub>3</sub> (t = 10 min). The salt treatment was released by lowering the KCl/KNO<sub>3</sub> concentration every 10 min. Each curve is the average of at least 4 independent experiments. The data were normalized by the mean of the time interval 2 min ≤ t ≤ 10min. Error bars represent StDv.

### 3.2.4 Expression and purification of AtCIC-A in bacterial system

The expression and purification of transmembrane proteins is due to their different molecular properties a difficult task. The right expression system, buffer composition, and detergents have to be chosen and tested. If problems are occurring at this stage, the denaturing purification procedure and re-folding of the protein needs to be considered as an alternative. Different non-ionic detergents were tested in order to solubilize the AtCIC-A protein (e.g. Brij® 35, Brij® 56, Tween 20, Triton X-100 and others). Nevertheless, only with n-dodecyl-β-D-maltoside a protein band of the approximate AtCIC-A protein size could be visualized by SDS-PAGE.

For purification of AtCIC-A a bacterial expression system was chosen. AtCIC-A was cloned into a pQE30 vector (Suppl\_material 17) suitable for expression in SG13009 or M15 cells. Difficulties occurred already during the first steps, since a contaminant appeared to compete with the AtCIC-A for the binding sites on the Ni<sup>2+</sup>-NTA column. It turned out, that an endogenous metal binding or histidine rich bacterial protein bound onto the column.



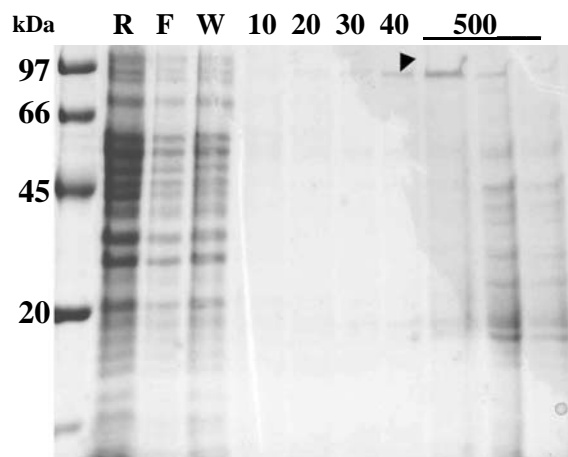
**Figure 48: 45 kDa endogenous bacterial protein is binding on the Ni<sup>2+</sup>-NTA column**

SDS-PAGE gel performed with the eluates (500 mM imidazole) from a gravity flow Ni<sup>2+</sup>-NTA column. As a source material SG13009 and M15 cells carrying an empty pQE30 vector were used. The arrow indicates a ~45 kDa protein band binding on the column.



Consequently, the same induction and purification protocol as for AtCIC-A was applied on the bacterial cultures carrying no plasmid or an empty pQE30 plasmid, for control. One protein band of approximately 45 kDa was seen migrating in a SDS-PA gel when elution was carried out with 500 mM imidazole (**Figure 48**).

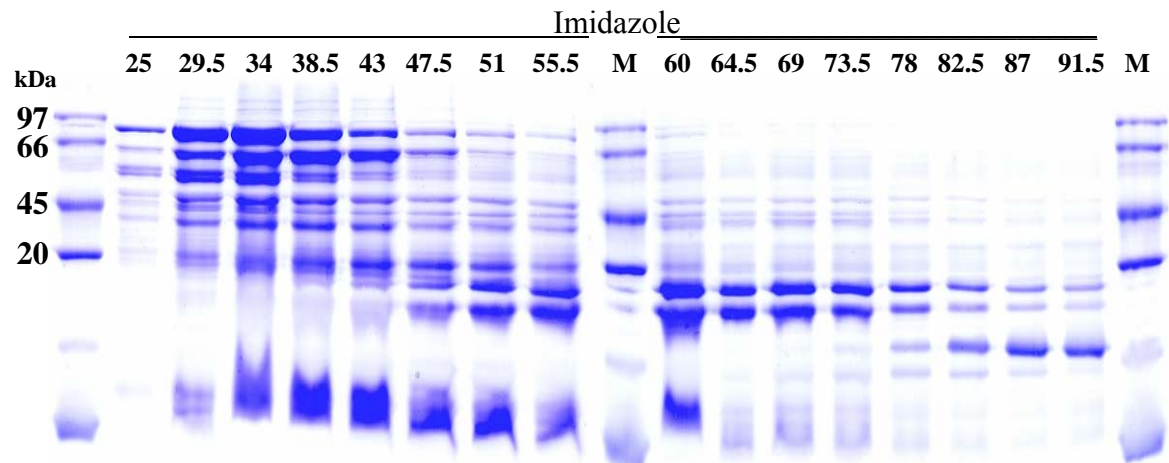
As a first approach to separate the unwanted contaminants from the putative AtCIC-A protein, an elution buffer gradient was run on a gravity flow Ni<sup>2+</sup>-NTA column (**Figure 49**) and in higher precision on an HPLC (**Figure 50**).



**Figure 49: Purification of AtCIC-A on a gravity-flow Ni<sup>2+</sup>-NTA column**

SDS-PA gel performed with the raw extracts (R), flow-through (F) and wash (W) fractions as well as eluates (10-500 mM imidazole, as indicated in the legend) from a gravity flow Ni<sup>2+</sup>-NTA column. As a source material M15 cells carrying the pQE30\_AtCICA vector were used. The arrow indicates a ~90 kDa protein band already eluted at 40 mM imidazole.

A protein band of ~90 kDa was eluted already at very low imidazole concentrations (30 mM) indicating a non-specific binding of the protein on the column material (**Figures 49** and **50**).

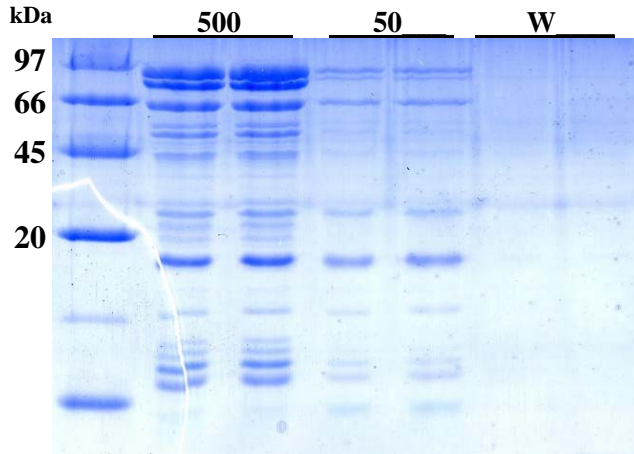


**Figure 50: Purification of AtCIC-A by the ÄKTA-purifier system**

SDS-PA gel performed with the 1 ml elution fractions (25-91.5 mM imidazole, as indicated in the legend) of a HisTrap HP column by the ÄKTA purifier system. As a source material M15 cells carrying the pQE30\_AtCICA vector were used. A ~90 kDa protein band is already eluted below 30 mM imidazole indicating a non-specific binding.

An explanation could be that the His-tag is buried within the expressed protein and not being able to interact properly with the column material. Therefore, with the obtained eluate a denaturing

purification on a gravity flow column was carried out. **Figure 51** shows that a ~ 90 kDa protein band was indeed partially eluted with 50 mM imidazole, but the major fraction came down with 500 mM imidazole.



**Figure 51: Purification of reduced AtCIC-A on a gravity-flow Ni<sup>2+</sup>-NTA column**

SDS-PA gel performed with wash (W) fraction as well as both eluates with 50 and 500 mM imidazole as indicated in the legend under reduced conditions (5 mM DTT in all buffers) from a gravity flow Ni<sup>2+</sup>-NTA column. As a source material M15 cells carrying the pQE30\_AtCICA vector were used. A ~90 kDa protein band is partially eluted at 50 mM imidazole, but the main fraction comes down at 500 mM.

### 3.3 DISCUSSION

#### 3.3.1 NaCl-induced chloride influx into *Arabidopsis* root cells exhibits two distinct phases

Teakle & Tyerman (2009) proposed a passive transport of chloride after onset of salt stress caused by the membrane depolarisation triggered by sodium uptake until the cytoplasmic concentration reaches a certain level. Above this level further chloride influx could be activated only by active transport mechanisms (for more details see **Chapter 1, Section 1.2.2**). Generally it is proposed, that the membrane depolarisation is caused by excessive uptake of sodium during salt treatment (Lurin *et al.* 1996; Shabala, 2003). However, Felle (1994) has shown, that in *Sinapis alba* the depolarisation is not necessarily only due to the imported sodium.

Furthermore, he has shown two different phases after elevating the external [Cl<sup>-</sup>] abruptly. The initial depolarisation of the plasma membrane was followed by a slow but substantial hyperpolarisation. The second phase was obviously not only caused by increasing [Cl<sup>-</sup>], but also due to an increasing acidification of the cytoplasm. This acidification was later explained by Beilby & Al-Khazaaly (2009) by activation of H<sup>+</sup>/OH<sup>-</sup> channels at the plasma membrane of *Chara australis* in the later stages of salt stress.

Taken together, after onset of salt stress a depolarisation of the plasma membrane occurs, followed by a second phase, where the membrane potential returns to more negative values or becomes even hyperpolarising. As proposed by Lorenzen *et al.* (2004) and later by Teakle & Tyerman (2009), an active (i.e. energy-driven) transport of chloride during the second phase is likely. Considering the

results from Felle (1994), the second phase in chloride influx can also be driven by hyperpolarisation activated anion channels.

The chloride influx triggered by 150 mM NaCl, as shown in **Figure 23A**, exhibits also two distinct phases. They are named here according to their proposed characteristics: “depolarisation” and “saturation” phase.

### 3.3.2 Internal and external calcium availability differ in their effect on NaCl-induced chloride entry

Calcium is known to ameliorate the influx / efflux of ions ( $\text{Na}^+$ ,  $\text{Cl}^-$  /  $\text{K}^+$ ) during salinity (Shabala *et al.*, 2006; El-Hendawy *et al.*, 2005; Lorenzen *et al.*, 2004; Essah *et al.*, 2003; Garg *et al.*, 1997). For example, only 10 mM  $\text{CaCl}_2$  applied during salt treatment on *Arabidopsis thaliana* plants expressing Clomeleon grown on full MS medium were able to block the chloride influx completely (Lorenzen *et al.*, 2004).

The results presented here (**Figures 24 – 26**) show that the calcium availability differentially acts on both phases of chloride influx. Externally applied calcium, even in very low concentrations (0.1 mM  $\text{CaCl}_2$ ) is able to reduce the NaCl-triggered chloride influx (**Figure 25**), while 10 mM  $\text{CaCl}_2$  inhibits the saturation phase almost completely. This finding corresponds to the data presented by Lorenzen *et al.* (2004). The “depolarisation phase” is inhibited, but not completely blocked due to this treatment. This is in line with the results from Shabala *et al.* (2006), where changes in the membrane potential of *Arabidopsis thaliana* cells exposed to different calcium concentrations were recorded. The steady state values of membrane potential of plants grown on full MS after bathing them for one hour in 0.1 mM  $\text{CaCl}_2$  and 10 mM  $\text{CaCl}_2$  have reached  $-127.5 \pm 4.8$  mV and  $-103.7 \pm 4.8$  mV, respectively (Shabala *et al.*, 2006). When 50 mM NaCl were applied to the plants, the less negative membrane potential caused by high  $[\text{Ca}^{2+}]$  lowered the amplitude of salt stress induced membrane depolarisation (Shabala *et al.*, 2006).

A different situation is given, when the  $[\text{Ca}^{2+}]$  is changed in the growth medium. When 10 mM  $\text{CaCl}_2$  is added, the plants show more pronounced NaCl-induced chloride influx (**Figure 24**, blue curve).

Also Ca depleted plants were used for measurements of NaCl-induced chloride influx (**Figure 26B, D**). Lowering internal  $[\text{Ca}^{2+}]$  leads surprisingly not to an accelerated chloride influx when plants are grown on half strength MS. In plants grown on full MS the acceleration of chloride influx due to Ca depletion is more pronounced but not significant. Ca deficiency may cause disintegration of the plasma membrane and thus alter the transport of all other ions too.

### 3.3.3 Salinity induced chloride transport and the role of pH

When tackling the question how chloride is transported into the cell while high NaCl concentrations are applied, an important factor cannot be omitted – the transport of  $H^+$ . Here, the effect of different pH of the superfusion solutions was tested (**Figure 23**). Application of 100 mM NaCl at a higher pH inhibits the influx of chloride (**Figure 23B**, red curve). Higher pH of the outside medium causes extrusion of protons from the cell, in order to maintain the proton gradient, which is important for ion transport. A slight alkalisation of the cytoplasm (~0.3 pH unit) could be measured by using the pH-indicator ptGFP (extrapolated from raw data shown in **Figure 36**), when applying solutions with different pH (pH 6 and pH 8). Moreover, the membrane potential recordings from Felle (1994) show that increased pH causes a membrane depolarisation. This is similar to the reaction of plants to an elevated calcium supply as described above (Shabala *et al.*, 2006). In its principle, this finding can be also applied on the experiments shown here. The less negative membrane potential caused by higher pH would in its consequence alleviate the chloride influx. Surprising here are the measurements with 150 mM NaCl at the pH 8. They show exactly the same chloride kinetic as plants with completely depleted calcium (**Figure 26D**, light blue curve).

### 3.3.4 Chloride flux is sensitive to diuretics and some anion channel inhibitors

It is proposed, that the second phase of the NaCl-induced chloride influx may be driven by electroneutral cation-chloride co-transporters (Lorenzen, *et al.*, 2004; Teakle & Tyerman, 2009). One of them (AtCCC1) was recently expressed in a *Xenopus* oocyte system and found to be a bumetanide-sensitive NKCC (Colmenero-Flores *et al.*, 2007). Moreover, they have shown that the transporter works only in the co-presence of  $Na^+$ ,  $K^+$ , and  $Cl^-$ . This would mean that under salt stress conditions (caused by excess NaCl) the transporter could only work when a sufficient amount of  $K^+$  is present. Anyway, the effect of loop diuretics, a group of substances, where bumetanide belongs to, was tested during the saturation phase of NaCl-induced chloride influx (**Figure 28**, **Table 7**). Torasemide, furosemide and bumetanide are able to inhibit the chloride flux by approximately 50 %. These results suggest, that although the NKCCs play a certain role, they do not cover the entire NaCl-induced chloride transport. Other cation-chloride-cotransport inhibitors, aiming specifically at NCCs and KCCs, show contrasting results (**Figure 29**). All of them lead to strong acidification of the cytoplasm and hence deliver results with Clomeleon, which may be misinterpreted. Since no data are available where the direct effect of the mentioned inhibitors on plants is described, it cannot be determined, whether they acidify the cytoplasm directly (all are weak acids) or by an other mode of action. Also DMSO, which was used for the solubilization of some of them, was tested on its effect on chloride transport (**Figure 30**). The same perfusion sequences as with diuretics were performed with DMSO only. DMSO, a plasma membrane

rigidifier, was shown to have an influence on the uptake of cations by excised barley root cells (Schmid, 1968). The sodium influx was severely inhibited by applying 10 % DMSO. Since the inhibition of sodium influx would consequently lead to an inhibited chloride influx, this mechanism could be an explanation for the results seen in **Figure 29**. Nevertheless, the results show, that DMSO does not cause acidifications of the cytoplasm, as seen with the inhibitors (data not shown).

Furthermore, anion channel blockers and inhibitors were tested for their effect on NaCl-induced chloride influx. It could be shown, that for example A9C was able to block the chloride influx nearly completely. Since the effect of the used anion channel inhibitors on different channels was described in several studies (Hedrich & Kurkdjian, 1988), this is in contrast to the hypothesis of a possible cation-chloride-cotransport during salt stress.

### 3.3.5 Block of chloride flux by trivalent ions $\text{La}^{3+}$ , $\text{Gd}^{3+}$ , and $\text{Al}^{3+}$

$\text{La}^{3+}$  and  $\text{Gd}^{3+}$  are usually used to block calcium permeable channels. However, Lewis and Spalding (1998) showed that  $\text{La}^{3+}$  is causing a non-selective channel block, also inhibiting anion channels. Also,  $\text{Al}^{3+}$  is well known to block calcium conducting channels (Plieth *et al.*, 1998). The data given here (**Figure 32**) suggest that  $\text{Gd}^{3+}$  and  $\text{Al}^{3+}$  are - like  $\text{La}^{3+}$  - also non selective channel blockers acting on a broad variety of ion-transporters. This leads to the assumption that the Cl<sup>-</sup> influx during salt treatment is possibly mediated by channels.

### 3.3.6 Inhibition of chloride influx by spermine

The accumulation of polyamines like putrescine, spermidine and spermine during abiotic stress was reported before (Evans & Malmberg, 1989, Alcazár *et al.*, 2006; 2010). In particular, during salt treatment this effect can be seen (Basu & Ghosh, 1991; Erdei *et al.*, 1996). Deletions in the polyamine metabolism by transgenic approach lead to salt hypersensitivity (Yamaguchi *et al.*, 2006, 2007). Furthermore, modulation and block of certain plant cation channels by polyamines have been reported (Colombo *et al.*, 1992; Dobrovinskaya *et al.*, 1999; Kusano *et al.*, 2007, Shabala *et al.*, 2007). The slight transient inhibition of the chloride kinetic by spermine (**Figure 33**) suggests once more a role of channels in the salt stress induced chloride influx.

### 3.3.7 Chloride influx is redox-sensitive

Applying the oxidative agents  $\text{H}_2\text{O}_2$  and aldrithiol on salt treated plants accelerates the chloride influx profoundly (**Figure 34**). Now, there are two possibly related phenomena: One is that that Cl<sup>-</sup> entry is activated by oxidative treatment. The activation of  $\text{Ca}^{2+}$ -permeable channels in plasma membranes by  $\text{H}_2\text{O}_2$  and other ROS causing  $\text{Ca}^{2+}$  elevation in the cytosol was described before (Pei *et al.* 2000; Demidchik *et al.* 2003, 2007; Foreman *et al.* 2003). For certain animal and human Cl<sup>-</sup> channels and cation chloride co-transporters the modulation by ROS has been shown (Kourie *et al.*,

1998 and references cited therein). Although no direct evidences are given, it is possible that similar mechanisms also work on the Cl<sup>-</sup> transport in plants.

The other phenomenon is that salt stress itself leads to the release of ROS (Hernandez *et al.* 1993; Fedoroff, 2006; Leshem *et al.*, 2006; Leshem & Levine, 2007). Leshem *et al.* (2006) reported H<sub>2</sub>O<sub>2</sub> release in plant cells under salt stress. They put forward a model by which H<sub>2</sub>O<sub>2</sub> is transported through the membranes and therefore is theoretically able to modulate plasma membrane channels. Bienert *et al.* (2007) presented the direct evidence that H<sub>2</sub>O<sub>2</sub> is transported through aquaporins between the cellular compartments. Hence, there are certain indications that a self amplifying positive feedback loop exists between NaCl treatment leading to ROS release thus facilitating increased anion entry and hence a further ROS-release. However, the redox-sensitivity of Clomeleon is hindering in framing a definite conclusion.

To confirm, that ROS are released during salt stress the changes in antioxidative capacity of *Arabidopsis thaliana* was measured (**Chapter 4**).

### 3.3.8 AtClC-A mediates the nitrate influx into the vacuoles of onion epidermal cells

The compartmentalisation of chloride in vacuoles can contribute to plant's salt tolerance (**Chapter 1**). Very recently, it has been shown, that AtClC-C plays a role in regulating chloride homeostasis during salt treatment in *Arabidopsis thaliana* (Jossier *et al.*, 2010).

The experiments with onion bulb epidermis cells co-bombarded with Clomeleon and different *Arabidopsis thaliana* chloride channels give an insight into the role of these channels in compartmentalisation of anions during salt treatment (**Figures 46** and **47**). The selectivity of the ClCs was assigned to specific residues (GXGIP, Dutzler *et al.*, 2000), where one amino acid exchange (S to P, or P to S) can lead to altered selectivity (chloride to nitrate and vice versa). This exchange was performed here with AtClC-A. The obtained construct (AtClCA\_mut) carries a serine instead proline in the selectivity filter and therefore was proposed – like the AtClC-C - to transport chloride preferentially. Clomeleon is an anion sensitive indicator (Kuner & Augustine, 2000). It is sensitive to chloride, but also to nitrate (Lorenzen *et al.*, 2004). This property was utilised to characterize the channel-mediated nitrate flux.

The chloride concentration while perfusing cells with KCl was lower when AtClC-C was expressed. In line with this data, were the chloride kinetics with AtClCA\_mut. In contrast, with AtClC-A the cells showed the same chloride kinetic (**Figure 46B**, blue curve) as the control experiments with Clomeleon only (**Figure 46B**, purple curve). Seemingly, AtClC-A, in its characteristic as a NO<sub>3</sub><sup>-</sup>/H<sup>+</sup> antiporter, is less able to transport chloride into the vacuole. When the same perfusion experiments were carried out with KNO<sub>3</sub>, the resulting kinetics for AtClC-A and AtClCAmut show opposite behaviour (**Figure 47**). These results are consistent with the data presented by Bergsdorf *et al.* (2009).

However, the localisation of the expressed anion channel in onion epidermal cells still needs to be demonstrated. Also the relatively low NaCl/KCl-induced chloride influx compared to *Arabidopsis thaliana*, might implicate, that onion cells are not optimal, to characterise channels residing on the membranes of intracellular compartments.

## CHAPTER 4

### FINGERPRINTING ANTIOXIDATIVE ACTIVITIES

To quantify changes in the antioxidative system of plants after abiotic stress summary parametric assays were developed from chemiluminescence assays. They allow the quantification of:

- 1) the total antioxidative capacity (TAC) of low-molecular-weight metabolites,
- 2) the luminol converting peroxidase activity (LUPO)
- 3) the total superoxide scavenging activity (SOSA) of high-molecular-weight compounds including SODs.

These summary parametric assays yield information about the general antioxidative status and about specific aspects of the antioxidative system, rather than exact data about single antioxidant species, their tissue concentration and distribution or the activity of particular antioxidative enzyme isoforms.

The relevant conditions for maximal long-lived light output and reproducibility were further optimised during this study. The chemiluminescence assays were extended by two common photometric assays for glutathione reductase (GR) and catalase (CAT). All 5 parameters displayed in a polygonal diagram, the so called 'fingerprint', give a general overview about changes in the entire antioxidative status in a plant exposed to different abiotic stimuli.

#### 4.1. MATERIAL AND METHODS

##### 4.1.1 Chemicals, consumables and equipment

All used chemicals, reagents and their sources as well as the used equipment are specified in the **Suppl\_materials 1-3**.

##### 4.1.2 Solutions and buffers

<u>0.5 x MS medium</u>	2.2 g/l ready to-use MS medium pH adjusted with KOH to 5.8 autoclaved
<u>Vertical agar plates 1xMS</u>	see Chapter 2 Section 2.1.2
<u>Vertical agar plates 1xMS-CaCl<sub>2</sub></u>	see Chapter 2 Section 2.1.2
<u>Bradford stock</u>	50 mg Coomassie Brilliant Blue G250 25 ml ethanol abs. 50 ml 85% orthophosphoric acid brought to 500 ml with Milli-Q water
<u>TriCa</u>	100 mM TRIS-HCl pH 8.6 2 mM CaCl <sub>2</sub> degassed by bubbling with N <sub>2</sub> and stored at 4°C
<u>TriCaT</u>	100 mM TRIS-HCl pH 8.6 2 mM CaCl <sub>2</sub>



	1 mM Triton <sup>®</sup> X-100
<u>Iodophenol stock</u>	100 mM colourless solution in ethanol abs.
<u>Luminol stock</u>	1 M solution in 5 M KOH
<u>HRP master mix</u> (sufficient for ca. 2000 samples)	20 µl ethanolic iodophenol stock 500 µl luminol stock 100 µl HRP suspension 660 µl Triton <sup>®</sup> X-100 1 l TriCa
<u>KPP buffer</u>	100 mM K <sub>2</sub> HPO <sub>4</sub> 100 mM KH <sub>2</sub> PO <sub>4</sub> adjusted to pH 7.4 by combining both solutions for dialysis stored at 4°C
<u>EDTA stock (2M)</u>	5.85 g dissolved in KOH
<u>KPET buffer</u>	KPP buffer 0.1 mM EDTA by diluting the EDTA stock 6 mM Triton <sup>®</sup> X-100
<u>Hypoxanthine stock</u>	1 M solution in 5 M KOH
<u>Xanthine stock</u>	4 mM in 1 M KOH

### 4.1.3 Processing of plant material

#### 4.1.3.1 Growing and stress treatment of garden cress (*Lepidium sativum*)

In a first approach, the antioxidative status of *Lepidium sativum* plants exposed to different abiotic stress treatments was analyzed. Garden cress was chosen for its ability to produce high fresh weight amounts in a short period. Seeds were obtained from Sperli (#42.953, Germany, [www.sperli-samen.de](http://www.sperli-samen.de)). 4 g of seeds were surface sterilized by vortexing (2 min) in 80 % ethanol and dried on filter paper. The seedlings were grown in a growth room at 21°C with 16 h photoperiod (50 µE, white fluorescent lamps Osram L36 W/77) for five to seven days before treatment with abiotic stress.

For salt and drought treatment *Lepidium sativum* was grown hydroponically on 0.5 x MS medium in the growth room in sterile Growtek<sup>™</sup> culture vessels (#BEL1768; BLD Science<sup>®</sup>, NC, USA; <http://www.bestlabdeals.com>). Salt stress was induced by replacing the nutrient medium by 150 mM NaCl in 0.5 x MS medium. Salinity was applied for 24 h in the growth room. For recovery, the salt solution was removed and the roots were rinsed with tap water to remove the excessive salt. The plants were then grown for further 24 h in Growtek<sup>™</sup> vessels with 0.5 x MS medium, under the previous growth conditions. To induce drought stress the nutrient medium of hydroponically grown plants was completely withdrawn. Drought was applied for 24 h. This period was sufficient to produce an appreciable limp appearance and yet short enough to maintain the ability for full recovery. For recovery, 0.5 x MS medium was added and plants were allowed to

grow for another 24 h under normal conditions. Green parts of the plants were harvested, portions of 4 g FW were snap-frozen in liquid nitrogen and stored at -80°C until processed.

For cold and heat treatment surface-sterilised seeds were sown on 2 layers of synthetic capillary matting (medical fleece "Rolta<sup>®</sup>-soft" # 932048, Hartmann, DE, <http://de.hartmann.info/>) soaked with 0.5 x MS medium placed in a mini propagator (26 x 11 x 7 cm, Windhager<sup>®</sup>; Austria; [www.windhager.at/](http://www.windhager.at/)). Cold and heat stress were applied by placing the whole mini-propagator for 12 h at 0°C, or for 6 h at 42°C, in the dark. Recovery times were allowed for 12 h and 6 h respectively in the growth room. Whole plants were harvested, snap-frozen in liquid nitrogen in portions of 4 g FW and stored at -80°C until processed.

Untreated controls for all four stress conditions were run in parallel.

#### 4.1.3.2 Growing and stress treatment of *Arabidopsis thaliana* and *Thellungiella salsuginea*

Seeds of *Arabidopsis thaliana* Col-0 and its salt tolerant relative *Thellungiella salsuginea* ecotype Shandong were grown on sterile vertical 1 x MS agar plates supplemented with 50 and 75 mM NaCl. Together with the respective controls they were grown as described previously (**Chapter 2, Section 2.1.3**).

#### 4.1.3.3 Processing of plant samples

*Lepidium sativum* plant material was ground with pre-cooled mortar and pestle on the day before measurements. Longer storage of ground material was found to alter the outcome of following experiments (data not shown).

The plant material from *Arabidopsis thaliana* and *Thellungiella salsuginea* was ground in pre-cooled 2 ml screw-cap tubes, provided with 5 glass beads ( $\varnothing = 1$  mm) in a tissue homogenizer (Precellys, PeqLab, Erlangen, DE) with 5800 rpm for 20 sec. The grinding time was long enough to get homogeneously pulverized material but not too long to let the samples thaw.

Ten volumes ice-cold TriCa (degassed by bubbling with N<sub>2</sub>) and 1 mM Triton<sup>®</sup>X-100 were added to the powder (ml/g), vortexed for 2 min, and filtered through a fluted paper filter in a 0°C cabinet under N<sub>2</sub>-atmosphere. This crude extract was aliquotted for membrane filtration (TAC) and for dialysis (LUPO, SOSA, CAT and GR assays). For analysis of low-molecular-weight total antioxidative capacity (TAC) the crude extract was passed through a membrane filter (MWCO = 10 kDa) by centrifugation at 0°C at maximum rotations accordingly to the manufacturer's instructions. For assaying enzyme activities the crude extract was dialysed in membrane tubing (MWCO = 10 kDa) against the two hundred-fold volume of ice-cold KPP buffer. The buffer was changed after 6 hours of dialysis. The overall duration of dialysis was 30 min per 100  $\mu$ l dialysate.

#### 4.1.4 Protein content measurements

Assay results have to be displayed with reference to an invariable parameter. However, dry weight is not invariable with salt treatment due to considerable salt uptake. The same is true when fresh weight is used as a reference, because of water uptake. Consequently, the total protein content as a reference parameter was employed, knowing that this may also vary within certain limits. Thus, the protein concentration of crude extracts and dialysed samples was determined by the Bradford assay (Bradford, 1976). The protein content of crude extracts was cross-checked with that of dialysed samples as an internal control of the dialysis process. 15 ml of the Bradford stock were diluted with 75 ml Milli-Q water in order to match with the protein concentration of undiluted plant extracts. A logarithmic dilution series of BSA (1.5; 3; 6; 12; 24; 48 and 96  $\mu\text{g}/\mu\text{l}$ ) was prepared in cuvettes in 3 ml diluted Bradford stock. 50  $\mu\text{l}$  of the dialysate and crude extract were added to 2.95 ml of the diluted Bradford stock. The samples were mixed well and let stand for at least 10 min. The absorption at 596 nm was recorded. Cross-sensitivities of the Bradford assay with low-molecular-weight compounds could not be detected. Before running the LUPO, SOSA, GR and CAT assays, all samples were supplemented with buffer in order to equalise differences in protein concentrations. The results of the TAC assay were equalized on the basis of the protein content of crude extracts.

#### 4.1.5 Total antioxidative activity (TAC) assay

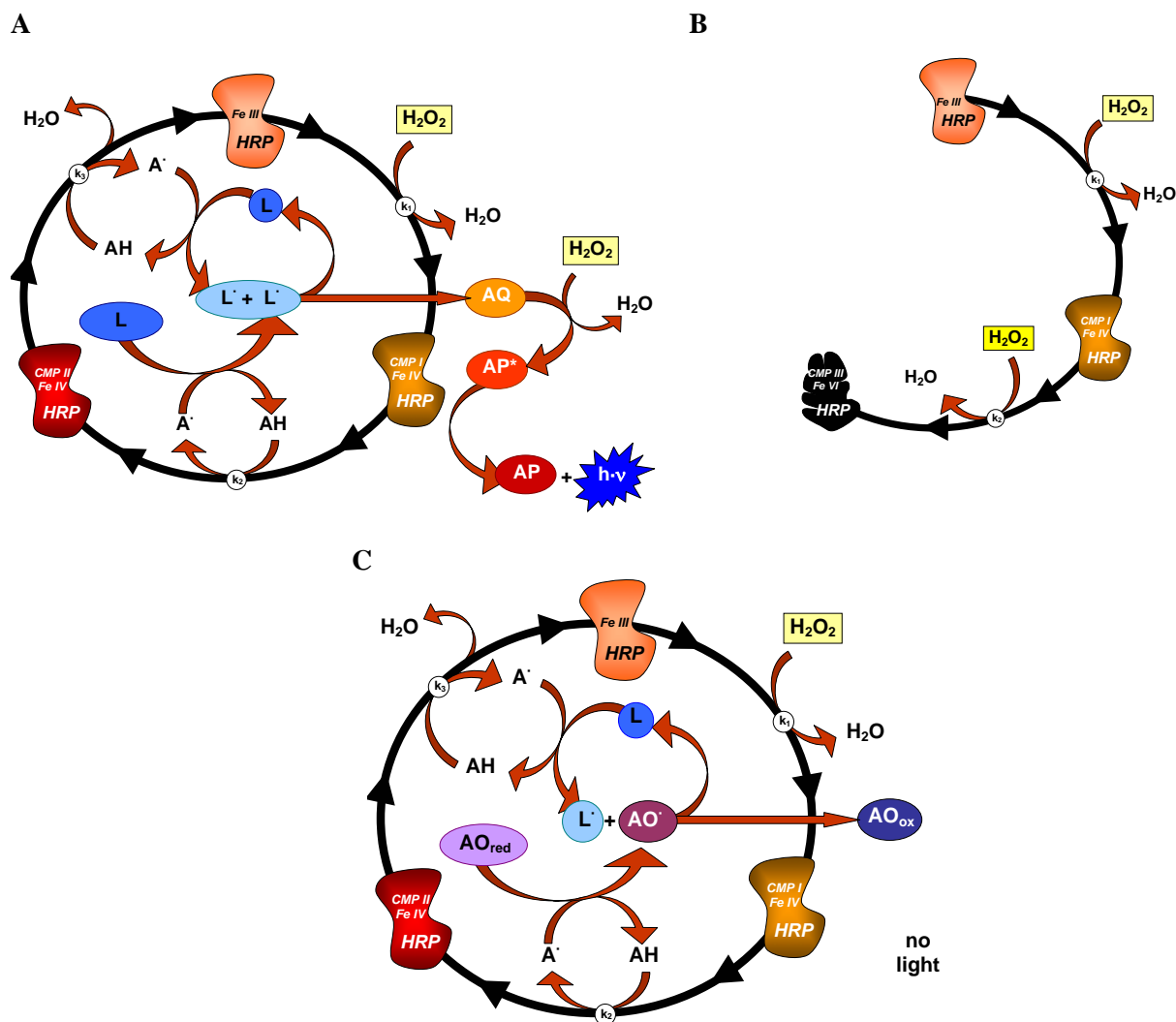
##### 4.1.5.1 Principle of the TAC assay

Luminol (L, 3-aminophthalhydrazide) is a frequently used reagent which emits light when oxidised by  $\text{H}_2\text{O}_2$  to aminophthalate (AP) under alkaline conditions. This chemiluminescence reaction can be catalysed by peroxidases (POs) such as horseradish peroxidase (HRP). The HRP-catalysed luminol reaction involves three steps by which the HRP protein undergoes conformational changes until functional HRP is regenerated (**Figure 52A**; Nazari et al., 2005; Veitch, 2004). This redox reaction driven by  $\text{H}_2\text{O}_2$  is the general basis of TAC assay. Phenolic electron donators (AH, **Figure 52A**) with higher affinity to HRP than luminol and with the OH group in *para*-position enhance the luminescence drastically (Sánchez *et al.*, 1995; Thorpe *et al.*, 1985). These enhancers (AH) serve as primary substrates for the HRP and their radicals ( $\text{A}^{\cdot}$ ) subduct electrons from luminol and thus form the radical luminol form ( $\text{L}^{\cdot}$ ). For the TAC assay as described here, 4-iodophenol was used as enhancer (**Suppl\_Material 19**; **Figure\_Suppl 6**).

Although the light reaction is driven by  $\text{H}_2\text{O}_2$ , an excess of it inactivates the HRP (**Figure 52B**, **Suppl\_Material 19**; **Figure\_Suppl 7B**; Nazari et al., 2005; Nicell & Wright, 1997). It gives a big light flash which decays to almost zero (**Suppl\_Material 19**; **Figure\_Suppl 7B**). The same is true, when the HRP-driven reaction is enhanced by 4-iodophenol (see Saleh & Plieth, 2009). The

optimal  $\text{H}_2\text{O}_2$ /HRP-ratio is given, when the signal, after  $\text{H}_2\text{O}_2$  injection, quickly increases and levels off to give a constant long lasting glow.

In contrast, peroxidases from *Lepidium sativum* show no direct inactivation even by high  $[\text{H}_2\text{O}_2]$  (Suppl\_Material 19; Figure\_Suppl 7A).

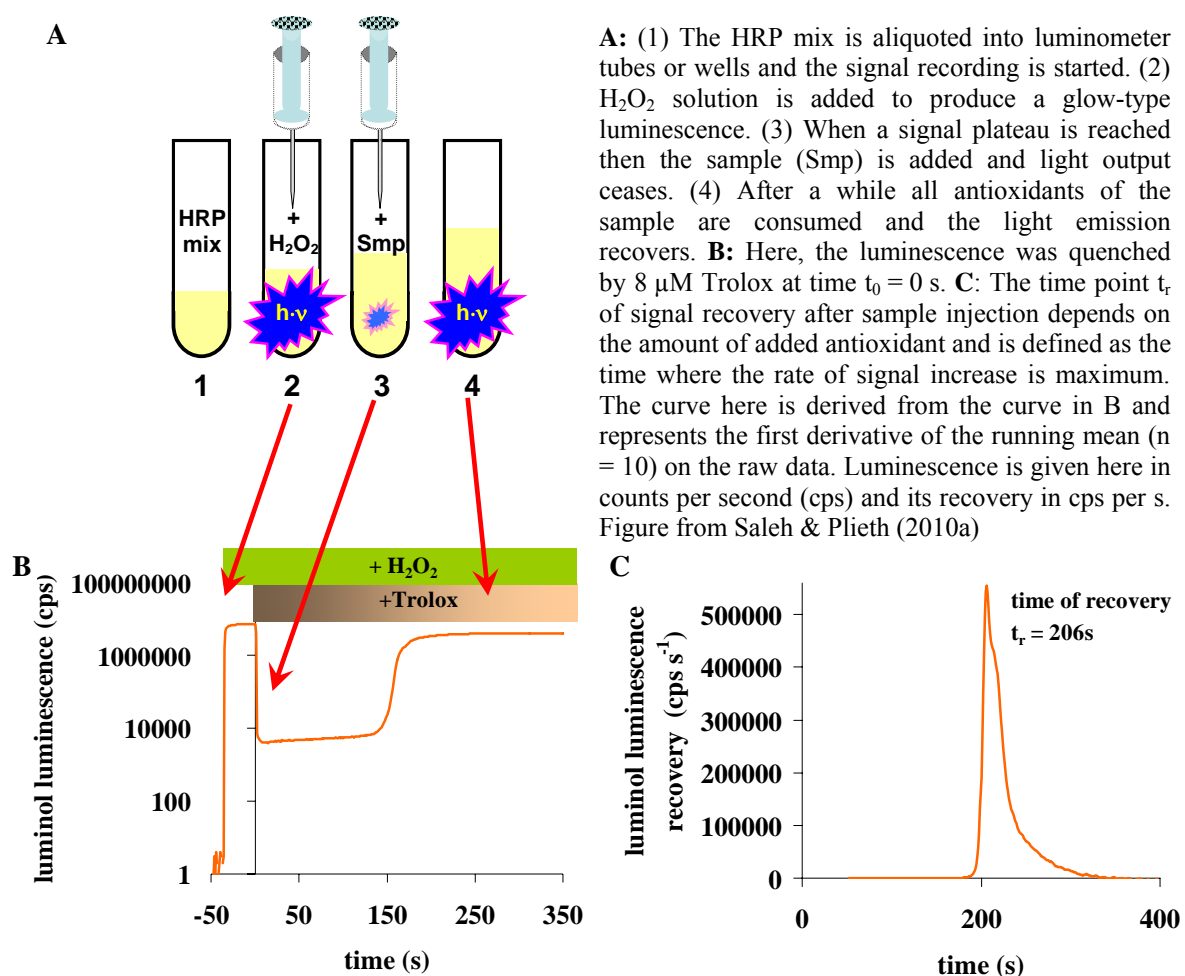


**Figure 52: HRP-driven reaction cycle**

**A:** An aromatic hydrogen donor (AH), serves as a primary substrate for the HRP and is oxidised in presence of  $\text{H}_2\text{O}_2$ . Its radical ( $\text{A}^\cdot$ ) subducts electrons from luminol (L), and forms the radical luminol form  $\text{L}^\cdot$ . During this reaction HRP undergoes conformational changes designated as compound-I state (CMP I) and compound-II state (CMP II). A di-aza-quinone (AQ) is formed as an intermediate of luminol by electron transfer between two  $\text{L}^\cdot$ . This in turn is oxidised by hydrogen peroxide ( $\text{H}_2\text{O}_2$ ) to form an excited state of aminophthalate ( $\text{AP}^*$ ). The final step is the emission of blue (420 nm) light ( $h\nu$ ) when the excited  $\text{AP}^*$  returns to its ground state (AP). **B:** The HRP CMP I state is sensitive to excess of  $\text{H}_2\text{O}_2$  and can undergo a so-called 'suicide reaction' when the  $\text{H}_2\text{O}_2$  is in excess. **C:** In presence of antioxidants (AO) with a reduction potential lower than that of luminol, electron transfer occurs between  $\text{L}^\cdot$  and  $\text{AO}^\cdot$ . Thereby the formation of AQ and thus luminescence is blocked. Scheme from Saleh & Plieth (2010b)

## 4.1.5.2 Setting up the TAC assay

For setting up the TAC assay, several factors were considered. At first, a suitable buffer system for the reaction had to be found. The pH-optimum was found to be around pH 8.7 (**Suppl\_Material 19; Figure\_Suppl 8**). Even though molecular oxygen ( $O_2$ ) is not involved in the HRP-reaction (Baker *et al.*, 2000; Cercek *et al.*, 1994; Nakamura & Nakamura, 1998), other additives that enhance enzyme turnover and stability, such as calcium and surfactants, are required. Calcium is an essential cofactor for HRP (Chattopadhyay & Mazumdar, 2000; Morishima *et al.*, 1986; Veitch, 2004). Light output ceases, when free calcium is present in concentrations below  $0.01 \mu\text{M}$  (**Suppl\_Material 19; Figure\_Suppl 9**). The most suitable concentration lies between 1-2 mM  $\text{Ca}^{2+}$ . Surfactants are also beneficial, as they seem to stabilise the protein, and thus enhance the light output (Ilyna *et al.*, 2000; Nicell & Wright, 1997). Non-ionic detergents, such as Triton<sup>®</sup>-X-100 (1 mM), were found to be optimal.



Light output is started by adding  $\text{H}_2\text{O}_2$  to the reaction mixture (**Figure 53A, B**). Antioxidants (AO, i.e. compounds of a reduction potential lower than that of L) added to the assay compete with L in donating electrons and protons and neutralize luminol radicals (**Figure 52C**). Light output is

therefore quenched according to the amount of antioxidant and recovers as soon as all antioxidants are oxidized. The delay time (time of light recovery) is used to quantify the amount of antioxidants added with the sample (**Figure 53C**).

Samples from living organisms always contain the full complement of their antioxidative factors. This includes peroxidases and catalases which may compete with HRP in the assay and thus influence the light output and lead to erroneous TAC values (**Suppl\_Material 19; Figure\_Suppl 10**). Hence, the low molecular weight antioxidants to be quantified have to be separated from enzymatic activities. Therefore the plant extract was divided into low- and high-molecular-weight fractions with an MWCO of 10 kDa.

In the low-molecular-weight fraction of plant extracts phenolic compounds (e.g. flavonoids) may be present. They possess antioxidative capacity *in vitro* (**Suppl\_Material 19; Figure\_Suppl 11**, Sichel *et al.*, 1991; Rice-Evans *et al.*, 1997). However, those with activating substituent in the *para*-position (such as naringenin, saponarin, lutoarin) are able to enhance the HRP-driven light output. Different concentrations of naringenin and 4-iodophenol were therefore tested by means of the not-enhanced TAC assay (**Suppl\_Material 19; Figure\_Suppl 12**). Since plant extracts typically contain compounds such as shown in **Suppl\_Material 19; Figure\_Suppl 12**, it may happen that they enhance the HRP-driven luminescence. For instance, high amounts of saponarin and lutoarin have been found in barley (Benedet *et al.*, 2007; Burchard, 2001; Liu *et al.*, 1995). At high dilution (between 1:200 and 1:20) the antioxidant effect (luminescence quenching) of the extract of 8-day-old barley plants is overrun by the enhancing effect of the present flavonoids (**Suppl\_Material 19; Figure\_Suppl 13**). The enhancing effect saturates at sample dilution of 1:10. At higher extract concentrations the quenching effect is more pronounced. Thus, if measuring plant samples containing endogenous enhancer of the HRP-activity, it is necessary to appropriately concentrate the extract, in order to measure antioxidative capacity of low-molecular weight antioxidants.

#### 4.1.5.3 Assaying the plant samples

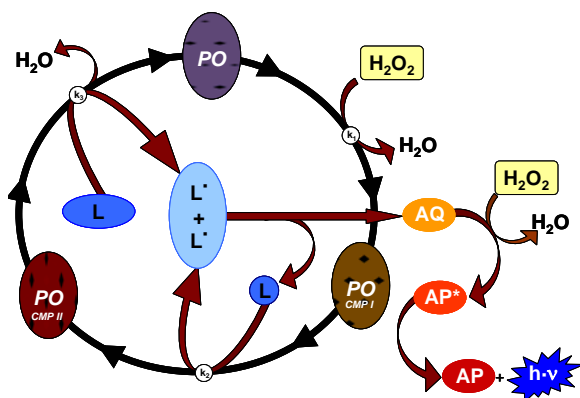
0.5 ml of HRP mix (stable for several weeks, when stored at 4°C) was aliquotted 1 hour before starting measurements into luminometer vials. H<sub>2</sub>O<sub>2</sub> (1.1 mM) solution was prepared by diluting H<sub>2</sub>O<sub>2</sub> -stock (30%) 1:8000 in 100 ml of TriCa buffer. The samples obtained from membrane filtration were diluted 1:200 (*Lepidium sativum*) and 1:100 (*A. thaliana* and *T. salsuginea*) in TriCaT buffer. Antioxidants are quickly oxidized by ambient air. The stability in presence of ambient oxygen is different for each type of antioxidant (**Suppl\_Material 19; Figure\_Suppl 14**). Therefore, it is essential to minimize the contact of samples with ambient air during the processing.

To avoid oxidation of antioxidant compounds by ambient oxygen, the dilution was carried out only few minutes before starting the measurements. The vial with 0.5 ml HRP mix was placed into the luminometer. The luminescence background signal was recorded for 12 s. The light emitting reaction was started by adding 0.5 ml  $\text{H}_2\text{O}_2$  solution at the time point 36 s. After establishment of a constant signal, the luminescence was quenched by injecting the diluted sample (500  $\mu\text{l}$ ). Light recording was continued until luminescence recovery.

#### 4.1.6 Luminol converting peroxidase assay

##### 4.1.6.1 LUPO assay principle

Peroxidases are widely distributed among living organisms and perform multiple physiological roles (Azevedo *et al.*, 2003; Bowler *et al.*, 1992b; Hiraga *et al.*, 2001; Mittler, 2002). They are considered important members of the antioxidative system since they remove detrimental peroxides. They have broad substrate specificity and need organic substrates such as flavonoids for catalysis (Kawano, 2003). Some of them also accept artificial electron donors such as luminol (L, **Figure 54**). Hence, the light generating process can be used for quantification of peroxidase activity. The luminol converting peroxidase (LUPO) assay is derived from the TAC assay. The LUPO assay is not enhanced by 4-iodophenol (**Figure 54**) and only the total light output is recorded as a measure for the amount of peroxidase activity in the sample.



**Figure 54: The luminol converting peroxidase (LUPO) cycle.**

Luminol (L) is accepted as substrate by many plant peroxidases (PO). Hence, the light generating process can be used for the quantification of peroxidase activities. In contrast to the HRP cycle (**Figure 52**), there is no inactivation of the light emitting reaction at higher  $\text{H}_2\text{O}_2$  concentrations. Scheme from Saleh & Plieth (2009).

##### 4.1.6.2 Assaying the plant samples

Low molecular weight  $\text{H}_2\text{O}_2$ -scavengers may interfere with the LUPO reaction. Therefore, the protein fraction was purified by dialysis (**Section 4.1.3.3**). Luminol (1 mM) solution was prepared by diluting 1 M luminol stock in TriCaT. A 6.6 mM  $\text{H}_2\text{O}_2$  solution was prepared from  $\text{H}_2\text{O}_2$  (30 %) in TriCaT for assaying the *Arabidopsis thaliana* and *Thellungiella salsuginea* samples. For *Lepidium sativum* a 17.6 mM  $\text{H}_2\text{O}_2$  solution was diluted from  $\text{H}_2\text{O}_2$  (30 %) in TriCaT. All dialysed samples were diluted 1:100 in TriCaT.

0.5 ml of diluted sample was then mixed with 0.5 ml luminol solution in a luminometer vial, adjusted to RT in the dark for 1 hour and background luminescence was recorded. The light reaction was started by adding 0.5 ml 6.6 mM (*A.thaliana* and *T.salsuginea*) or 17.6 mM H<sub>2</sub>O<sub>2</sub> (*L.sativum*) solution. Light output was recorded for several minutes and integrated counts were used as measure for peroxidase activity of the sample.

#### 4.1.7 Superoxide scavenging activity (SOSA) assay

Since XOD was employed for superoxide production in the SOSA assay, it was necessary to rule out the presence of XOD-inhibitors or endogenous XOD activity in the screened plant samples. Furthermore, the light output of the SOSA assay is dependent on the efficiency of this enzyme. Thus, the detailed knowledge of XOD, its reaction mechanism, and the relevant frame conditions was inevitable.

##### 4.1.7.1 XOD reaction mechanism

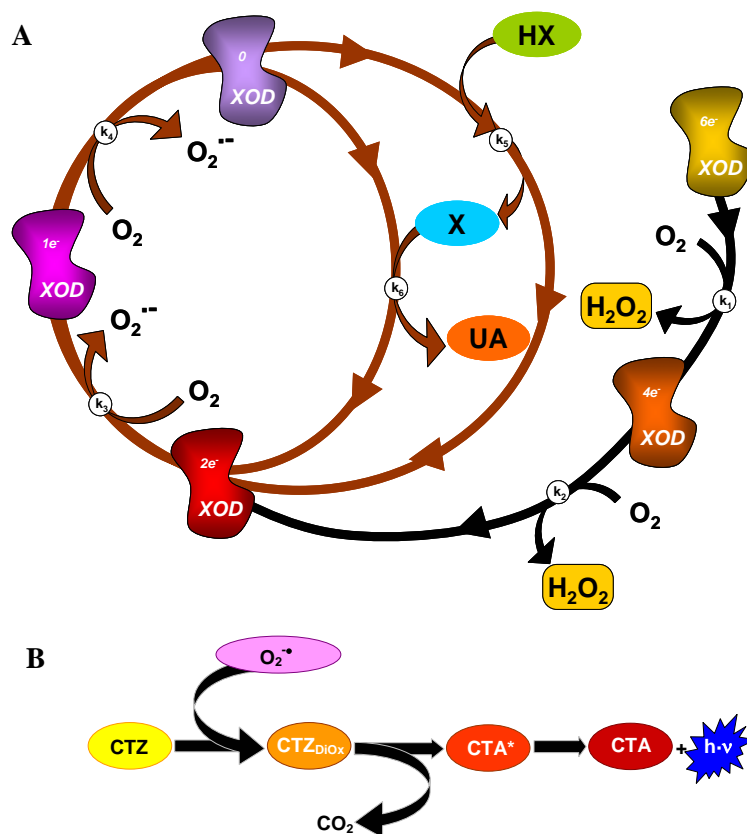
XOD from cow's milk is a homodimer with a molecular mass of 300 kDa, with catalytically independent subunits possessing four prosthetic groups: one molybdenum centre, one FAD, and two Fe<sub>2</sub>S<sub>2</sub>(Cys)<sub>4</sub> centres (Xia *et al.*, 1999). The enzyme catalyzes the oxidative hydroxylation of hypoxanthine to xanthine and the subsequent hydroxylation of xanthine to uric acid (**Figure 55A**, brown cycle). However, it can hydroxylate a wide variety of other purines, pteridines, and related aromatic heterocycles.

Substrate hydroxylation takes place at the molybdenum centre of the enzyme, which becomes reduced from Mo<sup>VI</sup> to Mo<sup>IV</sup> in the process (Hille *et al.*, 1993; Olson *et al.*, 1974). The reducing equivalents are subsequently passed via intramolecular electron transfer to the flavin centre, where reaction with O<sub>2</sub> takes place to give peroxide or superoxide; depending on the level of enzyme reduction (Porras *et al.*, 1981). The oxidative half-reaction (**Figure 55A**, black cycle) takes place in order to re-oxidize the fully reduced XOD (6-electron reduction). During the whole re-oxidation process two molecules of H<sub>2</sub>O<sub>2</sub> and two molecules of O<sub>2</sub><sup>•-</sup> are produced.

The reductive half-reaction (**Figure 55A**, brown cycle) occurs in presence of hypoxanthine, working here as a two electron donator. Thereby the enzyme is reduced (XOD 2e-) and subsequently the slow phase of the oxidative half-reaction with oxygen initiated. Here, two superoxide molecules are released. Depending on the XOD reduction state, it is possible, that also H<sub>2</sub>O<sub>2</sub> is produced. Therefore, if using this reaction to produce superoxide in situ, it is necessary to work with fully oxidized enzyme.

Xanthine oxidase is very sensitive to excess H<sub>2</sub>O<sub>2</sub> in presence of a substrate. Here, H<sub>2</sub>O<sub>2</sub> acts as an electron acceptor. Millimolar concentrations are able to interfere with the reductive reaction (Lynch & Fridovich, 1979; Terada *et al.*, 1991). Thereby hydroxyl radical is produced.





**Figure 55: Proposed mechanism of oxidative (black cycle) and reductive (brown cycle) half-reactions of XOD and the interaction of superoxide with coelenterazine in the SOSA assay**

**A:** During the oxidative half-reaction reaction two phases can be distinguished. In the fast phase oxygen binds rapidly to fully reduced flavin and a flavin semiquinone-superoxide complex is generated due to one-electron transfer. If more than 2 electrons are left in the enzyme, FADH<sub>2</sub> is regenerated by intramolecular transfer from the reduced iron-sulphur cluster and Mo. The second electron is transferred to O<sub>2</sub><sup>•-</sup> to produce H<sub>2</sub>O<sub>2</sub>. When XOD(2e-) is produced the slow phase initiates. Here, oxygen binds at the same rate, but the flavin cannot be regenerated, since the Fe cluster exhibits up to 10-fold greater affinity to electrons (Porrás *et al.*, 1981). Thus, the O<sub>2</sub><sup>•-</sup> molecule's released. The removal of the last electron from the enzyme produces O<sub>2</sub><sup>•-</sup> too. In contrast, the reductive half-reaction occurs at Mo, where the enzyme accepts two electrons from either hypoxanthine or xanthine, reducing Mo<sup>IV</sup> to Mo<sup>VI</sup>. **B:** The XOD reaction is used to produce superoxide in situ. The presence of superoxide is indicated by CTZ luminescence. The formed superoxide (O<sub>2</sub><sup>•-</sup>) attacks CTZ. A dioxetanone (CTZ<sub>DIOX</sub>) is formed which releases carbon dioxide (CO<sub>2</sub>) to form an excited state of coelenteramide (CTA\*). CTA\* relaxes to its ground state (CTA) by emission of blue (470 nm) light (hν). Figure from Saleh & Plieth (2010a)

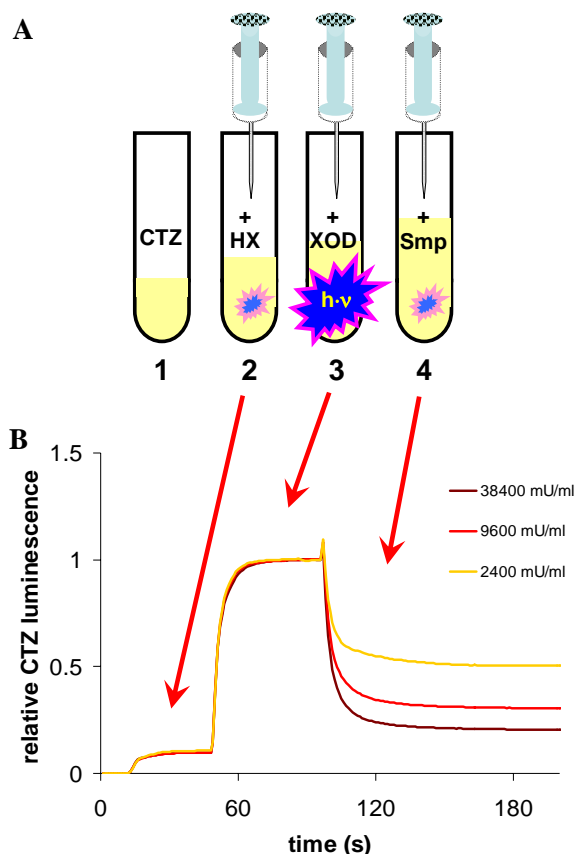
#### 4.1.7.2 XOD assay

Measurement of possible XOD inhibiting and/or endogenous XOD activities of plant samples was carried out before starting the SOSA assay by recording UV- absorption ( $\lambda_{\text{ABS}} = 293 \text{ nm}$ ) of uric acid (Praetorius & Poulsen, 1953) in UV- transparent cuvettes in a spectrophotometer (Ultraspec 2100pro; GE-Healthcare, München, DE). XOD from bovine milk was diluted 1:5, xanthine stock 1:100 (end concentration 0.04 mM), both in KPP. 945  $\mu\text{l}$  of diluted xanthine stock were pipetted into a cuvette and the background was recorded for 30 s. Then 5  $\mu\text{l}$  of XOD solution (end dilution of 1:3000) were added to start the reaction and mixed thoroughly. The uric acid production was recorded for further 2 min. 50  $\mu\text{l}$  undiluted dialysed sample were injected to see any detectable

effect on the XOD activity. As a negative control 50  $\mu\text{l}$  KPP were injected, in order to get hold of possible dilution effects. However, for the SOSA assay, a 'matrix'-induced inhibition of XOD as measured by a decreased urate production ( $A_{293}$ ) was different from species to species, but negligible (data not shown). If the dialysate contains XOD activity, this would produce additional superoxide, which could be then misleadingly interpreted in terms of less scavenging activity in the SOSA assay. Also this effect is negligible with the sample dilutions used here (data not shown).

#### 4.1.7.3 SOSA assay principle

The procedure for assaying the superoxide anion scavenging activity (SOSA) is based on the quenching of chemiluminescence from the light-yielding substrate coelenterazine (CTZ). CTZ is a specific superoxide indicator (Lucas & Solano, 1992; Molecular\_Probes, 2001; Teranishi & Shimomura, 1997). Since superoxide is disproportionated to oxygen and  $\text{H}_2\text{O}_2$  within milliseconds (Chen *et al.*, 1991; Elstner, 1990), it has to be produced *in situ*. For this reason XOD has been employed (Section 4.1.7.1).



**Figure 56: The SOSA assay procedure and data evaluation**

**A:** (1) The CTZ solution is aliquotted into luminometer tubes or wells. (2) HX and (3) XOD are added sequentially to produce a glow-type luminescence and the signal is recorded. When a signal plateau is reached then the sample (Smp) is added and light output ceases due to the presence of superoxide scavengers. **B:** In this experiment HX was added at  $t = 12\text{s}$  and light generation was triggered by XOD at time  $t = 48\text{s}$ . Luminescence was quenched by different amounts of superoxide dismutase at  $t = 96\text{s}$  as indicated on the legend. The percentage of light reduction is a quantitative measure for superoxide scavenging activity. Figure from Saleh & Plieth (2010b).

The superoxide produced by XOD oxidizes the coelenterazine, which forms a dioxetanone and by release of carbon dioxide ( $\text{CO}_2$ ) is converted into an excited state (coelenteramide). With relaxation to its ground state (CTZ) blue light ( $\lambda \approx 470 \text{ nm}$ ) is emitted (**Figure 55B**).

While XOD is generating  $\text{O}_2^{\cdot-}$  and thus producing light ( $h\nu$ ) in presence of CTZ, any  $\text{O}_2^{\cdot-}$ -scavengers in the assay reduce the steady state  $\text{O}_2^{\cdot-}$  concentration and thus light output (**Figure 56**). The percentage inhibition of CTZ luminescence is used to quantify the superoxide scavenging activity (**Suppl\_Material 20; Figure\_Suppl 15A**). The sensitivity of the assay spans two orders of magnitude of scavenger concentrations and follows a typical sigmoidal calibration curve (**Suppl\_Material 20; Figure\_Suppl 15B**). Apart from different SOD-isoenzymes, plants possess also non-enzymatic superoxide scavengers. It is possible to distinguish both kinds of scavengers simply by assaying heat-inactivated samples in parallel.

The XOD needs a physiological pH and calcium buffering for high superoxide anion yield. Calcium impairs the light yielding reaction triggered by coelenterazine (Reimer, 2010). However, the production of uric acid and the consumption of oxygen are not impaired (Reimer, 2010). Since enzyme turnover appears unaffected by calcium, there have to be other, as yet unknown, mechanisms of light output inhibition.

In high phosphate buffers  $\text{Ca}^{2+}$  is reasonably low and specific divalent-chelators can be omitted. Other buffer systems, however, require a chelator (e.g. EGTA, EDTA) to buffer divalent cations. Moreover, the activity of XOD is stabilized by non-ionic detergents, like Triton-X-100<sup>®</sup> or Tween 20.

#### 4.1.7.4 Assaying plant samples

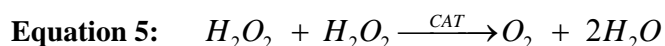
Coelenterazine (50  $\mu\text{M}$ ) solution was prepared by diluting a 5 mM methanolic stock solution in thoroughly de-gassed KPP buffer. This solution was aliquotted to 0.25 ml portions in luminometer vials under oxygen-free atmosphere and capped. The portions were stored at  $-80^\circ\text{C}$ . At the day of measurements HX (1 mM) was prepared by dilution of the alkaline 1 M stock 1:1000 in KPET. Xanthine oxidase mix was prepared by diluting XOD suspension (XOD from bovine milk, Roche, DE) 1:3000 in KPET to have a final activity of ca. 150 mU/ml. The enzyme has to be fully oxidized before usage, in order to produce superoxide with hypoxanthine as a substrate (**Figure 55B**). Dialysed samples from *Arabidopsis thaliana* and *Thellungiella salsuginea* were diluted 1:3 in KPET and the samples from *Lepidium sativum* 1:8. For subsequent quantification of non-enzymatic superoxide scavengers portions of dialysed samples were heated to  $95^\circ\text{C}$  for 20 min and subsequently diluted in KPET.

The CTZ- aliquots were taken out and equilibrated to room temperature for one hour. Dark background from uncapped CTZ aliquots was recorded before injecting 0.25 ml HX-solution (after

12 s). A background luminescence was recorded for 36 s after HX addition and then 0.5 ml XOD mix was injected to initiate the superoxide-CTZ reaction and a long lasting steady-state glow. 0.5 ml of diluted dialysed sample was injected (time point of injection: 96 s) to quench luminescence and light recording was continued for several minutes.

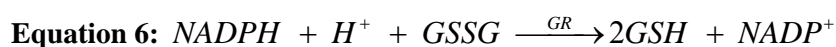
#### 4.1.8 Catalase (CAT) assay

CAT catalyses the conversion of two molecules  $H_2O_2$  to molecular oxygen and two molecules of water (**Equation 5**). The catalase assay used here for quantification of CAT activity is based on UV-absorption ( $\lambda_{\text{ABS}} = 240 \text{ nm}$ ) of  $H_2O_2$  (Beers & Sizer, 1952). The assay buffer consisted of 8.8 mM  $H_2O_2$  (i.e. 1:1000 dilution of 30%  $H_2O_2$ ) in KPP buffer. 1.95 ml of the assay buffer were placed in a quartz cuvette and the  $H_2O_2$  background was recorded for 30 sec in a spectrophotometer (Ultrospec 2100pro; GE-Healthcare, München, DE). The sample was added and the consumption of  $H_2O_2$  was recorded for further 3.5 min. The linear decay of  $A_{240 \text{ nm}}$  was recorded and catalase activity was calculated.



#### 4.1.9 Glutathione reductase (GR) assay

The assay is based on the absorption of light by NADPH, the co-substrate of the GR at  $\lambda_{\text{ABS}} = 340 \text{ nm}$  (**Equation 6**, (Halliwell & Foyer, 1978)). KPP buffer containing 0.1 mM NADPH and 1 mM GSSG was used for assaying the plant samples for the GR activity. 50  $\mu\text{l}$  of dialysed undiluted samples were injected into 450  $\mu\text{l}$  of the assay buffer in a UV-transparent cuvette after recording the NADPH background for 30 sec. The decrease in absorption was assayed with a spectrophotometer (Ultrospec 2100pro; GE-Healthcare, München, DE). The linear decay of  $A_{340 \text{ nm}}$  was recorded for further 3.5 min, and the GR-activity was calculated.



## 4.2 RESULTS

### 4.2.1 Fingerprinting the antioxidative activities of *Lepidium sativum* during different abiotic stress situations

Garden cress (*Lepidium sativum*) was used here as model organism to show how salt stress impacts on the antioxidative system (TAC, LUPO, SOSA, CAT, and GR). Other abiotic stress treatments (i.e. drought, heat and cold) were run in parallel for comparison. Drought stress symptoms have similarities to salt stress, since both impair the ion balance. Heat is also associated with salt and drought stress, since heat leads to increase of evaporation and consequently to elevated salt concentrations in the soil. Formation of low-molecular-weight antioxidants, up- and down-

regulation of enzymes are dependent on the kind of abiotic stress (**Figure 57**). The fingerprints drawn for the measured parameters reveal similarities between seemingly different abiotic stress situations like salt, drought and heat (**Figure 57**, fingerprints). The area of each polygon then gives a quantitative impression of changes in total antioxidative power of the sample. Antioxidative enzymes are individually adapted and regulated back as soon as the plant is allowed to recover from stress (**Figure 57**, gray columns). Only salt stress makes a difference in this regard.

#### 4.2.1.1 Salt stress

The plant's response to salt stress involves two different defence mechanisms: defence against the osmotic component of high salinity and against the toxic ion levels (more details in **Chapter 1**). The combination of both seems to inhibit many of the antioxidative enzymes involved in the examined antioxidative activities (**Figure 57**).

While LUPO, CAT, and GR activities are decreased (**Figure 57**), the results show a significant increase of the superoxide scavenging activity (SOSA; **Figure 57**). After recovery, the activity of the low molecular weight antioxidants (TAC) is up-regulated by more than 60% compared with the control (**Figure 57**). SOSA and GR return towards the control level, whereas LUPO and CAT activities are inhibited even more.

#### 4.2.1.2 Drought stress

Drought stress (i.e. water deficiency) is often said to depend on osmotic pressure changes. Since 'drought' cannot be precisely adjusted in the same way as temperature or salt concentration, in many previous studies osmotic stress produced by mannitol solutions was taken as a surrogate for drought (e.g. Knight *et al.*, 1998). Some studies however considered mannitol a potential antioxidant (Jennings *et al.*, 1998; Smirnoff & Cumbes, 1989). However, subsequent tests have revealed no particular scavenging activity for mannitol (**Suppl\_Material 21**; **Figure\_Suppl 20**). Nevertheless, here drought was induced by total withdrawal of nutrient medium from hydroponically grown plants, to avoid any side effects which may occur with mannitol. Withered plants completely regained turgor during the following recovery period after the nutrient solution was replaced.

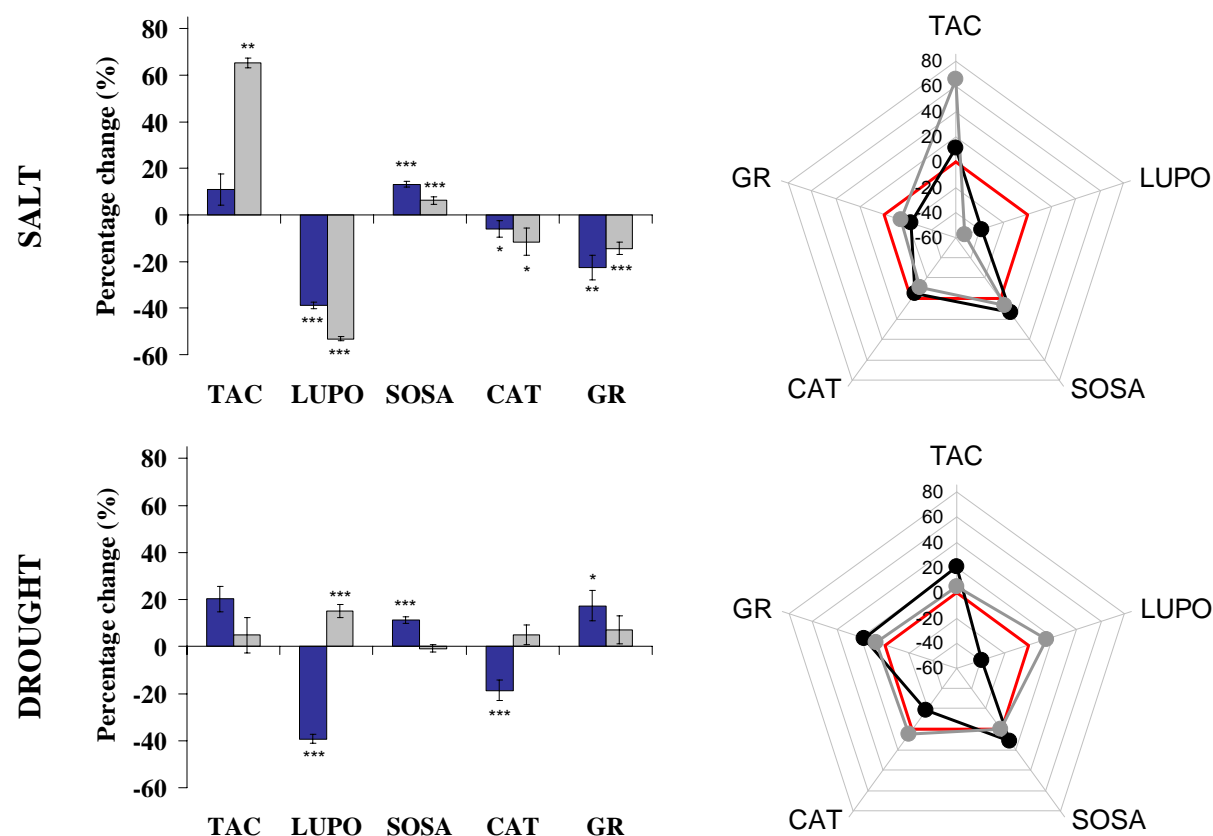
Similar to salt and heat (**Figure 57**) there are certain patterns in the antioxidative parameters, so that the area of the corresponding polygon remains almost unchanged (**Figure 57**). LUPO is decreased, however TAC and SOSA are increased similar to the salt stressed plants. These three parameters are regulated in the same way also during heat stress (**Figure 57**), suggesting similarities between all three stress kinds.

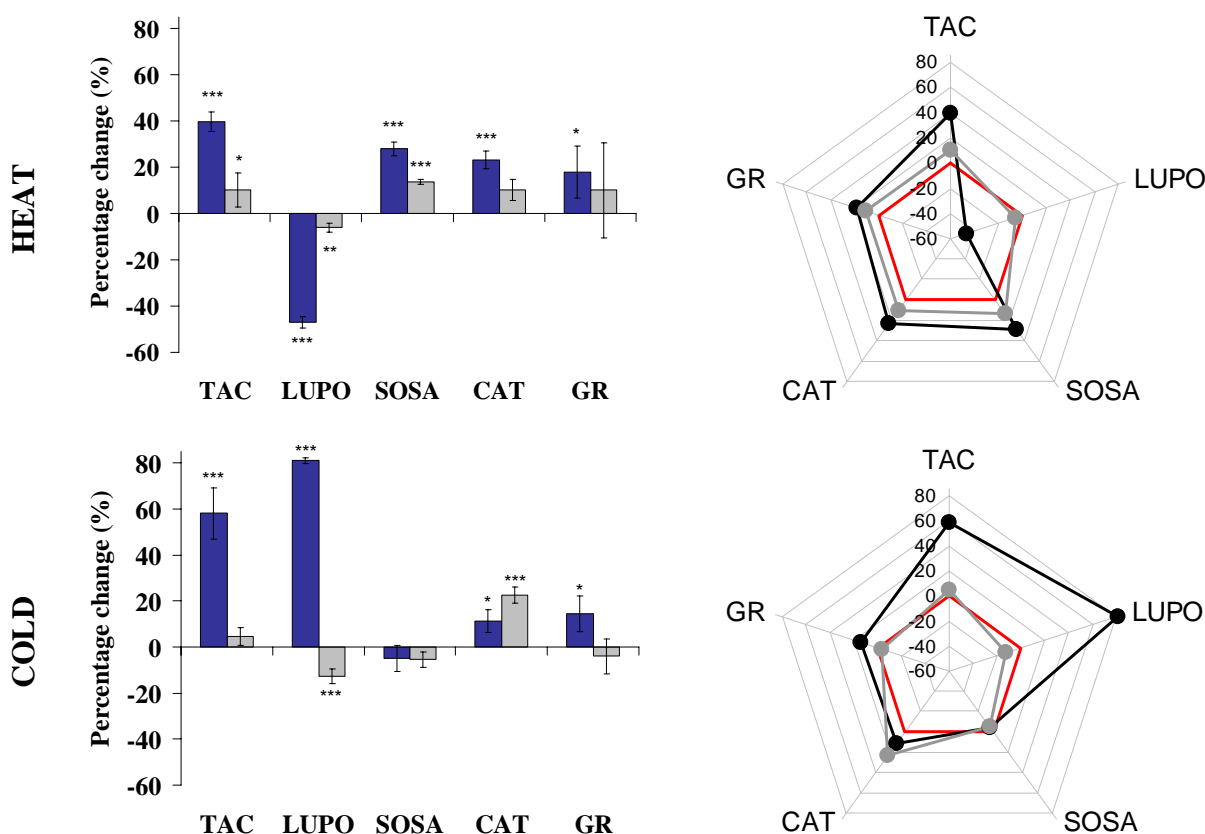
### 4.2.1.3 Heat stress

Heat stress has mainly been studied in terms of transcript profiling and proteomics (Ferreira *et al.*, 2006). Up-regulation of genes and expression of heat-shock proteins (HSP) are well known responses (Gong *et al.*, 1998, Larkindale & Knight, 2002 and references cited therein). Heat increases enzyme turnover and causes substrate/product and thus redox imbalances. This leads to oxidative damage. Cellular protection mechanisms directed against oxidative stress involve  $\text{Ca}^{2+}$ , ethylene, ABA and salicylic acid (Larkindale & Knight, 2002).

A dark incubator was chosen for heat treatment of *Lepidium sativum* to avoid light-induced additive effects which have been reported earlier (Larkindale & Knight, 2002). The treatment was started in the morning and the plants were harvested about midday. The plants were collected after 6 h recovery. Due to the diurnal rhythms and the variability of control plants, the different harvesting times should be considered with the experimental design (Asard *et al.*, 2000)

The fingerprint representation (**Figure 57**) of all screened parameters reveals a mobilisation of TAC, SOSA, CAT, and GR. However, most prominent is the cutback in LUPO activity, unveiling a heat sensitivity of plant peroxidases (see Supplemental data in Saleh & Plieth, 2009).





**Figure 57: Stress-induced alterations in the antioxidative system of *Lepidium***

In the left panel the percentage change in respect to the control experiments (zero line) for each parameter is summarised (left panel) and significance is marked with asterisks (\*  $p < 0.05$ ; \*\*  $p < 0.01$ ; \*\*\*  $p < 0.001$ , Student's T test). The plants were treated (blue bars) with salt (24 h at 150 mM NaCl in 0.5xMS medium); drought (withdrawal of nutrient medium for 24 h); heat (6 h at 42°C); and cold (12h at 0°C). The gray bars represent the change in antioxidative status of plants after recovery. Error bars represent StDv. Fingerprints in the right panel represent another graphic display of data shown in the left panel. The red pentagon in each panel represents the line of no change. Black polygons represent the antioxidative status immediately after stress treatment. Gray polygons represent the status after stress recovery. Each column represents the average of five technical replicates run on pooled plant material from three independent growth and treatment experiments. Standard deviations and significances are given in figures on the left side.

#### 4.2.1.4 Cold stress

Adaptation to cold and formation of freezing tolerance involves a plethora of cellular events beginning with  $\text{Ca}^{2+}$ - and  $\text{IP}_3$ -mediated signal transduction (Carpaneto *et al.*, 2007; Knight *et al.*, 1996; Plieth *et al.*, 1999; Ruelland *et al.*, 2002) with protein phosphorylation (Martin & Busconi, 2001) and gene induction (Knight, 2002; Knight *et al.*, 1999; Polisensky & Braam, 1996; Thomashow, 2001), leading to metabolic changes such as proline and carbohydrate accumulation (Charest & Phan, 1990) and growth retardation (Guy, 1990). The involvement of the cellular antioxidative system in the cold response has also been investigated (Prasad, 1995; 1997; Prasad *et al.*, 1994).

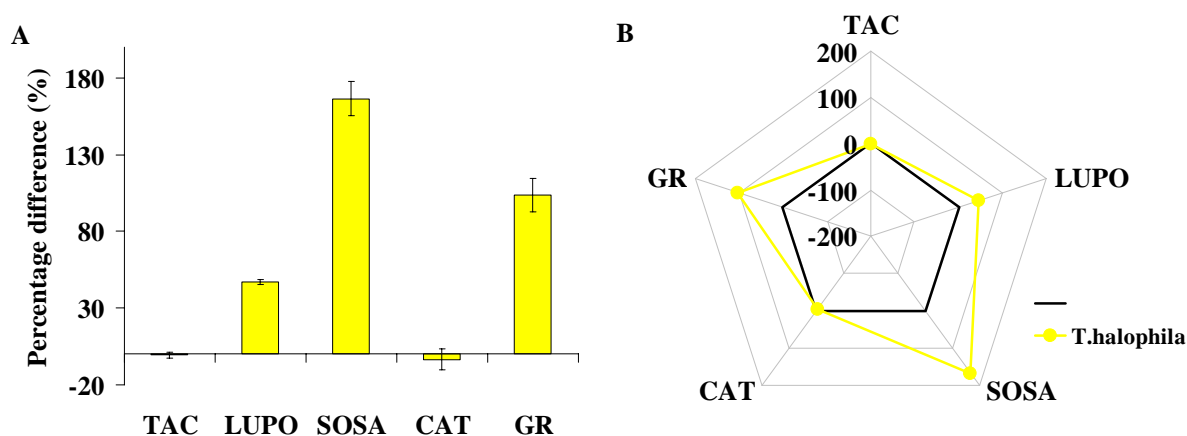
The total low-molecular-weight antioxidative capacity (TAC) was significantly increased in *Lepidium* during the cold period (Figure 57). This increase falls back to normal level during the

recovery period under normal growth conditions. In contrast, the superoxide anion scavenging activity (SOSA) mediated by high molecular weight compounds appears to be unaltered (**Figure 57**). The enzyme activities (LUPO, GR, CAT) are also up-regulated during cold (**Figure 57**). Most prominent is LUPO activity which increases by about 80 %. CAT up-regulation seems to continue during the recovery period, while LUPO and GR are regulated back to normal. When inspecting the cold stress fingerprint (**Figure 57**) it becomes obvious that during cold additional antioxidative activities have been mobilized.

#### 4.2.2 Fingerprinting the antioxidative activities of *Arabidopsis thaliana* and *Thellungiella salsuginea* during salt stress

For fingerprinting antioxidative activities in *A. thaliana* and *T. salsuginea*, seeds of both plant species were sown on 1 x MS vertical agar plates containing 50 mM and 75 mM NaCl and grown for 6 weeks. The salt stress experiment was carried out in parallel on agar plates containing 1 x MS lacking CaCl<sub>2</sub>.

When both plant species are compared in terms of their constitutive antioxidative activities (**Figure 58**), it becomes obvious that *T. salsuginea* has much higher background LUPO, SOSA, and GR activity than its salt sensitive relative (displayed in **Figure 57B** as black polygon).



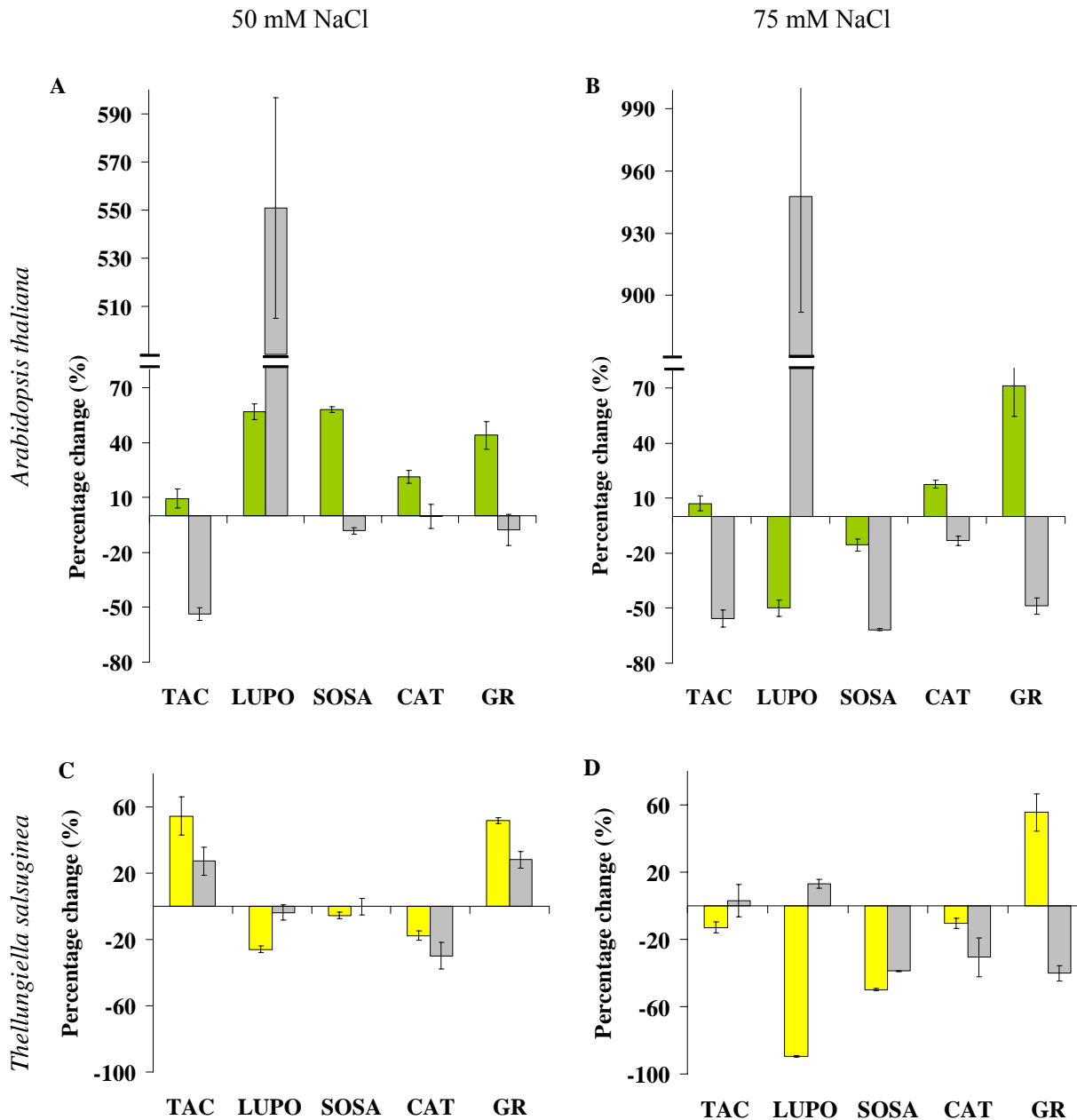
**Figure 58: Comparison of constitutive antioxidative parameters in *Arabidopsis* and *Thellungiella***

**A:** Displayed is the percentage difference of *Thellungiella*'s antioxidative parameters relative to those of *Arabidopsis* (= 100 %). Each column represents the average of five technical replicates run on pooled plant material from three independent growth and treatment experiments. Error bars represent StDv. **B:** Fingerprint display of data presented in A. Black polygon represents the antioxidative state of *Arabidopsis*. Both species had been grown under identical conditions without salt stress on 1 x MS agar plates. Standard deviations are given in A.

During mild salt stress (50 mM NaCl), CAT and GR are increased in *A. thaliana* by ca. 25 % and 40 % respectively (**Figure 59A**, green columns). Most prominent is the activation of peroxidases and superoxide scavengers by nearly 60 % compared to the control plants (**Figure 59A**, green columns). The up-regulation of SOSA suggests an excess production of superoxide during mild salt



stress. Up to 50 mM NaCl the plants are able to mobilize SOSA in order to keep increased superoxide amounts in check (**Figure 59A**, yellow columns). During dismutation of superoxide  $H_2O_2$  is produced (see **Chapter 1, Section 1.1.3, Equation 2**). The increase in LUPO in parallel to SOSA (ca. 60 %) implies a connection between these processes. TAC in contrast rises only marginally.



**Figure 59: Percentage change in TAC, LUPO, SOSA, CAT, and GR of plants exposed to salinity in comparison to untreated control plants.**

For each of the five screened parameters (TAC, LUPO, SOSA, CAT, GR) the percentage change of plants grown on 50 mM NaCl **A: *Arabidopsis thaliana*** and **C: *Thellungiella salsuginea*** and at 75 mM NaCl **B: *Arabidopsis thaliana*** and **D: *Thellungiella salsuginea*** is given in comparison to the control of untreated plants (zero line). The green/yellow bars represent plants grown on full MS and the grey bars represent plants grown on full MS without calcium. Each column represents the average of five technical replicates run on pooled plant material from three independent growth and treatment experiments. Error bars represent StDv.

A different picture is obtained, when inspecting *Arabidopsis* plants grown on 75 mM NaCl (**Figure 59B**, green columns). Here, only TAC and CAT show the same pattern as with 50 mM NaCl. GR is increased by 30 %; LUPO and SOSA are decreased by 50 % and 15 % respectively when compared to control plants.

When applying salt stress (50 mM NaCl) and calcium deficiency simultaneously (**Figure 59A**, grey columns) an exceptional increase in LUPO activity (ca. 5-times higher than control plants) takes place. In contrast, TAC, SOSA, CAT, and GR activities are impaired. At 75 mM NaCl (**Figure 59B**, grey columns) the LUPO activity increases nearly tenfold, whereas the other four parameters decrease even more, when compared to the plants grown on 50 mM NaCl without calcium. This phenomenon is discussed later.

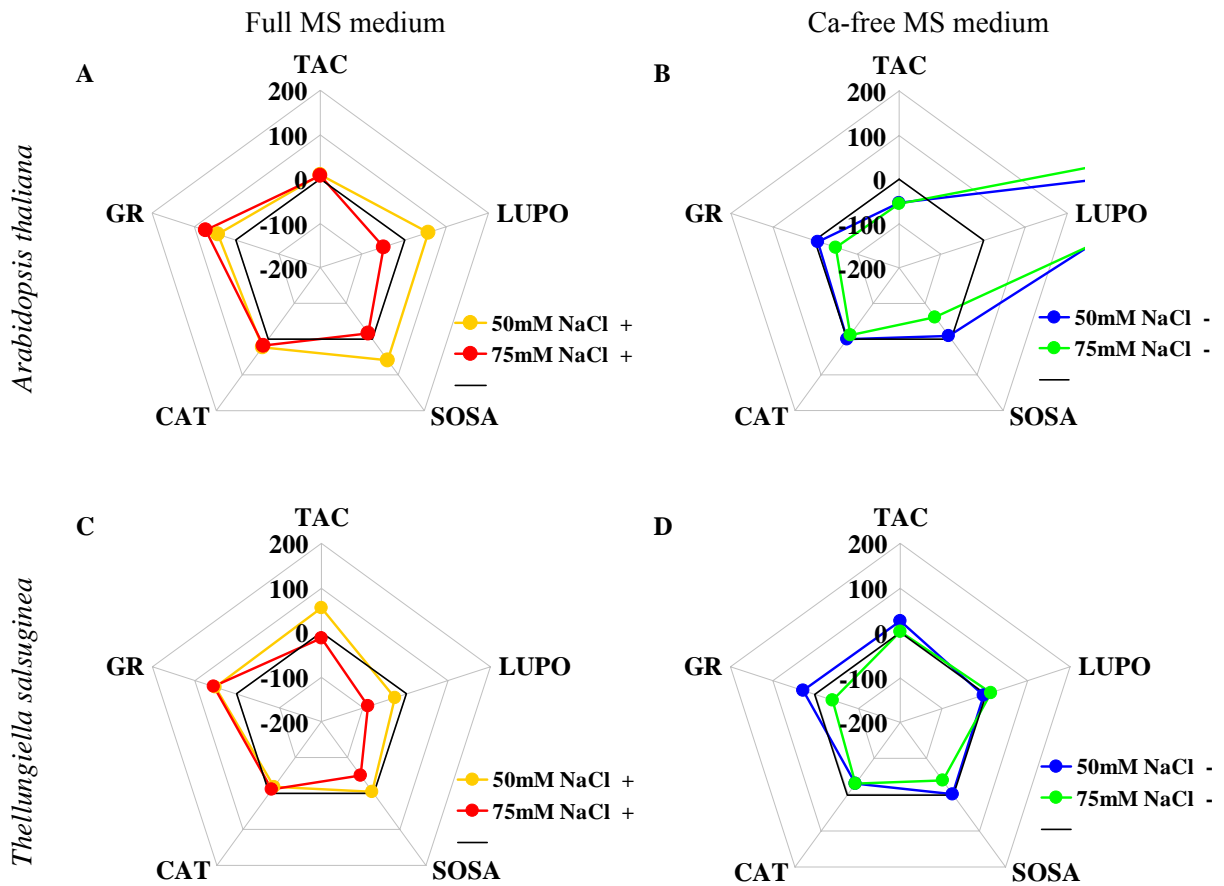
In *Thellungiella salsuginea* 50 mM NaCl (**Figure 59C**, yellow columns) in the growth medium cause an increase in TAC by 55 %. The same change occurs in GR, implicating that the major low-molecular-weight antioxidant is glutathione. The other screened parameters decline. Elevating the NaCl concentration in the growth medium to 75 mM (**Figure 59D**, yellow columns), causes a decrease in TAC, LUPO and SOSA, whereas CAT and GR hold the same level.

A simultaneous calcium deficiency (**Figure 59C, D**, grey columns) shows a similar pattern as in *A. thaliana*. The levels of TAC, LUPO, SOSA, and GR are about the control values. Only CAT activity is more impaired. The higher salt concentration (75 mM NaCl, **Figure 59D**, grey columns) causes in comparison to 50 mM NaCl (**Figure 59C**, grey columns) a reduction in TAC, SOSA and GR. LUPO is slightly increased. Since 75 mM NaCl in the medium cause a significant decrease in iron concentration (**Figure 11E, J, Chapter 2**), even more prominent than in its salt sensitive relative, it is not surprising, that LUPO and SOSA decline in the same way as described before. No significant changes in CAT were observed.

The data displayed as column graphs in **Figure 59** have been rearranged and are displayed as polygons in the **Figure 60**. Those fingerprints reveal the individual adaptation mechanisms of the two relatives to long-term salt treatment (**Figure 60A, C**) combined with calcium withdrawal (**Figure 60B, D**). The zero lines displayed as black polygons represent the control experiments (i.e. material from untreated plants) for each condition. In **Figure 60A, C** they are equivalent to plants grown on full MS medium, whereas in **Figure 60B, D** they correspond with plants grown on full MS lacking CaCl<sub>2</sub>.

An increase in the polygon area (**Figure 60A, C**) due to higher salt concentration occurs in both species. Certain similarity between both can be seen when looking at the polygons from plants grown on 75 mM NaCl (**Figure 60A, C**, red polygons). In contrast, the reaction to simultaneous salt stress and calcium deficiency is very different. Whereas *A. thaliana* (**Figure 60B**) reacts to the high salinity with a prominently increased LUPO activity, *T. salsuginea* (**Figure 60D**) seems to be generally inhibited in mobilisation of its antioxidative resources. This effect is the more

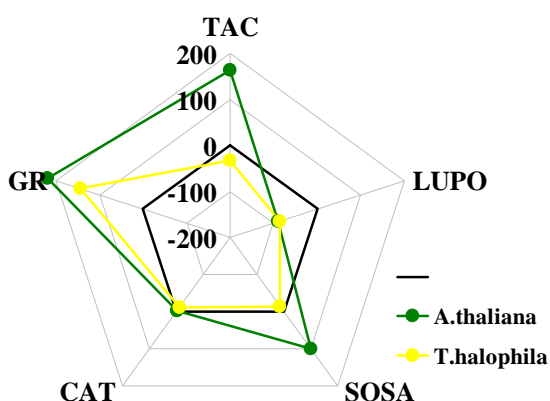
pronounced, the higher the concentration of salt in the growth medium (**Figure 60D**, green polygon).



**Figure 60: Fingerprints of antioxidant activities of salt-grown relatives differing in their salt tolerance**

**A:** *Arabidopsis thaliana* and **B:** *Thellungiella salsuginea* after salt stress challenge. The percentage in change of the five screened parameters is given (data from **Figure 59**). The black pentagon in each panel represents the line of no change. Yellow and red polygons represent the antioxidative status of plants grown on full MS medium supplemented with 50 and 75 mM NaCl, respectively. **C:** *Arabidopsis thaliana* and **D:** *Thellungiella salsuginea* after combined salt and calcium deficiency stress. Blue and green polygons in C, D represent the status of plants grown on MS medium without calcium supplemented with 50 and 75 mM NaCl, respectively. Each point is average of 5 technical replicates run on pooled biological material.

The pure effect of calcium deficiency can be seen in **Figure 61**. Here, plants grown on full MS displayed as black polygon are compared to plants grown on medium lacking calcium. There are some parallels between both plant species. While a cutback in LUPO activity is observable, GR is massively induced and CAT remains unaltered. In contrast, a slight lowering of the activity of low-molecular-weight antioxidants in *T. salsuginea* is seen, whereas in *A. thaliana* it is increased. The same pattern is observable in SOSA, while highly increased in the salt sensitive species; in *T. salsuginea* no additional superoxide scavengers are employed.



**Figure 61: Influence of calcium deficiency on the antioxidative system of *Arabidopsis thaliana* and *Thellungiella salsuginea* plants**

Displayed is the percentage difference of antioxidative parameters of plants grown on medium lacking calcium (yellow and green polygon) relative to plants grown on full MS (= 100 %, black polygon). Fingerprints display data calculated from data presented in **Figure 59**. Both species were grown under identical conditions without salt stress on 1 x MS agar plates or 1xMS without calcium.

## 4.3 DISCUSSION

### 4.3.1 Salt stress: a “two in one” challenge

There are numerous studies where the salt-stress induced response of antioxidative enzymes was investigated (Sanchez *et al.*, 2008; Eraslan *et al.*, 2007; Hernandez *et al.*, 2001; Ruiz & Blumwald, 2002; Rout & Shaw, 2001; Sreenivasulu *et al.*, 2000). The data presented here (**Figures 57, 59 and 60**) share similarities with these studies. However, in some cases the results are contradictory. This can be explained by the different time scales used for challenging plants with abiotic stress.

For fingerprinting garden cress a short term challenge (hours) was used. In contrast, seeds of *A. thaliana* and *T. salsuginea* were sown directly on salt - containing medium and grown for 6 weeks. This is a rather different approach to study impact of salinity on plants, since in most studies the salt treatment is applied on seedlings or fully developed plants. This may be the reason, why unexpected results were obtained (**Figures 59 and 60**).

The comparison of constitutive antioxidative activities of *Thellungiella salsuginea* and *Arabidopsis thaliana* depicted in **Figure 58** shows a higher SOSA, LUPO and GR activity. This is at least for SOSA supported by the comparative genomic study from Taji *et al.* (2004). They found a prominent up-regulation of the Fe-superoxide dismutase (FeSOD) gene in *Thellungiella salsuginea* under normal growth conditions. Since also other genes induced by environmental stress in *Arabidopsis* are constitutively overexpressed in *Thellungiella*, they suggest that this constitutive up-regulation of stress-inducible genes confers to higher stress tolerance in salt cress. A subsequent treatment of both plants with paraquat, causing superoxide and singlet oxygen formation, supported their finding, that *Thellungiella salsuginea* is more tolerant to oxidative stress. Also other studies revealed that plants having a higher capability to neutralize ROS have a higher salt tolerance (Tsugane *et al.*, 1999).

In *Thellungiella salsuginea* plants grown on 50 mM NaCl low-molecular-weight antioxidants are primarily activated, and the parallel increase of GR activity suggests that the preferred low-molecular-weight compound is GSH (Meyer *et al.*, 2007; **Figure 59C**). The other screened enzymatic activities are, in contrast to previous studies, lower. In particular, Demiral & Türkan (2005) have shown an increase in the SOSA, CAT and APX activity of the salt tolerant rice cultivar Pokkali. The same results were reported by Meloni *et al.* (2003) screening two cultivars of cotton differing in their salt tolerance. The salt tolerant cultivar exhibited an increased SOD, POX and GR activity. Gosset *et al.* (1994) have shown a significant increase in the activity of antioxidative enzymes in the salt tolerant cultivar of cotton during salt stress. De Azevedo Neto *et al.* (2006) described an activation of SOD, APX and GR in a salt tolerant cultivar of maize when compared to the salt sensitive one. Generally SOD activity has several times been shown to increase during salt stress (Gomez *et al.*, 2004; Hernandez *et al.*, 2001; Sreenivasulu *et al.*, 2000).

Surprisingly, the fingerprint of *A. thaliana* grown on 50 mM NaCl (**Figure 59A**) corresponds to these findings, the area of the polygon increases due to enhanced activity of all screened antioxidative enzymes (SOSA, LUPO, CAT, and GR). This shows that although *A. thaliana* is a salt sensitive plant, it is still able to mobilize its antioxidative system in order to cope with the effects of salt concentrations up to 50 mM NaCl.

The screening of plants grown on 75 mM NaCl (**Figure 59B**) shows a decrease in the area of polygon, mostly due to a decrease in LUPO and SOSA activity. Since iron deficiency occurs over 75 mM NaCl (**Chapter 2, Figure 11E**), the plant is not longer able to mobilize heme containing enzymes. Being a typical iron-sulphur protein, FeSOD is engaged in the detoxifying of superoxide anion in plastids and in the cytoplasm. An iron deficiency would impair the functionality of the enzyme and subsequently the antioxidative capacity of the plant. Consequently, the SOSA activity decreases to lower values than the control plants (**Figure 59B**). This corresponds to the results of Kurepa *et al.* (1997), who have shown that tobacco Fe-superoxide dismutases gene expression is repressed at the transcriptional level in response to iron deficiency.

Catalases and also many other peroxidases are heme enzymes; their activity depends also on the iron availability which may decline during iron deficiency. This case can be seen in the results of the LUPO assay. Catalase activity in contrast exhibits no significant changes.

The results obtained from fingerprinting *Lepidium sativum* after salt stress treatment backup previous findings (Gomez *et al.*, 2004; Sreenivasulu *et al.*, 2000) since they show that SOSA is higher during salt stress (**Figure 57**). On the other hand, they contrast with other studies. Peroxidase activity, for instance, increased significantly under salt stress in *Trigonella* species (Niknam *et al.*, 2006). However, this increase is strongly dependent on the applied conditions and is reversed at very high salt concentrations. The results here (**Figure 57**) mainly reveal an

inhibition of LUPO, which also corresponds to the findings in *A. thaliana* and *T. salsuginea*. The level of low molecular weight antioxidants is comparable with that of control plants. This is in line with the down-regulation of GR observed in parallel (**Figure 57**), supporting once more the importance of GSH during stress response (Meyer *et al.*, 2007).

The salt stress response fingerprint does not return to normal when the salt stress is released (**Figure 57**, grey polygon). This is because the 'recovery treatment' (exchange of salt solution by normal nutrition medium) implies an additional challenge, (hypo-osmotic stress), which provokes another shift of the antioxidative system. TAC is restored and even significantly increased when plants are returned from salt stress back to normal medium (**Figure 57**). As all measured H<sub>2</sub>O<sub>2</sub> scavenging enzymatic activities are highly impaired, only the ascorbate-glutathione pathway is available for the plant (see **Introduction, Section 1.1.2**) to diminish the negative effects of oxidative stress, in which also GR is strictly involved. Here, it cannot be distinguished whether the salt-induced oxidative burst is an effect of the concurrent hypo-osmotic shock or simply a relief of the 'high ion'-effect on the involved enzymes.

#### 4.3.2 Calcium controls the oxidative stress response in *Arabidopsis thaliana*

Ca<sup>2+</sup> has several functions within the cell (Plieth, 2005), including stabilisation of the endomembranes and the cell wall (Ferguson 1984), and the regulation of certain biochemical reactions directly or indirectly via calmodulin (Dieter 1984, Bouché *et al.*, 2005). If any of these physiological roles could not be fulfilled, excessive formation of ROS might be the result. Experiments with *A. thaliana* and *T. salsuginea* show (**Figure 61**), that the functionality of LUPOs is impaired due to calcium deficiency. This is consistent with the measurements of calcium dependency of HRP (**Suppl\_Material 19; Figure\_Suppl 9**). As seen in *A. thaliana* TAC and GR are massively induced (**Figure 61**), suggesting the scavenging of ROS by the glutathione-ascorbate pathway. SOSA shows a prominent up-regulation and CAT is not induced. Although no chlorotic tissue as a symptom of iron toxicity (Stephens *et al.*, 1990) could be perceived (**Chapter 2, Figure 8**), iron content is elevated due to calcium deficiency (**Chapter 2, Figure 11E**). Since iron and low-molecular-weight iron chelates are known to generate ROS in plants (**Chapter 2, Section 2.3.4**), the increase in SOSA suggests a superoxide formation. Induction of plant Fe- and Mn-superoxide dismutases by different metals has been reported before (Del Río *et al.*, 1998). H<sub>2</sub>O<sub>2</sub> generated during dismutation of superoxide is then probably scavenged by GSH. In *Thellungiella salsuginea* calcium deficiency has not such a big impact on the antioxidative system. Although LUPO activity is reduced and GR activity is increased, the other screened parameters do not change (**Figure 61**).

The measurements of Fe content in *Thellungiella salsuginea* grown on Ca-lacking medium (**Suppl\_material 4**) show a prominent increase of [Fe], which is much higher than in *Arabidopsis*.

The constitutive superoxide scavenging activity of *Theilungiella* is nearly 1.5 times higher than in *Arabidopsis* (**Figure 58**) and does not change due to calcium deficiency (**Figure 59**). Therefore, it is also possible, that superoxide is as a result of calcium deficiency-induced iron overload produced in excess.

Nevertheless, the outcome of experiments with calcium deficiency presented here (**Figure 61**) is in contrast to the results from Schmitz-Eiberger *et al.* (2002), who tested the influence of deficient calcium supply on the antioxidative system of *Lycopersicon lycopersicon cv. Panovy*. They observed a lower tocopherol and ascorbate content, a decline in the SOD activity and an increase in the peroxidase activity. However, they did not measure the Fe content in parallel, so if the tomato plants suffer from simultaneously increased Fe level remains unclear.

Salt stress in calcium deficient *Arabidopsis* plants leads to a massive up-regulation of LUPO (**Figure 59**). At 75 mM NaCl it reaches nearly the tenfold of the control (calcium deficient plants) values. This corresponds to the findings obtained from *Catharanthus roseus* (Abdul Jaleel *et al.*, 2007), from *Vigna radiata* (Manivannan *et al.*, 2007a) and *Dioscorea rotundata* (Abdul Jaleel *et al.*, 2008). When comparing the LUPO activity of Ca-deficient plants with Ca-rich plants grown both on 50 mM NaCl a reduction of LUPO by 60 % is seen (data calculated from experiments shown in **Figure 59**). In contrast, Ca-deficient plants grown on 75 mM NaCl show compared to the Ca-rich plants an increase of LUPO activity by more than 90 %. This can be explained by looking at the results of cation content measurements (**Chapter 2, Figure 11**). The Fe content is much higher in Ca-deficient *A. thaliana* plants, than in plants grown on full MS, meaning that they do not suffer from concomitant iron deficiency above 75 mM NaCl. Possible reasons for the higher Fe content in Ca-deficient plants are described in **Chapter 2, Section 2.3.4**.

### 4.3.3 Drought stress

Gogorcena *et al.* (1995) demonstrated that in pea (*Pisum sativum*) nodules drought causes a decrease in all relevant antioxidative enzymes and markers. They conclude that the decline of antioxidative capacity is due to an exhausted NAD(P)H pool. In contrast, Moran *et al.* (1994) and Zhang & Kirkham (1994) both reported a down-regulation of CAT and up-regulation of peroxidases in response to drought. The former is in line, the latter is opposite to the findings presented here (**Figure 57**). The reduction in LUPO (**Figure 57**) is in contrast to Moran *et al.* (1994) and Zhang & Kirkham (1994), suggesting either a loss of function at high ionic strength or a down-regulation due to a decreased demand of peroxidase activity in *Lepidium*. Therefore, the LUPO assay was performed in buffers of different ionic strengths (5 to 500 mM NaCl). No loss of function at high salt concentrations could be found (data not shown). Therefore, a demand-driven decrease in *Lepidium sativum* is more likely.

The increase in SOSA (**Figure 57**) is also seen with heat and salt treatment and is not observed with cold stress. Drought, heat and salt treatment produce an increase in cellular ionic strength that may increase a demand for superoxide scavengers.

The slight expansion of the polygon after recovery (**Figure 57**, grey polygon) suggests a collective formation or mobilisation of all assayed antioxidative activities. This may constitute an imprint on the metabolism memory for future challenges.

#### 4.3.4 Heat stress

Heat generally leads to an increase in metabolic turnover. Up-regulation of genes and expression of heat-shock proteins (HSP) are well established responses to heat stress in plants (Gong *et al.*, 1998; Larkindale & Knight, 2002).

The first prominent finding, up-regulation of SOSA, implies that there is apparently a demand for  $O_2^{\cdot-}$  scavengers, suggesting formation of superoxide during heat treatment. Thus, in order to cope with high concentrations of hydrogen peroxide generated during superoxide dismutation, the plant seems to mobilise low molecular weight antioxidants and catalases as well (**Figure 57**).

The second finding is a massive down-regulation of LUPO. In accordance with the data presented here, are the results obtained by heat treatment of *Arabidopsis* plants (Panchuk *et al.*, 2002). They found, that the total activity of ascorbate peroxidase in *Arabidopsis* was strongly reduced after several hours exposure to 44°C. Although peroxidases are generally believed to be heat stable, it has been shown that they suffer even from moderately raised temperature (42°C, Lee & Pennesi, 1984). In order to prove that this is also the case for the LUPO activity in *Lepidium* control experiment was performed (Saleh & Plieth, 2009). The results show that LUPO is very heat sensitive. Thus the reduction in LUPO is probably due to direct heat inactivation of the enzymes.

#### 4.3.5 Cold stress

Sudden cold (i.e. 0°C) is expected to halt many metabolic processes. Nevertheless, during a 12 h cold period, enzymatic activities (particularly peroxidases) are accumulated or activated and TAC is increased (**Figure 57**). There are many adaptive processes running during cold stress and a considerable number of involved metabolites and enzymes have been identified (Guy *et al.*, 2008; Prasad, 1996; Guy, 1990). However, the whole activation cascade (from  $Ca^{2+}$  signalling and transcription factor activation via gene transcription and translation) is expected to work very slowly at 0°C. Thus, it seems that other posttranslational events are involved. This has been shown in particular for GR. For instance, Edwards *et al.* (1993) described rather an increase in substrate affinity after cold treatment, than an increase in enzyme level or in GR transcripts.



Low temperature treatment influences metabolism far more profoundly than high temperature treatment (Guy *et al.*, 2008). This is substantiated here by the marked increase in the polygon area (compare e.g. **Figure 57** cold and heat). For many physiological responses the rate of temperature change (i.e. cooling rate) and not the steady state temperature is of importance (Minchin & Thorpe, 1983; for review see Minorsky, 1989). This has in particular been shown for  $\text{Ca}^{2+}$  signalling (Plieth *et al.*, 1999; Plieth, 1999). Thus, it would be no surprise if this was also the case for the antioxidative parameters studied here. The substantial increase in the antioxidants and peroxidases during cold treatment (**Figure 57**) is probably due to the cold shock applied. A more moderate treatment (slow cooling) may have less impact on the antioxidative system.

#### 4.3.6 Tolerance and robustness

Robustness of a plant is defined as the ability not only to withstand adverse conditions but also to propagate, and to produce a yield of sufficient quality in non-optimal environments. Tolerance to abiotic stress and robustness has often been directly linked to the efficiency of the antioxidative system (Pastori *et al.*, 2000 and references cited therein; Matsumura *et al.*, 2002). The current understanding of metabolic adaptation in response to abiotic challenges assumes genetic induction and the formation and mobilisation of antioxidative activities. If abiotic stress challenge only led to the formation of antioxidative capacity, then this would appear as an increase in area when plotting the changes in any set of screened parameters as a polygon. In *Lepidium sativum* this is true only for cold and heat treatment (**Figure 57**). For the other abiotic stimuli no remarkable increases in the polygon area are seen (**Figure 57**). Here, any expanding corner representing an up-regulated parameter is compensated by a contraction elsewhere in the polygon representing a down-regulation. This is particularly obvious when comparing LUPO and SOSA. These two parameters run anti-parallel under all investigated stress conditions, i.e. SOSA is increased while LUPO is down-regulated and *vice versa*. This is reasonable, since SODs form  $\text{H}_2\text{O}_2$  and peroxidases may also produce superoxide (Kawano, 2003). From the results of fingerprinting *Lepidium sativum* seedlings, another facet of this response emerges, namely a shift of function, i.e. the down-regulation of a selected function in favour of another. Consequently, the fingerprint may yield information as to what kind of ROS is mainly involved in each type of abiotic stress. Thus, if there is no increase in CAT, then there is probably no demand for additional  $\text{H}_2\text{O}_2$  scavengers. Conversely, if there is a shift towards SOSA then superoxide anions may be the major ROS. Apart from salt stress the areas of all grey polygons in **Figure 57**, representing the antioxidative status of *Lepidium sativum* after recovery, are close to the red pentagons (i.e. zero alterations). This shows that the antioxidative system is very flexible and that any changes are quickly adjusted to normal when stress factors are removed. Nevertheless, heat and drought (**Figure 57**) show a slightly increased polygon area even after recovery. This could be interpreted as a gain in tolerance and is

in line with findings that abiotic stress stimuli leave an imprint on plant metabolism (Knight *et al.* 1998; Evans *et al.*, 2005).

Many studies show, that an activation of the entire antioxidative system during stress treatment constitutes a tolerant plant. However, the comparison of tolerant and sensitive species under normal growth conditions may be helpful to complete the picture of adaptation to stress in plants. The screening of antioxidative properties of two cultivars of barley (Saleh *et al.*, 2010) different in their salt tolerance showed that the tolerant plant possessing lower entire antioxidant capacity at normal conditions is able to mobilize its resources in order to cope with salt stress. In contrast, the salt sensitive relative has a higher overall antioxidative capacity (comparable to that of salt treated tolerant line); nevertheless being unable to cope with high salinity. Contrasting are the results obtained from *A.thaliana* and *T.salsuginea* screening (**Figure 58**). Here, the tolerant plants have a higher constitutive antioxidative capacity. Since for *Thellungiella*, the conditions as applied here are not favourable, it is not possible to conclude on this point.

However, from the fingerprinting studies presented here it can be stated that a more robust plant is able to activate its antioxidative systems faster, or to shift antioxidative functions more effectively.

#### 4.3.7 Redundancies in the ROS-scavenging system

Certain redundancies between the different antioxidative activities have been revealed in transgenic plants with suppressed production of ROS-detoxifying mechanisms. Thus, suppressed APX production induces SOD, CAT and GR, whereas plants with suppressed CAT production induce APX and GPX (Willekens *et al.*, 1997; Rhizsky *et al.*, 2002). CAT and APX are not completely redundant since they do not compensate for the lack of each other (Mittler *et al.*, 1998). Surprisingly, plants with simultaneous suppression of APX and CAT appeared, at least under a defined set of unfavourable conditions, to suffer less from oxidative stress than plants with lowered APX or CAT levels, respectively (Rhizsky *et al.*, 2002).

Among the five screened parameters in *Lepidium sativum* (i.e. TAC, LUPO, SOSA, CAT, GR) redundancies appear to be present (**Figure 57**). TAC and GR in many cases run in parallel. This coincidence suggests that during drought, cold and heat the majority of low-molecular-weight antioxidants (i.e. TAC) employed for non-enzymatic detoxification of H<sub>2</sub>O<sub>2</sub> in the plant is represented by GSH. Since GR is involved in the ascorbate-glutathione pathway, it is also possible, that ascorbate may play a role. In order to test this, the activities of MDHAR or DHAR should be measured in parallel. Further, if an interdependency of LUPO and SOSA can be consolidated then their behaviour could also be regarded as redundant. In *Lepidium sativum* (**Figure 57**) during all abiotic treatments they run anti-parallel, whereas in *Thellungiella salsuginea* and *Arabidopsis thaliana* plants (**Figure 59**) grown on salt containing medium they exhibit the same trend.

On the one hand low redundancy is helpful within a multi-parametric set of assays to increase the informative value. But generally, redundancies within a group of screened parameters reduce the informative value. On the other hand, however, some redundancy can be used as an internal cross-check to identify errors and to minimise misinterpretation.

## 5 GENERAL DISCUSSION

The long-term salt stress experiments presented here (**Chapter 2**) were aimed on the comparison of two in their salt tolerance differing but related plant species - *Thellungiella salsuginea* and *Arabidopsis thaliana*. The results are in line with findings (Inan *et al.*, 2004; Orsini *et al.*, 2010), that *Thellungiella salsuginea* although salt tolerant, is not capable to germinate on medium containing high salt concentrations. Obviously it gains its tolerance only in later developmental stages. Knowing the time point would help to resolve the triggering signals and the cellular mechanisms contributing to its salt tolerance. Also comparative studies (on transcriptomic, proteomic and metabolomic levels) with both plants at different developmental stages would contribute to the present knowledge of salt tolerance mechanisms.

Calcium has a meliorative effect on the salt stress symptoms (Shabala *et al.*, 2003; Husain *et al.*, 2004). NaCl-triggered chloride influx into root cells is dependent on  $\text{Ca}^{2+}$ - availability in the surrounding medium (**Chapter 3, Figure 25**; Lorenzen *et al.*, 2004). This corresponds to results obtained by germination and primary root length screening on different salt concentrations. They clearly show that calcium meliorates the effects of high salt concentrations in *Arabidopsis* (**Chapter 2, Figures 5 and 6**). However, the germination of *Thellungiella salsuginea* on salt underlies different mechanisms than with its salt sensitive relative (**Chapter 2**). Although calcium has a positive effect on the growth parameters, the accumulation of  $\text{Na}^+$  and  $\text{Cl}^-$  is less pronounced when calcium is omitted in the growth medium (**Chapter 2, Figures 9 and 11**). This is in contrast with previous findings, that calcium inhibits sodium accumulation (Cramer, 1992; Essah *et al.*, 2003; Kinraide, 1999; Tyerman *et al.*, 1997). Another interesting point arises from the cation content measurements. Calcium has an inhibiting effect on the iron uptake (**Chapter 2, Figure 11E, J**). At higher salt concentrations certain iron deficiency symptoms were visible in both plant species (**Chapter 2, Figure 8**). It is widely accepted, that salt stress causes excessive production of ROS in plants (Rout & Shaw, 2001; Sreenivasulu *et al.*, 2000). Free iron, as a redox active transition metal, is capable to react with these (Fenton reaction) and thereby produce a more toxic oxygen species – hydroxyl radical (Mithöfer *et al.*, 2004; Wojtazsek, 1997). Therefore, minimising freely available iron could be a strategy of plants to cope with oxidative stress during salinity treatment. Calcium obviously plays an important role in this process, since omitting of calcium leads to over-accumulation of iron (**Chapter 2, Figure 11**). These results are underpinned with measurements of antioxidative activities (**Chapter 4**). In *Arabidopsis thaliana*, obviously superoxide is the main ROS produced in excess, since superoxide scavenging activity (SOSA) is prominently increased (**Chapter 4, Figure 59A**). The lack of iron caused by higher salt

concentrations leads to a break-down in the activity of heme-containing enzymes like SODs and LUPOs (**Chapter 4, Figure 59B**).

Calcium deficiency alone leads to an increased Fe content and an increase in SOSA (**Chapter 2, Figure 11E**, and **Chapter 4, Figure 61**) suggesting an excess production of superoxide. Simultaneous salinity treatment leads to an exaggerated LUPO activity in *Arabidopsis thaliana* and an inhibition of SOSA (**Chapter 4, Figure 59**). This result suggests that H<sub>2</sub>O<sub>2</sub> and not superoxide is produced in excess. Moreover, both treatments applied simultaneously lead obviously to a higher production of flavonoids (**Suppl\_material 21**). This is in line with studies describing that during metal toxicity flavonoids are produced in excess (Winkel-Shirley, 2002). They are able to chelate iron ions and thereby suppress the Fenton reaction (Rice-Evans *et al.*, 1997). On the other hand, Fe-chelates may involve the Haber-Weiß-reaction. However, although these compounds possess a ROS-scavenging activity *in vitro* (**Suppl\_material 19, Figure Suppl\_11**) no direct evidence was given until now, whether this is also true *in vivo*. Since flavonoids can also serve as electron donors for certain peroxidases (e.g. cell wall-bound peroxidases), it is imaginable, that the presence of flavonoids leads to an increased peroxidase activity as seen in **Chapter 4, Figure 59** (Mehlhorn *et al.*, 1996). However, these flavonoids obviously do not possess activating substituents in the para-position of their phenolic ring, since they are not able to trigger the HRP-driven reaction within the TAC assay.

However, it is possible, that the prominently increased peroxidase activity *in vitro* (**Chapter 4, Figure 59**) does not correlate with the peroxidase activity *in vivo*, since peroxidases need calcium for their activity.

The question of what kind of transporters are responsible for chloride influx into the cell and how the NaCl-triggered influx is regulated was tackled out by using a chloride sensitive ratiometric indicator – Clomeleon. *In vivo* superfusion experiments suggest that NaCl-induced chloride influx is mediated by channels. However to date no anion channel is known that is - as shown by Lorenzen *et al.* (2004) and the data presented here (**Chapter 3, Figure 25**) - inhibited by calcium. In contrary, there are anion channels known which are activated by Ca<sup>2+</sup> (Lewis *et al.*, 1997). So there is a discrepancy. On one hand the trivalent block of Cl<sup>-</sup> flux (**Chapter 3, Figure 32**) and the block by anion channel inhibitors (**Chapter 3, Figure 28 and Table 7**) suggest a channel; on the other hand however the partial inhibition by loop diuretics and the calcium induced inhibition suggest the involvement of CCCs.

It can be concluded, that H<sup>+</sup> ( $\Delta$  pH) and Ca<sup>2+</sup> together play a very important role in maintaining the cellular ion homeostasis in plants when salt stress occurs. Anyway, their precisely adjusted concentrations within the cell are fundamental for salinity tolerance processes connected with ion uptake. The measurements presented here (**Chapter 3, Figures 24 and 25**) show that Ca is able to

alleviate NaCl-induced chloride uptake only when applied during or short before the stress period (external Ca). When supplementing plants with high Ca long before the stress occurs (internal Ca), other mechanisms seem to be working. When the import of Ca is blocked by nifedipine (**Chapter 3, Figure 27**), the salt-induced chloride influx is pronounced and is comparable to plants perfused with solutions lacking calcium (**Chapter 3, Figure 26**). These results suggest that the influx of Ca through cation channels is necessary for hindering excess amounts of chloride to enter the cell.

Taking once more the results of Felle *et al.* (1994) into account and supposing, that during the second phase of chloride influx a hyperpolarisation of membrane in *Arabidopsis* occurs, another possibility of how chloride can be transported during salt stress arises. In *Arabidopsis* root cells a hyperpolarisation activated calcium channel was described previously by Véry & Davies (2000). This channel is selective for  $\text{Ca}^{2+}$  over  $\text{K}^+$  and  $\text{Cl}^-$  ( $P_{\text{Ca}}/P_{\text{K}} = 15$ ;  $P_{\text{Ca}}/P_{\text{Cl}} = 25$ ) and is fully blocked by  $<100 \mu\text{M}$  trivalent cations ( $\text{La}^{3+}$ ,  $\text{Al}^{3+}$ ,  $\text{Gd}^{3+}$ ). All properties described for this channel, fit with the findings presented here. Moreover, supposedly chloride is transported through this channel, when in excess, a part of the mechanisms; how Ca can alleviate chloride influx would be revealed.

The mechanisms of salt tolerance enclose also compartmentalisation of chloride within vacuoles. The over-expression of tonoplast-residing chloride channel AtClC-C in onion epidermal cells shows that this channel is capable to translocate excess chloride from the cytoplasm into the vacuole (**Chapter 3, Figure 46**). A mutation within the motif responsible for anion selectivity in AtClC-A, a  $\text{NO}_3^-/\text{H}^+$  antiporter, leads to a shift of the translocated anion from  $\text{NO}_3^-$  to  $\text{Cl}^-$  (**Chapter 3, Figure 47**).

## AKNOWLEDGMENTS

First of all my special thanks belong to PD Dr. Christoph Plieth for being an excellent advisor and for his unlimited help throughout the entire thesis.

My thanks also go to Prof. Dr. Axel Scheidig (Structural Biology Group, CAU, Kiel) for the opportunity to finish my thesis in his group and to the members of Structural biology group for their advices in protein purification and especially to Uli Zander for helping me with the PyMol-software. Many thanks go to Prof. Dr. Ulf-Peter Hansen and Dr. Indra Schröder (Former Biophysics Group, CAU, Kiel) for their valuable support in the “channel” research and patch clamp technique and for the nice tea times.

My thanks also go to Sonja Vollbehr from Zentrum für Biochemie und Molekularbiologie (ZBM, CAU, Kiel), for sharing with me the office and for her help in the lab.

I thank the former students and trainees for their assistance and help, namely: Gesche Weppner, Silja Hesterberg, Judith Pohanke, Sünne Anderson, Hendrik Röttger, Anne Wiedenhöft, Liliane Bartsch, Stefan Düsterhöft, Björn Reimer, Katharina Kolbe and Sabine Schmelz.

I greatly appreciate the opportunity given to me by Prof. Dr. Bilger (Ecophysiology of plants, CAU, Kiel) to share in their group seminars.

For the gift of *Thellungiella salsuginea* seeds and her support in transformation of *Thellungiella* I am much obliged to Prof. Dr. Jutta Papenbrock (Botanical Institute, Leibniz-University, Hannover).

I thank Prof. Dr. Karl-Hermann Mühling and Dr. Katja Witzel (Institute of Plant Breeding, CAU, Kiel) for the fruitful on-going cooperation and for the access to the AAS and IC facilities and the muffle furnace. Special thank goes in this context to the technical assistants Anne Thiessen for her help with dry ashing and AAS and Stefanie ThorStraten for being a great help with IC.

I gratefully acknowledge the financial support of the Deutsche Forschungsgemeinschaft (Grant No.: PL253/5) as well as access to the core facilities of the ZBM (CAU, Kiel), the access to the fluorescence binocular (Zoological institute, CAU Kiel) and the CLSM (Zentrale Mikroskopie, CAU, Kiel).

And last but not least I would like to express my deepest thankfulness to my whole family, especially my beloved husband, my mother and my grandparents for their trust in me, and for supporting me with their unlimited love, belief and hope.

## EIDESSTATTLICHE ERKLÄRUNG

Ich versichere an Eides statt, dass ich bis zum heutigen Tage weder an der Christian-Albrechts-Universität zu Kiel noch an einer anderen Hochschule ein Promotionsverfahren endgültig nicht bestanden habe oder mich in einem entsprechenden Verfahren befinde.

Ich versichere an Eides statt, dass die Abhandlung nach Inhalt und Form die eigene Arbeit ist und dass ich die Inanspruchnahme fremder Hilfen aufgeführt habe, sowie, dass ich die wörtlich oder inhaltlich aus anderen Quellen entnommen Stellen als solche gekennzeichnet habe.

Ich versichere an Eides statt, dass die Arbeit unter Einhaltung der Regeln guter wissenschaftlicher Praxis der Deutschen Forschungsgemeinschaft entstanden ist.

Kiel, den 22.12.2010



## REFERENCES

- Abarca, D.; Roldan, M.; Martin, M. and Sabater, B. (2001). "Arabidopsis thaliana ecotype Cvi shows an increased tolerance to photo-oxidative stress and contains a new chloroplastic copper/zinc superoxide dismutase isoenzyme." *Journal of Experimental Botany* **52**(360): 1417-1425.
- Abdolzadeh, A.; Shima, K.; Lambers, H. and Chiba, K. (2008). "Change in uptake, transport and accumulation of ions in *Nerium oleander* (Rosebay) as affected by different nitrogen sources and salinity." *Annals of Botany* **102**(5): 735-746.
- Abdul Jaleel, C.; Gopi, R.; Gomathinayagam, M. and Paneerselvam, R. (2008). "Effects of calcium chloride on metabolism of salt-stressed *Dioscorea rotundata*." *Acta Biologica Cracoviensia Series Botanica* **50**(1): 63-67.
- Abdul Jaleel, C.; Manivannan, P.; Sankar, B.; Kishorekumar, A. and Paneerselvam, R. (2007). "Calcium chloride effects on salinity-induced oxidative stress, proline metabolism and indole alkaloid accumulation in *Catharanthus roseus*." *Comptes Rendus Biologies* **330**(9): 674-683.
- Accardi, A. and Miller, C. (2004). "Secondary active transport mediated by a prokaryotic homologue of ClC Cl<sup>-</sup> channels." *Nature* **427**: 803-807.
- Accardi, A.; Walden, M.; Nguitragool, W.; Jayaram, H.; Williams, C. and Miller, C. (2005). "Separate ion pathways in a Cl<sup>-</sup>/H<sup>+</sup> exchanger." *The Journal of General Physiology* **126**(6): 563-570.
- Adler, P. R. and Wilcox, G. E. (1995). "Ammonium increases the net rate of sodium influx and partitioning to the leaf of muskmelon." *Journal of Plant Nutrition* **18**(9): 1951-1962.
- Alcázar, R.; Altabella, T.; Marco, F.; Bortolotti, C.; Reymond, M.; Koncz, C.; Carrasco, P. and Tiburcio, A. (2010). "Polyamines: molecules with regulatory functions in plant abiotic stress tolerance." *Planta* **231**(6): 1237-1249.
- Alcázar, R.; Marco, F.; Cuevas, J.; Patron, M.; Ferrando, A.; Carrasco, P.; Tiburcio, A. and Altabella, T. (2006). "Involvement of polyamines in plant response to abiotic stress." *Biotechnology Letters* **28**(23): 1867-1876.
- Almagro, L.; Gómez Ros, L. V.; Belchi-Navarro, S.; Bru, R.; Ros Barceló, A. and Pedréño, M. A. (2009). "Class III peroxidases in plant defence reactions." *Journal of Experimental Botany* **60**(2): 377-390.
- Alscher, R. G.; Erturk, N. and Heath, L. S. (2002). "Role of superoxide dismutases (SODs) in controlling oxidative stress in plants." *Journal of Experimental Botany* **53**(372): 1331-1341.
- Apse, M. P.; Aharon, G. S.; Snedden, W. A. and Blumwald, E. (1999). "Salt tolerance conferred by overexpression of a vacuolar Na<sup>+</sup>/H<sup>+</sup> antiporter in Arabidopsis." *Science* **285**(5431): 1256-1258.
- Apse, M. P. and Blumwald, E. (2002). "Engineering salt tolerance in plants." *Current Opinion in Biotechnology* **13**(2): 146-150.
- Asada, K. (2006). "Production and scavenging of reactive oxygen species in chloroplasts and their functions." *Journal of Plant Physiology* **141**: 391-396.
- Asard, H.; Horemans, N.; Pooters, G. and Caubergs, R. (2000). Plasma membrane electron transport and the control of cellular redox status and circadian rhythms. *The Redox State and Circadian Rhythms*. Vanden Driessche, T.; Guisset, J.-L. and Petiau-de Vries, G., Springer: 163-176S.
- Asch, F.; Dingkuhn, M.; Dörffling, K. and Miezán, K. (2000). "Leaf K/Na ratio predicts salinity induced yield loss in irrigated rice." *Euphytica* **113**(2): 109-118.
- Aslam, M.; Huffaker, R. C. and Rains, D. W. (1984). "Early effects of salinity on nitrate assimilation in barley seedlings." *Journal of Plant Physiology* **76**(2): 321-325.
- Azevedo, A. M.; Martins, V. C.; Prazeres, D. M. F.; Vojinovic, V.; Cabral, J. M. S. and Fonseca, L. P. (2003). "Horseradish peroxidase: a valuable tool in biotechnology." *Biotechnology: Annual Reviews* **5**: 199-247.
- Baker, C. J.; Deahl, K.; Domek, J. and Orlandi, E. W. (2000). "Scavenging of H<sub>2</sub>O<sub>2</sub> and production of oxygen by horseradish peroxidase." *Archives of Biochemistry and Biophysics* **382**(2): 232-237.
- Bar, Y.; Apelbaum, A.; Kafkafi, U. and Goren, R. (1997). "Relationship between chloride and nitrate and its effect on growth and mineral composition of avocado and citrus plants." *Journal of Plant Nutrition* **20**(6): 715-731.

- Barbier-Brygoo, H.; Vinauger, M.; Colcombet, J.; Ephritikhine, G.; Frachisse, J.-M. and Maurel, C. (2000). "Anion channels in higher plants: functional characterization, molecular structure and physiological role." Biochimica et Biophysica Acta (BBA) - Biomembranes **1465**(1-2): 199-218.
- Bartosz, G. and Bartosz, M. (1999). "Antioxidant activity: what do we measure?" Acta Biochimica Polonica **46**(1): 23-29.
- Basu, R. and Ghosh, B. (1991). "Polyamines in various rice (*Oryza sativa*) genotypes with respect to sodium chloride salinity." Physiologia Plantarum **82**(4): 575-581.
- Beers, R. F. and Sizer, I. W. (1952). "A spectrophotometric method for measuring the breakdown of hydrogen peroxide by catalase." Journal of Biological Chemistry **195**(1): 133-140.
- Beilby, M. and Al Khazaaly, S. (2009). "The role of H<sup>+</sup>/OH<sup>-</sup> channels in the salt stress response of *Chara australis*." Journal of Membrane Biology **230**(1): 21-34.
- Benedet, J. A.; Umeda, H. and Shibamoto, T. (2007). "Antioxidant activity of flavonoids isolated from young green barley leaves toward biological lipid samples." Journal of Agricultural and Food Chemistry **55**(14): 5499-5504.
- Berzi, A. and Moller, I. M. (1998). "NADH-monodehydroascorbate oxidoreductase is one of the redox enzymes in spinach leaf plasma membranes." Journal of Plant Physiology **116**(3): 1029-1036.
- Bergsdorf, E.-Y.; Zdebik, A. A. and Jentsch, T. J. (2009). "Residues important for nitrate/proton coupling in plant and mammalian CLC transporters." Journal of Biological Chemistry **284**(17): 11184-11193.
- Bhandal, I. S.; Malik, C. P.; Bourne, G. H.; Jeon, K. W. and Friedlander, M. (1988). Potassium estimation, uptake, and its role in the physiology and metabolism of flowering plants. International Review of Cytology, Academic Press. **110**: 205-254S.
- Bienert, G. P.; Møller, A. L. B.; Kristiansen, K. A.; Schulz, A.; Møller, I. M.; Schjoerring, J. K. and Jahn, T. P. (2007). "Specific aquaporins facilitate the diffusion of hydrogen peroxide across membranes." Journal of Biological Chemistry **282**: 1183-1192.
- Bienfait, H. F. (1988). "Mechanisms in Fe-efficiency reactions of higher plants." Journal of Plant Nutrition **11**(6): 605-629.
- Binzel, M. L. (1995). "NaCl-induced accumulation of tonoplast and plasma membrane H<sup>+</sup>-ATPase message in tomato." Physiologia Plantarum **94**(4): 722-728.
- Blumwald, E.; Aharon, G. S. and Apse, M. P. (2000). "Sodium transport in plant cells." Biochimica et Biophysica Acta (BBA) - Biomembranes **1465**(1-2): 140-151.
- Blumwald, E. and Poole, R. J. (1987). "Salt tolerance in suspension cultures of sugar beet: induction of Na<sup>+</sup>/H<sup>+</sup> antiport activity at the tonoplast by growth in salt." Journal of Plant Physiology **83**(4): 884-887.
- Bolwell, G. P. and Wojtaszek, P. (1997). "Mechanisms for the generation of reactive oxygen species in plant defence - a broad perspective." Physiological and Molecular Plant Pathology **51**(6): 347-366.
- Böszörményi, Z. and Cseh, E. (1961). "The uptake of halide ions and their relationships in absorption." Physiologia Plantarum **14**(2): 242-252.
- Bouché, N.; Yellin, A.; Snedden, W. A. and Fromm, H. (2005). "Plant-specific calmodulin-binding proteins." Annual Review of Plant Biology **56**(1): 435-466.
- Bowler, C.; Alliotte, T.; Van den Bulcke, M.; Bauw, G.; Vandekerckhove, J.; Van Montagu, M. and Inzé, D. (1989). "A plant manganese superoxide dismutase is efficiently imported and correctly processed by yeast mitochondria." Proceedings of the National Academy of Sciences USA **86**(9): 3237-3241.
- Bowler, C.; Montagu, M. v. and Inzé, D. (1992). "Superoxide dismutase and stress tolerance." Annual Reviews of Plant Physiology and Plant Molecular Biology **43**: 83-116.
- Bradford, M. M. (1976). "A rapid and sensitive method for the quantitation of microgram quantities of protein utilizing the principle of protein-dye binding." Analytical Biochemistry **72**(1-2): 248-254.
- Briat, J.-F.; Fobis-Loisy, I.; Grignon, N.; Lobréaux, S.; Pascal, N.; Savino, G.; Thoiron, S.; von Wirén, N. and Van Wuytswinkel, O. (1995). "Cellular and molecular aspects of iron metabolism in plants." Biology of the Cell **84**(1-2): 69-81.
- Briat, J.-F.; Ravet, K.; Arnaud, N.; Duc, C. I.; Boucherez, J.; Touraine, B.; Cellier, F. and Gaynard, F. (2010). "New insights into ferritin synthesis and function highlight a link between iron homeostasis and oxidative stress in plants." Annals of Botany **105**(5): 811-822.

- Brini, F.; Hanin, M.; Mezghani, I.; Berkowitz, G. A. and Masmoudi, K. (2007). "Overexpression of wheat  $\text{Na}^+/\text{H}^+$  antiporter TNHX1 and  $\text{H}^+$ -pyrophosphatase TVP1 improve salt- and drought-stress tolerance in *Arabidopsis thaliana* plants." Journal of Experimental Botany **58**(2): 301-308.
- Britto, D. T.; Ruth, T. J.; Lapi, S. and Kronzucker, H. J. (2004). "Cellular and whole-plant chloride dynamics in barley: insights into chloride-nitrogen interactions and salinity responses." Planta **218**(4): 615-622.
- Burchard, P. (2001). Lösliche Phenylpropane im Primärblatt von Gerste (*Hordeum vulgare* L.) und ihre Bedeutung als UV-B Schutzsubstanzen für die Photosynthese. Köln. **Dissertation**: 192 p.
- Cakmak, I.; van de Wetering, D. A. M.; Marschner, H. and Bienfait, H. F. (1987). "Involvement of superoxide radical in extracellular ferric reduction by iron-deficient bean roots." Journal of Plant Physiology **85**(1): 310-314.
- Caldwell, C. R. and Haug, A. (1981). "Temperature dependence of the barley root plasma membrane-bound  $\text{Ca}^{2+}$ - and  $\text{Mg}^{2+}$ -dependent ATPase." Physiologia Plantarum **53**(2): 117-124.
- Carpaneto, A.; Ivashikina, N.; Levchenko, V.; Krol, E.; Jeworutzki, E.; Zhu, J. K. and Hedrich, R. (2007). "Cold transiently activates calcium-permeable channels in *Arabidopsis* mesophyll cells." Journal of Plant Physiology **143**: 487-494.
- Carpita, N.; Sabularse, D.; Montezinos, D. and Delmer, D. P. (1979). "Determination of the pore size of cell walls of living plant cells." Science **205**(4411): 1144-1147.
- Caspary, R. (1865/66). "Bemerkungen über die Schutzscheide und die Bildung des Stammes und der Wurzel." Jahrbuch für Wissenschaftliche Botanik **4**: 101-124
- Cercek, B.; Cercek, B.; Roby, K. and Cercek, L. (1994). "Effect of oxygen abstraction on the peroxidase-luminol-perborate system: Relevance to the HRP enhanced chemiluminescence mechanism." Journal of Bioluminescence and Chemiluminescence **9**: 273-277.
- Cerda, A. and Martinez, V. (1988). "Nitrogen fertilization under saline conditions in tomato and cucumber plants." Journal of Horticultural Science **63**(3): 451-458.
- Cerezo, M.; García-Agustín, P. and Primo-Millo, E. (1999). "Influence of chloride and transpiration on net  $^{15}\text{NO}_3^-$  uptake rate by citrus roots." Annals of Botany **84**(1): 117-120.
- Chalfie, M.; Tu, Y.; Euskirchen, G.; Ward, W. and Prasher, D. (1994). "Green fluorescent protein as a marker for gene expression." Science **263**(5148): 802-805.
- Charest, C. and Phan, C. T. (1990). "Cold acclimation of wheat (*Triticum aestivum*): Properties of enzymes involved in proline metabolism." Physiologia Plantarum **80**: 159-168.
- Chattopadhyay, K. and Mazumdar, S. (2000). "Structural and conformational stability of horseradish peroxidase: Effect of temperature and pH." Biochemistry **39**(1): 263-270.
- Chen, S.; Yan, G.; Schwartz, M. A.; Perrin, J. H. and Schulman, S. G. (1991). "Penicillin-enhanced chemiluminescence of the luminol- $\text{H}_2\text{O}_2$ - $\text{Co}^{2+}$  system." Journal of Pharmacological Science **80**(11): 1017-1019.
- Chen, T.-Y. (2004). "Structure and function of  $\text{Cl}^-$  channels." Annual Review of Physiology **67**(1): 809-839.
- Chen, T. Y. and Miller, C. (1996). "Nonequilibrium gating and voltage dependence of the  $\text{Cl}^-$  channel." The Journal of General Physiology **108**(4): 237-250.
- Chen, Z.; Cuin, T. A.; Zhou, M.; Twomey, A.; Naidu, B. P. and Shabala, S. (2007a). "Compatible solute accumulation and stress-mitigating effects in barley genotypes contrasting in their salt tolerance." Journal of Experimental Botany **58**(15-16): 4245-4255.
- Chen, Z.; Pottosin, I. I.; Cuin, T. A.; Fuglsang, A. T.; Tester, M.; Jha, D.; Zepeda-Jazo, I.; Zhou, M.; Palmgren, M. G.; Newman, I. A. and Shabala, S. (2007b). "Root plasma membrane transporters controlling  $\text{K}^+/\text{Na}^+$  homeostasis in salt-stressed barley." Journal of Plant Physiology **145**(4): 1714-1725.
- Chinnusamy, V.; Zhu, J. and Zhu, J. K. (2006). "Salt stress signaling and mechanisms of plant salt tolerance." Genetic Engineering **27**: 141-177.
- Clarkson, D. T. (1993). "Roots and the delivery of solutes to the xylem." Philosophical Transactions of the Royal Society of London. Series B: Biological Sciences **341**(1295): 5-17.
- Clarkson, D. T. and Hanson, J. B. (1980). "The mineral nutrition of higher plants." Annual Review of Plant Physiology **31**(1): 239-298.
- Clough, S. J. and Bent, A. F. (1998). "Floral dip: a simplified method for *Agrobacterium*-mediated transformation of *Arabidopsis thaliana*." The Plant Journal **16**(6): 735-743.

- Colmenero-Flores, J. M.; Martínez, G.; Gamba, G.; Vázquez, N.; Iglesias, D. J.; Brumós, J. and Talón, M. (2007). "Identification and functional characterization of cation-chloride cotransporters in plants." The Plant Journal **50**(2): 278-292.
- Colombo, R.; Cerana, R. and Bagni, N. (1992). "Evidence for polyamine channels in protoplasts and vacuoles of cells." Biochemical and Biophysical Research Communications **182**(3): 1187-1192.
- Cosio, C. and Dunand, C. (2009). "Specific functions of individual class III peroxidase genes." Journal of Experimental Botany **60**(2): 391-408.
- Cramer, G. R. (2002). Sodium-calcium interactions under salinity stress, Kluwer Academic Publishers.
- Dajic, Z. (2006). Salt stress. Physiology and molecular biology of stress tolerance in plants. Madhava Rao, K. V.; Raghavendra, A. S. and Janardhan Reddy, K., Springer Netherlands: 41-99S.
- Davis, S. J. and Vierstra, R. D. (1998). "Soluble, highly fluorescent variants of green fluorescent protein (GFP) for use in higher plants." Plant Molecular Biology **36**(4): 521-528.
- Day, R. N. and Davidson, M. W. (2009). "The fluorescent protein palette: tools for cellular imaging." Chemical Society Reviews **38**(10): 2887-2921.
- De Angeli, A.; Monachello, D.; Ephritikhine, G.; Frachisse, J. M.; Thomine, S.; Gambale, F. and Barbier-Brygoo, H. (2006). "The nitrate/proton antiporter AtCLCa mediates nitrate accumulation in plant vacuoles." Nature **442**(7105): 939-942.
- de Azevedo Neto, A. D.; Prisco, J. T.; Enéas-Filho, J.; Abreu, C. E. B. d. and Gomes-Filho, E. (2006). "Effect of salt stress on antioxidative enzymes and lipid peroxidation in leaves and roots of salt-tolerant and salt-sensitive maize genotypes." Environmental and Experimental Botany **56**(1): 87-94.
- de Vos, C. R.; Lubberding, H. J. and Bienfait, H. F. (1986). "Rhizosphere acidification as a response to iron deficiency in bean plants." Journal of Plant Physiology **81**(3): 842-846.
- del Rio, L. A.; Palma, J. M.; Sandalio, L. M.; Corpas, F. J.; Pastori, G. M.; Bueno, P. and Lopez-Huertas, E. (1996). "Peroxisomes as a source of superoxide and hydrogen peroxide in stressed plants." Biochem. Soc. Trans. **24**(2): 434-438.
- del Rio, L. A.; Pastori, G. M.; Palma, J. M.; Sandalio, L. M.; Sevilla, F.; Corpas, F. J.; Jimenez, A.; Lopez-Huertas, E. and Hernandez, J. A. (1998). "The activated oxygen role of peroxisomes in senescence." Journal of Plant Physiology **116**(4): 1195-1200.
- Delpire, E. and Mount, D. B. (2002). "Human and murine phenotypes associated with defects in cation-chloride cotransport." Annual Review of Physiology **64**(1): 803-843.
- Demidchik, V.; Shabala, S. N.; Coutts, K. B.; Tester, M. A. and Davies, J. M. (2003). "Free oxygen radicals regulate plasma membrane Ca<sup>2+</sup>- and K<sup>+</sup>-permeable channels in plant root cells." Journal of Cell Science **116**(1): 81-88.
- Demidchik, V.; Shabala, S. N. and Davies, J. M. (2007). "Spatial variation in H<sub>2</sub>O<sub>2</sub> response of *Arabidopsis thaliana* root epidermal Ca<sup>2+</sup> flux and plasma membrane Ca<sup>2+</sup> channels." The Plant Journal **49**(3): 377-386.
- Demiral, T. and Türkan, I. (2005). "Comparative lipid peroxidation, antioxidant defense systems and proline content in roots of two rice cultivars differing in salt tolerance." Environmental and Experimental Botany **53**: 247-257.
- Desikan, R.; Cheung, M.-K.; Bright, J.; Henson, D.; Hancock, J. T. and Neill, S. J. (2004). "ABA, hydrogen peroxide and nitric oxide signalling in stomatal guard cells." Journal of Experimental Botany **55**(395): 205-212.
- Desikan, R.; Mackerness, S. A.-H.; Hancock, J. T. and Neill, S. J. (2001). "Regulation of the *Arabidopsis* transcriptome by oxidative stress." Journal of Plant Physiology **127**(1): 159-172.
- Dias, M. A. and Costa, M. M. (1983). "Effect of Low Salt Concentrations on Nitrate Reductase and Peroxidase of Sugar Beet Leaves." Journal of Experimental Botany **34**(5): 537-543.
- Dieter, P. (1984). "Calmodulin and calmodulin-mediated processes in plants." Plant, Cell & Environment **7**(6): 371-380.
- Dietz, K. J.; Tavakoli, N.; Kluge, C.; Mimura, T.; Sharma, S. S.; Harris, G. C.; Chardonnens, A. N. and Gollack, D. (2001). "Significance of the V-type ATPase for the adaptation to stressful growth conditions and its regulation on the molecular and biochemical level." Journal of Experimental Botany **52**(363): 1969-1980.
- Dobrovinskaya, O. R.; Muñiz, J. and Pottosin, I. I. (1999). "Inhibition of vacuolar ion channels by polyamines." Journal of Membrane Biology **167**(2): 127-140.

- Dooley, C.; Dore, T.; Hanson, G.; Jackson, W.; Remington, S. and Tsien, R. (2004). "Imaging dynamic redox changes in mammalian cells with green fluorescent protein indicators." Journal of Biological Chemistry **279**(21): 22284-22293.
- Dutzler, R. (2006). "The CIC family of chloride channels and transporters." Current Opinion in Structural Biology **16**(4): 439-446.
- Dutzler, R. (2007). "A structural perspective on CIC channel and transporter function." FEBS Letters **581**(15): 2839-2844.
- Dutzler, R.; Campbell, E. B.; Cadene, M.; Chait, B. T. and MacKinnon, R. (2002). "X-ray structure of a CIC chloride channel at 3.0Å reveals the molecular basis of anion selectivity." Nature **415**(6869): 287-294.
- Dutzler, R.; Campbell, E. B. and MacKinnon, R. (2003). "Gating the selectivity filter in CIC chloride channels." Science **300**(5616): 108-112.
- Edwards, E. A.; Enard, C.; Creissen, G. P. and Mullineaux, P. M. (1994). "Synthesis and properties of glutathione reductase in stressed peas." Planta **192**: 137-143.
- Eide, D.; Broderius, M.; Fett, J. and Gueriot, M. L. (1996). "A novel iron-regulated metal transporter from plants identified by functional expression in yeast." Proceedings of the National Academy of Sciences USA **93**(11): 5624-5628.
- El-Hendawy, S. E.; Hu, Y. and Schmidhalter, U. (2005). "Growth, ion content, gas exchange, and water relations of wheat genotypes differing in salt tolerances." Australian Journal of Agricultural Research **56**(2): 123-134.
- Elstner, E. F. (1990). Der Sauerstoff - Biochemie, Biologie, Medizin. Mannheim, Germany, BI-Wissenschaftsverlag.
- Eraslan, F.; Inal, A.; Savasturk, O. and Gunes, A. (2007). "Changes in antioxidative system and membrane damage of lettuce in response to salinity and boron toxicity." Scientia Horticulturae **114**: 5-10.
- Erdei, L.; Szegletes, Z.; Barabas, K. and Pestenacz, A. (1996). "Responses in polyamine titer under osmotic and salt stress in sorghum and maize seedlings." Journal of Plant Physiology **147**(5): 599-603.
- Essah, P. A.; Davenport, R. and Tester, M. (2003). "Sodium influx and accumulation in Arabidopsis." Journal of Plant Physiology **133**(1): 307-318.
- Evans, N. H.; McAinsh, M. R.; Hetherington, A. M. and Knight, M. R. (2005). "ROS perception in *Arabidopsis thaliana*: the ozone-induced calcium response." The Plant Journal **41**(4): 615-626.
- Evans, P. T. and Malmberg, R. L. (1989). "Do polyamines have roles in plant development?" Annual Review of Plant Physiology and Plant Molecular Biology **40**(1): 235-269.
- Fahlke, C. (2001). "Ion permeation and selectivity in CIC-type chloride channels." American Journal of Physiology - Renal Physiology **280**(5): 748-757.
- Fedoroff, N. (2006). "Redox regulatory mechanisms in cellular stress responses." Annals of Botany **98**(2): 289-300.
- Felle, H. (1994). "The H<sup>+</sup>/Cl<sup>-</sup> symporter in root-hair cells of *Sinapis alba*." Journal of Plant Physiology **106**: 1131-1136.
- Ferguson, I. B. (1984). "Calcium in plant senescence and fruit ripening." Plant, Cell & Environment **7**(6): 477-489.
- Ferreira, S.; Hjerna, K.; Larsen, M.; Wingsle, G.; Larsen, P.; Fey, S.; Roepstorff, P. and Salomé Pais, M. (2006). "Proteome profiling of *Populus euphratica* Oliv. upon heat stress." Annals of Botany **98**(2): 361-377.
- Flowers, T. J. and Colmer, T. D. (2008). "Salinity tolerance in halophytes." New Phytologist **179**(4): 945-963.
- Flowers, T. J.; Troke, P. F. and Yeo, A. R. (1977). "The mechanisms of salt tolerance in halophytes." Annual Reviews in Plant Physiology **28**: 89-121.
- Fobis-Loisy, I.; Loidon, K.; Lobréaux, S.; Lebrun, M. and Briat, J.-F. (1995). "Structure and differential expression of two maize ferritin genes in response to iron and abscisic acid." European Journal of Biochemistry **231**(3): 609-619.
- Foreman, J.; Demidchik, V.; Bothwell, J. H. F.; Mylona, P.; Miedema, H.; Torres, M. A.; Linstead, P.; Costa, S.; Brownlee, C.; Jones, J. D. G.; Davies, J. M. and Dolan, L. (2003). "Reactive oxygen species produced by NADPH oxidase regulate plant cell growth." Nature **422**(6930): 442-446.

- Foyer, C. H. and Noctor, G. (2005). "Redox homeostasis and antioxidant signaling: A metabolic interface between stress perception and physiological responses." *The Plant Cell* **17**(7): 1866-1875.
- Fricker, M.; Runions, J. and Moore, I. (2006). "Quantitative fluorescence microscopy: from art to science." *Annual Review of Plant Biology* **57**(1): 79-107.
- Gadjev, I.; Vanderauwera, S.; Gechev, T. S.; Laloi, C.; Minkov, I. N.; Shulaev, V.; Apel, K.; Inze, D.; Mittler, R. and Van Breusegem, F. (2006). "Transcriptomic footprints disclose specificity of reactive oxygen species signaling in Arabidopsis." *Journal of Plant Physiology* **141**(2): 436-445.
- Gamba, G. (2005). "Molecular physiology and pathophysiology of electroneutral cation-chloride cotransporters." *Physiological Reviews* **85**(2): 423-493.
- Gao, D.; Knight, M. R.; Trewavas, A. J.; Sattelmacher, B. and Plieth, C. (2004). "Self-reporting Arabidopsis expressing pH and  $[Ca^{2+}]$  indicators unveil ion dynamics in the cytoplasm and in the apoplast under abiotic stress." *Journal of Plant Physiology* **134**(3): 898-908.
- Gao, F.; Gao, Q.; Duan, X.; Yue, G.; Yang, A. and Zhang, J. (2006). "Cloning of an  $H^+$ -PPase gene from *Thellungiella halophila* and its heterologous expression to improve tobacco salt tolerance." *Journal of Experimental Botany* **57**(12): 3259-3270.
- Garbarino, J. and DuPont, F. M. (1988). "NaCl induces a  $Na^+/H^+$  antiport in tonoplast vesicles from barley roots." *Journal of Plant Physiology* **86**(1): 231-236.
- García-Sánchez, F.; Carvajal, M.; Porras, I.; Botía, P. and Martínez, V. (2003). "Effects of salinity and rate of irrigation on yield, fruit quality and mineral composition of "Fino 49" lemon." *European Journal of Agronomy* **19**(3): 427-437.
- Garg, B. K.; Kathju, S.; Vyas, S. P. and Lahiri, A. N. (1997). "Alleviation of sodium chloride induced inhibition of growth and nitrogen metabolism of clusterbean by calcium." *Biologia Plantarum* **39**(3): 395-401.
- Garthwaite, A. J.; von Bothmer, R. and Colmer, T. D. (2005). "Salt tolerance in wild *Hordeum* species is associated with restricted entry of  $Na^+$  and  $Cl^-$  into the shoots." *Journal of Experimental Botany* **56**(419): 2365-2378.
- Gaxiola, R. A.; Fink, G. R. and Hirschi, K. D. (2002). "Genetic manipulation of vacuolar proton pumps and transporters." *Journal of Plant Physiology* **129**(3): 967-973.
- Gaxiola, R. A.; Li, J.; Undurraga, S.; Dang, L. M.; Allen, G. J.; Alper, S. L. and Fink, G. R. (2001). "Drought- and salt-tolerant plants result from overexpression of the AVP1  $H^+$ -pump." *Proceedings of the National Academy of Sciences USA* **98**(20): 11444-11449.
- Gechev, T.; Minkov, I. and Hille, J. (2005). "Hydrogen peroxide-induced cell death in Arabidopsis: transcriptional and mutant analysis reveals a role of an oxoglutarate-dependent dioxygenase gene in the cell death process." *IUBMB Life* **57**(3): 181-188.
- Geelen, D.; Lurin, C.; Bouchez, D.; Frachisse, J.-M.; Lelièvre, F.; Courtial, B.; Barbier-Brygoo, H. and Maurel, C. (2000). "Disruption of putative anion channel gene AtCLC-a in Arabidopsis suggests a role in the regulation of nitrate content." *The Plant Journal* **21**(3): 259-267.
- Glass, A. D. M. and Siddiqi, M. Y. (1985). "Nitrate inhibition of chloride influx in barley: Implications for a proposed chloride homeostat." *Journal of Experimental Botany* **36**(4): 556-566.
- Glenn, E.; Brown, J. J. and Blumwald, E. (1999). "Salt tolerance and crop potential of halophytes." *Critical Reviews in Plant Sciences* **18**: 227-255.
- Gogorcena, Y.; Iturbe-Ormaetxe, I.; Escuredo, P. R. and Becana, M. (1995). "Antioxidant defenses against activated oxygen in pea nodules subjected to water stress." *Journal of Plant Physiology* **108**(2): 753-759.
- Golldack, D. and Dietz, K.-J. (2001). "Salt-induced expression of the vacuolar  $H^+$ -ATPase in the common ice plant is developmentally controlled and tissue specific." *Journal of Plant Physiology* **125**(4): 1643-1654.
- Gomez, J. M.; Jimenez, A.; Olmos, E. and Sevilla, F. (2004). "Location and effects of long-term NaCl stress on superoxide dismutase and ascorbate peroxidase isoenzymes of pea (*Pisum sativum* cv. Puget) chloroplasts." *Journal of Experimental Botany* **55**(394): 119-130.
- Gong, M.; van der Luit, A. H.; Knight, M. R. and Trewavas, A. J. (1998). "Heat-shock-induced changes in intracellular  $Ca^{2+}$  level in tobacco seedlings in relation to thermotolerance." *Journal of Plant Physiology* **116**(1): 429-437.

- Gossett, D. R.; Millhollon, E. P. and Lucas, M. C. (1994). "Antioxidant response to NaCl stress in salt-tolerant and salt-sensitive cultivars of cotton." Crop Science **34**(3): 706-714.
- Grant, J. J. and Loake, G. J. (2000). "Role of reactive oxygen intermediates and cognate redox signaling in disease resistance." Journal of Plant Physiology **124**(1): 21-30.
- Grattan, S. R. and Grieve, C. M. (1998). "Salinity-mineral nutrient relations in horticultural crops." Scientia Horticulturae **78**(1-4): 127-157.
- Greenway, H. (1965). "Plant responses to saline substrates. IV. Chloride uptake by *Hordeum vulgare* as affected by inhibitors, transpiration, and nutrients in the medium." Australian Journal of Biological Science **18**: 249-268.
- Greenway, H. and Munns, R. (1980). "Mechanisms of salt tolerance in non-halophytes." Annual Reviews in Plant Physiology **31**: 149-190.
- Gurnett, C.; Kahl, S.; Anderson, R. and Campbell, K. (1995). "Absence of the skeletal muscle sarcolemma chloride channel CLC-1 in myotonic mice." Journal of Biological Chemistry **270**(16): 9035-9038.
- Gutschner, M.; Pauleau, A.-L.; Marty, L.; Brach, T.; Wabnitz, G. H.; Samstag, Y.; Meyer, A. J. and Dick, T. P. (2008). "Real-time imaging of the intracellular glutathione redox potential." Nature Methods **5**(6): 553-559.
- Guy, C. L. (1990). "Cold acclimation and freezing stress tolerance: Role of protein metabolism." Annual Reviews in Plant Physiology and Plant Molecular Biology **41**: 187-223.
- Guy, C. L.; Kaplan, F.; Kopka, J.; Selbig, J. and Hincha, D. K. (2008). "Metabolomics of temperature stress." Physiologia Plantarum **132**: 220-235.
- Haas, M. and Forbush, B. (1998). "The Na-K-Cl cotransporters." Journal of Bioenergetics and Biomembranes **30**: 161-172.
- Halliwell, B. (2006). "Reactive species and antioxidants. Redox biology is a fundamental theme of aerobic life." Journal of Plant Physiology **141**: 312-322.
- Halliwell, B. and Foyer, C. H. (1978). "Properties and physiological function of a glutathione reductase purified from spinach leaves by affinity chromatography." Planta **139**(1): 9-17.
- Halliwell, B. and Gutteridge, J. (1986). "Oxygen free radicals and iron in relation to biology and medicine: some problems and concepts." Archives of Biochemistry and Biophysics **246**(2): 501-514.
- Hancock, J.; Desikan, R.; Harrison, J.; Bright, J.; Hooley, R. and Neill, S. (2006). "Doing the unexpected: proteins involved in hydrogen peroxide perception." Journal of Experimental Botany **57**(8): 1711-1718.
- Hanson, G. T.; Aggeler, R.; Oglesbee, D.; Cannon, M.; Capaldi, R. A.; Tsien, R. Y. and Remington, S. J. (2004). "Investigating mitochondrial redox potential with redox-sensitive green fluorescent protein indicators." Journal of Biological Chemistry **279**: 13044-13053.
- Harada, H.; Kuromori, T.; Hirayama, T.; Shinozaki, K. and Leigh, R. A. (2004). "Quantitative trait loci analysis of nitrate storage in Arabidopsis leading to an investigation of the contribution of the anion channel gene, AtCLC-c, to variation in nitrate levels." Journal of Experimental Botany **55**(405): 2005-2014.
- Harling, H.; Czaja, I.; Schell, J. and Walden, R. (1997). "A plant cation-chloride co-transporter promoting auxin-independent tobacco protoplast division." EMBO Journal **16**(19): 5855-5866.
- Hashida, S.-n.; Takahashi, H. and Uchimiya, H. (2009). "The role of NAD biosynthesis in plant development and stress responses." Annals of Botany **103**(6): 819-824.
- Häussling, M.; Römheld, V. and Marschner, H. (1985). "Beziehungen zwischen Chlorosegrad, Eisengehalten und Blattwachstum von Weinreben auf verschiedenen Standorten." Vitis **24**: 158-168.
- Hechenberger, M. (1996). "A family of putative chloride channels from Arabidopsis and functional complementation of a yeast strain with a CLC gene disruption." Journal of Biological Chemistry **271**: 33632-33638.
- Hecht-Buchholz, C. (1979). "Calcium deficiency and plant ultrastructure." Communications in Soil Science and Plant Analysis **10**(1): 67-81.
- Hedrich, R. and Kurkdjian, A. (1988). "Characterization of an anion-permeable channel from sugar beet vacuoles: effect of inhibitors." EMBO Journal **7**(12): 3661-3666.
- Henriksson, E. and Henriksson, K. N. (2005). "Salt-stress signalling and the role of calcium in the regulation of the Arabidopsis ATHB7 gene." Plant, Cell & Environment **28**(2): 202-210.

- Hernández, J. A.; Corpas, F. J.; Gómez, M.; del Río, L. A. and Sevilla, F. (1993). "Salt-induced oxidative stress mediated by activated oxygen species in pea leaf mitochondria." Physiologia Plantarum **89**(1): 103-110.
- Hernandez, J. A.; Ferrer, M. A.; Jimenez, A.; Barcelo, A. R. and Sevilla, F. (2001). "Antioxidant systems and O<sub>2</sub><sup>-</sup>/H<sub>2</sub>O<sub>2</sub> production in the apoplast of pea leaves. Its relation with salt-induced necrotic lesions in minor veins." Journal of Plant Physiology **127**(3): 817-831.
- Hibbard, P. L. (1922). "Some experiments on reclamation of infertile alkali soils by means of gypsum and other treatments." Soil Science **13**(2).
- Hille, R.; Kim, J. H. and Hemann, C. (1993). "Reductive half-reaction of xanthine oxidase: Mechanistic role of the species giving rise to the "rapid type 1" molybdenum(V) electron paramagnetic resonance signal." Biochemistry **32**(15): 3973-3980.
- Hiraga, S.; Sasaki, K.; Ito, H.; Ohashi, Y. and Matsui, H. (2001). "A large family of class III plant peroxidases." Plant and Cell Physiology **42**(5): 462-468.
- Holmström, K. O.; Somersalo, S.; Mandal, A.; Palva, T. E. and Welin, B. (2000). "Improved tolerance to salinity and low temperature in transgenic tobacco producing glycine betaine." Journal of Experimental Botany **51**(343): 177-185.
- Husain, S.; Caemmerer, S. v. and Munns, R. (2004). "Control of salt transport from roots to shoots of wheat in saline soil." Functional Plant Biology **31**: 1115-1126.
- Ilyna, A. D.; Mauricio, B. J. E.; Sifuentes, S. I. P.; Martinez, H. J. L.; Bogatcheva, E. S.; Romero, G. J. and Rodriguez, M. J. (2000). "Behaviour of enhanced chemiluminescence peroxidase-catalysed peroxidation of luminol in the system of surfactant-water-organic solvent." Biocatalysis: Fundamentals and applications **41**(6): 109-113.
- Inan, G.; Zhang, Q.; Li, P.; Wang, Z.; Cao, Z.; Zhang, H.; Zhang, C.; Quist, T. M.; Goodwin, S. M.; Zhu, J.; Shi, H.; Damsz, B.; Charbaji, T.; Gong, Q.; Ma, S.; Fredricksen, M.; Galbraith, D. W.; Jenks, M. A.; Rhodes, D.; Hasegawa, P. M.; Bohnert, H. J.; Joly, R. J.; Bressan, R. A. and Zhu, J.-K. (2004). "Salt cress. A halophyte and cryophyte Arabidopsis relative model system and its applicability to molecular genetic analyses of growth and development of extremophiles." Journal of Plant Physiology **135**(3): 1718-1737.
- Jabeen, R. and Ahmad, R. (2009). "Alleviation of the adverse effects of salt stress by foliar application of sodium antagonistic essential minerals on cotton (*Gossypium hirsutum*)." Pakistan Journal of Botany **41**(5): 2199-2208.
- Jennings, D. B.; Ehrenshaft, M.; Pharr, D. M. and Williamson, J. D. (1998). "Roles for mannitol and mannitol dehydrogenase in active oxygen-mediated plant defense." Proceedings of the National Academy of Sciences USA **95**(25): 15129-15133.
- Jentsch, T. J. (2008). "CLC chloride channels and transporters: from genes to protein structure, pathology and physiology." Critical Reviews in Biochemistry and Molecular Biology **43**(1): 3-36.
- Jentsch, T. J.; Friedrich, T.; Schriever, A. and Yamada, H. (1999). "The CLC chloride channel family." Pflügers Archiv, European Journal of Physiology **437**(6): 783-795.
- Jentsch, T. J.; Steinmeyer, K. and Schwarz, G. (1990). "Primary structure of *Torpedo marmorata* chloride channel isolated by expression cloning in *Xenopus* oocytes." Nature **348**(6301): 510-514.
- Jeschke, W. D.; Pate, J. S. and Atkins, C. A. (1986). "Effects of NaCl salinity on growth, development, ion transport and ion storage in white lupin (*Lupinus albus* L. cv. Ultra)." Journal of Plant Physiology **124**(3-4): 257-274.
- Jeschke, W. D. and Wolf, O. (1988). "External Potassium Supply is not Required for Root Growth in Saline Conditions: Experiments with *Ricinus communis* L. Grown in a Reciprocal Split-Root System." Journal of Experimental Botany **39**(9): 1149-1167.
- Jossier, M.; Kroniewicz, L.; Dalmas, F.; Le Thiec, D.; Ephritikhine, G.; Thomine, S.; Barbier-Brygoo, H.; Vavasseur, A.; Filleur, S. and Leonhardt, N. (2010). "The Arabidopsis vacuolar anion transporter, AtCLCc, is involved in the regulation of stomatal movements and contributes to salt tolerance." The Plant Journal **64**(4): 563-576.
- Kabala, K. and Klobus, G. (2008). "Modification of vacuolar proton pumps in cucumber roots under salt stress." Journal of Plant Physiology **165**(17): 1830-1837.
- Kafkafi, U.; Valoras, N. and Letey, J. (1982). "Chloride interaction with nitrate and phosphate nutrition in tomato (*Lycopersicon esculentum* L.)." Journal of Plant Nutrition **5**(12): 1369-1385.



- Kawano, T. (2003). "Roles of reactive oxygen species-generating peroxidase reactions in plant defense and growth induction." Plant Cell Reports **21**: 829-837.
- Keller, T.; Damude, H. G.; Werner, D.; Doerner, P.; Dixon, R. A. and Lamb, C. (1998). "A plant homolog of the neutrophil NADPH oxidase gp91<sup>phox</sup> subunit gene encodes a plasma membrane protein with Ca<sup>2+</sup> binding motifs." The Plant Cell **10**(2): 255-266.
- Keutgen, A. J. and Pawelzik, E. (2009). "Impacts of NaCl stress on plant growth and mineral nutrient assimilation in two cultivars of strawberry." Environmental and Experimental Botany **65**(2-3): 170-176.
- Khan, M. A. and Gul, B. (2002). Salt tolerant plants of coastal sabkhas of Pakistan. Netherlands, Kluwer Academic Press.
- Khan, M. A.; Weber, D. J.; Gul, B. and Khan, M. A. (2006). Role of calcium in alleviating salinity effects in coastal halophytes. Ecophysiology of high salinity tolerant plants, Springer Netherlands. **40**: 107-114S.
- Khedr, A. H. A.; Abbas, M. A.; Wahid, A. A. A.; Quick, W. P. and Abogadallah, G. M. (2003). "Proline induces the expression of salt-stress-responsive proteins and may improve the adaptation of *Pancreaticum maritimum* L. to salt stress." Journal of Experimental Botany **54**(392): 2553-2562.
- Kinraide, T. B. (1999). "Interactions among Ca<sup>2+</sup>, Na<sup>+</sup> and K<sup>+</sup> in salinity toxicity: quantitative resolution of multiple toxic and ameliorative effects." Journal of Experimental Botany **50**(338): 1495-1505.
- Kishor, P. B. K.; Hong, Z.; Miao, G. H.; Hu, C. A. A. and Verma, D. P. S. (1995). "Overexpression of  $\delta$ -pyrroline-5-carboxylate synthetase increases proline production and confers osmotolerance in transgenic plants." Journal of Plant Physiology **108**(4): 1387-1394.
- Klein, T. M.; Wolf, E. D.; Wu, R. and Sanford, J. C. (1987). "High-velocity microprojectiles for delivering nucleic acids into living cells." Nature **327**(6117): 70-73.
- Klocke, R.; Steinmeyer, K.; Jentsch, T. J. and Jockusch, H. (1994). "Role of innervation, excitability, and myogenic factors in the expression of the muscular chloride channel ClC-1. A study on normal and myotonic muscle. ." Journal of Biological Chemistry **269**: 27635-27639.
- Knight, H.; Brandt, S. and Knight, M. R. (1998). "A history of stress alters drought calcium signalling pathways in Arabidopsis." The Plant Journal **16**(6): 681-687.
- Knight, H.; Trewavas, A. J. and Knight, M. R. (1996). "Cold calcium signaling in Arabidopsis involves two cellular pools and a change in calcium signature after acclimation." The Plant Cell **8**(3): 489-503.
- Kohler, B. and Raschke, K. (2000). "The delivery of salts to the xylem. Three types of anion conductance in the plasmalemma of the xylem parenchyma of roots of barley." Journal of Plant Physiology **122**(1): 243-254.
- Kourie, J. I. (1998). "Interaction of reactive oxygen species with ion transport mechanisms." American Journal of Physiology - Cell Physiology **275**(1): 1-24.
- Kuda, T.; Hishi, T. and Maekawa, S. (2006). "Antioxidant properties of dried product of 'haba-nori', an edible brown alga, *Petalonia binghamiae* (J. Agardh) Vinogradova." Food Chemistry **98**: 545-550.
- Kuner, T. and Augustine, G. J. (2000). "A genetically encoded ratiometric indicator for chloride: capturing chloride transients in cultured hippocampal neurons." Neuron **27**(3): 447-459.
- Kurepa, J.; Hérouart, D.; van Montagu, M. and Inzé, D. (1997). "Differential expression of CuZn- and Fe-superoxide dismutase genes of tobacco during development, oxidative stress, and hormonal treatments." Plant and Cell Physiology **38**(4): 463-470.
- Kusano, T.; Yamaguchi, K.; Berberich, T. and Takahashi, Y. (2007). "Advances in polyamine research in 2007." Journal of Plant Research **120**(3): 345-350-350.
- Lahaye, P. A. and Epstein, E. (1971). "Calcium and salt toleration by bean plants." Physiologia Plantarum **25**(2): 213-218.
- Lakra, N.; Mishra, S. N.; Singh, D. B. and Tomar, P. C. (2006). "Exogenous putrescine effect on cation concentration in leaf of *Brassica juncea* seedlings subjected to Cd and Pb along with salinity stress." Journal of Environmental Biology **27**(2): 263-269.
- Landsberg, E. C. (1996). "Hormonal regulation of iron-stress response in sunflower roots: a morphological and cytological investigation." Protoplasma **194**(1): 69-80.
- Larkindale, J. and Knight, M. R. (2002). "Protection against heat stress-induced oxidative damage in Arabidopsis involves calcium, abscisic acid, ethylene, and salicylic acid." Journal of Plant Physiology **128**(2): 682-695.

- Lee, C. Y. and Pennesi, A. P. (1984). "Isolation and further characterization of a heat resistant peroxidase isoenzyme from Cauliflower." Journal of Food Science **49**(6): 1616-1617.
- Legge, R. L.; Thompson, J. E.; Baker, J. E. and Lieberman, M. (1982). "The effect of calcium on the fluidity and phase properties of microsomal membranes isolated from postclimacteric Golden Delicious apples." Plant and Cell Physiology **23**(2): 161-169.
- Leshem, Y. and Levine, A. (2007). "Intracellular ROS – What does it do there?" Plant Signaling & Behaviour **2**(3): 155-156.
- Leshem, Y.; Melamed-Book, N.; Cagnac, O.; Ronen, G.; Nishri, Y.; Solomon, M.; Cohen, G. and Levine, A. (2006). "Suppression of Arabidopsis vesicle-SNARE expression inhibited fusion of H<sub>2</sub>O<sub>2</sub>-containing vesicles with tonoplast and increased salt tolerance." Proceedings of the National Academy of Sciences **103**(47): 18008-18013.
- Lewis, B. D.; Karlin-Neumann, G.; Davis, R. W. and Spalding, E. P. (1997). "Ca<sup>2+</sup>-activated anion channels and membrane depolarizations induced by blue light and cold in Arabidopsis seedlings." Journal of Plant Physiology **114**(4): 1327-1334.
- Lewis, B. D. and Spalding, E. P. (1998). "Nonselective block by La<sup>3+</sup> of Arabidopsis ion channels involved in signal transduction." Journal of Membrane Biology **162**(1): 81-90.
- Lim, H.-H. and Miller, C. (2009). "Intracellular proton-transfer mutants in a CLC Cl<sup>-</sup>/H<sup>+</sup> exchanger." The Journal of General Physiology **133**(2): 131-138.
- Lindsay, W. L. (1984). "Soil and plant relationship associated with iron deficiency with emphasis on nutrient interactions." Journal of Plant Nutrition **7**: 489-500.
- Lino, B.; Baizabal-Aguirre, V. M. and González de la Vara, L. E. (1998). "The plasma-membrane H<sup>+</sup>-ATPase from beet root is inhibited by a calcium-dependent phosphorylation." Planta **204**(3): 352-359.
- Lísal, J. and Maduke, M. (2009). "Proton-coupled gating in chloride channels." Philosophical Transactions of the Royal Society B: Biological Sciences **364**(1514): 181-187.
- Liu, J. and Zhu, J.-K. (1997). "An Arabidopsis mutant that requires increased calcium for potassium nutrition and salt tolerance." Proceedings of the National Academy of Sciences USA **94**(26): 14960-14964.
- Liu, L.; Gitz, D. C. and McClure, J. W. (1995). "Effects of UV-B on flavonoids, ferulic acid, growth and photosynthesis in barley primary leaves." Physiologia Plantarum **93**(4): 725-733.
- López-Huertas, E.; Sandalio, L. M.; Gómez, M. and Del Río, L. A. (1997). "Superoxide radical generation in peroxisomal membranes: evidence for the participation of the 18-kDa integral membrane polypeptide." Free Radical Research **26**(6): 497-506.
- Lorenzen, I.; Aberle, T. and Plieth, C. (2004). "Salt stress-induced chloride flux: a study using transgenic Arabidopsis expressing a fluorescent anion probe." The Plant Journal **38**(3): 539-544.
- Loudet, O.; Chaillou, S.; Krapp, A. and Daniel-Vedel, F. (2003). "Quantitative trait loci analysis of water and anion content in interaction with nitrogen availability in *Arabidopsis thaliana*." Genetics **163**: 711-722.
- Lucas, M. and Solano, F. (1992). "Coelenterazine is a superoxide anion-sensitive chemiluminescent probe: its usefulness in the assay of respiratory burst in neutrophils." Analytical Biochemistry **206**: 273-277.
- Lurin, C.; Geelen, D.; Barbier-Brygoo, H.; Guern, J. and Maurel, C. (1996). "Cloning and functional expression of a plant voltage-dependent chloride channel." The Plant Cell **8**(4): 701-711.
- Lüttge, U.; Ratajczak, R.; Leigh, R. A.; Sanders, D. and Callow, J. A. (1997). The physiology, biochemistry and molecular biology of the plant vacuolar ATPase. Advances in Botanical Research, Academic Press. **25**: 253-296S.
- Lv, Q. d.; Tang, R. j.; Liu, H.; Gao, X. s.; Li, Y. z.; Zheng, H. q. and Zhang, H. x. (2009). "Cloning and molecular analyses of the *Arabidopsis thaliana* chloride channel gene family." Plant Science **176**(5): 650-661.
- Lynch, J.; Cramer, G. R. and Lauchli, A. (1987). "Salinity reduces membrane-associated calcium in corn root protoplasts." Journal of Plant Physiology **83**(2): 390-394.
- Lynch, R. E. and Fridovich, I. (1979). "Autoinactivation of xanthine oxidase: The role of superoxide radical and hydrogen peroxide." Biochimica et Biophysica Acta (BBA) - Enzymology **571**(2): 195-200.
- Maathuis, F. J. M. and Amtmann, A. (1999). "K<sup>+</sup> nutrition and Na<sup>+</sup> toxicity: the basis of cellular K<sup>+</sup>/Na<sup>+</sup> ratios." Annals of Botany **84**(2): 123-133.

- Maduke, M.; Miller, C. and Mindell, J. A. (2000). "A decade of CLC chloride channels: Structure, mechanism, and many unsettled questions." Annual Review of Biophysics and Biomolecular Structure **29**(1): 411-438.
- Manivannan, P.; Cheruth, A. J.; Beemrao, S.; Ramamurthy, S.; Pallipalayam, V. M.; Ramalingam, S. and Rajaram, P. (2007). "Salt stress mitigation by calcium chloride in *Vigna radiata* (L.) Wilczek." Acta Biologica Cracoviensia Series Botanica **49**(2): 105-109.
- Marmagne, A.; Vinauger-Douard, M.; Monachello, D.; de Longevialle, A. o. F.; Charon, C. I.; Allot, M. I.; Rappaport, F.; Wollman, F.-A.; Barbier-Brygoo, H. I. n. and Ephritikhine, G. v. (2007). "Two members of the Arabidopsis CLC (chloride channel) family, AtCLCe and AtCLCf, are associated with thylakoid and Golgi membranes, respectively." Journal of Experimental Botany **58**(12): 3385-3393.
- Marschner, H. (1995). Mineral Nutrition of Higher Plants (Second Edition). London, Academic Press.
- Martin, M. L. and Busconi, L. (2001). "A rice membrane-bound calcium-dependent protein kinase is activated in response to low temperature." Journal of Plant Physiology **125**(3): 1442-1449.
- Matsumura, T.; Tabayashi, N.; Kamagata, Y.; Souma, C. and Saruyama, H. (2002). "Wheat catalase expressed in transgenic rice can improve tolerance against low temperature stress." Physiologia Plantarum **116**(3): 317-327.
- Mehlhorn, H.; Lelandais, M.; Korth, H. G. and Foyer, C. H. (1996). "Ascorbate is the natural substrate for plant peroxidases." FEBS Letters **378**(3): 203-206.
- Meloni, D. A.; Oliva, M. A.; Martinez, C. A. and Cambraia, J. (2003). "Photosynthesis and activity of superoxide dismutase, peroxidase and glutathione reductase in cotton under salt stress." Environmental and Experimental Botany **49**(1): 69-76.
- Meyer, A. J.; Brach, T.; Marty, L.; Kreye, S.; Rouhier, N.; Jacquot, J.-P. and Hell, R. (2007). "Redox-sensitive GFP in *Arabidopsis thaliana* is a quantitative biosensor for the redox potential of the cellular glutathione redox buffer." The Plant Journal **52**(5): 973-986.
- Miesenböck, G.; De Angelis, D. A. and Rothman, J. E. (1998). "Visualizing secretion and synaptic transmission with pH-sensitive green fluorescent proteins." Nature **394**(6689): 192-195.
- Miller, C. (1982). "Open-state substructure of single chloride channels from *Torpedo* electroplax." Philosophical Transactions of the Royal Society of London. B, Biological Sciences **299**(1097): 401-411.
- Miller, C. (2006). "ClC chloride channels viewed through a transporter lens." Nature **440**: 484-489.
- Minchin, P. E. H. and Thorpe, M. R. (1983). "A rate of cooling response in phloem translocation." Journal of Experimental Botany **34**(142): 529-536.
- Minorsky, P. V. (1989). "Temperature sensing by plants: a review and hypothesis." Plant Cell & Environment **12**: 119-135.
- Mithöfer, A.; Schulze, B. and Boland, W. (2004). "Biotic and heavy metal stress response in plants: evidence for common signals." FEBS Letters **566**(1-3): 1-5.
- Mittler, R. (2002). "Oxidative stress, antioxidants and stress tolerance." Trends in Plant Science **7**(9): 405-410.
- Mittler, R.; Feng, X. and Cohen, M. (1998). "Post-transcriptional suppression of cytosolic ascorbate peroxidase expression during pathogen-induced programmed cell death in tobacco." The Plant Cell **10**(3): 461-474.
- Mittler, R.; Vanderauwera, S.; Gollery, M. and Van Breusegem, F. (2004). "Reactive oxygen gene network of plants." Trends in Plant Science **9**(10): 490-498.
- Molecular\_Probes (2001). Coelenterazine and coelenterazine derivatives. Eugene, OR, USA, Molecular Probes, Inc.: 1-3.
- Moog, P. R.; Kooij, T. A. W.; Brüggemann, W.; Schiefelbein, J. W. and Kuiper, P. J. C. (1995). "Responses to iron deficiency in *Arabidopsis thaliana*: The Turbo iron reductase does not depend on the formation of root hairs and transfer cells." Planta **195**(4): 505-513.
- Moradi, H. (2009). Characterization of ClC transporter proteins : functional analysis of clc mutants in *Arabidopsis thaliana*. CEES; Faculty of Mathematics and Natural Sciences. Groningen, University of Groningen. **Dissertation**: 119 p.
- Moran, J. F.; Becana, M.; Iturbe-Ormaetxe, I.; Frechilla, S.; Klucas, R. V. and Aparicio-Tejo, P. (1994). "Drought induces oxidative stress in pea plants." Planta **194**(3): 346-352.

- Moran, J. F.; James, E. K.; Rubio, M. C.; Sarath, G.; Klucas, R. V. and Becana, M. (2003). "Functional characterization and expression of a cytosolic iron-superoxide dismutase from cowpea root nodules." Journal of Plant Physiology **133**(2): 773-782.
- Morgan, M. J.; Lehmann, M.; Schwarzländer, M.; Baxter, C. J.; Sienkiewicz-Porzucek, A.; Williams, T. C. R.; Schauer, N.; Fernie, A. R.; Fricker, M. D.; Ratcliffe, R. G.; Sweetlove, L. J. and Finkemeier, I. (2008). "Decrease in manganese superoxide dismutase leads to reduced root growth and affects tricarboxylic acid cycle flux and mitochondrial redox homeostasis." Journal of Plant Physiology **147**(1): 101-114.
- Morishima, I.; Kurono, M. and Shiro, Y. (1986). "Presence of endogeneous calcium ion in horseradish peroxidase." Journal of Biological Chemistry **261**(20): 9391-9399.
- Moya, J. L.; Primo-Millo, E. and Talon, M. (1999). "Morphological factors determining salt tolerance in citrus seedlings: the shoot to root ratio modulates passive root uptake of chloride ions and their accumulation in leaves." Plant, Cell & Environment **22**(11): 1425-1433.
- Murphy, T. M.; Vu, H. and Nguyen, T. (1998). "The superoxide synthases of rose cells. Comparison of assays." Journal of Plant Physiology **117**(4): 1301-1305.
- Nakamura, M. and Nakamura, S. (1998). "One- and two-electron oxidations of luminol by peroxidase systems." Free Radical Biology and Medicine **24**(4): 537-544.
- Nazari, K.; Mahmoudi, A.; R., K.; Moosavi-Movahedi, A. A. and Mohebi, A. (2005). "Stabilizing and suicide-peroxide protecting effect of Ni<sup>2+</sup> on horseradish peroxidase." Journal of the Iranian Chemical Society **2**(3): 232-237.
- Ndayiragije, A. and Lutts, S. (2006). "Do exogenous polyamines have an impact on the response of a salt-sensitive rice cultivar to NaCl?" Journal of Plant Physiology **163**(5): 506-516.
- Neill, S.; Desikan, R. and Hancock, J. (2002a). "Hydrogen peroxide signalling." Current Opinion in Plant Biology **5**: 388-395.
- Neill, S. J.; Desikan, R.; Clarke, A.; Hurst, R. D. and Hancock, J. T. (2002b). "Hydrogen peroxide and nitric oxide as signalling molecules in plants." Journal of Experimental Botany **53**(372): 1237-1247.
- Nicell, J. A. and Wright, H. (1997). "A model of peroxidase activity with inhibition by hydrogen peroxide." Enzyme Microbial Technology **21**: 302-310.
- Niknam, V.; Razavi, N.; Ebrahimzadeh, H. and Sharifzadeh, B. (2006). "Effect of NaCl on biomass, protein and proline contents, and antioxidant enzymes in seedlings and calli of two *Trigonella* species." Biologia Plantarum **50**(4): 591-596.
- Niu, X.; Bressan, R. A.; Hasegawa, P. M. and Pardo, J. M. (1995). "Ion homeostasis in NaCl stress environments." Journal of Plant Physiology **109**(3): 735-742.
- Noctor, G. (2006). "Metabolic signalling in defence and stress: the central roles of soluble redox couples." Plant, Cell & Environment **29**(3): 409-425.
- Noctor, G. and Foyer, C. H. (1998). "Ascorbate and glutathione: Keeping active oxygen under control." Annual Reviews of Plant Physiology and Plant Molecular Biology **49**: 249-279.
- Olson, J. S.; Ballou, D. P.; Palmer, G. and Massey, V. (1974). "The Mechanism of Action of Xanthine Oxidase." Journal of Biological Chemistry **249**(14): 4363-4382.
- Orsini, F.; D'Urzo, M. P.; Inan, G.; Serra, S.; Oh, D.-H.; Mickelbart, M. V.; Consiglio, F.; Li, X.; Jeong, J. C.; Yun, D.-J.; Bohnert, H. J.; Bressan, R. A. and Maggio, A. (2010). "A comparative study of salt tolerance parameters in 11 wild relatives of *Arabidopsis thaliana*." Journal of Experimental Botany **61**(13): 3787-3798.
- Panchuk, I. I.; Volkov, R. A. and Schoffl, F. (2002). "Heat stress- and heat shock transcription factor-dependent expression and activity of ascorbate peroxidase in *Arabidopsis*." Journal of Plant Physiology **129**(2): 838-853.
- Pardo, J. M.; Reddy, M. P.; Yang, S.; Maggio, A.; Huh, G.-H.; Matsumoto, T.; Coca, M. A.; Paino-Daurzo, M.; Koiwa, H.; Yun, D.-J.; Watad, A. A.; Bressan, R. A. and Hasegawa, P. M. (1998). "Stress signaling through Ca<sup>2+</sup>/calmodulin-dependent protein phosphatase calcineurin mediates salt adaptation in plants." Proceedings of the National Academy of Sciences USA **95**(16): 9681-9686.
- Pastori, G.; Foyer, C. H. and Mullineaux, P. (2000). "Low temperature-induced changes in the distribution of H<sub>2</sub>O<sub>2</sub> and antioxidants between the bundle sheath and mesophyll cells of maize leaves." Journal of Experimental Botany **51**(342): 107-113.

- Pei, Z.-M.; Murata, Y.; Benning, G.; Thomine, S.; Klusener, B.; Allen, G. J.; Grill, E. and Schroeder, J. I. (2000). "Calcium channels activated by hydrogen peroxide mediate abscisic acid signalling in guard cells." *Nature* **406**(6797): 731-734.
- Pitman, M. G. (1971). "Uptake and transport of ions in barley seedlings I. Estimation of chloride fluxes in cells of excised roots. ." *Australian Journal of Biological Science* **24**: 407-421.
- Pitman, M. G. (1982). "Transport across plant roots." *Quarterly Reviews of Biophysics* **15**(03): 481-554.
- Plieth, C. (2005). "Calcium: Just another regulator in the machinery of life?" *Annals of Botany* **96**(1): 1-8.
- Plieth, C.; Hansen, U.-P.; Knight, H. and Knight, M. R. (1999a). "Temperature sensing by plants: the primary characteristics of signal perception and calcium response." *The Plant Journal* **18**(5): 491-497.
- Plieth, C.; Sattelmacher, B.; Hansen, U.-P. and Knight, M. R. (1999b). "Low-pH-mediated elevations in cytosolic calcium are inhibited by aluminium: a potential mechanism for aluminium toxicity." *The Plant Journal* **18**(6): 643-650.
- Plieth, C.; Sattelmacher, B. and Hansen, U. P. (1997). "Cytoplasmic  $\text{Ca}^{2+}$ - $\text{H}^{+}$ -exchange buffers in green algae." *Protoplasma* **198**(1): 107-124.
- Porras, A. G.; Olson, J. S. and Palmer, G. (1981). "The reaction of reduced xanthine oxidase with oxygen. Kinetics of peroxide and superoxide formation." *Journal of Biological Chemistry* **256**(17): 9096-9103.
- Potters, G.; De Gara, L.; Asard, H. and Horemans, N. (2002). "Ascorbate and glutathione: guardians of the cell cycle, partners in crime?" *Plant Physiology and Biochemistry* **40**(6-8): 537-548.
- Praetorius, E. and Poulsen, H. (1953). "Enzymatic determination of uric acid with detailed directions." *Scandinavian Journal of Clinical and Laboratory Investigation* **5**(3): 273-280.
- Prasad, T. K. (1996). "Mechanisms of chilling-induced oxidative stress injury and tolerance in developing maize seedlings: changes in antioxidant system, oxidation of proteins and lipids, and protease activities." *The Plant Journal* **10**(6): 1017-1026.
- Prasad, T. K. (1997). "Role of catalase in inducing chilling tolerance in pre-emergent Maize seedlings." *Journal of Plant Physiology* **114**(4): 1369-1376.
- Prasad, T. K.; Anderson, M. D.; Martin, B. A. and Stewart, C. R. (1994). "Evidence for chilling-induced oxidative stress in Maize seedlings and a regulatory role for hydrogen peroxide." *Plant Cell* **6**(1): 65-74.
- Pusch, M.; Ludewig, U.; Rehfeldt, A. and Jentsch, T. J. (1995). "Gating of the voltage-dependent chloride channel CIC-0 by the permeant anion." *Nature* **373**(6514): 527-531.
- Pusch, M.; Zifarelli, G.; Murgia, A. R.; Picollo, A. and Babini, E. (2006). "Channel or transporter? The CLC saga continues." *Experimental Physiology* **91**(1): 149-152.
- Ratajczak, R.; Richter, J. and Lüttge, U. (1994). "Adaptation of the tonoplast V-type  $\text{H}^{+}$ -ATPase of *Mesembryanthemum crystallinum* to salt stress, C3-CAM transition and plant age." *Plant, Cell & Environment* **17**(10): 1101-1112.
- Raven, J. A. (1985). "Regulation of pH and generation of osmolarity in vascular plants: A cost-benefit analysis in relation to efficiency of use of energy, nitrogen and water." *New Phytologist* **101**(1): 25-77.
- Reimer, B. (2010). Funktionelle Charakterisierung der Xanthin Oxidase. *ZBM*. Kiel. **Bachelor thesis**: 46 p.
- Rengel, Z. and Elliott, D. C. (1992). "Mechanism of aluminum inhibition of net  $^{45}\text{Ca}^{2+}$  uptake by *Amaranthus* protoplasts." *Journal of Plant Physiology* **98**(2): 632-638.
- Rentel, M. C.; Lecourieux, D.; Ouaked, F.; Usher, S. L.; Petersen, L.; Okamoto, H.; Knight, H.; Peck, S. C.; Grierson, C. S.; Hirt, H. and Knight, M. R. (2004). "OXI1 kinase is necessary for oxidative burst-mediated signalling in Arabidopsis." *Nature* **427**: 858-861.
- Rhoads, D. M.; Umbach, A. L.; Subbaiah, C. C. and Siedow, J. N. (2006). "Mitochondrial reactive oxygen species. Contribution to oxidative stress and interorganellar signaling " *Journal of Plant Physiology* **141**: 357-366.
- Rice-Evans, C.; Miller, N. and Paganga, G. (1997). "Antioxidant properties of phenolic compounds." *Trends in Plant Science* **2**(4): 152-159.
- Richard, E. A. and Miller, C. (1990). "Steady-state coupling of ion-channel conformations to a transmembrane ion gradient." *Science* **247**(4947): 1208-1210.
- Rizhsky, L.; Halak-Herr, E.; van Breusegem, F.; Rachmilevitch, S.; Barr, J. E.; Rodermel, S.; Inze, D. and Mittler, R. (2002). "Double antisense plants lacking ascorbate peroxidase and catalase are less

- sensitive to oxidative stress than single antisense plants lacking ascorbate peroxidase or catalase." The Plant Journal **32**: 329-342.
- Rodríguez, A. A.; Ramiro Lascano, H.; Bustos, D. and Taleisnik, E. (2007). "Salinity-induced decrease in NADPH oxidase activity in the maize leaf blade elongation zone." Journal of Plant Physiology **164**(3): 223-230.
- Römheld, V. and Marschner, H. (1981). "Rhythmic iron stress reactions in sunflower at suboptimal iron supply." Physiologia Plantarum **53**(3): 347-353.
- Rosenwasser, S.; Rot, I.; Meyer, A. J.; Feldman, L.; Jiang, K. and Friedman, H. (2010). "A fluorometer-based method for monitoring oxidation of redox-sensitive GFP (roGFP) during development and extended dark stress." Physiologia Plantarum **138**(4): 493-502.
- Rout, N. P. and Shaw, B. P. (2001). "Salt tolerance in aquatic macrophytes: possible involvement of the antioxidative enzymes." Plant Science **160**(3): 415-423.
- Ruelland, E.; Cantrel, C.; Gawer, M.; Kader, J.-C. and Zachowski, A. (2002). "Activation of phospholipases C and D is an early response to a cold exposure in Arabidopsis suspension cells." Journal of Plant Physiology **130**(2): 999-1007.
- Ruiz, J. M. and Blumwald, E. (2002). "Salinity-induced glutathione synthesis in *Brassica napus*." Planta **214**: 965-969.
- Rychkov, G. Y.; Pusch, M.; Roberts, M. L.; Jentsch, T. J. and Bretag, A. H. (1998). "Permeation and block of the skeletal muscle chloride channel, ClC-1, by foreign anions." The Journal of General Physiology **111**(5): 653-665.
- Sagi, M. and Fluhr, R. (2001). "Superoxide production by plant homologues of the gp91<sup>phox</sup> NADPH oxidase. Modulation of activity by calcium and by tobacco mosaic virus infection." Journal of Plant Physiology **126**(3): 1281-1290.
- Sagi, M. and Fluhr, R. (2006). "Production of reactive oxygen species by plant NADPH oxidases." Journal of Plant Physiology **141**(2): 336-340.
- Saleh, L. and Plieth, C. (2009). "Fingerprinting antioxidative activities in plants." Plant Methods **5**(1): 2.
- Saleh, L. and Plieth, C. (2010a). "A coelenterazine-based luminescence assay to quantify high-molecular-weight superoxide anion scavenger activities." Nature Protocols **5**(10): 1635-1641.
- Saleh, L. and Plieth, C. (2010b). "Total low-molecular-weight antioxidants as a summary parameter, quantified in biological samples by a chemiluminescence inhibition assay." Nature Protocols **5**(10): 1627-1634.
- Saleh, L.; Plieth, C.; Mock, H.-P.; Mühling, K.-H. and Witzel, K. (2010). Antioxidative Defence Mechanisms in Two Contrasting Barley Genotypes under Salt Stress. Symposium Genetics of Plant Mineral Nutrition, Hannover.
- Sanchez, D. H.; Siahpoosh, M. R.; Roessner, U.; Udvardi, M. and Kopka, J. (2008). "Plant metabolomics reveals conserved and divergent metabolic responses to salinity." Physiologia Plantarum **132**: 209-219.
- Sánchez, F. G.; Díaz, A. N. and García, J. A. G. (1995). "*P*-phenol derivatives as enhancers of the chemiluminescent luminol-horseradish peroxidase-H<sub>2</sub>O<sub>2</sub> reaction: substituent effects." Journal of Luminescence **65**(1): 33-39.
- Sanford, J. C.; Klein, T. M.; Wolf, E. D. and Allen, N. (1987). "Delivery of substances into cells and tissues using a particle bombardment process." Particulate Science and Technology: An International Journal **5**(1): 27-37.
- Scandalios, J. G. (1993). "Oxygen stress and superoxide dismutases." Journal of Plant Physiology **101**(1): 7-12.
- Schachtman, D. P.; Tyerman, S. D. and Terry, B. R. (1991). "The K<sup>+</sup>/Na<sup>+</sup> selectivity of a cation channel in the plasma membrane of root cells does not differ in salt-tolerant and salt-sensitive wheat species." Journal of Plant Physiology **97**(2): 598-605.
- Schell, J.; Bisseling, T.; Dülz, M.; Franssen, H.; Fritze, K.; John, M.; Kleinow, T.; Leßnick, A.; Miklashevichs, E.; Pawlowski, K.; Röhrig, H.; van de Sande, K.; Schmidt, J.; Steinbiß, H.-H. and Stoll, M. (1999). "Re-evaluation of phytohormone-independent division of tobacco protoplast-derived cells." The Plant Journal **17**(5): 461-466.
- Schmid, W. E. (1968). "On the effects of DMSO in cation transport by excised barley roots." American Journal of Botany **55**(7): 757-761.

- Schmidt, H. (2005). Entwicklung fluoreszierender Redoxindikatoren und deren gezielte Expression in pflanzlichen Organellen. ZBM. Kiel. Diploma thesis: 107 p.
- Schmidt, H.; Thierbach, K. and Plieth, C. (2007). Anoxia-induced sub-cellular pH- and redox-crosstalk monitored with PtGFP and sm2roGFP. Botanikertagung 2007, Hamburg.
- Schmidt, W. (2003). "Iron solutions: acquisition strategies and signaling pathways in plants." Trends in Plant Science **8**(4): 188-193.
- Schmitz-Eiberger, M.; Haefs, R. and Noga, G. (2002). "Calcium deficiency - Influence on the antioxidative defense system in tomato plants." Journal of Plant Physiology **159**(7): 733-742.
- Schulte, A.; Lorenzen, I.; Bottcher, M. and Plieth, C. (2006). "A novel fluorescent pH probe for expression in plants." Plant Methods **2**(1): 7.
- Schwarzländer, M.; Fricker, M. D.; C., M.; Marty, L.; Brach, T.; Novak, J.; Sweetlove, L. J.; R., H. and Meyer, A. J. (2008). "Confocal imaging of glutathione redox potential in living plant cells." Journal of Microscopy **231**(2): 299-316.
- Serrano, R. and Kwang, W. J. (1996). "Salt tolerance in plants and microorganisms: toxicity targets and defense responses." International Review of Cytology **165**: 1-52.
- Serrano, R. and Rodriguez-Navarro, A. (2001). "Ion homeostasis during salt stress in plants." Current Opinion in Cell Biology **13**(4): 399-404.
- Shabala, L.; Cuin, T.; Newman, I. and Shabala, S. (2005). "Salinity-induced ion flux patterns from the excised roots of *Arabidopsis sos* mutants." Planta **222**(6): 1041-1050.
- Shabala, S. (2000). "Ionic and osmotic components of salt stress specifically modulate net ion fluxes from bean leaf mesophyll." Plant, Cell & Environment **23**(8): 825-837.
- Shabala, S. (2003). "Regulation of potassium transport in leaves: from molecular to tissue level." Annals of Botany **92**(5): 627-634.
- Shabala, S. and Cuin, T. A. (2008). "Potassium transport and plant salt tolerance." Physiologia Plantarum **133**: 651-669.
- Shabala, S.; Cuin, T. A. and Pottosin, I. (2007). "Polyamines prevent NaCl-induced K<sup>+</sup> efflux from pea mesophyll by blocking non-selective cation channels." FEBS Letters **581**(10): 1993-1999.
- Shabala, S.; Demidchik, V.; Shabala, L.; Cuin, T. A.; Smith, S. J.; Miller, A. J.; Davies, J. M. and Newman, I. A. (2006). "Extracellular Ca<sup>2+</sup> ameliorates NaCl-induced K<sup>+</sup> loss from *Arabidopsis* root and leaf cells by controlling plasma membrane K<sup>+</sup>-permeable channels." Journal of Plant Physiology **141**(4): 1653-1665.
- Shannon, M. C. (1997). Adaptation of plants to salinity. Advances in Agronomy. Donald, L. S., Academic Press. **60**: 75-120S.
- Shi, H.; Ishitani, M.; Kim, C. and Zhu, J.-K. (2000). "The *Arabidopsis thaliana* salt tolerance gene SOS1 encodes a putative Na<sup>+</sup>/H<sup>+</sup> antiporter." Proceedings of the National Academy of Sciences USA **97**(12): 6896-6901.
- Shi, H.; Lee, B.-h.; Wu, S.-J. and Zhu, J.-K. (2003). "Overexpression of a plasma membrane Na<sup>+</sup>/H<sup>+</sup> antiporter gene improves salt tolerance in *Arabidopsis thaliana*." Nature Biotechnology **21**(1): 81-85.
- Shi, H.; Quintero, F. J.; Pardo, J. M. and Zhu, J.-K. (2002). "The putative plasma membrane Na<sup>+</sup>/H<sup>+</sup> antiporter SOS1 controls long-distance Na<sup>+</sup> transport in plants." The Plant Cell **14**(2): 465-477.
- Shigeoka, S.; Ishikawa, T.; Tamoi, M.; Miyagawa, Y.; Takeda, T.; Yabuta, Y. and Yoshimura, K. (2002). "Regulation and function of ascorbate peroxidase isoenzymes." Journal of Experimental Botany **53**(372): 1305-1319.
- Shimomura, O.; Johnson, F. H. and Saiga, Y. (1962). "Extraction, purification and properties of aequorin, a bioluminescent protein from the luminous hydromedusa, *Aequorea*." Journal of Cellular and Comparative Physiology **59**(3): 223-239.
- Shrivastava, A. K.; Darash, R.; Shukla, S. P.; Kumar, A. and Singh, G. B. (1993). "Effect of NaCl induced salt stress on iron uptake, partitioning and accumulation in sugar cane." Sugar cane **4**: 17-21.
- Sichel, G.; Corsaro, C.; Scalia, M.; Di Bilio, A. J. and Bonomo, R. P. (1991). "In vitro scavenger activity of some flavonoids and melanins against O<sub>2</sub><sup>•-</sup>." Free Radical Biology and Medicine **11**(1): 1-8.
- Sies, H. (1991). "Role of reactive oxygen species in biological processes." Journal of Molecular Medicine **69**(21): 965-968.

- Skerrett, M. and Tyerman, S. D. (1994). "A channel that allows inwardly directed fluxes of anions in protoplasts derived from wheat roots." *Planta* **192**(3): 295-305.
- Smirnoff, N. and Cumbes, Q. J. (1989). "Hydroxyl radical scavenging activity of compatible solutes." *Phytochemistry* **28**(4): 1057-1060.
- Song, J.; Shi, G.; Xing, S.; Yin, C.; Fan, H. and Wang, B. (2009). "Ecophysiological responses of the euhalophyte *Suaeda salsa* to the interactive effects of salinity and nitrate availability." *Aquatic Botany* **91**(4): 311-317.
- Sreenivasulu, N.; Grimm, B.; Wobus, U. and Weschke, W. (2000). "Differential response of antioxidant compounds to salinity stress in salt-tolerant and salt-sensitive seedlings of foxtail millet (*Setaria italica*)." *Physiologia Plantarum* **109**: 435-442.
- Sridha, S. and Wu, K. (2006). "Identification of AtHD2C as a novel regulator of abscisic acid responses in Arabidopsis." *The Plant Journal* **46**(1): 124-133.
- Staal, M.; Maathuis, F. J. M.; Elzenga, J. T. M.; Overbeek, J. H. M. and Prins, H. B. A. (1991). "Na<sup>+</sup>/H<sup>+</sup> antiport activity in tonoplast vesicles from roots of the salt-tolerant *Plantago maritima* and the salt-sensitive *Plantago media*." *Physiologia Plantarum* **82**(2): 179-184.
- Stephens, P. A.; Widholm, J. M. and Nickell, C. D. (1990). "Iron-deficiency chlorosis evaluation of soybean with tissue culture." *Theoretical and Applied Genetics* **80**(3): 417-420.
- Storey, R. (1995). "Salt tolerance, ion relations and the effect of root medium on the response of citrus to salinity." *Australian Journal of Plant Physiology* **22**: 101-114.
- Storey, R. and Walker, R. R. (1987). "Some effects of root anatomy on K, Na and Cl loading of citrus roots and leaves." *Journal of Experimental Botany* **38**(11): 1769-1780.
- Szabados, L. and Saviouré, A. (2010). "Proline: a multifunctional amino acid." *Trends in Plant Science* **15**(2): 89-97.
- Sze, H.; Li, X. and Palmgren, M. G. (1999). "Energization of plant cell membranes by H<sup>+</sup>-pumping ATPases: regulation and biosynthesis." *The Plant Cell* **11**(4): 677-690.
- Taji, T.; Seki, M.; Satou, M.; Sakurai, T.; Kobayashi, M.; Ishiyama, K.; Narusaka, Y.; Narusaka, M.; Zhu, J.-K. and Shinozaki, K. (2004). "Comparative genomics in salt tolerance between Arabidopsis and Arabidopsis-related halophyte salt cress using Arabidopsis microarray." *Journal of Plant Physiology* **135**: 1697-1709.
- Tarczynski, M. C.; Jensen, R. G. and Bohnert, H. J. (1993). "Stress protection of transgenic tobacco by production of the osmolyte mannitol." *Science* **259**(5094): 508-510.
- Teakle, N. L. and Tyerman, S. D. (2009). "Mechanisms of Cl<sup>-</sup> transport contributing to salt tolerance." *Plant, Cell & Environment* **33**(4): 566-589.
- Teardo, E.; Frare, E.; Segalla, A.; Marco, V. D.; Giacometti, G. M. and Szabò, I. (2005). "Localization of a putative ClC chloride channel in spinach chloroplasts." *FEBS Letters* **579**(22): 4991-4996.
- Terada, L. S.; Leff, J. A.; Guidot, D. M.; Willingham, I. R. and Repine, J. E. (1991). "Inactivation of xanthine oxidase by hydrogen peroxide involves site-directed hydroxyl radical formation." *Free Radical Biology and Medicine* **10**(1): 61-68.
- Teranishi, K. and Shimomura, O. (1997). "Coelenterazine analogs as chemiluminescent probe for superoxide anion." *Analytical Biochemistry* **249**: 37-43.
- Tester, M. and Davenport, R. (2003). "Na<sup>+</sup> Tolerance and Na<sup>+</sup> Transport in Higher Plants." *Annals of Botany* **91**(5): 503-527.
- Thierbach, K. (2006). Expression und Verifikation von pH- und Redoxindikatoren in subzellulären Domänen pflanzlicher Zellen. *ZBM, Kiel. Diploma thesis*: 100 p.
- Thorpe, G. H.; Kricka, L. J.; Moseley, S. B. and Whitehead, T. P. (1985). "Phenols as enhancers of the chemiluminescent horseradish peroxidase- luminol-hydrogen peroxide reaction: application in luminescence- monitored enzyme immunoassays." *Clinical Chemistry* **31**(8): 1335-1341.
- Tsien, R. W. and Tsien, R. Y. (1990). "Calcium channels, stores, and oscillations." *Annual Review of Cell Biology* **6**(1): 715-760.
- Tsugane, K.; Kobayashi, K.; Niwa, Y.; Ohba, Y.; Wada, K. and Kobayashi, H. (1999). "A recessive Arabidopsis mutant that grows photoautotrophically under salt stress shows enhanced active oxygen detoxification." *The Plant Cell* **11**: 1195-1206.



- Turan, M. A.; Elkarim, A. H. A.; Taban, N. and Taban, S. (2010). "Effect of salt stress on growth and ion distribution accumulation in shoot and root of maize plant." African Journal of Agricultural Research **5**(7): 584-588.
- Tyerman, S. D. and Skerrett, I. M. (1998). "Root ion channels and salinity." Scientia Horticulturae **78**(1-4): 175-235.
- Tyerman, S. D.; Skerrett, M.; Garill, A.; Findlay, G. P. and Leigh, R. A. (1997). "Pathways for the permeation of Na<sup>+</sup> and Cl<sup>-</sup> into protoplasts derived from the cortex of wheat roots." Journal of Experimental Botany **48**(459-480).
- Van Breusegem, F.; Bailey-Serres, J. and Mittler, R. (2008). "Unraveling the tapestry of networks involving reactive oxygen species in plants." Journal of Plant Physiology **147**(3): 978-984.
- Van Breusegem, F. and Dat, J. F. (2006). "Reactive oxygen species in plant cell death." Journal of Plant Physiology **141**(2): 384-390.
- Van Goor, B. J. (1968). "The role of calcium and cell permeability in the disease blossom-end rot of tomatoes." Physiologia Plantarum **21**(5): 1110-1121.
- Vanderauwera, S.; Zimmermann, P.; Rombauts, S.; Vandenabeele, S.; Langebartels, C.; Gruijsem, W.; Inze, D. and Van Breusegem, F. (2005). "Genome-wide analysis of hydrogen peroxide-regulated gene expression in Arabidopsis reveals a high light-induced transcriptional cluster involved in anthocyanin biosynthesis." Journal of Plant Physiology **139**(2): 806-821.
- Veitch, N. C. (2004). "Horseradish peroxidase: a modern view of a classic enzyme." Phytochemistry **65**: 249-259.
- Vera-Estrella, R.; Barkla, B. J.; Bohnert, H. J. and Pantoja, O. (1999). "Salt stress in *Mesembryanthemum crystallinum* L. cell suspensions activates adaptive mechanisms similar to those observed in the whole plant." Planta **207**(3): 426-435.
- Vert, G.; Grotz, N.; Dedaldechamp, F.; Gaymard, F.; Guerinot, M. L.; Briat, J.-F. and Curie, C. (2002). "IRT1, an Arabidopsis transporter essential for iron uptake from the soil and for plant growth." The Plant Cell **14**(6): 1223-1233.
- Véry, A.-A. and Davies, J. M. (2000). "Hyperpolarization-activated calcium channels at the tip of Arabidopsis root hairs." Proceedings of the National Academy of Sciences USA **97**(17): 9801-9806.
- Volkov, V. and Amtmann, A. (2006). "*Thellungiella halophila*, a salt-tolerant relative of *Arabidopsis thaliana*, has specific root ion-channel features supporting K<sup>+</sup>/Na<sup>+</sup> homeostasis under salinity stress." The Plant Journal **48**(3): 342-353.
- Von der Fecht-Bartenbach, J.; Bogner, M.; Dynowski, M. and Ludewig, U. (2010). "CLC-b-mediated NO<sub>3</sub><sup>-</sup>/H<sup>+</sup> exchange across the tonoplast of Arabidopsis vacuoles." Plant and Cell Physiology **51**(6): 960-968.
- Von der Fecht-Bartenbach, J.; Bogner, M.; Krebs, M.; Stierhof, Y.-D.; Schumacher, K. and Ludewig, U. (2007). "Function of the anion transporter AtCLC-d in the trans-Golgi network." The Plant Journal **50**(3): 466-474.
- Vranova, E.; Inze, D. and Van Breusegem, F. (2002). "Signal transduction during oxidative stress." Journal of Experimental Botany **53**(372): 1227-1236.
- Wachter, R. M.; Yarbrough, D.; Kallio, K. and Remington, S. J. (2000). "Crystallographic and energetic analysis of binding of selected anions to the yellow variants of green fluorescent protein." Journal of Molecular Biology **301**(1): 157-171.
- Wallace, A.; Frolich, E. and Lunt, O. R. (1966). "Calcium requirements of higher plants." Nature **209**(5023): 634-634.
- Wang, W.; Vinocur, B. and Altman, A. (2003). "Plant responses to drought, salinity and extreme temperatures: towards genetic engineering for stress tolerance." Planta **218**(1): 1-14.
- White, P. J. and Broadley, M. R. (2001). "Chloride in soils and its uptake and movement within the plant: A review." Annals of Botany **88**(6): 967-988.
- Willekens, H.; Chamnongpol, S.; Davey, M.; Schraudner, M.; Langebartels, C.; Van Montagu, M.; Inze, D. and Van Camp, W. (1997). "Catalase is a sink for H<sub>2</sub>O<sub>2</sub> and is indispensable for stress defence in C<sub>3</sub> plants." EMBO Journal **16**(16): 4806-4816.
- Williams, K. (1997). "Modulation and block of ion channels: a new biology of polyamines." Cellular Signalling **9**(1): 1-13.

- Winkel-Shirley, B. (2002). "Biosynthesis of flavonoids and effects of stress." Current Opinion in Plant Biology **5**(3): 218-223.
- Wiseman, H. and Halliwell, B. (1996). "Damage to DNA by reactive oxygen and nitrogen species: role in inflammatory disease and progression to cancer." Biochemical Journal **313**(1): 17-29.
- Wojtaszek, P. (1997). "Oxidative burst: an early response to pathogen infection." Biochemical Journal **322**: 681-692.
- Xia, M.; Dempski, R. and Hille, R. (1999). "The reductive half-reaction of xanthine oxidase." Journal of Biological Chemistry **274**(6): 3323-3330.
- Yamaguchi, K.; Takahashi, Y.; Berberich, T.; Imai, A.; Miyazaki, A.; Takahashi, T.; Michael, A. and Kusano, T. (2006). "The polyamine spermine protects against high salt stress in *Arabidopsis thaliana*." FEBS Letters **580**(30): 6783-6788.
- Yamaguchi, K.; Takahashi, Y.; Berberich, T.; Imai, A.; Takahashi, T.; Michael, A. J. and Kusano, T. (2007). "A protective role for the polyamine spermine against drought stress in *Arabidopsis*." Biochemical and Biophysical Research Communications **352**(2): 486-490.
- Yang, Q.; Chen, Z.-Z.; Zhou, X.-F.; Yin, H.-B.; Li, X.; Xin, X.-F.; Hong, X.-H.; Zhu, J.-K. and Gong, Z. (2009). "Overexpression of SOS (Salt Overly Sensitive) genes increases salt tolerance in transgenic *Arabidopsis*." Molecular Plant **2**(1): 22-31.
- Yousfi, S.; Wissal, M. s.; Mahmoudi, H.; Abdelly, C. and Gharsalli, M. (2007). "Effect of salt on physiological responses of barley to iron deficiency." Plant Physiology and Biochemistry **45**(5): 309-314.
- Zdebik, A. A.; Zifarelli, G.; Bergsdorf, E.-Y.; Soliani, P.; Scheel, O.; Jentsch, T. J. and Pusch, M. (2008). "Determinants of anion-proton coupling in mammalian endosomal CLC proteins." Journal of Biological Chemistry **283**: 4219-4227.
- Zhang, H.-X.; Hodson, J. N.; Williams, J. P. and Blumwald, E. (2001). "Engineering salt-tolerant Brassica plants: Characterization of yield and seed oil quality in transgenic plants with increased vacuolar sodium accumulation." Proceedings of the National Academy of Sciences USA **98**(22): 12832-12836.
- Zhang, J. and Kirkham, M. B. (1994). "Drought-stress-induced changes in activities of superoxide dismutase, catalase, and peroxidase in Wheat species." Plant Cell Physiology **35**(5): 785-791.
- Zhen, R. G.; Kim, E. J.; Rea, P. A.; Leigh, R. A.; Sanders, D. and Callow, J. A. (1997). The molecular and biochemical basis of pyrophosphate-energized proton translocation at the vacuolar membrane. Advances in Botanical Research, Academic Press. **25**: 297-337S.
- Zhu, C.; Schraut, D.; Hartung, W. and Schäffner, A. R. (2005). "Differential responses of maize MIP genes to salt stress and ABA." Journal of Experimental Botany **56**(421): 2971-2981.
- Zhu, J.-K. (2001). "Plant salt tolerance." Trends in Plant Science **6**(2): 66-71.
- Zifarelli, G. and Pusch, M. (2007). "CLC chloride channels and transporters: a biophysical and physiological perspective." Reviews of Physiology, Biochemistry and Pharmacology: 23-76.
- Zifarelli, G. and Pusch, M. (2009). "Conversion of the 2 Cl<sup>-</sup>/1 H<sup>+</sup> antiporter CLC-5 in a NO<sub>3</sub><sup>-</sup>/H<sup>+</sup> antiporter by a single point mutation." EMBO Journal **28**(3): 175-182.

## SUPPLEMENTAL MATERIAL

<b>Supplemental material 1: Chemicals</b>	<b>140</b>
<b>Supplemental material 2: Equipment</b>	<b>142</b>
<b>Supplemental material 3: Other consumables</b>	<b>143</b>
<b>Supplemental material 4: Comparison of cation content</b>	<b>145</b>
<b>Supplemental material 5: Buffer composition for <i>in vitro</i> calibration</b>	<b>146</b>
<b>Supplemental material 6: Primer Table</b>	<b>147</b>
<b>Supplemental material 7: Chloride channel AtCIC-A</b>	<b>148</b>
<b>Supplemental material 8: Chloride channel AtCIC-A mut</b>	<b>150</b>
<b>Supplemental material 9: Chloride channel AtCIC-B</b>	<b>151</b>
<b>Supplemental material 10: Chloride channel AtCIC-C</b>	<b>153</b>
<b>Supplemental material 11: Chloride channel AtCIC-D</b>	<b>155</b>
<b>Supplemental material 12: Chloride channel AtCIC-E</b>	<b>157</b>
<b>Supplemental material 13: Chloride channel AtCIC-F</b>	<b>159</b>
<b>Supplemental material 14: Chloride channel AtCIC-G</b>	<b>161</b>
<b>Supplemental material 15: Cation-chloride-cotransporter AtCCC</b>	<b>163</b>
<b>Supplemental material 16: Destination vector maps</b>	<b>165</b>
<b>Supplemental material 17: Cloning strategy for Clom_Strep</b>	<b>167</b>
<b>Supplemental material 18: Blockers and Inhibitors</b>	<b>168</b>
<b>Supplemental Material 19: TAC Assay</b>	<b>169</b>
<b>Supplemental Material 20: SOSA Assay</b>	<b>172</b>
<b>Supplemental Material 21: Antioxidative activity of different osmolytes</b>	<b>173</b>
<b>Supplemental Material 22: Flavonoids in plant extracts</b>	<b>173</b>

## Supplemental material 1: Chemicals

(±)cis, trans Abscisic acid	[ <b>ABA</b> ; Sigma, #A1049; MW = 264.3 g/mol]
2-dodecoxyethanol	[ <b>Brij@35</b> ; Roth, #CN21; MW = 1198.57 g/mol]
2-morpholinoethanesulfonic acid	[ <b>MES</b> ; Roth, #4256; MW = 195.2 g/mol]
4-(2-hydroxyethyl)-1-piperazineethanesulfonic acid	[ <b>HEPES</b> ; Fluka, #54457; MW = 238.3 g/mol]
Acetic acid	[Roth, #3738; MW = 60.05 g/mol]
Acrylamide/ N,N'-methylenebisacrylamide	30 % [37.5:1, Roth, #3029]
Agarose	[Invitrogen, # 15510]
Aldrithiol	[Aldrich, # 143057; MW = 220.32 g/mol]
Aluminium chloride anhydrous	[Fluka, # 06220; MW = 133.34 g/mol]
Ammonium nitrate	[Serva, #13373; MW = 80.04 g/mol]
Ammonium persulfate	[ <b>APS</b> ; Roth, #9592; MW = 228.2 g/mol]
Ampicillin sodium salt	[Roth, #K029]
Boric acid	[Fluka, #15670; MW = 61.83 g/mol]
Bovine serum albumin	[ <b>BSA</b> ; Roth, #0052]
Bromophenol Blue	[Riedel de Haën, # 32712]
Caesium chloride	[Sigma, #289329; MW = 168.36 g/mol]
Calcium chloride	[ <b>CaCl<sub>2</sub> · 6 H<sub>2</sub>O</b> ; Riedel deHaen, #12074; MW= 220 g/mol]
Carbenicillin disodium salt	[Roth, #6344]
Chloroform	[Roth, #3313; MW = 119.38 g/mol]
Coelenterazine	[NanoLight Technologies, #303; MW = 423 g/mol]
Complete Mini (Protease Inhibitor)	[Roche, # 13218400]
Coomassie Brilliant Blue R 250	[Fluka, #27816; MW = 833 g/mol]
Coomassie Brilliant Blue G 250	[Serva, #17524; MW = 833 g/mol]
Di methyl sulphoxide	[Fluka, #41648; MW = 78.13 g/mol]
Di-potassium hydrogen phosphate	[Roth, #T875; MW = 174 g/mol]
Di-Sodium-acetamido-isothiocyanostilbene	[ <b>SITS</b> ; Fluka, #00309; MW = 498.46 g/mol]
Dithiothreitol	[ <b>DTT</b> ; Roth, #6908; MW = 154.2 g/mol]
D-mannit	[Roth, # 4175.1; MW = 182.17 g/mol]
Ethanol abs.	[Walter; MW = 46.07 g/mol]
Ethanol denatured	[Walter; MW = 46.07 g/mol]
Ethidiumbromide	[M.P.I., #802511]
Ethylenediaminetetraacetic acid	[ <b>EDTA</b> ; Sigma, #E5134; MW = 372.24 g/mol]
Gadolinium chloride	[ <b>GaCl<sub>3</sub> · 6 H<sub>2</sub>O</b> ; Aldrich, #203289; MW = 371.7 g/mol]
Glutathione - oxidised	[ <b>GSSG</b> ; Roth, #6378; MW = 612 g/mol]
Glycine	[Roth, #3790; MW = 75.07 g/mol]
Horseradish peroxidase	[ <b>HRP</b> ; Sigma, #P6140, ca. 2 kU/ml]
Hydrochloric acid	[Roth, #4625; 1 M, i.e. 34% 1:10 diluted in H <sub>2</sub> O]
Hydrogen peroxide solution	[ <b>H<sub>2</sub>O<sub>2</sub></b> ; Merck, #1.08597; MW = 34 g/mol]
Hypoxanthine	[Fluka, #56700; MW = 136 g/mol]
Imidazole	[Fluka, #56750; MW = 68.077 g/mol]
Iodophenol	[Fluka, #58020; MW = 220 g/mol]
Isopropanol	[Roth, #9865; MW = 60.10 g/mol]
Isopropyl β-D-1-thiogalactopyranoside	[ <b>IPTG</b> ; Roth, #CN08, MW = 238.3 g/mol]
Kanamycin sulphate	[Roth, #T832.3]
Lanthanum chloride	[Merck, #1.12219, MW = 371.18 g/mol]
Luminol	[Fluka, #09253; MW = 177 g/mol]
Luria Broth.(LB) agar	[Roth, #X969; 40 g/l]
Luria Broth.(LB) medium	[Roth, #X968; 25 g/l]
Lysozyme	[Serva, # 28262; 178 000 units/mg]
Magnesium chloride	[ <b>MgCl<sub>2</sub> · 6 H<sub>2</sub>O</b> ; Merck, #1.05832; MW = 203.3 g/mol]
Magnesium sulphate	[Serva, #28308; MW = 120.36 g/mol]
Methanol abs.	[Roth, #HN41; MW = 32.04 g/mol]
Murashige&Skoog (MS) medium	[Duchefa, #M0222]
Murashige&Skoog micro salts	[Duchefa, #M0301]
Murashige&Skoog vitamins	[Duchefa, #M0409]
N, N, N', N'-tetramethylethylenediamine	[ <b>TEMED</b> ; Promage, #V3161]

NADPH	[Roth, #AE14; MW = 833.4 g/mol]
n-dodecyl- $\beta$ -D-maltoside	[Roth, #CN26; MW = 510.63 g/mol]
Nifedipine	[ <b>Nifedipine</b> ; Hennig Arzneimittel, 10mg per tablet]
Nitric acid	[Roth, #9274; MW = 63 g/mol]
Octylphenolpoly(ethyleneglycolether) <sub>x</sub>	[ <b>Triton<sup>®</sup>X-100</b> ; Sigma, #X100; MW = 647]
Orthophosphoric acid 85 %	[Roth, #6366]
Plant agar	[Duchefa, #1001]
Polyethyleneglycol 1,000	[Fluka, #81188]
Polyethyleneglycol 1,500	[Hampton Research, #HR2-525]
Polyethyleneglycol 8,000	[Fluka, #81268]
Polyoxyethylene (10) cetylolether	[ <b>Brij<sup>®</sup>56</b> ; Sigma, #9004-95-9; MW = 1123.52 g/mol]
Polyoxyethylene sorbitan monolaurate	[ <b>Tween 20</b> ; Roth, #9127.1; MW = 354.57 g/mol]
Potassium buffered saline tablets	[ <b>PBS</b> ; Medicago, #69-9400]
Potassium chloride	[Roth, #6781; MW = 74.55 g/mol]
Potassium di-hydrogen phosphate	[Merck, #1.04873; MW = 136 g/mol]
Potassium hydroxide	[Roth, #6751; MW = 56 g/mol; 5 M in H <sub>2</sub> O]
Potassium nitrate	[Duchefa, #0519; MW = 101.1 g/mol]
Rifampicin	[Duchefa, #R0146]
Simethicon	[Ratiopharm; dimethicone 1000 - SiO <sub>2</sub> ; 94.5:5.5]
Sodium acetate	[Roth, #6773; MW = 82.03 g/mol]
Sodium dodecyl sulphate	[ <b>SDS</b> ; Sigma, #L4390; MW = 288.38 g/mol]
Sodium hydroxide	[Merck, #1.06498; MW = 39.9 g/mol]
Sodium chloride	[Fluka, #71378; MW = 58.44 g/mol]
Spectinomycin	[Duchefa, #S0188]
Spermidine	[Fluka, #85558; MW = 254.6 g/mol]
Spermine	[Fluka, #85605; MW = 202.34 g/mol]
Superoxide dismutase	[from bovine liver; Sigma, #S8409]
TRIS ultra pure	[ICN Biomedicals, #77861; MW = 121 g/mol]
Trolox	[Aldrich, #23,881; MW = 250 g/mol]
Tween 20	[Roth, #9127; MW = 1227 g/mol]
Xanthine oxidase	[from bovine milk; Roche Diagnostics, #10110434001]
$\beta$ -Mercaptoethanol	[Applichem, #A1108; MW = 78.13 g/mol]

**Supplemental material 2: Equipment**

AA spectrometer S-series	[Thermo Scientific Inc., Bonn, GER]
ÄKTA™ purifier	[GE-Healthcare Europe, München, GER]
Autoclave 5050 ELV	[Tuttnauer Europe B.V., Breda, NED]
Avanti J-25 equipped with rotors Ja-10/Ja-25.5	[Beckmann Coulter, Krefeld, GER]
Centrifuge 5417C	[Eppendorf, Hamburg, GER]
Centrifuge Heraeus 3SR with rotor 75006441	[Thermo Scientific Inc., Bonn, GER]
Conductivity detector module	[CD 20, Dionex, Idstein, GER]
Confocal laser scanning microscope Leica TCS SP2	[Leica Microsystems, Bensheim, GER]
Dual View - Optical insights	[Photometrics, Ottobrunn, GER]
Electroporator Gene-Pulser®II	[Biorad, München, GER]
Filter sets	[AHF Analysentechnik, Tübingen, GER]
Flow-through-chamber	[self-made, Supplemental material xxx]
Fluorescence microscope Leica MZFL III	[Leica Microsystems CMS, Wetzlar, GER]
Fluorescence spectrophotometer Varian	[PeqLab, Erlangen, GER]
Fluorescent lamp Osram L36 W/77	[Osram, München, GER]
Gel Doc 2000™	[Biorad, München, GER]
Gene-Gun (according to University Freiburg)	[self-made apparatus]
Imago QE CCD-Camera	[Till Photonics, Gräfelfing, GER]
Incubator Innova™ 4230	[New Brunswick Scientific, Nürtingen, GER]
Incubator Multitron	[Infors, Bottmingen, SUI]
Inverted Microscope (DIAPHOT-TMD)	[Nikon, Düsseldorf, GER]
Ion chromatograph DX300	[Dionex, Idstein, GER]
Laminar flow workbench HERAsafe	[Heraeus, Langenselbold, GER]
Lenses	[Zeiss, Jena, GER]
Luminometer PMT 9829A	[Electron Tubes Ltd. Ruislip, UK]
Magnetic stirrer RH basic	[IKA, Staufen, GER]
Milli-Q Biocel	[Millipore, Medford, USA]
Monochromator Polychrom IV	[Till Photonics, Gräfelfing, GER]
Nanodrop® ND-1000	[PeqLab, Erlangen, GER]
Osmometer 030	[Gonotec, Berlin, GER]
PCR-cycler	[Biometra, Göttingen, GER]
pH-meter Sentix-81	[WTW, Weilheim, GER]
Power Pac	[Biorad, München, GER]
Savant SpeedVac DNA 120	[Thermo Scientific Inc., Bonn, GER]
Sonoplus 2200	[Bandelin, Berlin, GER]
Sonorex Super Ak106 (sonicator)	[Bandelin, Berlin, GER]
Sonotrode MS 73	[Bandelin, Berlin, GER]
Spectrophotometer Ultrospec 2100pro	[GE-Healthcare Europe, München, GER]
Sub-Cell®GT, Agarose Gel Electrophoresis System	[Biorad, München, GER]
Thermomixer comfort	[Eppendorf, Hamburg, GER]
Thermomixer comfort	[Eppendorf, Hamburg, GER]
Three-way magnetic valve (S306 01Z350A)	[Sirai, Steinhöring, GER]
Tissue homogenizer Precellys	[PeqLab, Erlangen, GER]
UV Transilluminator 2000	[Biorad, München, GER]
Vacuum pump Type 400171	[ILMVAC, Ilmenau, GER]
Vertical electrophoresis system	[Biorad, München, GER]
Vibration-isolated bench	[Physik Instruments, Karlsruhe, GER]
Vibration-isolated underframe	[Physik Instruments, Karlsruhe, GER]
Vortex Genie 2	[Scientific Instruments, USA]

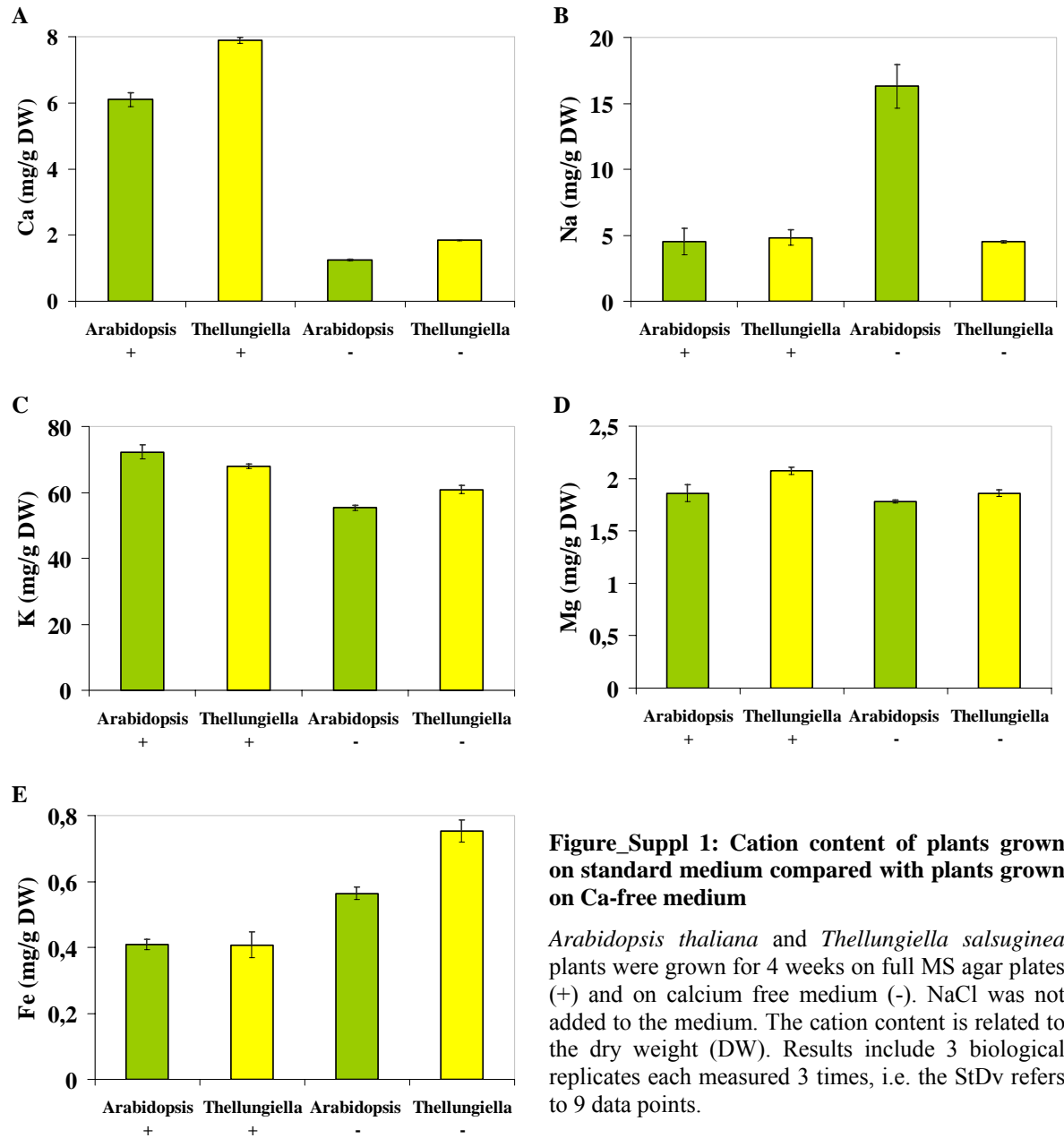
**Supplemental material 3: Other consumables**

0.5; 1.5 and 2 ml centrifuge tubes	[Sarstedt, #72.735; #72.695, #71.890]
15 ml polypropylene tubes	[Greiner bio-one, # 188271]
1kb DNA ladder	[Fermentas, #SM0311]
50 ml polypropylene tubes	[Sarstedt, #62.548]
Acrylic cuvettes	[Sarstedt, #02402017]
Ashless filter paper (Whatman® #42)	[Eydam, ]
Centrifugal filter devices MWCO = 10 kDa:	
Complete Mini (Protease Inhibitor)	[Roche, #13218400]
Cover slips Ø 60mm	[Thermo Scientific, #0047-10888]
Dialysis membrane tubing MWCO = 10 kDa	[Roth, #E668]
Electroporation cuvettes	[VWR, #732-2267]
Filter material	[JBL Symec, #6231100]
Firecly crucibles (Haldenwanger)	[Eydam,
Fluted filter Ø 240 mm	[Macherey-Nagel, #MN 612 1/4]
For 0.5 ml samples Microcon YM-10	[Millipore, #42407]
For 15 ml samples Ultracel-10k	[Millipore, #UFC901096]
Gold Powder (1.5-4 micron/99.9%)	[ChemPur, #009151]
HisTrap™ HP Columns	[GE Healthcare, #17-5247]
Injection syringes (1ml)	[Omnifix®, #9161309]
IonPac anion exchange column	
(AS4 and AS4a together, 4x250 mm)	[Dionex, # 053940]
LMW marker for SDS PAGE	[GE Healthcare, #17-0446-01]
Luminometer vials	[Sarstedt, #55.484]
Membrane filters 0.2 µm PVDF	[Roth, #KH54.1]
Membrane filters 0.2 µm, Cellulose acetate (47mm)	[Whatman, # 9057611]
Micro screw-cap tubes 2 ml	[Sarstedt, #72.694]
NAP™-25 colums	[GE Healthcare, #383393]
Ni <sup>2+</sup> NTA SuperFlow agarose beads	[Qiagen, #1018244]
Oligo(dT)18 Primer	[Fermentas, #SO131]
PCR stripes	[Sarstedt, #72.985]
Petri dishes for bacteria	[Sarstedt, # 82.1473]
Petri dishes for plants	[Greiner bio-one, # 633181]
Quartz cuvettes	[Hellma, # 100-10-40]
Reversed-phase Strata C18-E column	[Phenomenex, #8B_S001-DAK]
RNase Zap®	[Ambion, #9780.9782]
Set of dNTPs (10µmol 100mM each)	[Promega, # U1330]
Single-use scalpels	[Braun, #4501646716]
Spinal injection needle (0.8 x 100mm 2R2)	[UniMed®, #13.205]
Swinnex filter holder	[Millipore, # 16-8941]
Toothpicks KAYBEE	[Bray Health & Leisure, #622]
UV cuvettes	[Sarstedt, 67.758]
 Enzymes and Kits:	
BamHI	[Promega, # R6021]
BglII	[Promega, #R6081]
Go-Taq-DNA Polymerase	[Promega, # EP0401]
HindIII	[Promega, # R6041]
Kpn I	[Promega, # R6341]
Mfe I / Mun I	[NEB, # R0589S]
Pae I / Sph I	[Fermentas, # ER0601]
PCR Mastermix	[Promega, #M7502]
<i>Pfu</i> DNA Polymerase 100u	[Promega, #M7741]
RNaseA	[Macherey-Nagel, #740505]
RQ1 RNase-Free DNase	[Promega, # M6101]
Sal I	[Promega, # R6051]

Shrimp Alkaline Phosphatase	[Promega, # M8201]
SmaI	[Promega, # R6121]
T4 DNA Ligase	[Promega, # M1801]
Xba I	[Promega, # R6181]
Xho I	[Promega, # R6161]
Xma I	[Promega, # R6491]
PeqGOLD Plant RNA Kit	[PEQLab, # 12-6627]
Plasmid Quick Pure	[Macherey-Nagel, # 740615]
QIAfilter™ Plasmid Maxi Kit	[Qiagen, # 12262]
QIAGEN Plasmid Plus Midi	[Qiagen, # 12943]
QIAprep® Spin Miniprep Kit	[Qiagen, # 27106]



## Supplemental material 4: Comparison of cation content



**Supplemental material 5: Buffer composition for *in vitro* calibration**

Buffers for *in vitro* pH calibration of S3roGFP, ratiometric GFP and PtGFP:

pH	Buffering substance (50 mM)
5.5	MES
6.0	MES
6.5	MES
7.0	HEPES
7.5	HEPES
8.0	HEPES
8.5	TAPS
9.0	TAPS

For pH Calibration of Clomeleon 100 mM  $K_2HPO_4$  and 100 mM  $KH_2PO_4$  were combined together in order to obtain solutions with the pH values as listed above.

Oxidized buffers for NaCl calibration of Clomeleon:

1M Na Gluconate (ml)	1M NaCl (ml)	Chloride concentration
0	100	1M
50	50	500 mM
75	25	250 mM
87.5	12.5	125 mM
93.75	6.25	62.5 mM
96.875	3.125	31.25 mM
98.437	1.563	15.625 mM
99,219	0.781	7.8125 mM
100	0	0 mM

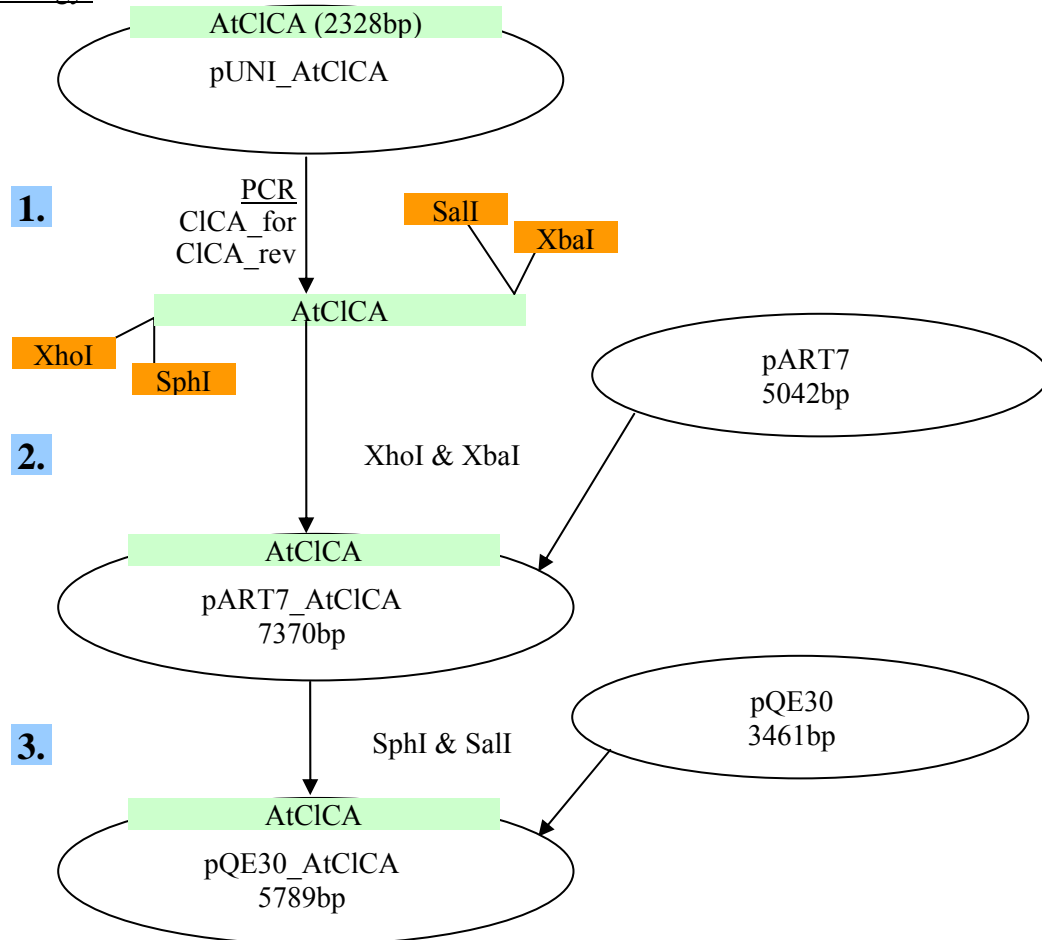
Reduced buffers were prepared by degassing the solutions listed above and the addition of 50 mM DTT

## Supplemental material 6: Primer table

Primer	Sequence 5' -> 3'	Length	Annealing temperature
CICA_for	GATATACCCGGGATGGATGAAGATGGAAACTTGC	34 bp	55°C
CICA_rev	CGGACTATCGATTTCATCTAGCTTTTCCACTTTT	33 bp	
CICA_mut1 rev	TCTCAGGGATCCCCGAACCAGCCGCCGTAGG	31 bp	65°C
CICB_for1	GATATAGGTACCATGGTGAAGAAGATTTAAACCAG	33 bp	62°C
CICB_rev1	CGGACTGTCGACGAATTGCAGATCTCTATGAACTCTC	37 bp	
CICB_for2	GATATAGGTACCTCATAGAGATCTGCAATTCAGGGA	36 bp	58-64°C
CICB_rev2	CGGACTGTCGACTCAATGTGTCTTTCCACCTTTGG	35 bp	
CICC_for	GATATAGGTACCATGGATGATCGGCACGAAGG	32 bp	60°C
CICC_rev	CGGACTCCCGGGTCACTTGAGGGGATCAATGT	32 bp	
CICD_for	GATATAGGTACCATGTTATCGAATCATCTCCAGA	34 bp	62°C
CICD_rev	CGGACTCCCGGGTTAACCTAAAAGATCGTCTAGA	34 bp	
CICE_for	GATATAGGTACCATGGCAGCCACGCTTCCACT	32 bp	60°C
CICE_rev	CGGACTCCCGGGTTACAGATACAGCGAATTTAGG	34 bp	
CICF_for	GATATAGGTACCATGTCATCGGGAGGAGAC	30 bp	60°C
CICF_rev	ACTTCGTCCCGGGTCAATGCCATTTGTAC	30 bp	
CICG_for	GATATAGGTACCATGCCAACTCAACGACGGAG	33 bp	60°C
CICG_rev	CGGACTCCCGGGTCATGAGAAGAAAGGCAG	30 bp	
CCC_for1	GATATAGGATCCGCGCTCGAGATGGATAGCGGCGACATTGAA	42 bp	58-64°C
CCC_rev1	CGGACTGTCGACTCTAGAAGGGAAAGGCCAAGCAATTGT	39 bp	
CCC_for2	GTACTAGGATCCCTCGAGACTTACTGCTACAATTGC	36 bp	62°C
CCC_rev2	CGGACTGTCGACTCTAGACTATGTAAACAAAGTAACAAC	39 bp	
pART7seq_for2	CAAGACCCTTCTCTATA	18 bp	45°C
pART7seq_rev1	CGATCATAGGCGTCTCGC	18 bp	
pQE30_for	GTATCACGAGGCCCTTTCGTCT	22 bp	55°C
pQE30_rev	CATTACTGGATCTATCAACAGGAG	24 bp	
T3	AATTAACCCTCACTAAAGGG	20 bp	55°C
T7	TAATACGACTCACTATAGGG	20 bp	
M13_for	TGAGTTTCGTCACCAGTA	18 bp	50°C
M13_rev	CAGGAAACAGCTATGACC	18 bp	
Clom_Strep	CATGCAAGCTTCTCGAACTGCGGGTGGCTCCACTTGTACAGCTCGTCCA	50 bp	55°C
ClomLNK_Strep	CATGCAAGCTTCTCGAACTGCGGGTGGCTCCAACCACCAGAA CCAGAACCCTTGTACAGCTCGTCC	67 bp	60°C

**Supplemental material 7: Chloride channel AtCIC-A**

Cloning strategy:



- 1) Amplification of the whole 2328 bp long fragment by PCR run with pUNI\_AtCICA as a template. The channel DNA was extended with XhoI and SphI restriction sites at the 5'-end and Sall and XbaI restriction sites at the 3'-end (see **Suppl\_material 6**).
- 2) Cloning into a pART7 vector with help of XhoI and XbaI
- 3) Subcloning into a pQE30 vector (SphI and Sall)

Sequencing results:

pART7\_CICA (pART7seq\_for2 primer)

	XhoI	SphI	
	AGAACTTCTTTGGAGAGAACG	CTCGAGGCATGC	pART7
ATGGATGAAGATGGAAACTTGCAGATTAGTAATAGTAATTACAATGGAGAAGAAGAAGGA	60		
GAAGATCCAGAGAACAACACTTTGAATCAACCACTGCTTAAGAGACATAGAACTCTTTCT	120		
TCAACTCCTCTTGCTTTGGTCGGTGCCAAGGTTTCACACATCGAGAGTTTATGATTATGAA	180		
ATAAACGAGAATGATCTGTTCAAGCATGACTGGAGAAGCAGATCAAAAGCACAAGTGT	240		
CAATACATATTCTTAAAATGGACATTAGCTTGCTTTGTTGGTCTCTTCACTGGTCTTATC	300		
GCTACTCTCATCAACCTTGCTGTCGAAAACATCGCCGGTTACAAACTTCTCGCCGTCGGC	360		
TACTACATTGCTCAAGATAGGTTTTGGACAGGTCTGATGGTCTTTACGGGGGCGAATTTG	420		
GGTCTGACTTTGGTGGCGACAGTACTTGTTGTTTACTTTGCTCCTACGGCGGCTGGTCCG	480		
GGGATCCCTGAGATTAAGCTTACCTTAATGGCATTGACACTCCCAATATGTTTGGTTTT	540		
ACCACCATGATGGTTAAGATTGTTGGAAGTATTGGAGCGGTTGCAGCTGGACTTGATCTT	600		
GGTAAAGAAGGGCCATTGGTTCATATTGGAAGTTGCATAGCTTCTTTGCTTGGTCAAGGT	660		
GGTCCAGATAATCACAGAATCAAATGGAGATGGCTTCGTTACTTCAACAACGATAGAGAT	720		
CGAAGAGATCTTATTACATGTGGATCTGCCTCTGGAGTATGTGCTGCTTTCAGGTCACCA	780		
GTAGGAGGAGTACTTTTCGCTCTTGAGGAAGTCGCTACGTGGTGGAGAAGCGCTCTCTTG	840		
TGGAGAACATTCTTCAGTACAGCCGTTGTGGTGGTTGTATTAAGAGCGTTCATTGAGATT	900		
TGTAACTCCGGGAAATGCGGACTTTTCGGCTCAGAGGACTCATTATGTTTCGATGTGAGTC	960		

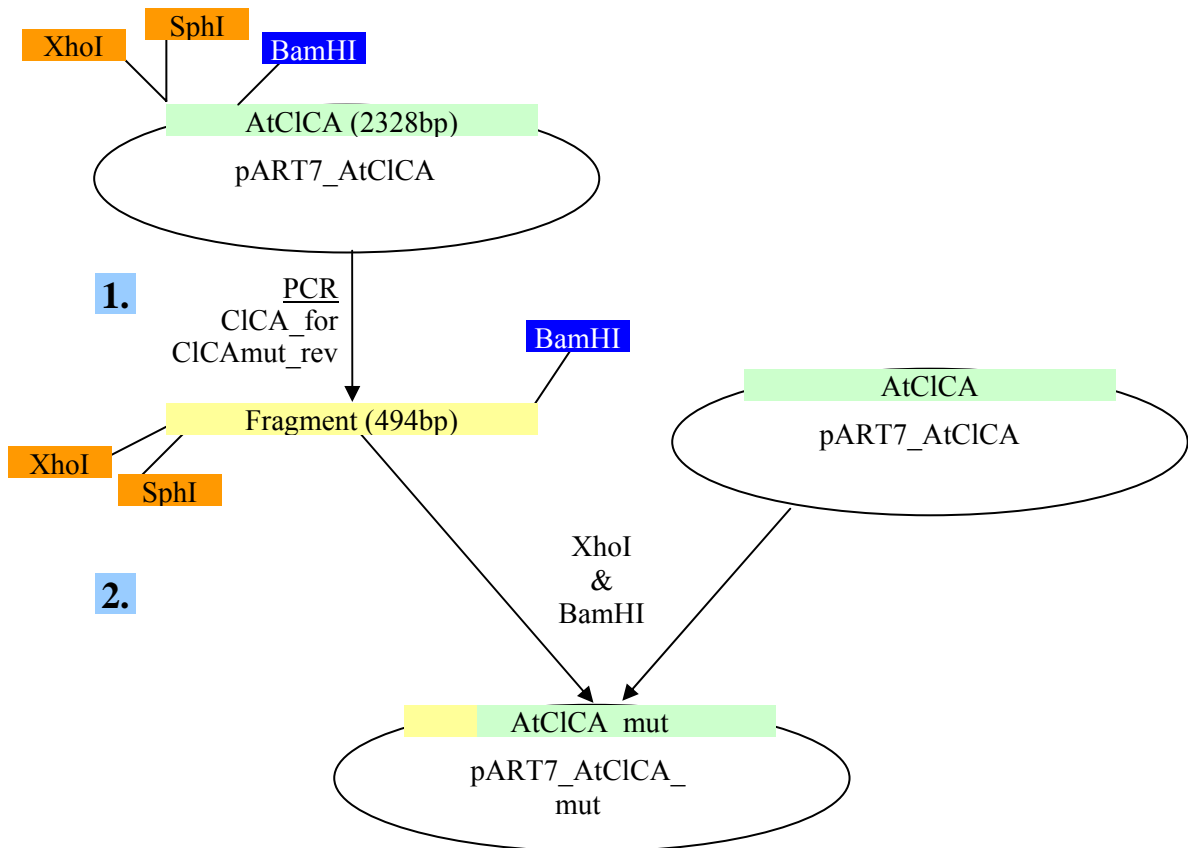
ATGTAGAGGTTAGGTACCACGCAGCAGATATAATCCCAGTCACATTGATTGAGTCTTTGG 1020  
TGGCATT 1027

pART7\_CICA (pART7seq\_rev1 primer)

CCAATGATGATGCAGTCAGAAAACATTTCTCTTCAAACACTCTAATGAGTTTGGCATGGTT 1300  
TCTCTCTGGATATTCTTTGGCCTCTACTGCATTTTGGGTCCTTATAACATTCGGTATAGCG 1368  
ACACCGTCGGGTCTCTTCCCTACCGATTATCCTCATGGGTTCTGCATACGGTAGGATGCTA 1428  
GGCACAGCAATGGGGTCTTACACAAACATAGATCAAGGGCTTTACGCGGTTCTTTGGTGCA 1488  
GCTTCACTCATGGCTGGTTCAATGAGAATGACTGTTTCACTCTGTGTTATATTTCTGGAA 1548  
CTCACCAACAACCTTCTTTTGTGTTGCCATTACAATGTTTGTGCTTCTGATAGCTAAAACA 1608  
GTAGGTGACAGCTTCAATCTAAGTATCTACGAGATCATCTCCATCTTAAGGGCTTACCT 1668  
TTCTTGAAGCAAATCCAGAGCCGTGGATGAGGAATCTCACTGTAGGTGAGCTTAACGAC 1728  
GCTAAGCCTCCGGTTGTAACACTTAACGGAGTAGAAAAAGTGGCAAATATAGTCGATGTA 1788  
CTAAGGAACACAACGCATAACGCATTCCCAGTCTTGGATGGAGCAGATCAAAACACTGGC 1848  
ACAGAGCTCCATGGTCTGATCCTAAGAGCTCACCTTGTGAAAGTTCGAAAAAGAGATGG 1908  
TTCTTGAATGAGAAAAGGAGAACAGAAGAGTGGGAAGTTAGGGAAAAGTTCACACCGGTT 1968  
GAATTAGCTGAGAGAGAAGATAACTTCGATGATGTTGCAATCACAAGCTCAGAGATGCAA 2028  
TTGTATGTTGATCTTCATCCTTTGACCAACACTACACCTTACACAGTGGTGCAAAGTATG 2088  
TCAGTGGCTAAAGCTTTGGTTCGTGTTCCGGTCAGTGGGTCAGACATTTACTGGTGGTT 2148  
CCCAAGATTCAAGCTTCAGGGATGTCACCTGTGATAGGGATCTTAACAAGGCAAGATCTC 2208  
AGGGCTTATAACATTTCTACAAGCATTTCCCTCACTTGGATAAACACAAAAGTGGAAAAGCT 2268  
AGATGA 2328  
GTCTGACTCTAGA CACTCGTCTAGAGTCGGCTAGT pART7  
Sali XbaI

**Supplemental material 8: Chloride channel AtClC-A mut**

Cloning strategy:



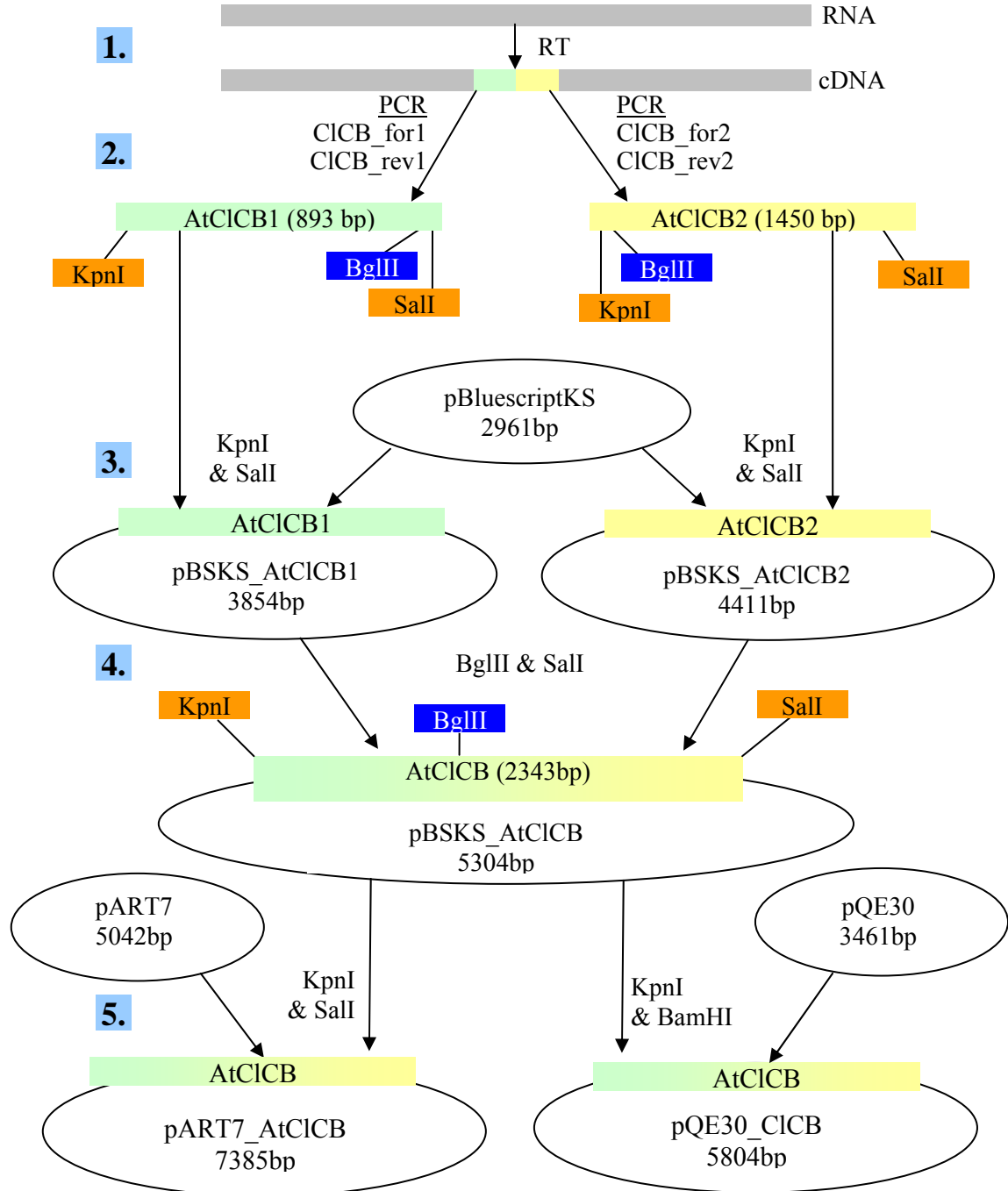
1) Amplification of a 494 bp long fragment by PCR run with pART7\_AtCICA as a template. The fragment was extended with XhoI and SphI restriction sites (see **Suppl\_material 6**) at the 5'-end and contained an endogenous BamHI restriction site at the 3'-end.

2) Cloning back into a pART7\_AtCICA vector with help of XhoI and BamHI

Sequencing results:

pART7\_CICA\_mut (pART7seq\_for2 primer)

	XhoI SphI	
	TTTGGAGAGGAACG	CTCGAGGCATGC pART7
ATGGATGAAGATGGAAACTTGCAGATTAGTAATAGTAATTACAATGGAGAAGAAGAAGGA		60
GAAGATCCAGAGAACAACACTTTGAATCAACCACTGCTTAAGAGACATAGAACTCTTTCT		120
TCAACTCCTCTTGGCTTGGTCGGTGCCAAGGTTTCACACATCGAGAGTTTAGATTATGAA		180
ATAAACGAGAATGATCTGTTCAAGCATGACTGGAGAAGCAGATCAAAAAGCACAAGTGTTT		240
CAATACATATTCTTAAAATGGACATTAGCTTGTCTTGGTGGTCTCTTCACTGGTCTTATC		300
GCTACTCTCATCAACCTTGTGTCGAAAACATCGCCGGTTACAAACTTCTCGCCGTCGGC		360
TACTACATTGCTCAAGATAGGTTTTGGACAGGTCTGATGGTCTTTACGGGGGCGAATTTG		420
GGTCTGACTTTGGTGGCGACAGTACTTGTGTTTACTTTGCTCCTACGGCGGCTGGTTCG		480
		160AA
GGGATCCCTGAGATTAAAGCTTACCTTAATGGCATTGACACTCCCAATATGTTTGGT		540
<b>C I P</b>		
BamHI		
ACCACCATGATGGTTAAGATTGTTGGAAGTATTGGAGCGGTTGCAGCTGGACTTGATCTT		600

**Supplemental material 9: Chloride channel AtCIC-B**Cloning strategy:

- 1) Reverse transcription of RNA isolated from *Arabidopsis thaliana* (cDNA)
- 2) Amplification of two fragments by PCR run with *Arabidopsis thaliana* cDNA:
  - #1 to #893 (from ATG to BglII-restriction site) – AtCICB1
  - #893 to #2343 (from BglII-restriction site to STOP) – AtCICB2
 Both fragments were extended with KpnI restriction site at the 5'-end and SalI restriction site at the 3'-end (see **Suppl\_material 6**).
- 3) Cloning into a pBluescript II KS+ vector with help of KpnI and SalI
- 4) Merging of both fragments in a pBluescript II KS+ vector with help of BglII and SalI
- 5) Subcloning into a pART7 vector (KpnI and SalI) and into a pQE30 vector (KpnI and BamHI)

Sequencing results:

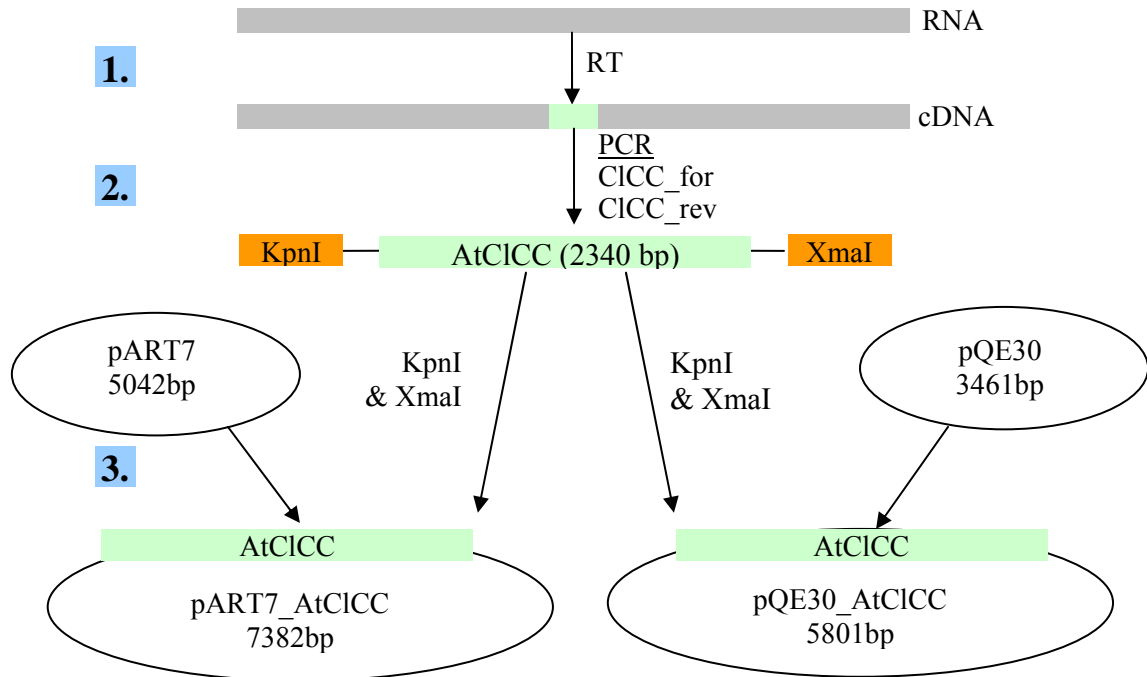
pBS\_ClCB1 (T3 and T7 primer)

	KpnI
	pBKS
	CAAAGCTGGGTACC
ATGGTGGAAGAAGATTTAAACCAGATTGGTGGTAATAGTAATTACAATGGAGAAGGAGGC	60
GACCCAGAGAGCAACACACTTAACCAACCTCTAGTTAAGGCTAATCGAACACTTTCTTCA	120
ACTCCACTTGCTTTGGTTGGTGCCAAAGTTTCCCATATCGAAAGCTTGGACTATGAAATA	180
AACGAGAACGATCTGTTTAAAGCATGATTGGAGAAAAAGATCAAAGGCACAAGTACTTCAA	240
TACGTGTTCTTGAAATGGACGTTAGCTTGTCTTGTGGTCTTTTCACTGGTTAATCGCT	300
ACTCTCATCAACTTAGCTGTTGAAAACATCGCCGGCTATAAGCTTTTAGCCGTGGTTCAC	360
TTCCCTCACTCAAGAAAGATATGTTACAGGTCTGATGGTGTCTTGTGGGGCGAATTTGGGA	420
CTGACGTTGGTGGCGTCTGTGCTTTGTGTGTGCTTTGTCTTACGGCGGTGGACCTGGA	480
ATCCCTGAGATCAAAGCTTATCTTAATGGTGTAGATACTCCCAACATGTTTGGTGTACT	540
ACTATGATCGTTAAGATTGTTGGAAGCATTGGAGCGGTTGCAGCTGGACTTGATCTAGGT	600
AAAGAGGGTCTCTAGTTTACATTGGAAGCTGCATAGCTTCTTTGCTTGGACAAGGTGGA	660
ACAGACAACCACCGTATCAAGTGGCGGTGGCTTCGTTACTTCAACAACGATAGAGACCGC	720
AGGGATCTGATTACATGTGGCTCAGCTGCAGGAGTGTGTGCAGCCTTCAGGTCACCTGTT	780
GGAGGTGTACTTTTCGCCCTCGAGGAAGTGTACTTGGTGGAGAAGTGCCTTATTTGTGG	840
CGGACTTTCTTTCAGCACAGCGGTTGTTGTGGTTGTTCTAAGAGAGTTTCATAGAGATCT	898
<b>GTTCGAC</b> GGTATCGATAAGCTTGATATCGAATTCTGCAGCCCCGGGGATCCACTAGTTCT	PBKS
AGAGCGGCCGCCACCGCGGTGGAGCTCC	PBKS
SaI I	

pBS\_ClCB2 (T3 and T7 primer)

	KpnI
	pBKS
	AAAGCTGGGTACC
	GCAAT
	903
TCAGGGAAGTGTGGGTTGTTTGGAAAAGGAGGGCTAATCATGTTTGATGTGAGTCATGTA	963
ACTTATACTTACCATGTAACCTGATATAATCCCTGTTCATGTTGATTGGTGTAAATCGGTGGA	1023
ATTTCTGGGAGCCTGTACAATCATCTTCTGCATAAAGTTCTCAGGCTTTACAATCTCATC	1083
AATGAGAAGGGTAAGATCCATAAGGTGCTTCTCAGTCTTACAGTATCACTCTTTACATCT	1143
GTTTGCCTTTATGGCCTTCCCTTTCTTAGCGAAATGCAAGCCTTGTGACCCCTCGATAGAT	1203
GAGATATGCCCGACGAATGGAAGATCGGGTAACCTTCAAACAGTTCATTTGCCCTAAAGGT	1263
TACTACAATGATCTAGCTACTCTGCTTCTCACCACCAACGATGATGCTGTGCAGAAACCTT	1323
TTCTCTTCCAACACTCCCAATGAGTTTGGTATGGGTTCCCTTTGGATATTTCTTTGTGCTA	1383
TACTGCATCTTGGGGCTTTTCACATTTGGTATTGCAACACCGTCTGGTCTCTTCCCTCCC	1443
ATCATCCTCATGGGTGCTGCATATGGCCGAATGCTTGGCGCTGCAATGGGATCATAACACA	1503
AGTATTGACCAAGGGCTTTATGCTGTCTTGGTGCAGCTGCACCTCATGGCTGGATCGATG	1563
AGAATGACTGTGTCACTCTGTGTTATATTCCCTTGAACCTCACCACAACCTTCTTTTGTCTT	1623
CCTATAACGATGATCGTGCTTCTGATAGCCAAAACCTGTGGGAGACAGCTTTAACCCGAGT	1683
ATATATGACATCATCTTGCATCTAAAGGGCTTACCTTTCTTAGAAGCAAATCCAGAGCCG	1743
TGGATGAGGAACCTCACCGTTGGTGGAGCTTGGTGTATGCTAAGCCCCGGTTGTAAACCTG	1803
CAAGGTGTTGAAAAGGTTTCAAATATAGTTGATGTGCTAAAAGAACACGACGCATAATGCA	1863
TTCCCTGTTTTAGATGAAGCAGAAGTACCTCAAGTGGGTCTAGCAACTGGGGCTACAGAA	1923
CTCCACGGGTTGATCTTGGAGAGCGCACCTCGTTAAAGTTCTGAAAAAGAGATGGTCTTTG	1983
ACAGAGAAAAGAAGAACAGAGGAGTGGGAGGTCAGAGAAAAGTTTCCATGGGATGAATTG	2043
GCTGAAAGAGAAGACAACCTTTGACGACGTGGCCATCACAAGCGCTGAAATGGAAATGTAT	2103
GTCGATCTTCACTCTCACCAACACAACACCTTACACAGTCATGGAGAACATGTCAGTG	2163
GCCAAGGCTTTAGTACTTTTCCGGCAAGTGGGACTCCGGCATTGCTTATTGTTCCCAAG	2223
ATTCAAGCCTCAGGAATGTGTCTTGTGGTAGGGATCTTAACCAGACAGGACCTAAGGGCA	2283
TACAACATTCTACAAGCCTTTCCCTCTCTTGGAAAAATCCAAAGGTGGAAAGACACATTGA	2343
<b>GTTCGAC</b> GGTATCGATAAGCTTGATATCGAATTCTGCAGCCCCGGGGATCCACTAGTTCT	PBKS
AGAGCGGCCGCCACCGCGGTGGAGCTCCCA	PBKS
SaI I	



**Supplemental material 10: Chloride channel AtCIC-C**Cloning strategy:

- 1) Reverse transcription of RNA isolated from *Arabidopsis thaliana* (cDNA)
- 2) Amplification of the whole 2835 bp long fragment by PCR run with *Arabidopsis thaliana* cDNA. The fragment was extended with KpnI restriction site at the 5'-end and XmaI restriction site at the 3'-end (see **Suppl\_material 6**).
- 3) Cloning into a pART7 vector and a pQE30 vector with help of KpnI and XmaI

Sequencing results:

pART7\_CICC (pART7seq\_for2 primer)

```

                                     GGGGCTTATTTTGGAGAGGAACGCTCGAGGATTCGGTACC KpnI
ATGGATGATCGGCACGAAGGAGACCATCATGATATAGAGGTTGAAGGAGGAGCTTTACAT pART7 60
GGTTTCGAGAGGAAGATATCTGGGATTCCTAGACGATGGATCTGTCCGATTTTCGACAGCCT 120
CTTCTCGCTAGGAATCGAAAAGAACACAACCTTCTCAGATCGCTATTTGTCCGGAGCTAATACT 180
TGTCCCATCGAAAGCCTTGATTACGAGATCTTCGAAAATGATTTTTTCAAGCAAGACTGG 240
AGGTCTAGGAAGAAGATTGAGATACTTCAGTATACGTTTTCTCAAATGGGCGCTTGC'TTTT 300
CTTATTGGT'TTAGCTACTGGACTTGT'TGGCTTTTTTGAATAACCTTGGTGT'TGAGAATATA 360
GCTGGATTTAAACTCTTGCTCATCGGTAATCTCATGCTCAAGGAAAAATATTTCCAGGCA 420
TTTTTTTGCATTTGCTGGT'TGTAACCTAATTTTTGGCAACTGCTGCTGCTTCACTCTGTGCT 480
TTTTATTGCTCCTGCGGCGGCAGGATCTGGCATAACCTGAGGTTAAAGCATATCTCAATGGT 540
ATAGATGCTTATTCAATATTTAGCTCCAAGCACCTCTTTGTTAAGATCTTTGGCTCTATA 600
TTTTGGAGTTGCTGCCGGATTTGTAGTTGGAAAAGAAGGGCCTATGGTTCATACTGGTGC'T 660
TGCATTGCTAATTTACTTGGACAAGGTGGT'TCCAAAAAGTACCGGTTGACTTGGAAAGTGG 720
CTCAGATTTCTCAAAAACGATAGAGACAGAAGAGACCTGATCACTTGC'GGGGCTGCTGC'T 780
GGTGTAGCAGCTGCCTTCCGTGCTCCAGTTGGAGGAGTGCTTTTTTCGCCCTTGAAGAAGCT 840
GCTTCATGGTGGAGGAATGCCTTCTCTGGAGGACATTCCTTCACTACCGCAGTTGTAGCAG 900
TGGTCTTACGAAGTTTGATTGAGTTCTGTGCTCTGGGAGATGTGGACTGTTTGGGAAGG 960
ACGTCTCATCATGTTTGGATGTAAACTCGGGACCAGGTGCTATATAGCCCTCCAGATTT 1020
GCTAGCATAGTTATTCCTTGGAGTTATTTGGTGGTGTGGCC'TTGAAGCCTTTACAAC'TAC 1080
CTTGTGG 1087

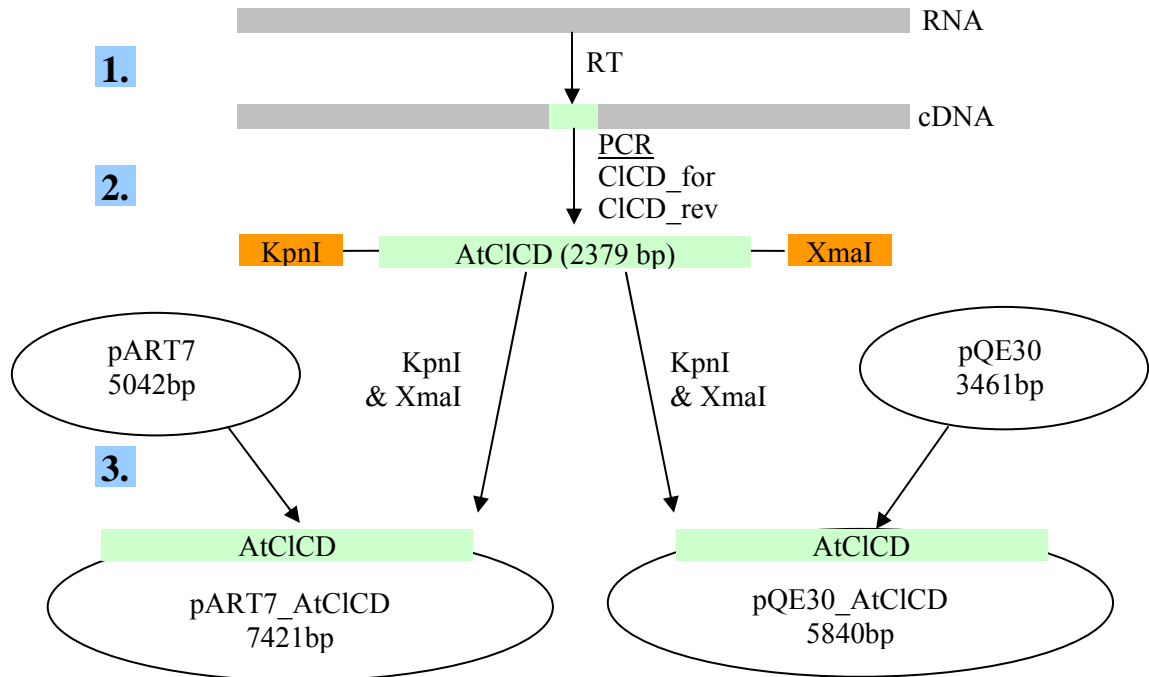
```

pART7\_CICC (pART7seq\_rev1 primer)

```

GTAGGTCG 1260
ATCCAGCATCTTAAGAGGTTGCCAGTGTCTCCCAAACCATTTACAATGACCTTCCCTCCCTA 1320
CTTCTCAACACCAATGATGATGCAATCCGTAATCTTTTCACATCCAGATCTGAAAAATGAA 1380
TTCCATATCTCTACCCTTGCCATCTTCTTTGTGCGCAGTGTACTGCCTTGGCATCATAACA 1440
TACGGCATAGCCATACCCTCTGGGCTTTTCATTCCCTGTCATTCTTGCTGGAGCCTCTTAT 1500
GGACGACTAGTGGGTAGACTGCTGGGTCCAGTATCTCAGCTTGATGTAGGTCTGTTTTCT 1560
CTGCTCGGAGCTGCTTCCTTCCTTGGAGGCACAATGAGAATGACGGTCTCTCTATGTGTT 1620
ATACTGCTCGAACTTACAAATAATCTCCTAATGCTGCCACTGGTGATGCTTGACTCCTT 1680
ATATCAAAAACGGTTGCAGATTGTTTCAACAGGGGGTCTATGACCAGATTGTAACAATG 1740
AAAGGACTGCCTTACATGGAAGACCATGCAGAGCCGTACATGCGCAATTTGGTTGCAAAG 1800
GACGTAGTTTCTGGAGCTTTGATATCCTTTTCGAGAGTTGAAAAGGTTGGGGTAATATGG 1860
CAGGCTTTAAAAATGACAAGACATAATGGTTTCCCTGTAATTGATGAGCCACCTTTCACA 1920
GAAGCTTCTGAGCTATGTGGGATTGCCTTGAGATCTCATCTCCTTGCTTCTCCAAGGG 1980
AAGAAATTCTCGAAGCAGAGAACAACCTTTGGTTCACAAATCTGAGAAGTTGCAAAGCC 2040
CGTGACTTTGGTAAAGCAGGGTTAGGTAAGGGGCTCAAGATTGAAGATTTGGATCTAAGT 2100
GAGGAGGAGATGGAGATGTATGTTGATCTCCATCCCATCACTAACACATCTCCTTACACT 2160
GTGCTTGAGACTCTGTCTCTAGCTAAGGCGGCTATTCTTTTCCGGCAACTTGGTCTTCGC 2220
CACTTGTGTGTGGTGCCTAAAACACCAGGGAGACCGCTATTGTGGAATACTGACAAGG 2280
CATGATTTTCATGCCGGAACATGTCCTGGGACTCTACCCTCACATTGATCCCCCAAGTGA 2340
CCCGGGTTTCGAAATCGATAAGCTTGGATCCTCTAGAGTCAGCTAGTT pART7
XmaI

```

**Supplemental material 11: Chloride channel AtClC-D**Cloning strategy:

- 1) Reverse transcription of RNA isolated from *Arabidopsis thaliana* (cDNA)
- 2) Amplification of the whole 2379 bp long fragment by PCR run with *Arabidopsis thaliana* cDNA. The fragment was extended with KpnI restriction site at the 5'-end and XmaI restriction site at the 3'-end (see **Suppl\_material 6**).
- 3) Cloning into a pART7 vector and a pQE30 vector with help of KpnI and XmaI

Sequencing results:

pART7\_CICD (pART7seq\_for2 primer)

```

GGGGCTTATTTTGGAGAGGAACGCTCGAGGATTCGGTACC KpnI
ATGGATGATCGGCACGAAGGAGACCATCATGATATAGAGGTTGAAGGAGGAGCTTTACAT pART7 60
GGTTTCGAGAGGAAGATATCTGGGATTCCTAGACGATGGATCTGTCTGGATTTTCGACAGCCT 120
CTTCTCGCTAGGAATCGAAAAGAACACAACCTTCTCAGATCGCTATTTGTCTGGAGCTAATACT 180
TGTCCCATCGAAAGCCTTGATTACGAGATCTTCGAAAATGATTTTTTCAAGCAAGACTGG 240
AGGTCTAGGAAGAAGATTGAGATACTTCAGTATACGTTTTCTCAAATGGGCGCTTGC'TTTT 300
CTTATTGGT'TTAGCTACTGGACTTGT'TGGCTTTTTTGAATAACCTTGGTGT'TGAGAATATA 360
GCTGGATTTAAACTCTTGCTCATCGGTAATCTCATGCTCAAGGAAAAATATTTCCAGGCA 420
TTTTTTTGCATTTGCTGGT'TGTAACCTAATTTTTGGCAACTGCTGCTGCTTCACTCTGTGCT 480
TTTATTGCTCCTGCGGCGGCAGGATCTGGCATACTGAGGTTAAAGCATATCTCAATGGT 540
ATAGATGCTTATTCAATATTAGCTCCAAGCACCTCTTTGTTAAGATCTTTGGCTCTATA 600
TTTGGAGTTGCTGCCGGATTTGTAGTTGGAAAAGAAGGGCCTATGGTTCATACTGGTGC'T 660
TGCATTGCTAATTTACTTGGACAAGGTGGT'TCCAAAAAGTACCGGTTGACTTGGAAAGTGG 720
CTCAGATTC'TTCAAAAACGATAGAGACAGAAGAGACCTGATCACTTGC'GGGGCTGCTGC'T 780
GGTGTAGCAGCTGCCTTCCGTGCTCCAGTTGGAGGAGTGCTTTTTTCGCCCTTGAAGAAGCT 840
GCTTCATGGTGGAGGAATGCCTTCTCTGGAGGACATTC'TTCACTACCGCAGTTGTAGCAG 900
TGGTCTTACGAAGTTTGATTGAGTTCTGTCTGCTCTGGGAGATGTGGACTGTTTGGGAAGG 960
ACGTCTCATCATGTTTGGATGTAAACTCGGGACCAGGTGCTATATAGCCCTCCAGATTT 1020
GCTAGCATAGTTATTCCTTGGAGTTATTTGGTGGTGTGGCC'TTGAAGCCTTTTACAAC'TAC 1080
CTTGTGG 1087

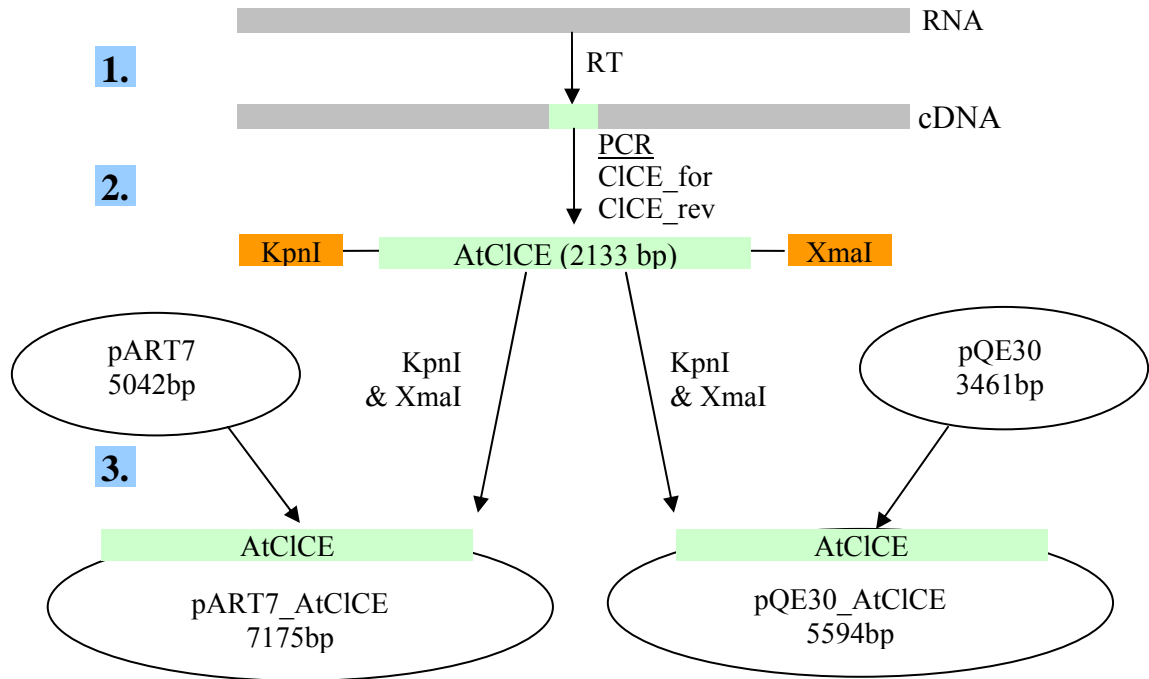
```

pART7\_ClCD (pART7seq\_rev1 primer)

```

GTAGGTCG 1260
ATCCAGCATCTTAAGAGGTTGCCAGTGTCTCCAAACCATTACAATGACCTTCCTCCCTA 1320
CTTCTCAACACCAATGATGATGCAATCCGTAATCTTTTCACATCCAGATCTGAAAATGAA 1380
TTCCATATCTCTACCCTTGCCATCTTCTTTGTGCGAGTGTACTGCCTTGGCATCATAACA 1440
TACGGCATAGCCATAACCCTCTGGGCTTTTCATTCCCTGTCATTCTTGCTGGAGCCTCTTAT 1500
GGACGACTAGTGGGTAGACTGCTGGGTCCAGTATCTCAGCTTGATGTAGGTCTGTTTTCT 1560
CTGCTCGGAGCTGCTTCCTTCCTTGGAGGCACAATGAGAATGACGGTCTCTCTATGTGTT 1620
ATACTGCTCGAACTTACAAATAATCTCCTAATGCTGCCACTGGTGATGCTTGACTCCTT 1680
ATATCAAAAACGGTTGCAGATTGTTTCAACAGGGGGTCTATGACCAGATTGTAACAATG 1740
AAAGGACTGCCTTACATGGAAGACCATGCAGAGCCGTACATGCGCAATTTGGTTGCAAAG 1800
GACGTAGTTTCTGGAGCTTTGATATCCTTTTCGAGAGTTGAAAAGGTTGGGGTAATATGG 1860
CAGGCTTTAAAAATGACAAGACATAATGGTTTCCCTGTAATTGATGAGCCACCTTTCACA 1920
GAAGCTTCTGAGCTATGTGGGATTGCCTTGAGATCTCATCTCCTTGCTTCTCCAAGGG 1980
AAGAAATTCTCGAAGCAGAGAACAACCTTTGGTTCACAAATTCTGAGAAGTTGCAAAGCC 2040
CGTGACTTTGGTAAAGCAGGGTTAGGTAAGGGGCTCAAGATTGAAGATTGGATCTAAGT 2100
GAGGAGGAGATGGAGATGTATGTTGATCTCCATCCCATCACTAACACATCTCCTTACACT 2160
GTGCTTGAGACTCTGTCTCTAGCTAAGGCGGCTATTCTTTTCCGGCAACTTGGTCTTCGC 2220
CACTTGTGTGTGGTGCCTAAAACACCAGGGAGACCGCTATGTGTGGAATACTGACAAGG 2280
CATGATTTTCATGCCGGAACATGTCCTGGGACTCTACCCTCACATTGATCCCCCAAGTGA 2340
CCCGGGTTTCGAAATCGATAAGCTTGGATCCTCTAGAGTCAGCTAGTT pART7
XmaI

```

**Supplemental material 12: Chloride channel AtClC-E**Cloning strategy:

- 1) Reverse transcription of RNA isolated from *Arabidopsis thaliana* (cDNA)
- 2) Amplification of the whole 2133 bp long fragment by PCR run with *Arabidopsis thaliana* cDNA. The fragment was extended with KpnI restriction site at the 5'-end and XmaI restriction site at the 3'-end (see **Suppl\_material 6**).
- 3) Cloning into a pART7 vector and a pQE30 vector with help of KpnI and XmaI

Sequencing results:

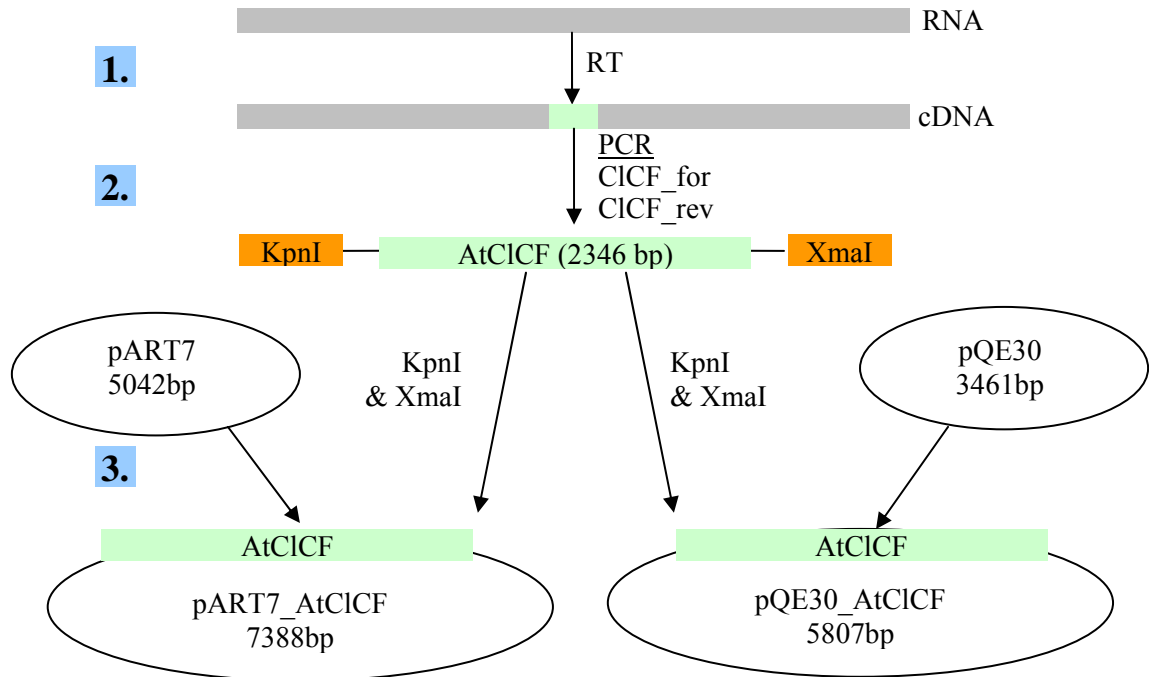
pART7\_CICE (pART7seq\_for2 and pART7seq\_rev1 primer)

	KpnI
	pART7
	GAACGCTCGAGGATTCGGTACC
ATGGCAGCCACGCTTCCACTCTGTGCTGCCCTCCGATCTCCCGTCTCTTCCCGGAGATTC	60
GCTCCAATTCACAAAACCGACGTTCCCTTTTCAGTTCAATGTCGTCCTTTCACCGTTTTTC	120
GGTTCGCTCGCTATTGGCGGTAGAATTTTCCCGCGTTTACC GGCGGCGAAGCAGGAGACT	180
GATCAGGATGAGGTTGGATTTGATCAGCAGCCGCTCAGGAGCTTGCGATAGCGTCGGT	240
TGTTTGGTTGGTGTCTCACTGGAGTTAGTGTGGTTCTATTCAACAACCTGTGTTCACTTG	300
CTTCGAGACTTTTCTGGGATGGGATTCCTGATCGTGGAGCTTCGTGGCTTAGAGAGGCA	360
CCGATCGGTTCCAATTGGTTGCGTGTATCCTTGTTCGGACTATCGGCGGTTTGGTGGTG	420
AGCATCCTCAATCAGCTTCGAGAATCTGCTGGAAAATCTACTGGAGATTCATTCATAGT	480
CTCGATCGCGTAAAGGCAGTGTTCGCTCCTTCCCTTAAGACTGTTGCCGCATGTGTGACG	540
CTTGGGACTGGAAATTCGCTGGGGCCGGAAGGTCCAAGTGTGAAATGGAGCGTCAAT	600
GCTAAAAGGTGTGAATTCCTGTTCAATAAAAAGTCCCTCAGACTGGCTTCTCACTTCTGCC	660
GCTGGCTCAGCTGCTGGCATTTCCTCTGGGTTCAATGCAGCTGTGGCTGGATGCTTCTTT	720
GCAGTTGAATCCGTTTTGTGGCCTTCTTCATCAACTGATTCATCAACTTCAC TTCCAAC	780
ACA ACTTCTATGGTTATTCTTAGTGCTGTACTGCTTCTGTGGTTTTCCGAAATCGGTCTC	840
GGCTCTGAACCTGCGTTTAAGGTTCTGACTATGACTTCCGCTCTCCTGGGAACTTCCA	900
CTCTATCTTTATTGGGCGCTCTGTGTGGCTTGGTCTCGTTGGCATATCTCGATGTACA	960
TCATCCATGACATCTGCTGTGACAGTCTTAACAAGGATGCTGGGATACCAAAGGCTGTA	1020
TTTCTGTAATGGGTGGATTAAGTGTGGTATCATAGCTTTGGTATACCC TGAAGTATTA	1080
TACTGGGGTTTTTCAGAATGTGGATATTTTGTGGAGAAACGTCATTTGTGAAGGGTCTT	1140
TCAGCTGATCTTTTGTTCAGCTGGTAGCGGTCAAGATAGCTGCAACCGCATGGTGTCCG	1200
GCTTCTGGACTTGTTCGGTGGATACTATGCTCCTTCTCTCTTTATTTGGCGGGGCAGCAGGA	1260
ATGGCCTATGGAAAGTTTATTGGACTTGTCTTTGGCTCAGAACCCTGATTTCAATCTCTCT	1320
ATCTTGGAAAGTGGCATCTCCACAAGCTTATGGTCTGGTTGGAATGGCTGCTACACTTGC	1380
GGGGTTTTGTCAAGTTCTCTTACAGCAGTACTACTGCTATTTGAACTTACACAGGATTAT	1440
CGTATAGTGTACCTCTACTGGGAGCTGTAGGCATGTCTTCATGGATTACATCTGGACAA	1500

```

TCAAAGAGACAAGAAACTAGAGAAACAAAAGAAACTAGGAAAAGAAAGAGCCAAGAAGCT 1560
GTACAGTCTCTGACGTCATCTGATGATGAATCATCAACGAATAACCTTTGTGAAGTTGAA 1620
AGTTCTCTTTGCCTTGATGATTCTCTCAACCAATCTGAGGAGCTGCCGAAGAGTATTTTT 1680
GTTTCAGAAGCCATGCGAACAAGATTTGCGACAGTTATGATGAGCACTTCTTTGGAAGAG 1740
GCATTAACCTCGTATGCTGATAGAGAAACAATCCTGCGCCTTGATTGTTGATCCTGACAAT 1800
ATCTTTCTCGGTATACTTACACTTTCAGACATTCAGGAATTCAGCAAAGCAAGAAAAAGAA 1860
GGAAATAATAGACCCAAGGATATTTTTTGTAAATGACATCTGTTTCGAGGAGTGGAGGAAAA 1920
TGTAAGGTGCCATGGACTGTTACACCTGATATGGATCTTCTCGCTGCCCAAACAATCATG 1980
AACAAGCATGAACTTTCTCATGTTGCAGTCGTTTCAGGCAGCATTGATGCTCCCAGAATA 2040
CACCTGTTGGGGTCCTGGATAGAGAATGTATCACTCTAACACGCAGGGCTCTAGCAACC 2100
AGAATGTACCTCCTAAATTCGCTGTATCTGTAA 2133
CCCGGGTTCGAAATCGATAAGCTTGGATCCTCTAGAGTCC pART7
XmaI

```

**Supplemental material 13: Chloride channel AtClC-F**Cloning strategy:

- 1) Reverse transcription of RNA isolated from *Arabidopsis thaliana* (cDNA)
- 2) Amplification of the whole 2346 bp long fragment by PCR run with *Arabidopsis thaliana* cDNA. The fragment was extended with KpnI restriction site at the 5'-end and XmaI restriction site at the 3'-end (see **Suppl\_material 6**).
- 3) Cloning into a pART7 vector and a pQE30 vector with help of KpnI and XmaI

Sequencing results:

pART7\_ClC-F (pART7seq\_for2 primer)

	TTTTGGAGAGGAACGCTCGAGGATTCGGTACC	KpnI
		pART7
ATGTCATCGGGAGGAGCCGGAGAGTATAACGAAGACAGACATCTGTTACGATCCACCGAC		60
GGAGATGAAGTCGGCATTTGGCGGAGGAGGGTGATCTAGATGTTGAATCTCAGTCTCCG		120
GCTATCAGAAGTGGAGCTGGAGGAGTTAGGGATCTGTTCAAGCATATAGATCGGAGATTT		180
TCTCTTTCCGGTCGTCGTTTAAAGTTTTAAACGGATGGAGAATATCAGAGTCGATAGAGAG		240
CGCCATAATCCTTCTTCTTCTTCAGCGTTTTTCGACTGCTGGAGAAGAAGATGGTGGTGGT		300
ATCAGTAATTTACATAGCGTTGATGATCGAAATGACGAGTACGGGTTTGATGAAGAAGTT		360
CTCGGAGATAGTGCTCCACCTGAGTGGGCTCTGCTTCTCATTGGCTGTCTTATTGGTGT		420
GCCGCTGGAATTTGTGTCGCCGGCTTCAATAAAGGGTTTCATGTCATTCATGAGTGGGCA		480
TGGGCTGGTACTCCCAACGAAGGTGCTGCAATGGCTTCGTCCTACAGAGACTAGCTGATACT		540
TGGCATCGGATTTCTTAATTCGGTCACTGGAGGTGTTATAGTAGGAATGATGCACGGT		600
TTGCTTGAGATCTTAGACCAAATAAGGCAATCTAATTTCTTCTCAAAGACAAGGACTAGAT		660
TTTCTTGCTGGTATTTATCCAGTGATAAAGGCCATCCAAGCTGCTGTGACCCCTTGGTACA		720
GGATGTTCACTGGGTCCTGAGGGACCTAGCGTTGACATTTGAAAATCATGTGCCAACGGT		780
TTTGCACTCATGATGGAAAACAACAGAGAAAGAATAGCTCTCACCGCAGCTGGTGGC		840
GCTTCTGGGATTCATCTGGTTTCAATGCAGCAGTGGCGGGTTGTTTCTTTGCTATTGAA		900
ACTGTTTTAAGACCTTACGTGCCGAGAATCGCCTCCATTTACCACCTGCAATGATAATA		960
TTGGCCCTCTGTTATATCATCGACTGTGTCAAATGCTCTGCTTGGGACTCAATCAGCTTT		1020
CACAGTTCCCTCATACTGACTGAAGTCTGCTGCAGAGCTCCTCTGTACTGATACTAGGCAT		1080
GCTTTCGGGTGCTGTCAGTGTGTTTTTTCTCGGCTCGTACAGTGTCT		1128

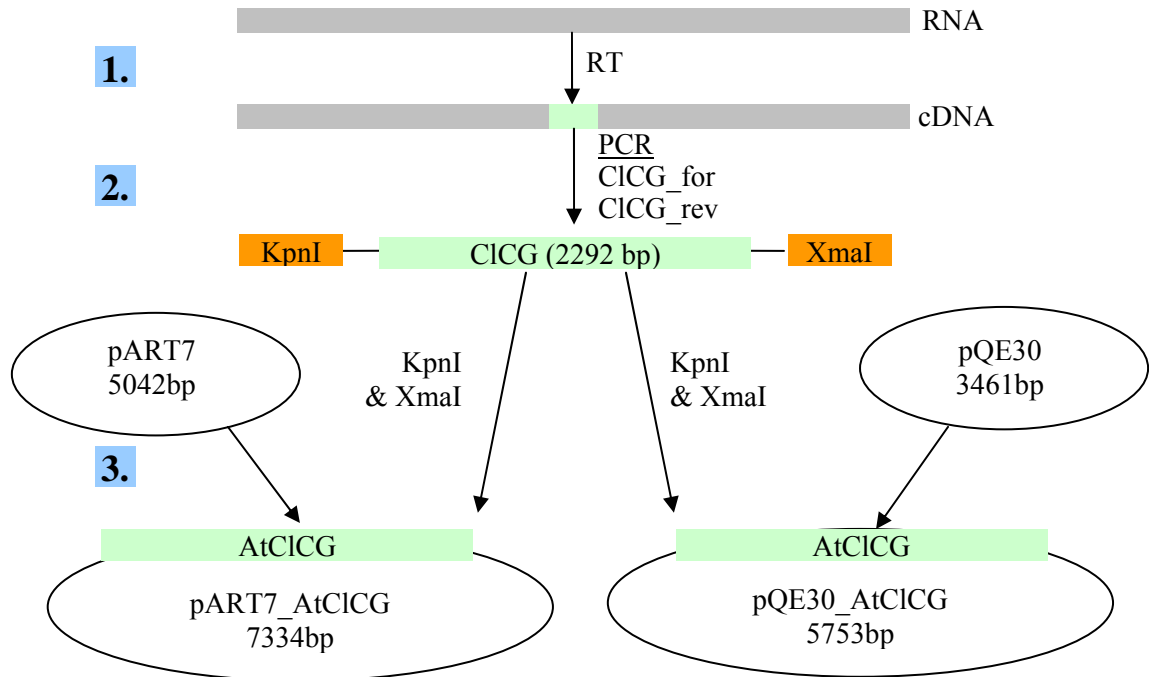
pART7\_ClCF (pART7seq\_rev1 primer)

```

AGCTCAG 1326
TTAGCCGCTGCAAAAGTGTGGCTACAGCTCTTGCAAAGGCTCTGGGCTGTAGGTGGTCTA 1386
TATGCACCAAGTTTGGATGATTGGTGCTGCCGTTGGTGCTGTATTTGGGGGTTCGGCTGCT 1446
GAGATTATTAACAGAGCTATTCCTGGTAATGCTGCTGTTGCTCAACCACAAGCTTATGCT 1506
CTGGTTGGAATGGCAGCGACACTAGCTTCAATGTGCTCTGTTCCCTTAACATCAGTATTA 1566
CTGCTGTTTCGAGCTAACGAAAGATTATAGAATTTTGCTTCCCCTCATGGGAGCAGTTGGT 1626
TTAGCAATATGGGTTCCCTCTGTGGCAAACCAAGGCAAAGAGAGTGATTTCATCTGAAGGT 1686
CGTAGCACAGGAAGAGGATACTCTTCTCTTTCACCTTCCGAACGTAAAACCGAAGGAGTC 1746
TGGAGACATACGGATAATGCTGACTCCCTTGAGCTTACCGTCATAGAGAACCCTGACCAT 1806
AATTCCTTTTTGGATGAAGAGACTATTCTGGAAGACTTAAAAGTTATGCGGGTTATGTCA 1866
AAGAACTATGTGAAAGTTTCTTCAGGAACAACCTAAGAGAAGCAAGAAACATCCTTAAA 1926
GAGAGCCACCAAAACTGCATTATGGTGGTTCGATGACGATGATTTTCTAGCTGGAATCCTA 1986
ACACACGGTGACATAAGAAGATACTTGTCCAATAACGCCTCTACAATCTTAGATGAGAAT 2046
ACATGTCCGGTTTCTTCTGTATGTACTAAGAAAATAAGCTATCGAGGCCAAGAACGCGGT 2106
TTACTTACTTGTATCCAGACGCCACAGTTGGTGTAGCCAAGGAGTTGATGGAGGCTAGA 2166
GGTGTAAAGCAATTACCTGTTGTAAAACGAGGTGAAGTAATTCACAAAGGGAAACGAAGG 2226
AAACTGCTTGGCCTCCTTACATTACGATTCCATTTGGACTTTTCTCAGAGATGAAATGAGT 2286
CGTAGGAGATCGATCAACGACCGGAGAAAAGACAAAGAGGTTGGTACAAATGGGCATTGA 2346
CCCGGTTTCGAAATCGATAAGCTTGGATCCTCTAGAGTCCTGCTAGT pART7
XmaI

```



**Supplemental material 14: Chloride channel AtCIC-G**Cloning strategy:

- 1) Reverse transcription of RNA isolated from *Arabidopsis thaliana* (cDNA)
- 2) Amplification of the whole 2292 bp long fragment by PCR run with *Arabidopsis thaliana* cDNA. The fragment was extended with KpnI restriction site at the 5'-end and XmaI restriction site at the 3'-end (see **Suppl\_material 6**).
- 3) Cloning into a pART7 vector and a pQE30 vector with help of KpnI and XmaI

Sequencing results:

pART7\_CICG (pART7seq\_for2 primer)

	KpnI
TTGGAGAGGAACGCTCGAGGATTC	GGTACC pART7
ATGCCAAACTCAACGACGGAGGACTCCGTCGCCGTTCCACTACTCCCCTCCCTCCGCCGC	60
GCTACTAACTCTACTTCTCAAGTAGCAATCGTCCGTCGCAACGCTCTGTCCAATAGAAAGT	120
CTCGATTACGAAATCGCGGAGAATGATTTCTTCAAGCAGGATTTGGAGAGGTCGTAGTAAG	180
GTAGAGATTTTCCAATACGTGTTTATGAAGTGGCTGCTTTTGTGTTTTGTATCGGCATTTAT	240
GTTAGTCTCATCGGATTCGCTAATAACCTCGCCGTTGAGAATCTCGCCGGTGTAAAGTTT	300
GTTGTTACTTCTAACATGATGATAGCCGGAAGGTTTGCATATGGGTTTTGTTGTTTTCTCT	360
GTTACAAATTTGATTTACTCTCTTTGCGTCGGTGATTACCGCTTTTGTGCTCCTGCT	420
GCGGCAGGTTCCGGTATACCGGAAGTTAAGGCTTATTTGAATGGTGTGATGCTCCAGAG	480
ATATTCTCACTTCGCACTTTGATCATTAAGATCATTTGGGAACATATCTGCAGTATCAGCG	540
TCTCTTCTCATTGGAAAGGCAGGGCTATGGTGCATACTGGTGCCTTGTGTTGCATCTATA	600
CTTGGTCAGGGTGGCTCCAAAAGATATAGATTGACCTGGAGATGGCTCAGATTTTTTCAA	660
AATGATAGAGACAGAAGAGATCTTGTAACTTGTGGGGCAGCTGCTGGTATCGCTGCTTCG	720
TTTCGTGCTCCGGTTGGTGGTGTCTTGTGCGCTTGAGGAAATGTCATCTTGGAGTGCA	780
CTTTTATGGAGAATCTTCTTTTCGACAGCTGTTGTGGCAATAGTTCTCAGAGCTCTAATC	840
GATGTGTGTTAAGTGGAAAAGTGTGGGTTATTTGGTAAAGGAGGCTTAATAATGTTTGAT	900
GTCTACTCAGAAAATGCGTCATATCATTTAGGGGATGTACTTCCGTGTTCTTCTTTGGG	960
GTTGTTGGTGGTATTTTAGGAAGCTTATACAACCTTCTTACTGGATAAGGTTCTGCGAGCT	1020
TACAACTACATATATGAGAAAAGGGTTACTTTGGAAAATC	1059

## pART7\_ClCG (pART7seq\_rev1 primer)

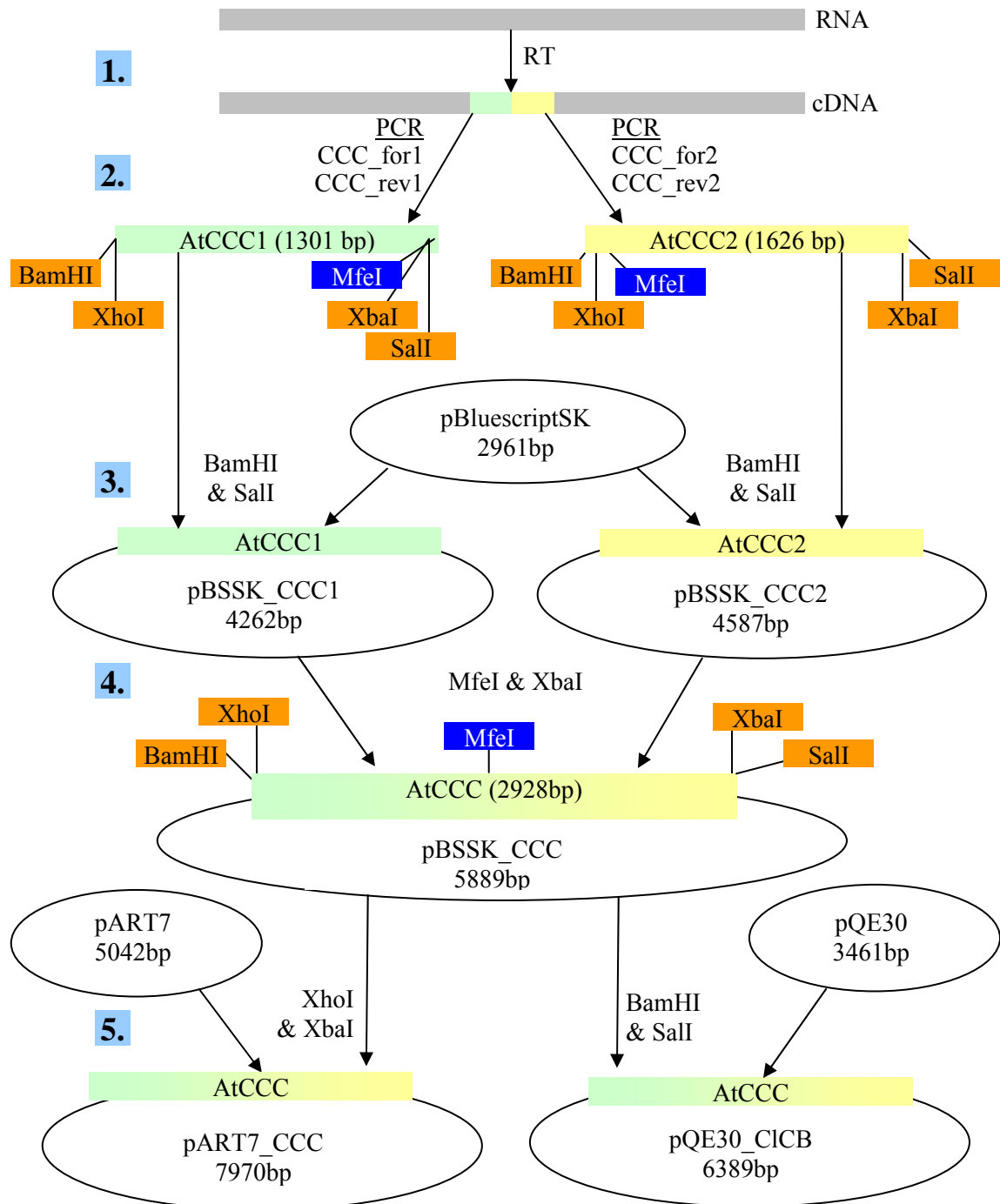
```

          TCTGGAAACTTTAAGAAATACCAATGCCCTCCTGGT 1212
CACTACAATGATCTAGCTAGCCTTATTTTCAACACAAATGATGATGCCATCAAAAACCTT 1272
TTCAGCAAAAACACTGACTTCGAGTTTCATTATTTTTCGGTTCTCGTATTTTTTGTCCACC 1332
TGCTTCTTCCCTCAGTATCTTTAGCTATGGCATTGTTGCTCCAGCAGGGCTCTTTGTGCCA 1392
GTTATTGTAACAGGAGCATCGTATGGACGGTTTGTAGGGATGCTGCTTGGTTCAAACCTCA 1452
AATCTTAATCATGGTCTGTTTGTGCTGCTCGGTGCTGCATCCTTTCTTGGCGGAACAATG 1512
AGGATGACAGTTTCCACTTGTGTTATTCTCCTTGAGCTGACCAACAATCTGCTGCTACTA 1572
CCTATGATGATGGTGGTCCTTCTGATTTCAAAAACAGTTGCTGATGGTTTCAATGCTAAC 1632
ATCTACAACCTCATCATGAAGTTAAAAGGATTTCCCTACCTCTACAGCCATGCAGAGCCT 1692
TACATGAGGCAGCTTCTAGTTGGTGTAGTGTAGTACCCGGCCCACTTCAAGTCTTCAATGGC 1752
ATTGAGAAAGTCGAGACTATTGTACACGTTCTCAAAACGACCAATCACAATGGCTTCCCC 1812
GTGGTTGATGGGCCACCACTAGCTGCAGCTCCTGTTCTACACGGTCTAATCCTCCGGGCT 1872
CATATTCTGACTCTGTTAAAGAAACGAGTATTCATGCCTAGTCCAGTAGCTTGTGACTCC 1932
AATACCCTTTCCAATTCAAGGCAGAGGAGTTTGCTAAGAAGGGTTCTGGGAGGAGTGAT 1992
AAGATAGAAGATGTGGAATTAAGCGAGGAAGAATGAATATGTATTTGGATTTGCACCCA 2052
TTCTCTAATGCCTCTCCGTACACTGTTGTGGAGACAATGTCACTTGCAAAGGCCCTTATT 2112
CTCTTCCGTGAGGTTGGCATAAGGCACCTTACTGGTTATACCAAAAACCTCCAATAGACCT 2172
CCAGTGGTAGGTATATTGACACGGCATGACTTCATGCCGGAACATATACTAGGCCTGCAT 2232
CCCTCCGTTTCTCGGAGCAAGTGGAAGGCTTCGGATTTCGGCTGCCTTTCTTCTCATGA 2292
CCCGGGTTCGAAATCGATAAGCTTGGATCCTCTAGAGTCCTGCTAG pART7
XmaI

```

## Supplemental material 15: Cation-chloride-cotransporter AtCCC

## Cloning strategy:



- 1) Reverse transcription of RNA isolated from *Arabidopsis thaliana* (cDNA)
- 2) Amplification of two fragments by PCR run with *Arabidopsis thaliana* cDNA:
  - #1 to #1301 (from ATG to MfeI-restriction site) – AtCCC1
  - #1302 to #2928 (from MfeI-restriction site to STOP) – AtCCC2
 Both fragments were extended with BamHI and XhoI restriction sites at the 5'-end and XbaI and Sall restriction sites at the 3'-end (**Suppl. material 6**).
- 3) Cloning into a pBluescript II SK+ vector with help of BamHI and Sall
- 4) Merging of both fragments in a pBluescript II KS+ vector with help of MfeI and XbaI
- 5) Subcloning into a pART7 vector (XhoI and XbaI) and into a pQE30 vector (BamHI and Sall)

**Sequencing results:****pBS\_CCC1 (T3 and T7 primer)**

	BamHI	XhoI	
	ACGCGGTGGCGGCCGCTCTAGAACTAGT	GGATCCGCGCTCGAG	pBSK
ATGGATAGCGGCGACATTGAAGAAGCCGGCGGGAATGGCGAAGAGGAATTC			60
CCACGTCTCGGCGGTAGCAAATACAGACCGGTGGTGGCGCACGATAGAGCGGTTGT			120
ATGTCTCCATCGATCCTGGATCTTCTCTTCCACCCTCAAGAACATAAAAAGTAG			180
CCAGGAGACGTGGGCGCTGGTGTAAAGGGACCAGAAGATGGAGTCAATGGCCATC			240
GAATCCAAGCTGGAATTTATTTGGTTTTCGACTCTCTTGTGAATATTTCTTGGCT			300
ATGACGGGGGAGCAAATTCAGGCACCATCTAGCCCTAGAGATGGGGAAAGATATCT			360
ACGCAAGGGCACCCAAAGCCTCCTGCTCTCAAGATGGGTACAATGATGGGAGTTT			420
CCCTGCTTGCAAAAACATATTAGGAATTATATATATATATCCGTTTCACATGGAT			480
ATGGCTGGTATCGGACAAGGCCCTAGTATTGGTATTTCTTTGTGGCTTATGTACAT			540
ACGACAATATCTTTGAGTGCTATTGCAACAAATGGTGAATGAAGGGTGGAGGACC			600
TACCTCATTGGTCGCGCTCTTGGTCCGGAAGTTGGGATTAGCATAGGTTTATGCT			660
CTTGGAATGCAGTTGCTGGAGCTCTGTATGTTTTGGGTGCTGTGGAGACTTTTCT			720
GCATTTCCCTGCTGCTGGGATTTTTAGAGAACTATCACAAAGGTTAACGGAAACAG			780
TCCGAATCAATACAAAGCCGAACCTCACATGACTTGCAGGTTTATGGAATGTTGT			840
ATCCTTCTTTGCTTCATTGTGTTTTGGTGGCGTGAAGATGATCAATCGGGTTCAC			900
TTCTCTGTAACCCGTTTTGCTCTCTATCTTCTGCATATTCATCGGGATATTTTT			960
ACAGATGATCCTGACAATGGAATTACGGGCTTGCCTTAAAAAGCTTTAAAGACA			1020
GGTTCTGCTTATCAAATGACAAATGATGCGGGAATTCCTGATCCAACCTGGAGGG			1080
TGGAGTTTCAATGAGCTGGTGGGTCTATTTTTTCTGCTGTAACAGGAATTTATG			1140
TCAAATCGATCAGCTTCACTTAAAGATACAAAAATCAATTCCTGTTGGTACAT			1200
GCCACTGTGACCACAACCTCACTATATTTGATTTCTGTGTTGTTTTTTGGAGCT			1260
ATCCCGTGACAAACTTTTGACTGATAGGCTACTTACTGCTACAATTGCTTGGCCT			1320
<b>TCTAGAGTCGAC</b> CTCGAGGGGGGGCC			pBSK
XbaI	SalI		

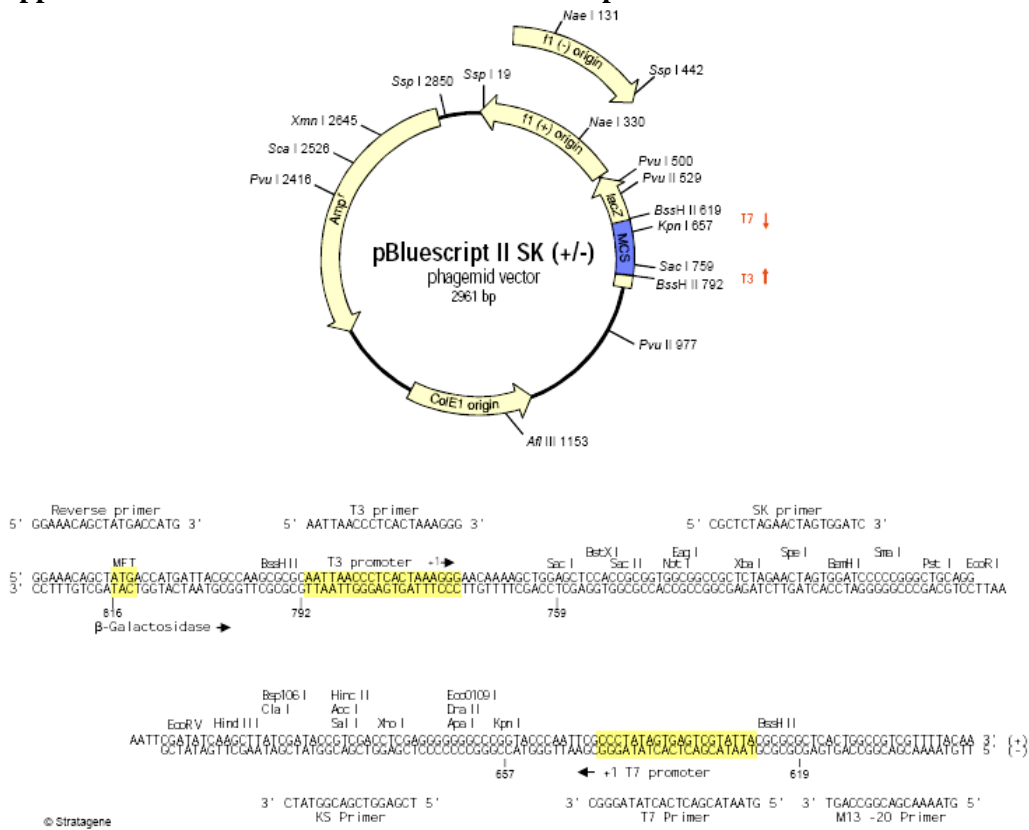
**pBS\_CCC2 (T3 primer)**

	BamHI	XhoI	
	TGGCGGCCGCTCTAGAACTAGT	GGATCCGCGCTCGAG	pBSK
CAATTGCTTGGCCTTTCCCTGCCATTGTTTACGCTTGGAAATCATCCTTTCAACCT			60
TTGCTCTCCAGAGTTTGACAGGGGCACCAAGGTTACTTGGCCGCTATAGCAAATGAT			120
TTCTCCCCATCTGAACTATTTCAAAGTTGCAGATACTAGTGAACCTCATATAGCGAC			180
TCTTACAGCATTATCTGCATTGGATGTGTTGTTATCGGAAATCTGGATCTTATCAC			240
CTACTGTGACCATGTTTTATCTTTTGTGCTATTTCGGGAGTAAACTTGTCTTGT			300
TCGATCTTCTTGATGCTCCAAGTTGGCGTCCACGGTGGAAATATCATCATTGGAGC			360
CCTTTGTTGGAGCCTCACTTTGCATAGGTATGAAATTTTCAAATACTCACGGAGAA			420
TCTTTCCAGTCTACCTATGTAGTCCATTTCTTATAGAAATTTCTGATTTGAACTAC			480
GGCTTCTTATCTACCTGAATCCTGAGATGTCTTATTACAAAGCCTTGTGAGTTTT			540
<b>ATTATATTTTTTCTATTCTTGCAGTGCATGTTCTTTGATATCTTGGTCATTCAC</b>			600
<b>GTGCCATTGCACTTGCAGTCTTATATACAAATACGTTGGCCTAAAAGGAAAGGCTGGG</b>			660
<b>GACTGGGGGGATGGTTTCAAGAGTGCATATTTTTCAGTTGGCCCTTCGTAGTCTCAGG</b>			720
<b>CTCGGAGGTATGAACCTGGCATATCTAAGTCTTGTTCATGTAACCCGTTGTCTATA</b>			780
<b>ACTAAATCTCTAAGTTCCATTATGCAGAACCTGCCATATCTAATTTGGTTTCAAT</b>			840
<b>GGTCCATGTATCTAAAGCTAATCTCATGTACTGTCAATTTCTTCAAATTCAGCGAAT</b>			900
GTGCACCCAA			

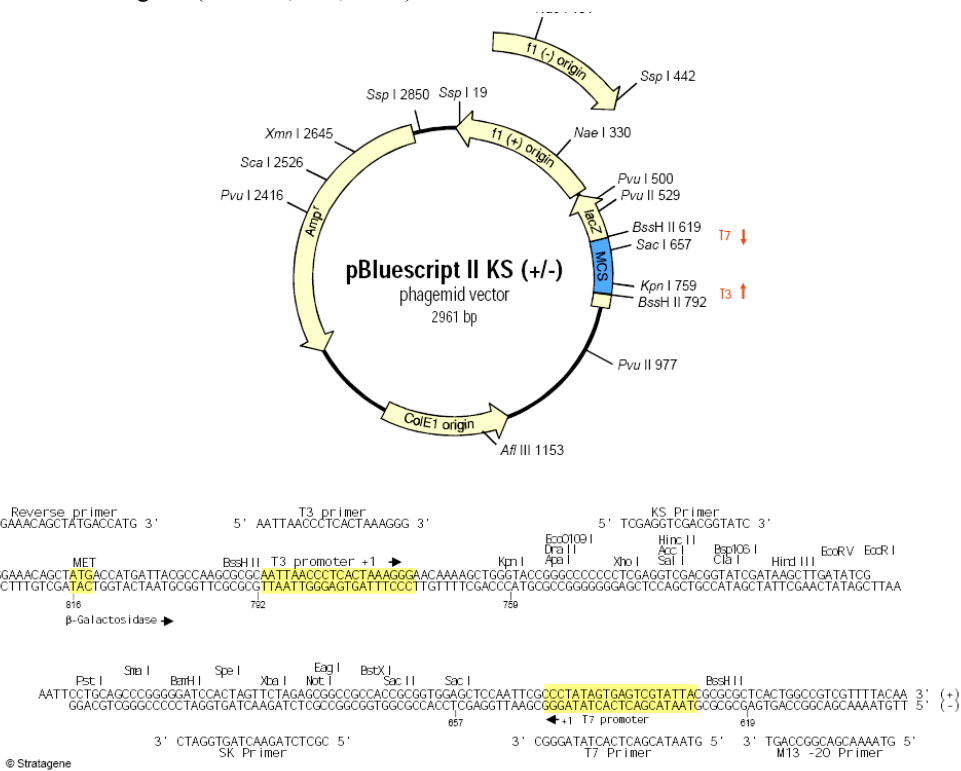
**pBS\_CCC2 (T7 primer)**

TGTGCTGAAGAAGCAAAGGAAGCTTGCAACAATTAGCCACCTACATTGAGTATAAGCGT	1131
TGTGAAGGTGTAGCTGAAATCGTTGTAGCCCCAAACATGACTGAAGGGTCCGTGGGATC	1191
ATCCAGACGATGGGACTCGGAAACCTCAAACCAACATTTGTGGTAATGAGGTACCCGTGAG	1251
ATCTGGCGCAGAGAAAATCTAACAGAGATTTCCATCCACATTTGTTGGGATAATCAATGAC	1311
TGCATAACAGCAAACAAAGCAGTTGTCATCATCAAAGGGTTAGACGAGTGGCCAAACGAG	1371
TACCAAAGACAGTATGGAACAATCGACTTGTACTGGATTGTGAGAGATGGTGGTCTCATG	1431
CTTCTTCTCTCACAGCTTCTTCTGACAAAAGAAAGCTTCGAAAGCTGCAAAAATCCAATC	1491
TTCTGCATAGCTGAAGAGGATTCAGACGCGGAAGCACTCAAAGCTGACGTGAAGAAGTTC	1551
CTCTACGATCTCAGAATGCATGCGAAGTAATCGTGGTCACAATGAAATCATGGGACATA	1611
AGATCCGAAGGAAACAGCCAAGAAGATTCATTTGGAAGCTTTTGTATGCTGCACAGAGACGA	1671
ATCTCAGATTACTTTGGGAGAGATCAAGAGACAAGGTTTCAATCCTTTGTTGGCTAATGGG	1731
AAACCGATGGTGGTGAATGAGCAACAAGTGGAGAAGTTCTTTACACAATGCTGAAACTG	1791
AACTCAACCATCTGAGTTATTCGAGAATGGCCGAGTGGTTCTGGTTAGTCTCCCCCCA	1851
CCTCCGTTGAATCACCCGGCGTATTTCTACATGGAATATATGGATTTGCTGGTGGAGAAT	1911
GTGCCAAGGATGTTGATCGTAAGAGGGTATCACAGAGACGTTGTTACTTTGTTTACATAG	1971
<b>TCTAGAGTCGAC</b> CTCGAGGGGGGGC	pBSK
XbaI	SalI

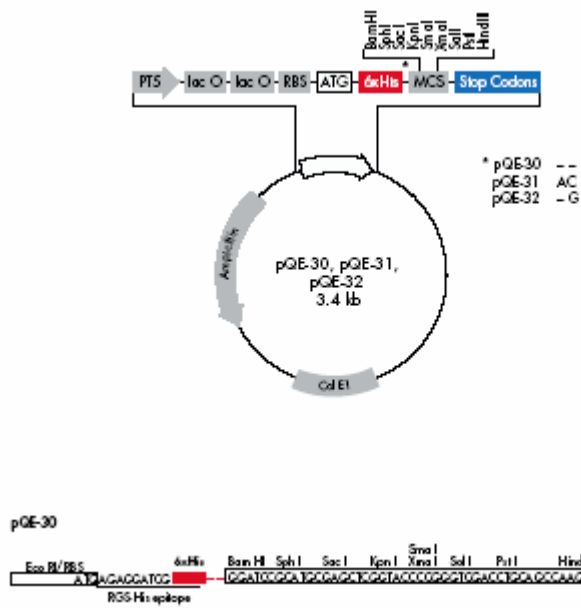
**Supplemental material 16: Destination vector maps**



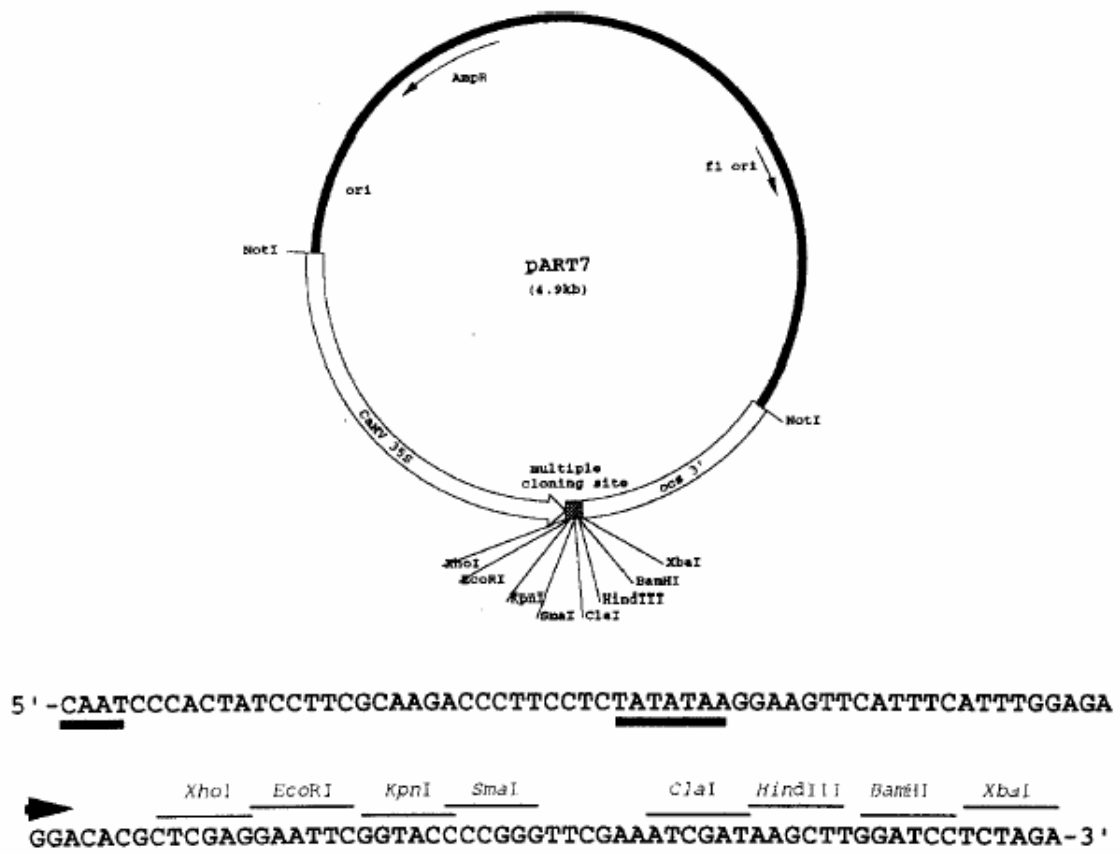
**Figure Suppl\_2: pBluescript II SK(+/-) vector**  
Figure from Stratagene (La Jolla, CA, USA).



**Figure Suppl\_3: pBluescript II KS(+/-) vector**  
Figure from Stratagene (La Jolla, CA, USA).



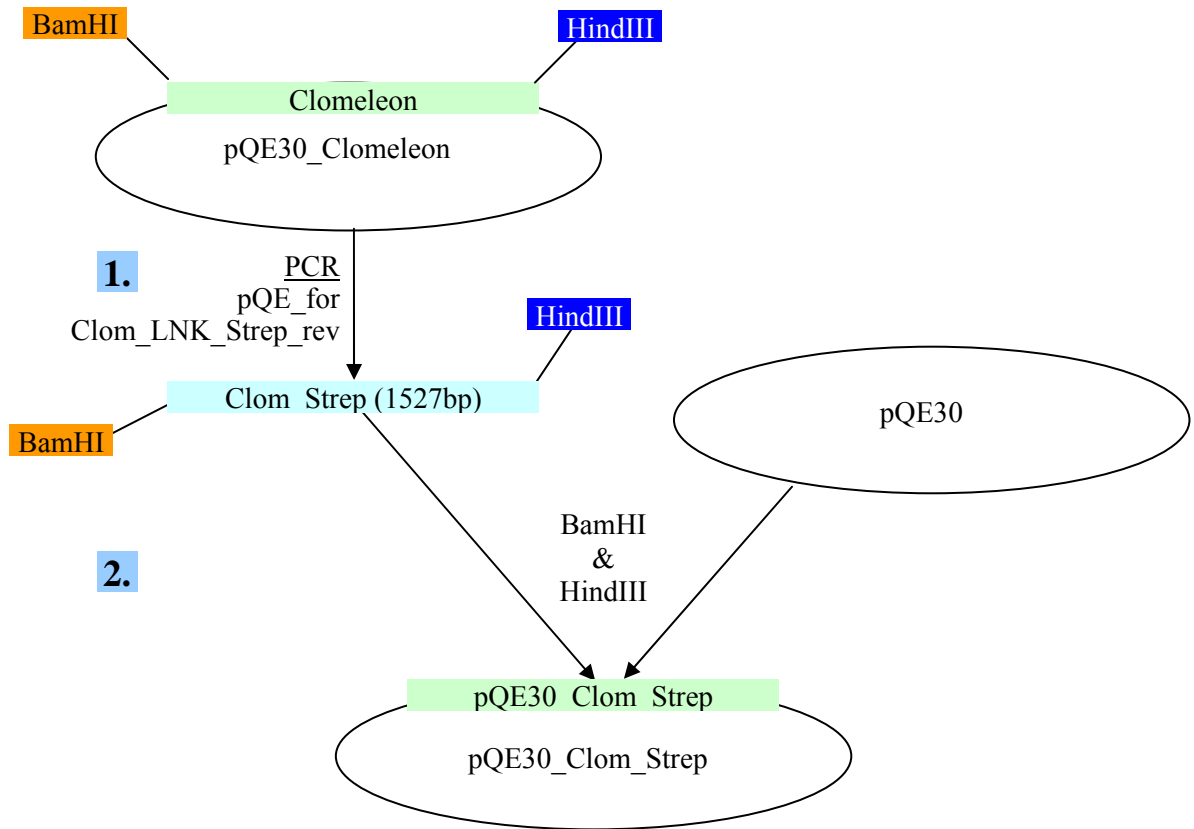
**Figure Suppl\_4: pQE30 vector**  
Figure from Qiagen (Hilden, DE).



**Figure Suppl\_5: pART7 vector**  
Figure from Gleave, 1992.

**Supplemental material 17: Cloning strategy for Clom\_Strep**

Cloning strategy:



- 1) Amplification of a 1527 bp long fragment by PCR run with pQE30\_Clom as a template. The fragment was extended with HindIII restriction site (see **Suppl\_material 6**) at the 3'-end.
- 2) Cloning back into a pQE30 vector with help of BamHI and HindIII

Sequencing results:

pQE30:Clom\_Strep (with pQerev primer):

```

                                CLOMELEON LINKERLINKERLINKER
                                CTCGGCATGGACGAGCTGTACAAG GGTTCGGTCTGGTGGT
1482 -----+-----+-----+-----
                                GAGCCGTACCTGCTCGACATGTTC CCAAGACCAAGACCACCA
                                L G M D E L Y K GlySerGlySerGlyGly
    
```

```

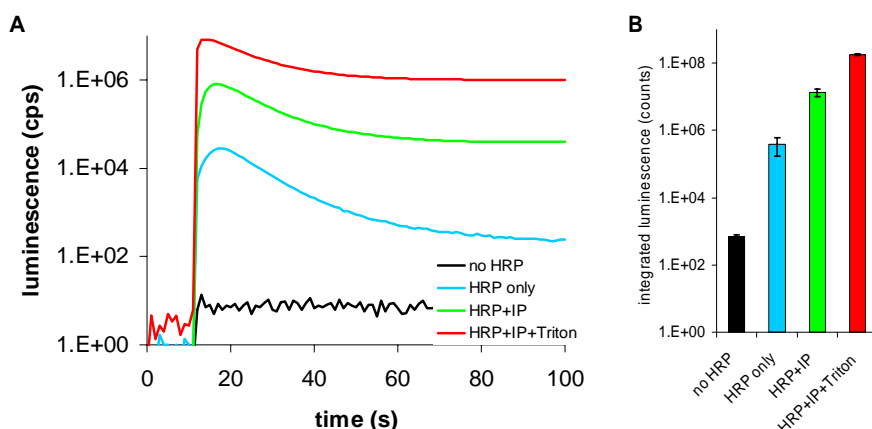
STREP-TAG                      HindIII
TGGAGCCACCCGCGAGTTCGAG AAGCTT
+-----+-----+-----+-----
ACCTCGGTGGGCGTCAAGCTC TCGAA
W S H P Q F E K L.
    
```

## Supplemental material 18: Blockers and Inhibitors

Group	Chemical	Company Order Nr.	MW (g/mol)	Solubility	Functioning
Anion channel blocker	<b>SITS</b> DiSodium-acetamido- isothiocyanostilbene	Fluka #00309	498.46	0.1 M KHCO <sub>3</sub> pH 8	Cl <sup>-</sup> channel blocker
	<b>DIDS</b> Diisothiocyanostilbene	Sigma #D3514	498.48	0.1 M KHCO <sub>3</sub> pH 8	Cl <sup>-</sup> channel blocker
	<b>IAA-94</b> Indanyloxyacetic acid	Sigma #I117	357.23	DMSO	Cl <sup>-</sup> channel blocker
	<b>NPPB</b> Nitro-phenylpropylamino-benzoic acid	Sigma #N4779	300.31	DMSO	potent chloride channel blocker
	<b>ACA9</b> Anthracene-9-carboxylic acid	Aldrich #A89405	222.24	Ethanol	Anion channel inhibitor
	<b>Niflumic acid</b>	Sigma #N0630	282.22	DMSO	Anion channel inhibitor
	<b>Flufenamic acid-</b> <i>N</i> -(3-[Trifluoromethyl] phenyl)anthranilic acid	Sigma #F9005	281.23	DMSO	Anion channel inhibitor
Loop diuretics	<b>Bumetanide</b>	Sigma #B3023	364.42	DMSO	Na <sup>+</sup> K <sup>+</sup> Cl <sup>-</sup> -cotransporter inhibitors
	<b>Furosemide</b> 1 tablet/40mg	Sigma #F4381	330.745	Water (0.006 mg/ml)	
	<b>Torasemide</b> 1 tablet /10mg	Sigma #T3202	348.421	Water	
Thiazide analoga	<b>Hydrochlorothiazide</b>	Sigma #H4759	297.73	1 M KOH	Na <sup>+</sup> Cl <sup>-</sup> -cotransporter inhibitors
	<b>Tensoflux</b> 1 tablet/ 2.5 mg bendroflumethiazide and 5 mg amiloride hydrochloride-2-hydrate	Hennig Arzneimittel	421.21 229.65	DMSO	
	<b>Xipamid</b> 1 tablet/40mg	Aquaphor®,Lilly GmbH	354.808	Ethanol	
	<b>R-(+)-DIOA</b>	Sigma #D129	399.31	Ethanol	K <sup>+</sup> Cl <sup>-</sup> cotransporter inhibitor

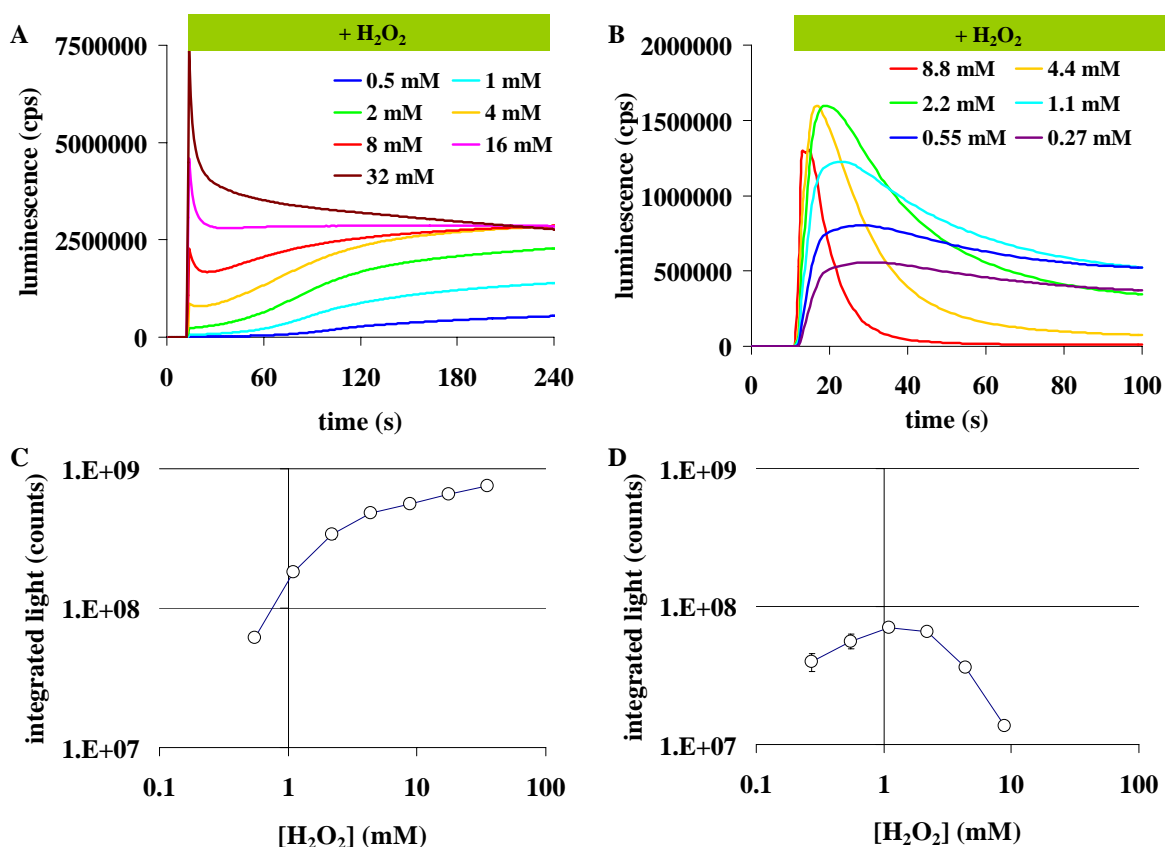


## Supplemental material 19: TAC Assay



**Figure Suppl\_6: Enhanced versus not enhanced HRP-catalysed luminol reaction**

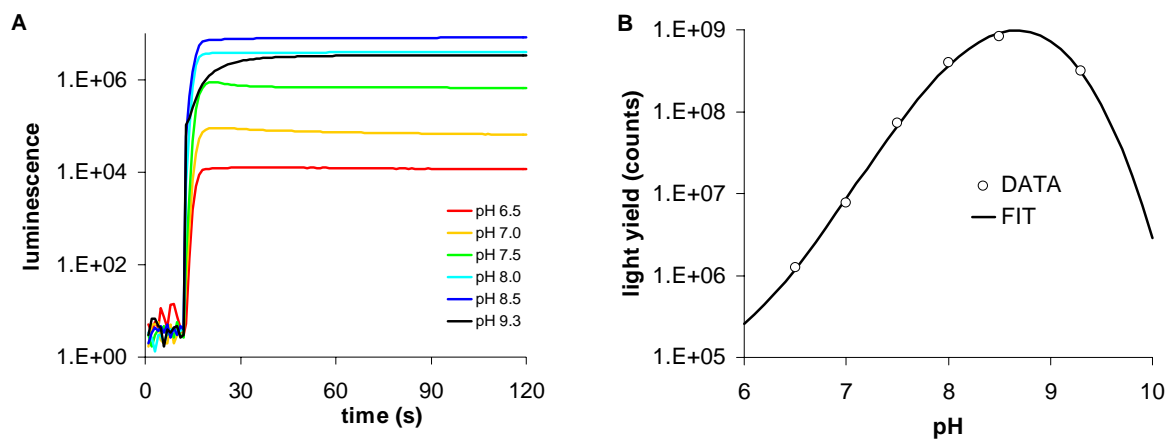
The light yield from HRP-catalysed reactions depends on the presence of enhancers (here: 4-iodophenol = IP) and a surfactant (here: Triton-X-100). **A:** Light emission from different luminol reaction mixtures (0.5 ml) was triggered at  $t = 12$  s by injecting 0.5 ml of 1.1 mM  $H_2O_2$  and recorded for 100 s. **B:** The light yield (integrated for 100 s) displayed for four different luminol reaction mixtures. Averages of  $n = 3$ . Error bars represent standard deviation. Figure from Saleh & Plieth (2009).



**Figure Suppl\_7: In contrast to HRP, luminol converting peroxidases from *Lepidium sativum* are not inactivated by  $H_2O_2$**

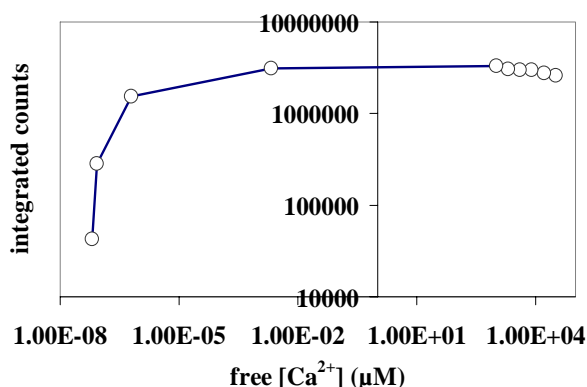
**A:** Light output of reactions during the first 4 min. The reactions were triggered by adding 0.5 ml  $H_2O_2$  (concentrations given in the legend) to 1 ml of peroxidases/luminol assay mix at  $t = 12$  s. The curves show that light yield increases with increasing  $H_2O_2$  concentration. *Lepidium* peroxidases appear to withstand even high  $H_2O_2$  concentrations when compared with HRP (**B**). **C:** Plot of integrated light yield (= sum of counts during the first 240 sec of reactions shown in A) against the concentration of added  $H_2O_2$  in log-log-scale. Traces given in A are averages of  $n = 3$  with StDv of less than 15% of peak value. Averages in C are calculated from data shown in A. Error bars are equal or below symbol size. Figures in A and C are from

Saleh & Plieth (2009) **D**: Plot of integrated light yield (= sum of counts during the first 100 sec of reactions shown in B) against the concentration of added H<sub>2</sub>O<sub>2</sub> in log-log-scale. Traces given in B are averages of n = 3 with StDv of less than 15% of peak value. Averages in D are calculated from data shown in B. Error bars are equal or below symbol size.



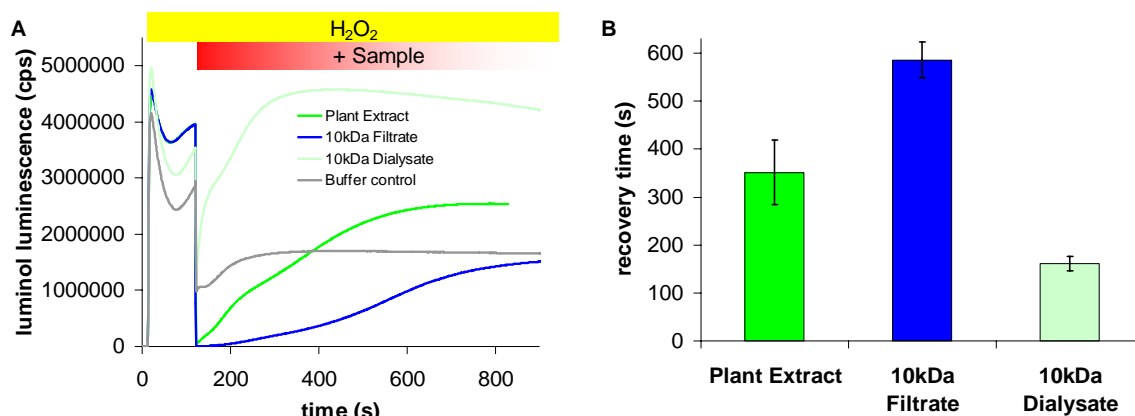
**Figure Suppl\_8: pH-optimium of the HRP-catalysed luminol reaction is around pH = 8.7**

**A**: HRP mix and H<sub>2</sub>O<sub>2</sub> were adjusted to the pH given in the legend. Reactions were started at t = 12 s by mixing 0.5 ml HRP mix with an equal amount of 1.1 mM H<sub>2</sub>O<sub>2</sub> of same pH. **B**: The integrated light output vs. pH. Data represent averages of n = 3. StDv is within symbol size. Figure from Saleh & Plieth (2009).



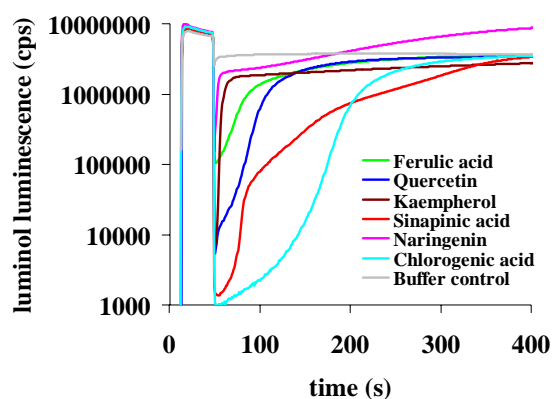
**Figure Suppl\_9: Calcium dependency of HRP catalyzed luminol luminescence.**

Plot of integrated light yield (sum of counts during the first 100 sec) against the free calcium concentration in the assay buffer. Free calcium concentrations were calculated from total [CaCl<sub>2</sub>] and [EGTA] in the HRP-master mix accordingly to Patton *et al.* (2004) <http://www.stanford.edu/~cpatton/webmaxcS.htm>.



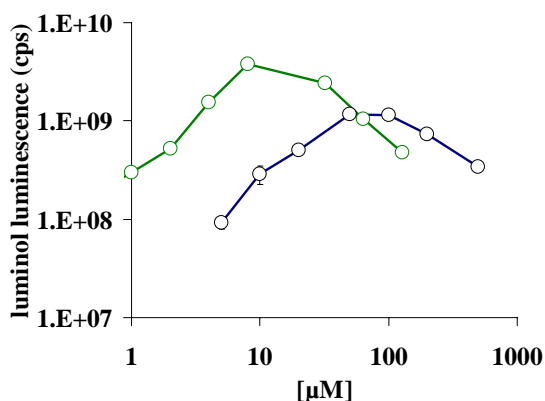
**Figure Suppl\_10: TAC of different molecular weight fractions (whole sample, filtrate and dialysate) from garden cress (*Lepidium sativum*).** The filtrate represents the low molecular weight fraction of the

samples (< 10 kDa) whereas the dialysate represents the high molecular weight fraction (> 10 kDa). **A, B:** Plant extract from garden cress (*Lepidium sativum*) was prepared, filtered and dialyzed as described in the Chapter 4. The signal from filtered samples (blue in **A**) completely recovers and reaches the control level (grey). In contrast the full extract (dark green in **A**) gives more light than the control (grey) indicating the presence of plant peroxidases in the sample, which add to the HRP activity in the assay. This effect is more pronounced with the dialysate (light green in **A**) because signal quenching antioxidants are absent. Data in **B** are averages of  $n = 5$ . Error bars represent StDv.



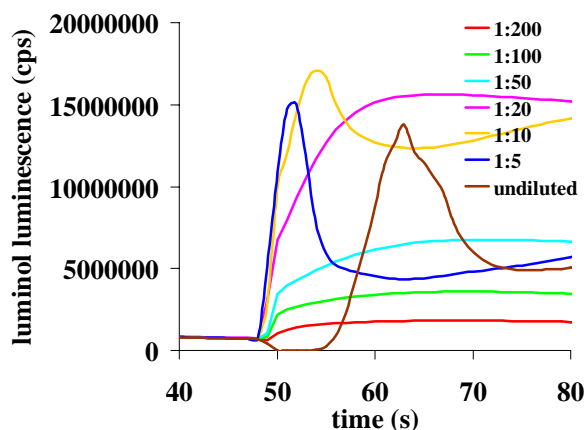
**Figure Suppl\_11 Antioxidative properties of different flavonoids**

Ferulic acid 2  $\mu\text{M}$ , quercetin 2 mM, kaempferol 200  $\mu\text{M}$ , sinapinic acid 2  $\mu\text{M}$ , naringenin 200  $\mu\text{M}$ , chlorogenic acid 2  $\mu\text{M}$  were measured by the means of TAC assay. Averages of three technical replicates are given. StDv are not included.



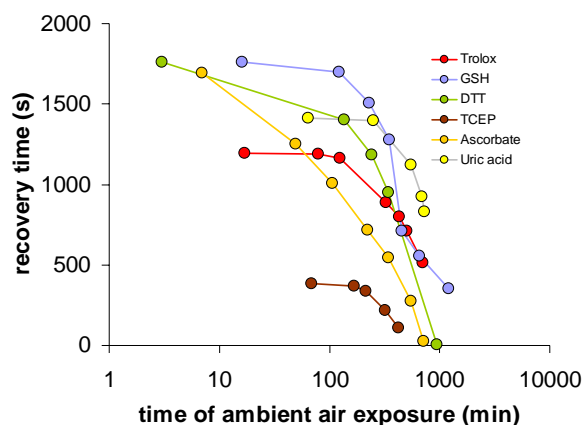
**Figure Suppl\_12: Naringenin and 4-iodophenol enhance the HRP-driven luminol light yield.**

Plot of integrated light yield (= sum of counts during the 240 sec) against the concentration of added enhancer in log-log-scale. Data are averages of  $n = 3$ . Error bars are equal or below symbol size. 0.5 ml not-enhanced HRP master mix was aliquotted into luminometer vials. The light reaction was started at 12 s by addition of 0.5 ml 1 mM  $\text{H}_2\text{O}_2$ . 0.5 ml of the enhancer were added at  $t = 48$  s. 1 M ethanolic solutions of 4-iodophenol and naringenin were prepared and diluted further in TriCaT.



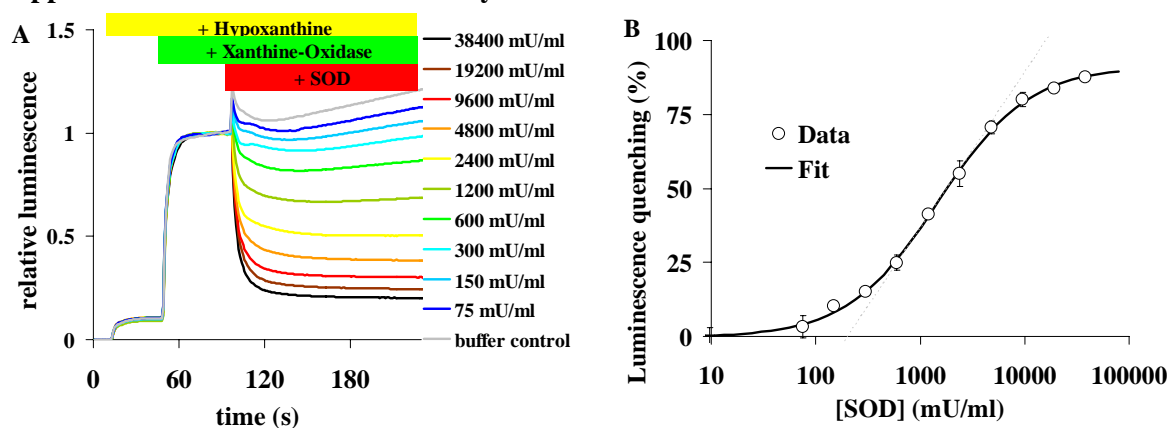
**Figure Suppl\_13: Barley extract enhances the HRP-driven luminol luminescence.**

Different dilutions (as depicted in the figure legend) of young barley leaves filtrate were tested by the not-enhanced TAC assay on their antioxidative and enhancing activity.



**Figure Suppl\_14: Decay of the antioxidative capacity of pure antioxidants** (Trolox 64  $\mu$ M, GSH 1 mM, DTT 1 mM, TCEP 20  $\mu$ M, ascorbate 1 mM, uric acid 100  $\mu$ M). Samples were assayed at different times after preparation. Recovery times are plotted against (log of) the time after preparation. Averages of three technical replicates are given. The standard deviation (StDv) is within the symbol size Data from Saleh & Plieth (2010a).

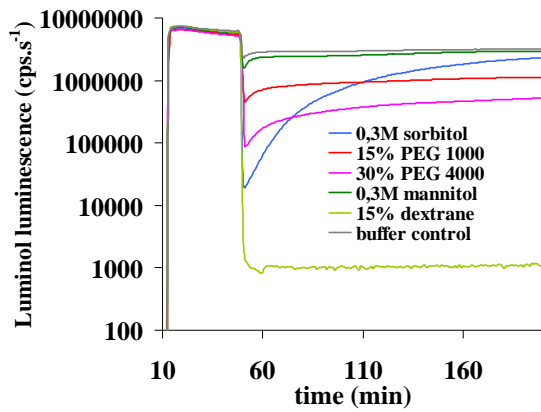
### Supplemental material 20: SOSA Assay



**Figure Suppl\_15 The luminescence quenching by SOSA correlates with the log of the amount of superoxide scavengers added.**

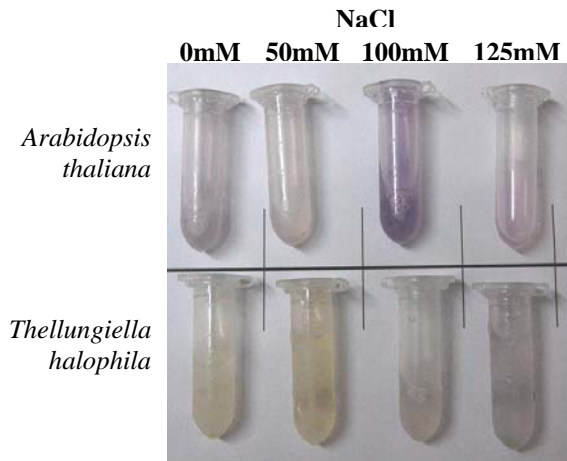
A: Purified SOD from bovine liver (Sigma #S8409) in concentrations indicated in the legend is injected into the SOSA assay, mixed and luminescence quenching is recorded for 2 min. The steady state luminescence after starting the reaction with XOD (62 s < t < 72 s) was used to normalise the data. B: Luminescence quenching calculated from the data in A is plotted against the SOD concentration. The plotted parameters are linearly correlated when quenching is between 20 and 80 % ( $r^2 = 0.996$ ). Data in B are averages of  $n = 3$ . Error bars represent StDv. Data from Saleh & Plieth (2009)

**Supplemental Material 21: Antioxidative activity of different osmolytes**



**Figure Suppl\_16: Antioxidative properties of different osmolytes measured by means of the TAC-assay**

**Supplemental Material 22: Flavonoids in plant extracts**



**Figure Suppl\_16: Pictures of water extracts prepared for IC.**

Plants were grown at different salt concentrations, as depicted in the legend on Ca-free medium. The water extract was prepared as described in the Chapter 2, Section 2.1.4.

